Development of a clean and simple biocatalysed flavin regeneration system to aid sustainable chemical synthesis



Shiny Joseph Srinivasan

St Edmund Hall, Hilary Term, 2022

A Thesis submitted to the Board of the Faculty of Physical Sciences, for the degree of Doctor of Philosophy, University of Oxford

Acknowledgements

First and foremost, my sincere thanks to Professor Kylie Vincent for her invaluable supervision and guidance throughout my DPhil. Kylie's patience and passion for chemistry was an inspiration for me that kept me moving during challenging times. I cannot thank her enough for offering me to take on this exciting project which I had absolutely enjoyed working on.

I am hugely indebted to Dr Sarah Cleary for the unfailing support she has offered me from day one – from discussing ideas about the project to running UV-visible activity assays to setting up organic chemical reactions, this thesis would not be where it is now without her. Thank you for proof reading all my abstracts, reports, conference presentations and many more. I am ever grateful for your patience in replying to all my silly doubts. I will cherish the moments we spent in the lab together and I hope our paths cross again in the future.

I would like to thank Dr Holly Reeve for her priceless advice at the various stages of this project. You have always welcomed me with a smiling face when I came for help, despite your extremely busy schedule. I am much obliged to Dr Jack Rowbotham for all his useful advice on my experiments, but most importantly for his uncomplaining assistance with the GC and the HPLC. I must thank Dr Miguel Ramirez for preparing Hyd1 and other enzymes that I used for this project.

I thank our collaborator, Dr Caroline Paul for kindly providing us with *Ts*OYE enzymes, and for her useful discussion in the flavin project. I thank all the members of the Vincent group, both past and present for every little help that was offered to me in one form or the other. You were such wonderful colleagues to work with and have made my time in the Vincent group a memorable one. I thank everyone from the Chemistry department who have indirectly contributed to the smooth running of my project experiments.

I thank all the wonderful friends that I made at Oxford – for giving me loads of beautiful memories to look back at and smile one day. A special word of thanks to my dearest friend, Carlson Alexander for having my back at all times – for the time we spent talking chemistry, cooking Indian food, doing grocery shopping and more.

I am ever grateful to all my teachers, supervisors and professors who motivated and supported me during different stages of my education in India.

Many thanks to my beloved husband, Kevin, for all the love, support and for the incredible patience to wait for me until I finish my DPhil. I am beyond grateful to my family – mummy, daddy and Shawn for believing in me and for being that pillar of support through this venture. I am thankful to my uncle, Fr John F Antony for keeping me in his prayers. Finally, I thank the Lord Almighty for the many blessings he has bestowed upon me during this stage of my life.

Development of a clean and simple biocatalysed flavin regeneration system to aid sustainable chemical synthesis

A Thesis Submitted for the degree of DPhil, Hilary Term, 2022

Shiny Joseph Srinivasan, St Edmund Hall

Over the years, biocatalysis has evolved as an extremely useful tool for synthetic applications due to the incredible selectivity it offers under relatively mild reaction conditions. With the advent of directed evolution and enzyme engineering, new reactivities previously unknown in nature are also being discovered by scientists. One of the main factors that determines the cost and efficiency of many biocatalytic reactions is their cofactor regeneration system. Cofactors are helper molecules that aid an enzyme to sustain catalysis. Their complex structure makes them prohibitively expensive such that their stoichiometric addition for a biocatalytic reaction is not viable. Cofactor regeneration involves the recycling of a catalytic quantity of the cofactor over and over again using a catalyst. Cofactor regeneration techniques for the nicotinamide cofactors have been widely resolved in the past to an extent that some enzymes dependent on these cofactors have found application in industry. This thesis looks at ways to recycle another useful class of cofactors – the flavins. Preliminary efforts to regenerate the deazaflavin cofactors are also presented. Enzymes that rely on flavin cofactors have valuable synthetic utility, however their application in industry is not well established perhaps due to the lack of efficient recycling methods. This project resulted in an exciting discovery that hydrogenases can reduce flavins under H_2, an atom economical reductant. The robust nature and exceptional stability of the hydrogenase, Hyd1 was exploited to supply reduced flavins for ene-reductases and nitroreductases to accomplish H_2-driven C=C double bond reductions and nitro reductions respectively with high selectivity.

Thus a new application for the hydrogenase enzyme has been uncovered. Demonstration of this novel, single-enzyme flavin regeneration system for application with several useful enzymes, with benefits over current flavin recycling methods, could make this Hyd1/ flavin system a promising choice for use in industry.

Publications and patents

1. S. Joseph Srinivasan, S. E. Cleary, M. A. Ramirez, H. A. Reeve, C. E. Paul and K. A. Vincent, *Angew. Chemie - Int. Ed.* **2021**, *60*, 13824 – 13828.

2. M. A. Ramirez, S. Joseph Srinivasan, S. E. Cleary, P. M. T. Todd, H. A. Reeve and K. A. Vincent, *Frontiers in Catalysis*, **2022**, 2, 1-9.

3. K. A. Vincent, S. E. Cleary, S. Joseph Srinivasan and H. A. Reeve, **2021**, *Method of reducing and recycling oxidized flavin cofactors*, WO 2021/214493 A1.

Oral and poster presentations at conferences

1. S. J. Srinivasan, Sarah E. Cleary, Holly A. Reeve, Kylie A. Vincent. *Biocatalysed H_2-Driven Flavin Regeneration for Clean, Chemoselective Alkene Reductions*. Poster presentation at the 5th RSC Dalton Division Southern Regional Meeting; September 2019; Oxford, United Kingdom.

2. S. J. Srinivasan, S. E. Cleary, M. A. Ramirez, H. A. Reeve, C. E. Paul, K. A. Vincent. *Hydrogenase is a robust flavin recycling catalyst: demonstrated for atom-economical, selective alkene hydrogenations by ene-reductases.* Oral presentation at NextGenBiocat 2021, February 2021, online.

3. S. J. Srinivasan, S. E. Cleary, M. A. Ramirez, H. A. Reeve, C. E. Paul, K. A. Vincent. *Mild Chemo- and Enantioselective Biocatalytic Hydrogenation of activated alkenes.* Oral presentation at SCI's 31st Postgraduate Symposium, May 2021, held online.

4. S. J. Srinivasan, S. E. Cleary, M. A. Ramirez, H. A. Reeve, C. E. Paul, K. A. Vincent. *Hydrogenase is a robust flavin recycling catalyst: demonstrated for atom-economical, selective alkene hydrogenations by ene-reductases.* Poster presentation at Biotrans 2021; July 2021; Graz, Austria (attended online)

Abbreviations

A	Absorption
BV	Benzyl viologen
c	Concentration
d	doublet
δ	Chemical shift
Da	Dalton
dd	doublet of doublets
DMF	Dimethyl formamide
DMSO	Dimethyl sulphoxide
e^-	Electron
ee	enantiomeric excess
ϵ	Molar extinction coefficient
FAD	Flavin Adenine Dinucleotide
FMN	Flavin Mononucleotide
g	grams
GC	Gas chromatography
HPLC	High Pressure Liquid Chromatography
IR	Infrared
J	Coupling constant
K_M	Michalis-Menten constant
λ_{max}	Wavelength of maximum absorption
M	Molar extinction coefficient
M	mass
MB	Methylene blue
NAD^+	Nicotinamide Adenine Dinucleotide
NMR/^{1}H NMR	1H Nuclear Magnetic Resonance Spectroscopy
OD	Optical Density
PDB	Protein Data Bank
pKa	Dissociation Constant for an acid
ppm	Parts per million
rpm	Rotations per minute
s	seconds
SH	Soluble Hydrogenase
t	time
T	Temperature
TN	Turnover Number
TOF	Turnover Frequency
TTN	Total Turnover Number
U	micromol/ min
UV-vis	Ultraviolet-visible

Table of Contents

Chapter 1 Introduction 1

1.1. Biocatalysis 2

1.2. Hydride transfer organic cofactors 3

1.2.1. Nicotinamides 3

1.2.2. Flavins 4

1.2.3. Deazaflavins 6

1.2.4. Pyrroloquinoline quinone (PQQ) 7

1.2.5. Cofactor regeneration 8

1.3. Important classes of redox reactions in biotechnology 10

1.3.1. C=O reductions (mostly NADH/NADPH dependent) 10

1.3.2. C=C reductions 11

1.3.3. C=N reductions (mostly NADH/NADPH dependent) 15

1.3.4. Oxidation 16

1.3.5. Halogenases 18

1.4. Emerging H_2-driven approaches for cofactor recycling 21

1.4.1. H_2 - a valuable and clean reductant 21

1.4.2. Biocatalytic approaches for H_2-driven NAD(P)H regeneration 22

1.4.3. Soluble hydrogenase from *Ralstonia eutropha* 23

1.4.4. Flavin reduction activity 23

1.4.5. Limitations of SH 24

1.4.6. Reduction of $NADP^+$ 25

1.4.7. The structural design of soluble hydrogenase (SH) from *R. eutropha* 26

1.4.8. The HydRegen system[117,118] 28

1.5. Hydrogenases and their classification 30

1.5.1. NiFe hydrogenases 32

1.5.2. General features of NiFe hydrogenases 32

1.5.3. Metal Active centre 33

1.5.4. FeS clusters 34

1.5.5. Hydrogenases from *E. coli* 34

1.6. Hydrogenase 1 from *E. coli* (Hyd1) 35

1.6.1. The crystal structure of Hyd1 35

1.6.2. Oxygen tolerance 36

1.6.3. Redox states of the NiFe active site in Hyd1 37
1.6.4. Predicted mechanism of flavin reduction by Hyd1 41
1.7. Hyd2 from *E. coli* **42**
1.8. DvMF (*Desulfovibrio vulgaris* Miyazaki F) hydrogenase **44**
1.9. The concept of this project **45**
Chapter 2 Methods **43**
2.1. Enzyme sources and preparation **44**
2.1.1. Hydrogenases 44
2.1.1.1. Hydrogenase 1 from *E. coli* (Hyd1) 44
2.1.1.2. Hydrogenase 2 from *E. coli* (Hyd2) 46
2.1.1.3. NiFe Hydrogenase from *Desulfovibrio vulgaris* Miyazaki F (DvMF) 47
2.1.2. Glucose dehydrogenase 47
2.1.2.1. GDH-101 47
2.1.3. Old Yellow Enzyme ene-reductases 47
2.1.3.1. Old Yellow Enzyme from *Thermus scotoductus* (*Ts*OYE) 47
2.1.3.2. Commercial ene-reductases 49
2.2. UV-visible spectroscopy **49**
2.2.1. Theory of UV-visible spectroscopy[178,179] 49
2.2.2. Electronic transitions in cofactor molecules 50
2.2.2.1. Nicotinamides - NAD^+ and NADH 51
2.2.2.2. Flavins - FAD, FMN and $FADH_2$, $FMNH_2$[180–182] 52
2.2.2.3. Deazaflavins 58
2.2.3. The Beer-Lambert law 60
2.2.4. Calculating enzyme activities 61
2.2.5. Plate reader 63
2.2.5.1. Bradford assay 63
2.3. Reaction set-up **64**
2.3.1. Pressure vessel 64
2.3.2. Procedure for setting up a pressure vessel reaction for alkene hydrogenation reactions 65
2.3.3. *In situ* UV-visible reactions in UV cuvettes 66
2.4. Analytical methods **67**
2.4.1. NMR spectroscopy 67
2.4.2. Gas Chromatography 68
2.4.3. GC method and parameters 68
2.4.4. Mass spectrometry 73

2.5. Enzyme Kinetics and Measurements[202,203] 74
2.5.1. Michaelis-Menten equation 75
2.5.2. Derivation of the Michaelis-Menten constant 76
2.5.3. Enzyme inhibition[202,203] 79
2.5.3.1. Reversible inhibition 79
2.5.3.2. Irreversible enzyme inhibition 82
2.6. Chemicals and reagents 83
2.6.1. Gases 83
2.6.2. Buffers 83
2.6.3. Cofactors 84
2.6.4. Glovebox 84
2.6.5. Substrates and standards 85
Chapter 3 Developing methods for H_2-driven flavin reduction 86
3.1. Reduction of FMN and FAD by Hyd1 87
3.2. Control experiments for Hyd1 catalysed flavin reduction 90
3.2.1. Flavin reduction in the absence of molecular hydrogen 90
3.2.2. Flavin reduction in the absence of Hyd1 90
3.2.3. Flavin reduction in the absence of H_2 and Hyd1 91
3.3. Effect of temperature on flavin reduction by Hyd1 93
3.4. Hyd1 samples with and without the cytochrome subunit 95
3.4.1. Reduction of FMN using Hyd1 enzyme that contains or lacks the cytochrome 96
3.5. Effect of pH on the reduction activity of Hyd1 97
3.6. Flavin reduction by other hydrogenases 99
3.6.1. Reduction of FMN and FAD by Hyd2 99
3.6.2. Reduction of FMN and FAD by DvMF hydrogenase 100
3.7. Kinetic studies to determine the K_M (Michaelis-Menten constant) of Hyd1 for FAD 102
3.8. Complete reduction of FMN to $FMNH_2$ 104
3.9. Overview 106
Chapter 4 Coupling flavin regeneration to ene-reductases 108
4.1. Introduction 109
4.2. Old Yellow Enzyme ene-reductases (OYE) 110
4.2.1. *Ts*OYE ene-reductase 111
4.2.1.1. Developing a H_2-driven system for the reduction of ketoisophorone (1) to (*R*)-levodione (2) using *Ts*OYE and the Hyd1 recycling system for flavins 113
4.2.1.2. Reaction setup and optimisation for the reduction of 1 114

4.2.1.3. Control experiments 121
4.2.1.4. Reproducibility 122
4.2.1.5. Comparison to other similar systems in the literature 122
4.2.2. Commercial ene-reductases from Johnson Matthey 131
4.2.2.1. Preliminary screening of various substrates and ene-reductases 131
4.2.2.2. Reaction optimisation 134
4.2.2.3. Comparison of the Hyd1 recycling system with the GDH/glucose recycling system for alkene reductions using ene-reductase from JM 139
4.2.2.4. Reproducibility of results for alkene reduction using GDH-101 and glucose recycling system 142
Chapter 5 Coupling Hyd1 to nitroreductases for the synthesis of amines 144
5.1. Amines 145
5.2. Synthesis of amines 146
5.2.1. Catalytic hydrogenation 146
5.2.2. Mechanism for the hydrogenation of nitro group to amine 148
5.2.3. Catalytic transfer hydrogenation 150
5.2.4. Hydride transfer reductions 150
5.2.5. Metal dissolving reductions 151
5.2.6. Metal free reductions 152
5.3. Biocatalytic synthesis of amines 153
5.3.1. Transaminases 153
5.3.2. Amine dehydrogenases 156
5.3.3. Amine oxidases 157
5.3.4. Imine reductases 160
5.4. Nitroreductase 163
5.4.1. Model crystal structure of a nitroreductase 165
5.5. Nitro reductions at Johnson Matthey (JM) 168
5.6. H_2-driven flavin catalysed reduction of 2-methyl-5-nitropyridine using commercial nitroreductases from Johnson Matthey 170
5.6.1. Reaction setup and enzyme screening 171
5.6.2. Analysis in GC 172
5.6.3. Synthesis of *N*-(6-methylpyridin-3-yl)hydroxylamine 177
5.6.4. Reproducibility of nitro reduction reactions 179
5.6.5. Control experiments 180
5.6.6. Evaluating the efficacy of control reactions in generating the final amine product 181
5.6.7. Reaction intensification 183

5.7. Summary ... **185**

Chapter 6 The Deazaflavin cofactor, F_{420} ... **186**

6.1. Deazaflavins ... **187**

6.1.1. Structure and chemistry of deazaflavins ... 188

6.1.2. F_{420} and F_O ... 189

6.1.3. Deazaflavins – nicotinamide in a flavin's clothing[192] ... 190

6.1.4. UV-visible spectroscopy of F_{420} ... 191

6.2. Potential cofactor recycling methods for F_{420} ... **191**

6.3. Classification of deazaflavoenzymes and their relevance for biotechnology applications ... **194**

6.4. Reducing deazaflavins with hydrogenases ... **198**

6.4.1. Synthesis of F_O ... 199

6.4.2. Characterisation of synthesised F_O ... 201

6.4.3. Reduction of F_O ... 202

6.4.4. Reduction of F_{420} ... 203

Chapter 7 Conclusion and Outlook ... **205**

References ... **210**

1

Chapter 1 Introduction

1.1. Biocatalysis

Biocatalysis can be defined as the 'mediation of chemical reactions by means of biological systems, including isolated enzymes, whole cells or cell-free extracts'.[1] Over the years, biocatalysis has emerged as a powerful synthetic tool, both in academia and industry owing to the advantages it offers over traditional chemistry methods.[2] Enzymes catalyse a plethora of chemical reactions with extraordinary chemo-, regio- and stereo-selectivity in aqueous solvents under ambient reaction conditions. They can also tolerate organic solvents, to a certain extent, which makes them suitable for carrying out many organic chemical reactions. Conventional hydrogenation and oxidation reactions usually depend on precious metals (like Pt, Rh) and heavy metal oxidants (like Cr (VI)) respectively that require careful separation techniques because of their toxicity. Enzymes on the other hand are non-toxic, renewable catalysts, and are produced themselves from biodegradable and renewable resources.[3,4] Moreover, with the rapid developments in protein engineering techniques, it has become possible to modify protein structures to enable them to perform desired reactions under favourable conditions, and hence achieve novel enzymatic reactions previously unknown in nature.[5,6] With the increasing demand for versatile yet benign catalysts, biocatalysis holds huge promise for cleaner and greener chemical synthesis in the future.

To date, several thousand enzymes have been identified and many hundreds of them are commercially available. Among them, the oxidoreductases are a synthetically interesting class of enzymes that are studied for the diverse range of redox reactions they catalyse[7] — oxidation of hydroxyl, aldehyde and keto groups, oxidation of primary and secondary amines, Baeyer-Villiger oxidation, double bond epoxidation, reduction of aldehydes, ketones, carboxylic acids and unsaturated carbon-carbon bonds are a few examples.[8]

1.2. Hydride transfer organic cofactors

Many important biological reactions are catalysed by enzymes that rely on helper molecules called cofactors.[9] Cofactor molecules can be inorganic such as metal ions in various oxidation states or organic molecules like nicotinamide and flavin cofactors.[10] About 80% of all oxidoreductases employ organic cofactors for their catalytic activity.[11] These include cofactors such as nicotinamides (NAD(P)H), flavins (FAD and FMN), deazaflavins (F_{420}) and quinones (PQQ) that are essential for electron, proton or hydride shuttling processes.

1.2.1. Nicotinamides

Nicotinamide Adenine Dinucleotide (NAD^+) and Nicotinamide Adenine Dinucleotide Phosphate ($NADP^+$) are ubiquitous in nature and are among the most extensively studied cofactors for biocatalysis. Upon reduction, $NAD(P)^+$ becomes NAD(P)H. Nicotinamide cofactors strictly undergo only two-electron reactions in biology and aid in hydride transfer processes. For example, during ketone reduction by alcohol dehydrogenases (ADH), NADH aids in hydride and proton transfer to the carbonyl group which is essential for the reduction to occur. The chemical structures of NAD^+ and $NADP^+$ are shown in Figure 1. 1. While the NAD^+/NADH and the $NADP^+$/NADPH couples have similar redox potentials, Nature employs them to perform two orthogonal sets of reactions, where redox interconversion is not possible, because NADH and NADPH do not interconvert spontaneously.[12] In general, NAD^+ is used in an oxidative manner for catabolic processes where it serves as an electron acceptor, whereas NADPH functions as an electron donor during reductive biosynthesis.[13,14] $NADP^+$ differs from NAD^+ in that it contains an additional phosphate group as shown in Figure 1. 1. The phosphate group however has no influence on the electron transfer properties of the two cofactors, because it remains far from the redox active site. However, it does give $NADP^+$ a different shape that allows the two sets of cofactors to bind to different set of enzymes that catalyse different reactions.

Moreover, inside the cell the NAD^+ to NADH ratio is kept high and the ratio of $NADP^+$ to NADPH is kept low to make sure there is enough supply of the NAD^+ for catabolic processes and sufficient NADPH to fuel anabolic reactions. It makes sense that this cannot be achieved simultaneously using just one cofactor.[15,16]

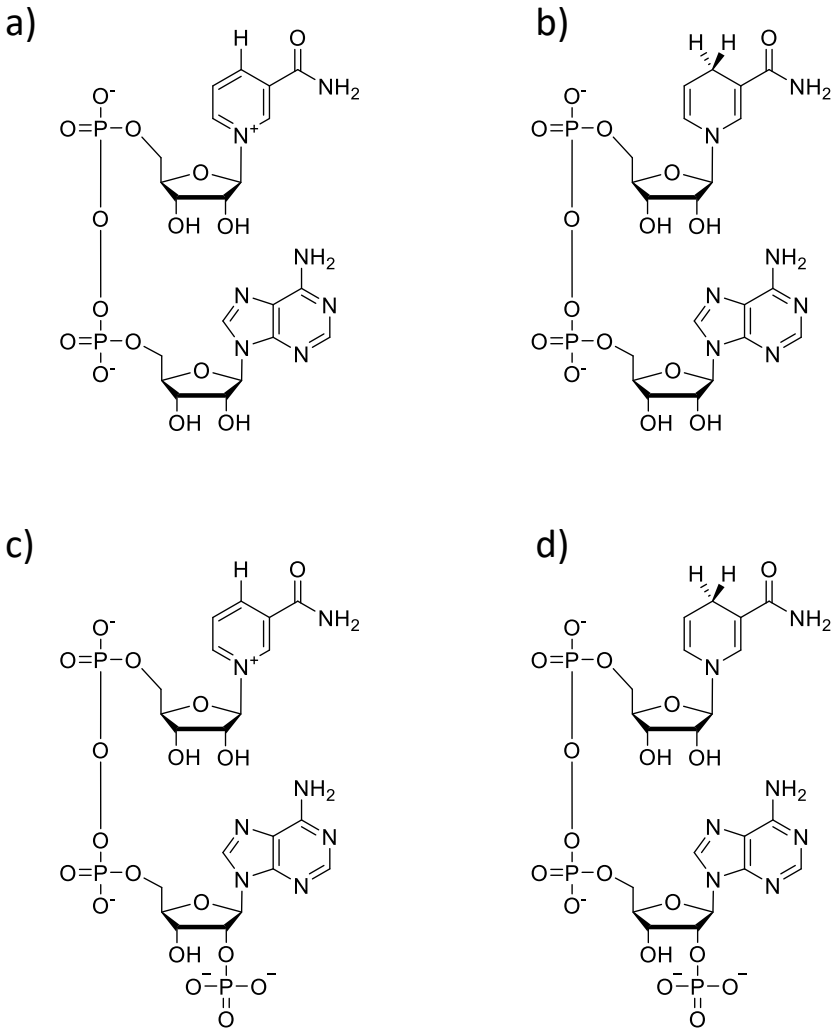


Figure 1. 1. Chemical structures of a) NAD^+, b) NADH, c) $NADP^+$ and d) NADPH

1.2.2. Flavins

Flavins are an interesting class of cofactors as they can undergo both one and two electron processes unlike nicotinamides that exclusively perform only two electron transfer processes. Figure 1. 2 shows

the chemical structures of the two biologically important cofactors: FAD (Flavin Adenine Dinucleotide) and FMN (Flavin Mononucleotide). For example, in the flavoenzyme, NADPH-cytochrome P-450 reductase, the flavin cofactor within the enzyme readily accepts two electrons from NADPH and transfers one electron at a time to cytochrome P-450 enzyme, thus acting as a two electron acceptor and one electron donor.[17]

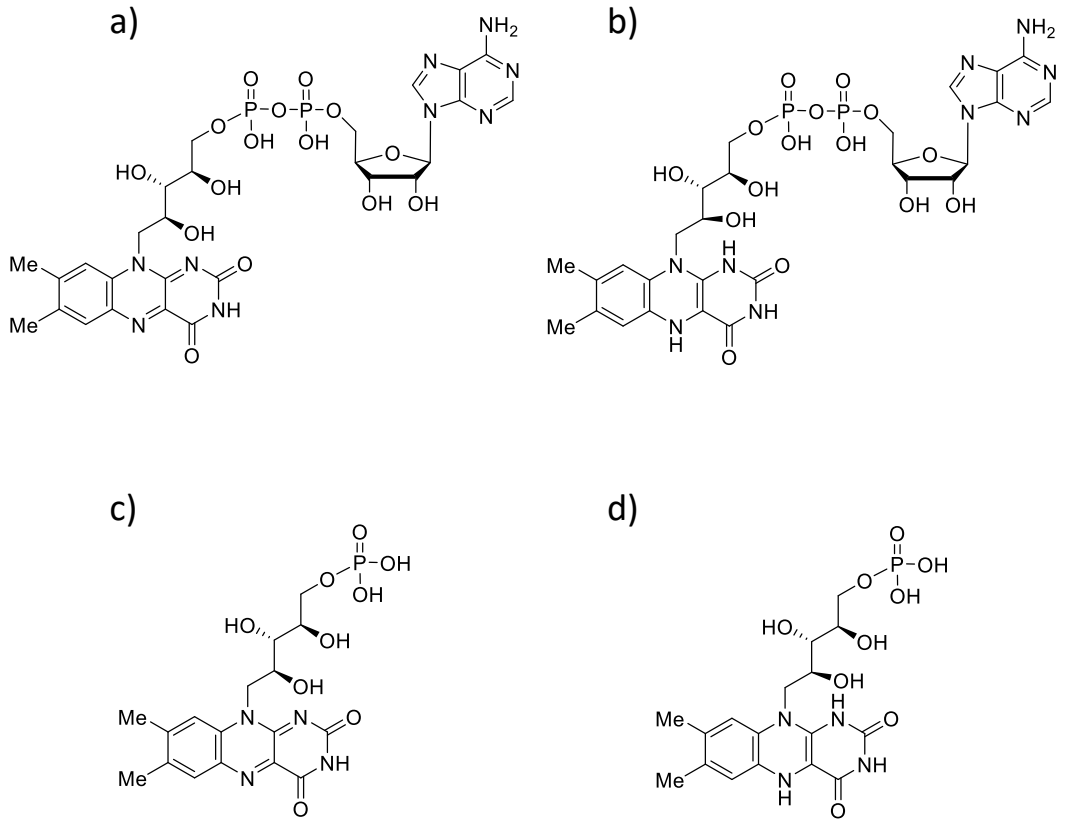


Figure 1. 2. Chemical structures of a) FAD, b) $FADH_2$, c) FMN and d) $FMNH_2$

Apart from general redox catalysis, flavins exhibit interesting photochemistry that has led to research resulting in new reactivities.[2,18] In nature, flavins are responsible for processes like bioluminescence and DNA repair.[19,20]

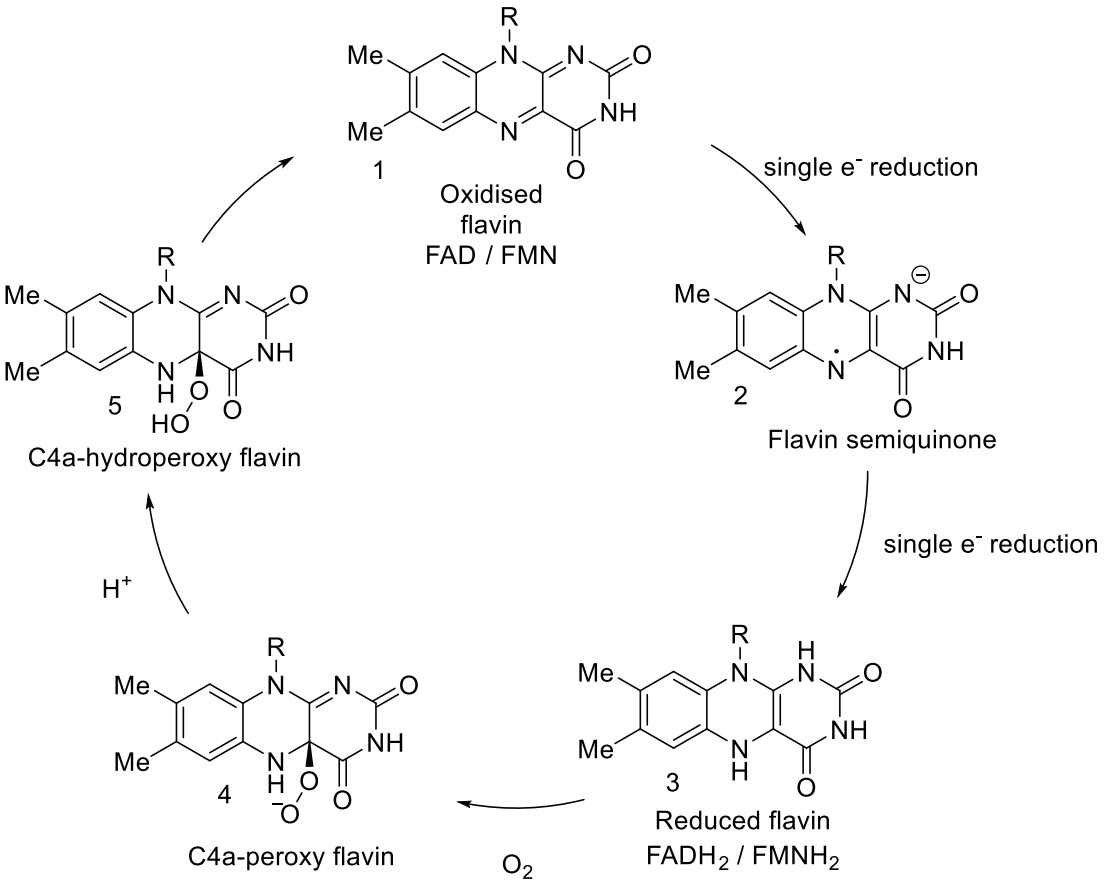


Figure 1. 3. Different redox states of flavin adapted from reference 21 with permission from Elsevier publisher: *Tetrahedron*, **2019**, *75*, 1115-1121.[21] License number: 5236261358063

1.2.3. Deazaflavins

The deazaflavin cofactor, F_{420} has gained interest lately due to new reactions catalysed by F_{420}-dependent enzymes. Reduction of C=C by deazaflavin-dependent enzymes have been shown to generate products with opposite stereochemistry to that obtained from flavin utilising enzymes.[22] Like nicotinamides, deazaflavins strictly perform only two-electron transfer reactions. Studies by Greening *et al*. have shown that mycobacterial $F_{420}H_2$-dependent reductases accomplish enantioselective alkene reductions through a common mechanism of hydride transfer from $F_{420}H_2$ to the electron deficient alkene group.[23] Figure 1. 4. shows the chemical structure of deazaflavin cofactor.

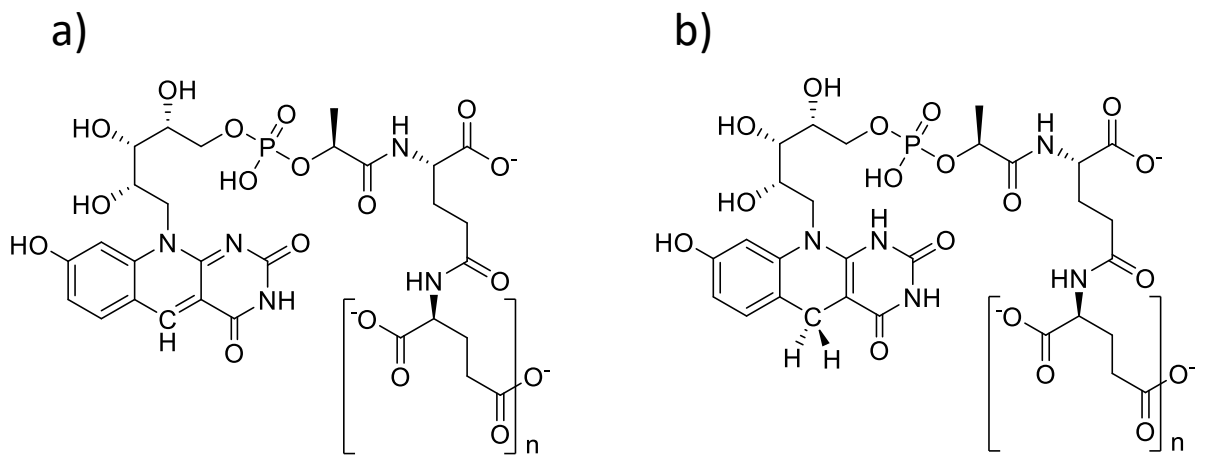


Figure 1. 4. Chemical structure of the deazaflavin cofactor a) F_{420} and b) $F_{420}H_2$.

1.2.4. Pyrroloquinoline quinone (PQQ)

Pyrroloquinoline quinone (PQQ) is a redox cofactor present in quinoproteins. These are nicotinamide-independent dehydrogenases widely present in bacterial enzymes and are involved in the oxidation of a variety of alcohols and sugars.[24] Nearly 88% of PQQ forming species were predicted to be in proteobacteria. The fact that PQQ generating enzymes are predominantly exclusive to bacterial species make their biosynthesis in bacteria an attractive target for new antibiotic design and development. Research into the development of inhibitors that can interfere with the biosynthesis of PQQ can suppress the growth of the respective bacterium.[25,26] In general, PQQ forms stable semiquinone intermediates which makes it possible to undergo both one and two electron transfers. In methanol dehydrogenases, the reductive half reaction involves oxidation of methanol to formaldehyde accompanying the reduction of PQQ through a hydride transfer mechanism. During the oxidative half reaction, the two-electron carrier PQQ, performs two one-electron transfers to the c-type cytochrome which is a one-electron carrier.[27] The exclusive Pyrroloquinoline quinone cofactors are not discussed further in this thesis but are mentioned here to give a complete overview of hydride transfer organic cofactors.

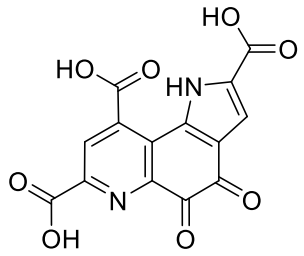


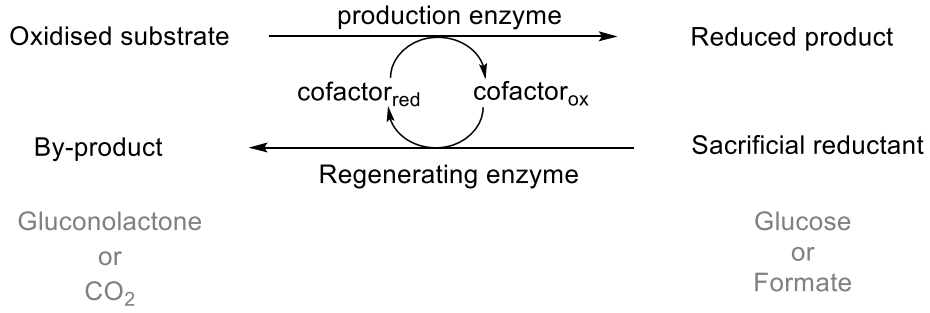
Figure 1. 5. Chemical structure of pyrroloquinoline quinone

1.2.5. Cofactor regeneration

Due to their complex structures, organic cofactor molecules are expensive to synthesise which means that their stoichiometric use in enzymatic reactions is off-putting. Much research in the past was devoted towards developing efficient cofactor regeneration techniques where a catalytic quantity of the expensive cofactor is regenerated in order to be available for the enzyme to use over and over again. While cofactor recycling has been largely resolved for NADH, development of efficient recycling techniques for other cofactors like reduced flavins and deazaflavins are still primitive.[14,28] New cofactor regeneration methods are frequently reported in the literature.[29,30] These include chemical, electrochemical and enzymatic methods with each technique possessing their own advantages and disadvantages. For instance, the different methods for NADH regeneration featuring potential synthetic utility include electrochemistry, chemical regeneration, photochemistry, enzymatic and chemo-enzymatic methods.[28] Extensive research in this field has also led to the development of nicotinamide biomimetics (mNADHs) that can replace the expensive natural cofactors required for catalysis, although recycling systems for these biomimetics remain poorly developed.[31] Enzymatic regeneration of the native cofactors, NAD(P)H still remains the most adopted technique for NAD(P)H regeneration on an industrial scale because of the high activity and mild reaction conditions, and because enzymatic regeneration leads to exclusively the enzyme-active form of NAD(P)H.[32] Several immobilisation strategies have also been developed to improve catalyst recycling and reuse, although for industrial application use of enzymes in solution remains the most

common approach.[32] Common problems pertaining to enzymatic cofactor recycling include cost, complexity (multi enzyme system, mutual inactivation of enzymes), separation issues at the end of the reaction and by-products. In 2000, an 80 kg scale enzymatic synthesis of allysine ethylene acetal (a vasopeptidase inhibitor) was demonstrated by Hanson *et al*. This enzymatic reaction was carried out using a phenylalanine dehydrogenase along with a formate dehydrogenase system for regenerating NADH.[33,34]

Glucose dehydrogenase is the most widely used cofactor recycling enzyme in industrial biotechnology, but still has a number of drawbacks. The by-product of glucose oxidation, gluconolactone, makes the reaction carbon-intensive, and also hydrolyses in water to gluconic acid. Gluconic acid has a pK_a value of ~3.6-3.8 and hence is a weak acid. However, accumulation of the acid over time has led to instances where the pH of the reaction mixture has been lowered requiring proper pH monitoring and adjustment.[35,36] Difficulties in cofactor recycling were important reasons why the industrial application of oxidoreductases was hampered at least until the early 2000s and industry still seeks better cofactor recycling methods.[37] This thesis explores new directions in this area with particular focus on solving the cofactor problem discussed above for flavin and deazaflavin cofactors.

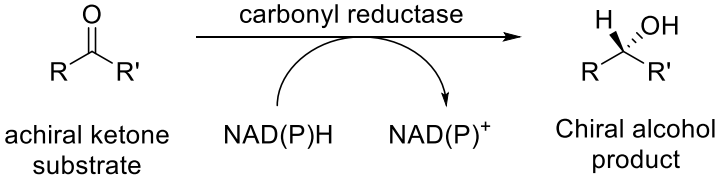


Scheme 1. 1. A general scheme showing the application of enzymatic cofactor recycling for an enzymatic reaction.

1.3. Important classes of redox reactions in biotechnology

1.3.1. C=O reductions (mostly NADH/NADPH dependent)

Asymmetric reduction of carbonyl groups is an important reaction that offers easy access to enantioenriched alcohols which represent valuable synthons in the making of industrially important chemicals. In conventional organic synthesis, this is generally accomplished through asymmetric catalysis where chiral catalysts, often chiral metal complexes facilitate this reaction. Chiral catalysts are highly stable making it easy to handle them during experiments. The possibility to separate them from the reaction mixture makes them attractive catalysts, however, on a large scale synthesis, catalyst separation still remains difficult. This becomes a disadvantage especially when there are severe regulatory restrictions on the acceptable amounts of metal present in drugs. A few chiral catalysts are also commercially available, for e.g. BINAP.[38,39] In biocatalysis, C=O reductions are predominantly done with the help of carbonyl reductases, a group of enzymes within the oxidoreductase family. Most carbonyl reductases, also known as ketoreductases (KRED) and alcohol dehydrogenases (ADH) demonstrate high turnovers and exceptional selectivity.[40] Up until the early 2000s, biocatalysis was dominated by two main enzymes, and carbonyl reductase was one of them, the other being lipases.[40,41]



Scheme 1. 2. A general reaction scheme showing an NAD(P)H-dependent carbonyl reductase reducing an achiral ketone substrate to its corresponding chiral alcohol product.

The mechanism of carbonyl reduction is already well established and firstly involves binding of the substrate carbonyl and NAD(P)H to the enzyme. This is followed by hydride transfer from NAD(P)H to

the substrate.[42] Oxidised nicotinamide cofactor $NAD(P)^+$ formed as a consequence is usually regenerated using a cofactor recycling system. Simple and low-cost cofactor regeneration systems that can fully harness nicotinamide-dependent enzymes for biotechnology have been an extensively researched topic. This eventually resulted in alcohol dehydrogenase catalysed carbonyl reduction as a commercially viable process displaying high catalytic turnover and selectivity operating with cost effective cofactor regeneration systems.[40,43]

1.3.2. C=C reductions

Asymmetric C=C reductions represent valuable reactions in chemistry as they generate chiral products important for the fine chemical and pharmaceutical industries. Biocatalytic routes for such reactions are highly competitive because of the high chemo and regio- selectivity that these enzymes offer. Over the last few decades, nicotinamide dependent alkene reductions catalysed by numerous enzyme families collectively called ene-reductases were explored widely and their potential application in the chemical industries was recognised.[44] The most predominant family of ene-reductases are the 'Old Yellow enzymes' (OYE).[45] These are FMN containing, NAD(P)H-dependent enzymes that selectively reduce α, β-unsaturated compounds containing an electron withdrawing group (EWG). The majority of the enzymes sold for biotechnology come under this family and by 2017 over 63 OYEs were identified and characterised.[46] The mechanism of hydrogenation occurs in a trans-fashion complementing the already well-established non-enzymatic cis-hydrogenation in organic chemistry.[41] The reaction follows a bi-bi ping-pong mechanism (consecutive binding of the substrate and the cofactor to the active site) and is hypothesised to comprise of two steps, (i) a reductive and (ii) an oxidative half reaction.[47]

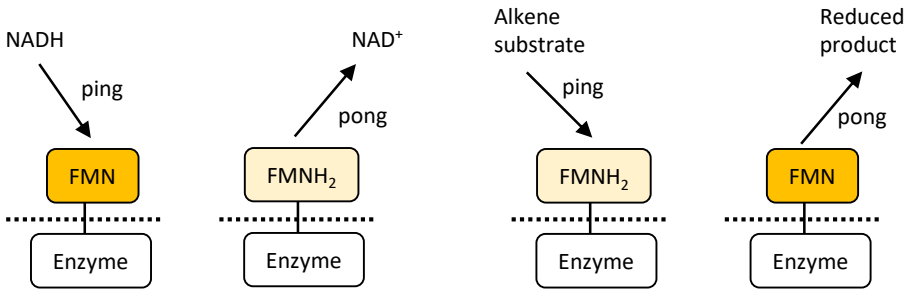


Figure 1. 6. Schematic representation of a bi-bi ping-pong mechanism.

Also called as a double displacement reaction, bi-bi ping-pong reactions are characterised by the formation of a temporary enzyme intermediate. The mechanism involves the binding and release of one product, in this case the NADH cofactor, before the binding of the second substrate (the alkene substrate here). This is opposed to the sequential reaction which requires the binding of both substrates to the enzyme in order to form the product. The name ping-pong arises from the manner in which the enzyme jumps between the two states: intermediate state and the normal state. In the case of ene-reductases, NADH binds and reacts with the enzyme bound flavin first, resulting in the release of oxidised NAD^+ as the product. Following this, the alkene substrate binds to the enzyme bound reduced flavin, releasing the hydrogenated product. Thus NADH and the alkene substrate alternate in reacting with the FMN showing a bi-bi ping-pong mechanism.[48,49] An illustration of this model is shown in Figure 1. 6

The ene-reduction reaction proceeds with a hydride transfer from NAD(P)H to the enzyme-bound flavin. The hydride from the reduced flavin is then transferred to the activated alkene, which on simultaneous protonation results in the product.[45,50,51] C=C double bond reductions by ene-reductases are further discussed in detail in chapter 4.

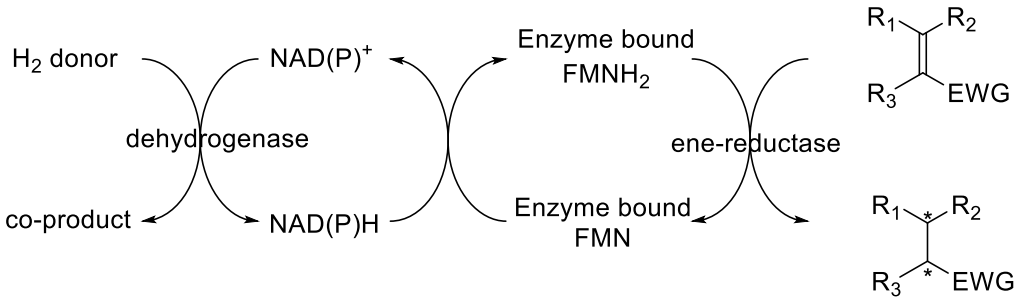
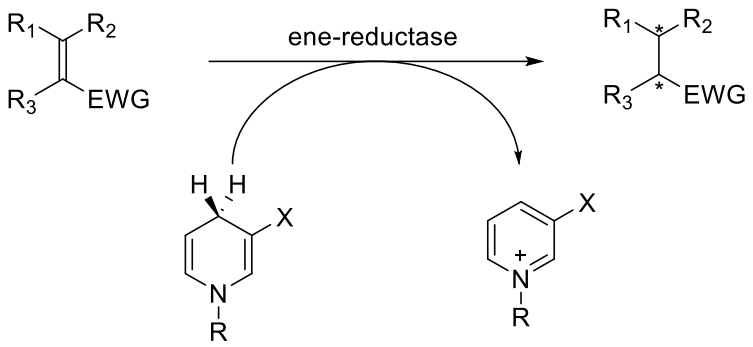


Figure 1. 7. Hydrogen transfer pathway by an ene-reductase for the reduction of an activated C=C double bond.

Although OYEs were believed to only accept nicotinamide cofactors as hydride donors, research later has shown that this process can be simplified by altering the supply of hydride source to the enzyme.[41,44,45] Reports show that a direct reduction of the enzyme bound flavin is possible through electron transfer from externally supplied reduced flavins.[7,52] This would allow a relatively simple system, provided there is an efficient recycling system for reduced flavins. One such example was the use of hydrogen donors like cyclohex-2-en-1-one that can directly reduce the enzyme bound flavin. This method circumvents the need for the expensive nicotinamide cofactor and a suitable nicotinamide recycling system.[53,54] Another approach is to use synthetic nicotinamide analogues called nicotinamide biomimetics (mNADHs) as hydride sources in place of natural cofactors (Figure 1. 8.). These functional mimics of nicotinamide cofactors are simple and cheap to synthesise and are attractive, cost efficient alternatives.[55] The applications of mNADHs is demonstrated with several OYE ene-reductases and have shown to perform better than natural cofactors. A cofactor recycling method for mNADHs is however not very well developed.[31]



R	X
benzyl	-$CONH_2$
n-butyl	-$CONH_2$
benzyl	-CO_2H
benzyl	-$COCH_3$
benzyl	-CN

Figure 1. 8. Asymmetric reduction of activated alkenes using mNADHs. The table inset shows the different mNADHs synthesised and tested for this reductive reaction.[55]

Direct photocatalysed reduction of enzyme bound flavins using organometallic photosensitisers in the presence of electron donors have also been reported to show relatively good conversions. These systems however, suffer from flavin decomposition after prolonged exposure to light.[56]

Simpler methods like electrochemistry and metal catalysis have also been reported, but these systems do encounter biocompatibility issues.[7,29,57] Milder enzymatic methods for flavin recycling are preferred, however, such systems are quite cumbersome.[29,44,58] They require a flavin reductase to reduce flavins at the expense of NAD(P)H which is then regenerated using a glucose/GDH system.[59,60] Such lack of efficient recycling techniques have hindered the exploitation of valuable flavin dependent enzymes.

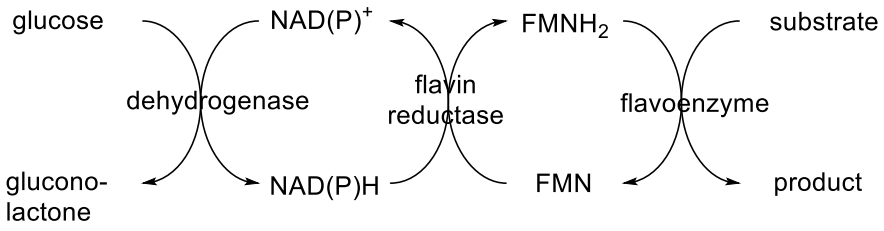


Figure 1. 9. A multi-enzymatic flavin reduction system comprising of a dehydrogenase and flavin reductase utilised by a flavoenzyme for its respective biotransformation.

This project uncovers a non-native reactivity of the hydrogenase enzyme which is used to develop an efficient flavin regeneration system using H_2 as the clean reductant.

Other families of ene-reductases include the FAD-containing enoate reductases that are specific to substrates containing carboxylic acids and esters. Ene-reductase activity is also observed in medium chain[61] and short chain dehydrogenases[62] that are flavin independent and require direct hydride transfer from nicotinamides, NAD(P)H.

Another recently discovered group of ene-reductases are those that depend on F_{420}, a deazaflavin cofactor found in certain methanogens and bacteria. F_{420}-dependent ene-reductases exhibit opposite enantioselectivities to that of OYE which make them interesting catalysts for synthetic chemistry.[22,63] These enzymes are not yet applied for biotechnology due to the lack of viable cofactor recycling methods for the F_{420} and also due to the high cost of F_{420}.[64]

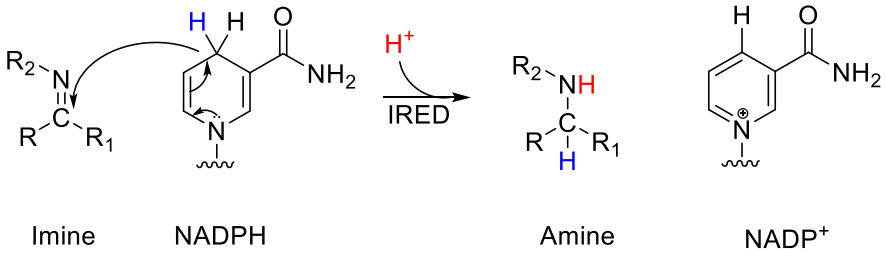
In this project, the newly developed flavin regeneration system was coupled for alkene reduction reactions catalysed by a thermophilic ene-reductase from *Ts*OYE and a range of commercial ene-reductases from Johnson Matthey (JM)[35,44] and attempts were made to extend to F_{420} reduction.

1.3.3. C=N reductions (mostly NADH/NADPH dependent)

Over the last two decades, asymmetric reduction of imines has become a popular method for synthesising chiral amines. Chiral amines are valuable intermediates in pharma and agrochemical industries, and development of efficient methods for their preparation is therefore of great significance.[65] While biocatalytic C=O and C=C reductions are well established in terms of enzyme discovery and reaction mechanism,[66] C=N reductions have only recently gained attention, probably due to the low stability of imine substrates that can degrade to their corresponding ketone/ aldehyde and amine counterparts in aqueous media – a typical reaction medium for biocatalysis.[66,67] Imine reductases (IRED) are an attractive route for the synthesis of 1°, 2°, 3° chiral amines, and have been extensively investigated for biocatalytic applications, since their discovery in 2011 by Mitsukura and co-workers.[68,69] Most imine reductases are NADPH dependent enzymes.[65,68,70] A few imine reductases

that utilise the unusual deazaflavin cofactor, F_{420}, have been identified at the DNA level[71] and have also been observed in the sibiromycin biosynthetic pathway, a potent antitumor antibiotic produced by *Streptosporangium sibiricum*.[72]

The general mechanism of imine reduction involves hydride transfer from the C-4 atom of nicotinamide cofactor to the imine carbon atom followed by proton transfer to the nitrogen atom of the imine moiety (Scheme 1. 3).[66,73] As mentioned earlier, poorly stable imine substrates are a major limitation for the application of imine reductases, and this greatly narrows the substrate scope of imine reductases limiting them to only water-stable cyclic imines. However, over time, IREDs were also reported to reduce imines formed from ketones and amines, basically performing reductive aminations, although with diminished activity.[74] Imine reductases have also been combined with other enzymes and used in cascade reactions to produce valuable chiral amines.[75,76] Protein engineering could be a valuable tool to address key challenges pertaining to C=N reduction by imine reductases, boosting their value in biotechnology.[74,77]

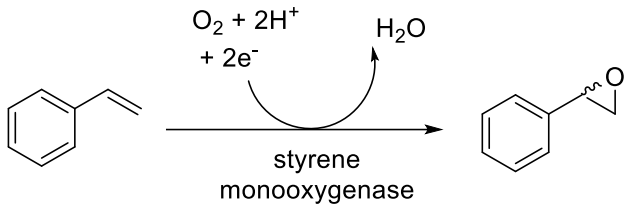


Scheme 1. 3. Mechanism for reaction catalyzed by imine reductase

1.3.4. Oxidation

Oxidising enzymes catalyse the oxidation of a substrate through electron transfer or hydrogen transfer. Enzymatic oxidation reactions offer high selectivity and control when compared to conventional chemical catalysis routes that depend on expensive and strong oxidising agents. Important oxidative enzymes include oxygenases, oxidases and dehydrogenases.

Monooxygenases catalyse the insertion of a single oxygen atom into an organic substrate molecule by activating molecular oxygen.[78]



Scheme 1. 4. Styrene monooxygenase catalysed oxygenation of styrene to styrene oxide.

The activation of molecular oxygen occurs through the formation of a reactive peroxy-intermediate that performs monooxygenation. This type of intermediate formed depends on the cofactor present within the monooxygenase. In some cases no cofactor is present and these enzymes are called internal monooxygenases where they obtain electrons from the substrate themselves. External monooxygenases utilise electrons from external sources like nicotinamide and flavin cofactors. Depending on the type of cofactor present, monooxygenases are classified into various families. Among them, the widely known haem-dependent and flavin-dependent monooxygenases will be discussed briefly here.

Haem-dependent monooxygenases, also called cytochrome P450 monooxygenases (CYP) are well-known in biotechnology, and their chemistry and mechanism of action have been extensively studied. These enzymes take electrons mostly from NAD(P)H cofactors for activating molecular oxygen.

Flavin-dependent monooxygenases catalyse various reactions like epoxidations, Baeyer-Villiger oxidations and halogenations. Most oxygenases of this category are FAD-dependent and rely on NAD(P)H cofactors as their electron source. Their catalytic mechanism involves the formation a flavin-oxygen reactive intermediate, the C4a-hydro(peroxy) flavin which then reacts with the substrate to form the product molecule. Flavin-dependent monooxygenases are attractive candidates for

biocatalytic applications not only because of their high chemo-, region- and enantioselectivity but also because they can be easily expressed in recombinant hosts as many of them are of bacterial origin.[79] Poor enzyme stability[80,81] and lack of efficient cofactor recycling methods[82] have been the limiting factors for the application of these enzymes. Copper-/ non-haem-iron/ pterin-dependent monooxygenases are other different types that are yet to be explored for biocataytic industrial applications.[79]

Oxidases use molecular oxygen as the oxidant for catalysis and produce hydrogen peroxide or water as a by-product during this process.[83] Flavin-dependent and copper-dependent oxidases are the two main oxidase families. Compared to dehydrogenases, which depend on (generally expensive) coenzymes, oxidases have the advantage of using just molecular oxygen. However, oxidases are quite rare in nature which makes it difficult to develop suitable overexpression systems to produce them for practical applications. Despite this hindrance, oxidases are becoming popular catalysts for C-N and C-O oxidations in biocatalysis and their applications have also extended to hydroxylation, oxidative C-C and C-O bond formation and oxidative ether bond cleavage.[84]

Other interesting enzymes that promise valuable biocatalytic applications, but are not yet commercially exploited include the halogenases and nitroreductases. These enzymes have gained increasing interest in recent times and are being keenly investigated by researchers.

1.3.5. Halogenases

Halogenated compounds are used in a range of pharmaceutical and agrochemical products, because of the improved bioactivity, achieved through the introduction of one or more halogen atoms. The presence of halogen substituents is also important for performing cross-coupling reactions. While conventional halogenation chemistry often involves hazardous, toxic reagents and solvents, enzymatic halogenation offers a mild, environmentally-friendly route with high regio- and

stereoselectivity. As a result, there is a growing interest in research related to the characterization and application of halogenases for synthetic utility. As a consequence, many reviews have been published on the classification and application of halogenases, also revealing the occurrence of a plethora of halogenated natural products in microorganisms.[82,85–88] Halogenases are divided into 4 major classes: 1) haloperoxidases (haem-dependent and vanadium-dependent), 2) flavin-dependent 3) non-haem-iron α-ketoglutarate-dependent and 4) S-adenosyl-L-methionine (SAM) dependent halogenases.

Halogenation activity was first reported in the enzyme chloroperoxidase from *Calariomyces fumago* that belongs to the haloperoxidase family. Depending on the type of cofactor they use, haloperoxidases are further classified as haem iron haloperoxidases and vanadium-dependent haloperoxidases that follow an electrophilic halogenation mechanism.

The next class are the flavin-dependent halogenases that come under the super-family of flavin monooxygenases. These enzymes are highly regioselective and have a very narrow substrate scope. The majority of these enzymes utilize free reduced flavin ($FADH_2$) that is made available by a second enzyme component, a flavin reductase. During biocatalysis *in vivo*, flavin reductases are supported with nicotinamide cofactors as hydride donors. The catalytic mechanism involves reaction between molecular oxygen and reduced flavin leading to the formation of a hydroperoxy flavin (FAD-OOH), which after nucleophilic attack by a halide ion forms hypohalous acid. The hypohalous moiety reaches the substrate binding site, where interaction with a lysine residue of the halogenase forms an enzyme-chloride adduct, whose exact structure is still under debate. Regioselectivity of the halogenated product is mainly governed by the orientation of this adduct moiety.

Non-haem-iron α-ketoglutarate (KG)-dependent enzymes are the only class of halogenases that undergo a radical mechanism and belong to the superfamily of α-ketoglutarate-dependent

oxygenases. The radical mechanism involves the formation of a high-valent Fe^{IV}-oxido species that is capable of selectively halogenating inactivated aliphatic carbon centres.

SAM-dependent halogenases undergo a nucleophilic mechanism for halogenation and are so far the only discovered enzymes that perform fluorination in microorganisms. This is attributed to the very low distribution of fluorinated compounds in nature as compared to organochlorine and organobromine compounds. Fluorine has been portrayed as a paradoxical element due to several of its physical and chemical properties.[89] For instance, fluorine is the most reactive halogen, but also forms the strongest bonds, especially C-F bonds, that are so strong that they remain unreacted for a long time. Fluorine is the 13th most abundant element on earth (present in minerals), however, much of it is present in an insoluble form which is biologically unavailable.[90,91] As a consequence, very few organofluorine compounds have been found in nature. Sea water contains only about 1.3 mg mL^{-1} of fluorine compared to 3000 mg mL^{-1} of aqueous chlorine.[92] This low availability of fluorine is perhaps due to the high heat of hydration of the fluoride that makes it a poor nucleophile, thus preventing it to participate efficiently in nucleophilic reactions.[90] This leads to the answer for why fluorine would not have been predominantly incorporated for biological mechanisms. The first fluorinase enzyme was reported by David *et al* that catalysed the formation of 5'-fluoro-5'-deoxyfluoroadenosine from fluoride ion and S-adenosylmethionine.[93] Since then, the search for new fluorinases have gained attention. Current interest in the application of fluorinases is focused on the synthesis of [^{18}F] labelled compounds that are used in biological imaging technologies.[91,92,94]

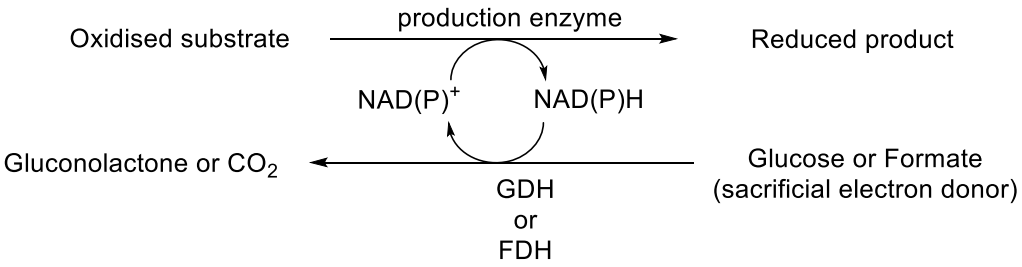
Among all the halogenase classes mentioned above, flavin-dependent and α-ketoglutarate halogenases afford a high regio- and steroselective halogenation and are hence the most promising classes for biocatalysis. Additionally, fluorinases, the only enzymes involved in enzymatic fluorination are most likely to be explored for application in biocatalysis.[82,85] The lack of viable regeneration

system for reduced flavin hinders the application of the flavin-dependent enzymes, and could be a future target for the system developed in this thesis.

1.4. Emerging H_2-driven approaches for cofactor recycling

1.4.1. H_2 - a valuable and clean reductant

Among various methods available for cofactor recycling, the use of H_2 for cofactor reduction provides the cleanest reaction with a high atom efficiency. As a cheap yet strong reducing agent, H_2 is a sustainable energy carrier too.[95,96] In industry, the reduction of NADH and NADPH are almost exclusively performed using a second regenerating enzyme (usually a dehydrogenase) that selectively consumes a sacrificial electron donor. It is essential to make sure that the donor does not inhibit or act as an alternative substrate for the production enzyme.



Scheme 1. 5. A general scheme showing an enzymatic reaction supported by an enzymatic regeneration system.

There are several dehydrogenases that are employed for NADH regeneration and their choice depends on the conditions and the nature of the reaction.[14,97,98] Some well-known dehydrogenases, their substrates and products are shown in Table 1. 1.

Table 1. 1. Different enzymes used for NAD(P)H regeneration along with their sacrificial reductants and final by-products.

Enzyme	Sacrificial substrate	Product
Glucose dehydrogenase (GDH)	D-glucose	D-gluconolactone
Formate dehydrogenase (FDH)	formate	$CO_{2\,(g)}$
Phosphite dehydrogenase (PtxD)	phosphite	phosphate
Alcohol dehydrogenase (ADH)	isopropanol	acetone

Sacrificial carbon based compounds that get oxidised during an enzymatic reaction remain as a waste by-product that needs to be removed during product purification. The environmental benefits of using an enzymatic transformation are therefore compromised due to the accumulation of unwanted waste. Some reactions may require pH monitoring as the pH of the reaction mixture may get altered over time due to by-product accumulation. Reaction conditions require proper optimisation to facilitate proper functioning of both the enzymes, and as a result, activities of both the enzymes might be compromised. Overall, such problems necessitate better cofactor regeneration methods and in this respect, the use of H_2 as an electron source provides an atom efficient method, as its consumption leaves no by-products. Glucose dehydrogenase has been developed sufficiently to allow widespread application of biocatalysis in pharma, but there is still room for improvement, especially for the manufacture of low value chemicals where the cost of glucose becomes much more significant.

1.4.2. Biocatalytic approaches for H_2-driven NAD(P)H regeneration

Hydrogenation reactions have been traditionally performed using H_2 and precious metal catalysts like Pt and Pd. In nature, on the other hand, organisms produce specific enzymes (broadly classified as hydrogenases), which facilitate the interconversion of H_2 into protons and electrons, which are then

used for substrate reduction during metabolic activities. Hydrogenases possess metal active sites made of non-precious metals like Ni and Fe, which make them attractive, in terms of harnessing the reducing power of H_2 as well as in the fabrication of bio-inspired catalysts like artificial metalloenzymes.

1.4.3. Soluble hydrogenase from *Ralstonia eutropha*

Lenz *et al*. reported a soluble hydrogenase (SH) from *Ralstonia eutropha* H16 (previously called *Alcaligenes eutrophus*) which exhibited an impressive tolerance to O_2 compared with many other hydrogenases.[99] In a study, two reactions, one containing SH and the other containing FDH as the NADH regeneration catalyst, together with a carbonyl reductase, were performed to reduce acetophenone to (*S*)-1-phenyl-ethanol. The SH showed a remarkably high total turnover number (*c.a.* up to 50,000) when compared to that observed for FDH (*c.a.* up to 490), and the specific activity of SH was estimated to be 60-fold greater than that determined for FDH.[100] Many examples of SH coupled for carbonyl reductions by ADHs, horse-liver alcohol dehydrogenase, lactate dehydrogenase etc. have been reported. For example, Nakada *et al*. coupled partly purified SH from *R. eutropha* for NADH regeneration with lactate dehydrogenase (LDH) for the conversion of pyruvate to lactate with 99% conversion.[96,101]

1.4.4. Flavin reduction activity

In addition to reducing NAD^+, purified SH from *R. eutropha* has also been known for a long time to reduce a range of other substrates including flavin cofactors, FAD and FMN.[102] Recently, Lauterbach and co-workers reported a H_2-driven, SH catalysed flavin recycling system for applications in biotechnology. Figure 1. 10. shows the different reactions that were performed using this system.[103]

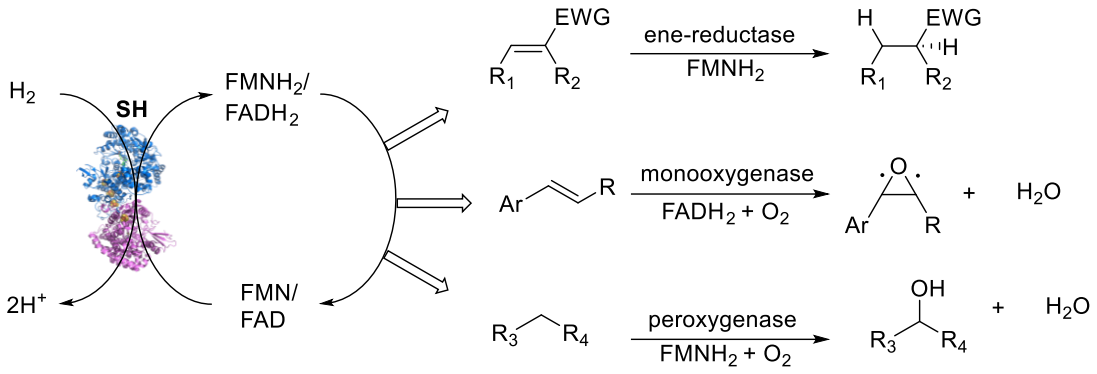


Figure 1. 10. H_2-driven flavin regeneration catalysed by soluble hydrogenase (SH) coupled to three biocatalysts – ene-reductase for C=C double bond reduction, monooxygenase for epoxidation and peroxygenase for selective hydroxylation.

1.4.5. Limitations of SH

The applications of SH for biotechnology is impeded by its limited stability under operational conditions like stirring or elevated temperature, poor tolerance to organic solvents and loss of activity upon storage for long durations.[100,104] Purified SH natively shows the highest activity at pH 8 and 30 °C. [96] Under technologically relevant conditions, this temperature has been shown to increase to 35 °C, with a half–life of just 5.3 h.[100,104] Greater stability is a desired trait while developing methods for biotechnological applications. This has led to investigations ranging from adaption of immobilisation strategies to studying the effect of different solvents on SH stability. An extensive study on immobilising SH on Amberlite™ FPA54 was conducted by Lauterbach and coworkers. With high immobilisation yields, both through adsorption and covalent binding, an SH catalytic activity of 48.9% and 39.3%, respectively were observed. Modification of the covalently bound SH using methoxy-poly(ethylene) glycol (mPEG) showed enhanced stability at elevated temperatures and during agitation. These modifications significantly contributed to the stability of SH showing improved half-lives of up to 161 h at 25 °C and 32 h at 35 °C.[104]

1.4.6. Reduction of $NADP^+$

The biocatalytic reduction of $NADP^+$ using H_2 as a reductant is rather more niche as there are not many hydrogenases that are specific to $NADP^+$. One interesting case was the discovery and over expression of SH1, an $NADP^+$ reducing hydrogenase from *Pyrococcus furiosus* by Adams and coworkers.[105] SH1 was identified to be an anaerobic, hyperthermophilic enzyme (100 °C). Although, it was found to be slightly oxygen sensitive, it functioned even at lower temperatures of 40 °C. Following this, SH1 from *Pyrococcus furiosus* also found application as the first H_2-driven NADPH regeneration catalyst demonstrated for reduction reactions catalysed by an alcohol dehydrogenase.[105] Later studies by Jones and coworkers, who probed the oxygen tolerance of SH1 showed that the H_2 oxidising activity is temperature dependent, with activity dropping to zero at just 1% O_2 and at 25 °C, however, up to 32% of the oxidation activity seem to be retained at 80 °C, even after 900 seconds of O_2 exposure.[106] Nevertheless, this enzyme is likely too O_2 sensitive for industrial biocatalytic applications.

More recently, Preissler *et al*. reported that site-directed amino acid exchanges in the O_2-tolerant NAD^+ reducing soluble hydrogenase from *R. eutropha* can allow for a switch in cofactor specificity, allowing this enzyme to accommodate $NADP^+$ and perform $NADP^+$ reduction even in the presence of O_2.[107] A rational designing of the binding pocket was performed using the crystal structure of Complex I from *Thermus thermophilus* as the basis, as this enzyme showed the closest homology to the *R. eutropha* SH. Among many variants tested by spectrophotometric analysis, $NADP^+$ reduction activity was the highest in the mutant, $SH^{E431/S342R}$ which corresponded to the replacement of glutamine (Glu314) and serine (Ser342) residues with alanine and arginine respectively. An $NADP^+$ reduction activity of

1 U mg^{-1} and a K_M of *c.a*. 0.6 mM was observed for $SH^{E431/S342R}$ which was selected to be the best variant for further applications. The NADPH recycling system was demonstrated for reduction

reaction with an imine reductase and alkane oxidation by an NADPH dependent P450 monooxygenase, $P450_{BM3}$ under aerobic conditions.[107]

1.4.7. The structural design of soluble hydrogenase (SH) from *R. eutropha*

R. eutropha is a knallgas bacterium that harbours three hydrogenases: a membrane bound, cytoplasmic and soluble hydrogenase (SH). 'Knallgas' is a German word that translates to 'boom-gas' or 'bang-gas' in English. It is used to denote the explosive oxygen-hydrogen gas mixture and hence the term knallgas bacteria, because the hydrogenases are expressed when the organism is grown under explosive mixtures of oxygen and hydrogen gas. The soluble hydrogenase is a bidirectional [NiFe] hydrogenase, biased towards hydrogen oxidation due to its physiological function.[108] Figure 1. 11. Shows the model crystal structure of the soluble hydrogenase from *R. eutropha*. This heterohexameric protein complex is about 207 kDa and is composed of 6 subunits, $HoxHYFUI_2$.[109] It is primarily categorised into two catalytic components, the HoxHY and HoxFU moieties, each functioning independent of each other.

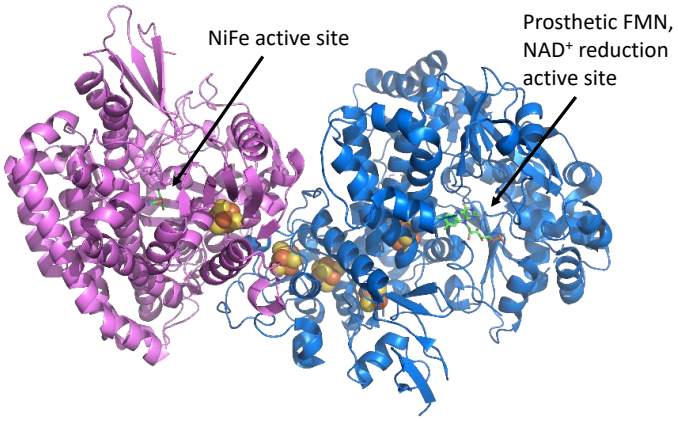


Figure 1. 11. Homology model of the crystal structure of NAD^+ reducing soluble hydrogenase from *R. eutropha* (PDB: 5FX9) based on the crystal structure of the NAD^+ reducing soluble hydrogenase from *Hydrogenophilus thermoluteolus* TH-1.[110]

The heterotetrameric structure of SH, HoxHYFU is relatively stable while the $HoxI_2$ is readily released under conditions used for purification and isolation. While H_2 oxidation takes place in the HoxHY

subunits, the HoxFU contains an NAD^+ reducing dehydrogenase component, also called the diaphorase subunit. HoxY accommodates one proximal 4Fe-4S and an FMN molecule.[100,109] The NiFe active centre is located in the HoxH subunit. The HoxFU diaphorase unit consists of a [2Fe2S] cluster, an FMN molecule and a series of [4Fe4S] clusters.[111] Both HoxHY and HoxFU have been separately isolated and characterised in the past.[111,112] Two copies of the non-essential HoxI subunit are primarily associated to HoxF with close proximity to HoxY. Purification protocols followed since 1983, have only focussed on the isolation of the tetrameric enzyme that was sufficient to accomplish H_2 oxidation and NAD^+ reduction. Isolation and purification of the hexameric protein (that contains the HoxI subunit) has aided understanding of the role of the HoxI subunit. While a rapid activation of the tetrameric form (that does not contain the HoxI unit) was achieved in the presence of NADH (but not NADPH), the hexameric form was found to be activated even with small amounts of NADPH as well as NADH, suggesting that the HoxI may provide a specific binding domain for NADPH.[109,113] Electron transfer between the hydrogenase active site and the NAD^+ binding site is facilitated by four [4Fe4S], one [2Fe2S] clusters and two FMN molecules. The FMN molecule present in HoxFU is designated as FMN-b while the other FMN, FMN-a is bound to the hydrogenase small subunit, HoxY. All NAD(H)-linked bidirectional hydrogenases have been found to contain at least one FMN molecule, typically in the HoxF subunit. The other FMN, FMN-a is often lost during SH purification and can be reconstituted by adding free FMN to the purified enzyme.[103] The ability of flavins to transfer electrons between one-electron FeS centres and the two electron cofactor, NADH validates this observation.

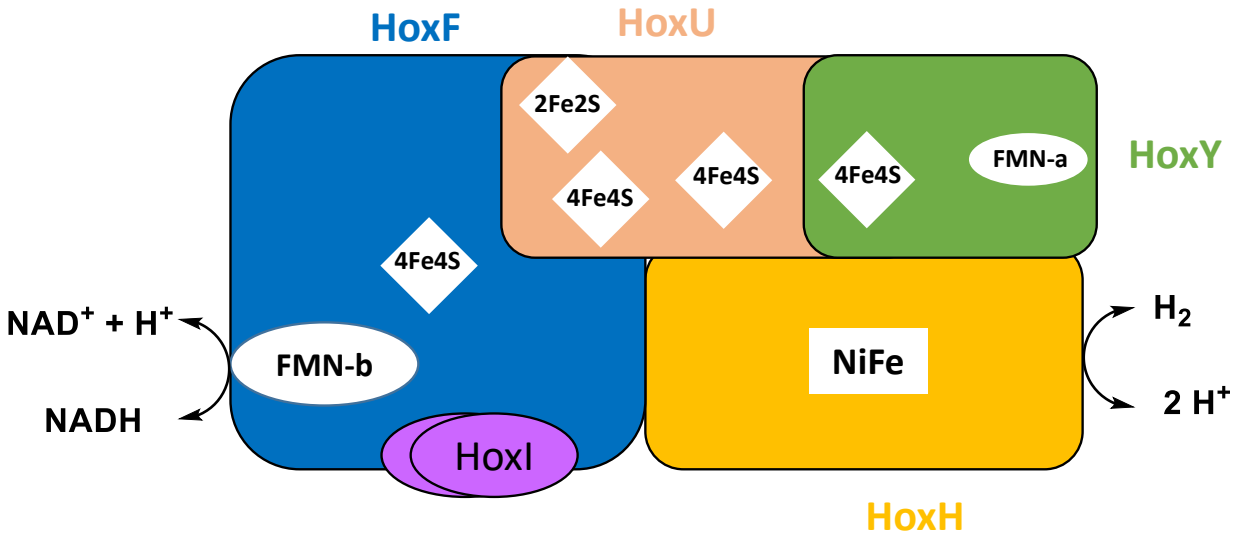


Figure 1. 12. Proposed arrangement of the different subunits of the soluble hydrogenase from *R. eutropha*. This figure is adapted from reference 111.[111]

A crystal structure of the SH from *R. eutropha* is not available yet, however, the diaphorase moiety closely resembles the peripheral arm of respiratory Complex I from *T. thermophilus*, which has been crystallised, and this is used as a model for conducting mechanistic studies of the SH.[114–116]

1.4.8. The HydRegen system[117,118]

The HydRegen system is based on the concept of uncoupling the hydrogenase and diaphorase components of SH, followed by recoupling the NAD^+ reducing, HoxFU moiety with a more robust hydrogenase like Hyd2 on an electronically conducting material, resulting in a more modular and heterogeneous catalyst.[117] This provides an opportunity to combine new and more robust hydrogenases with HoxFU, as it is known that the hydrogenase moiety from SH becomes quite unstable after losing its FMN molecule.[117] Lauterbach *et al*. showed that the HoxFU subunit of SH can be successfully isolated and characterised.[111] The diaphorase component also functioned as an efficient electrocatalyst upon adsorption on a pyrolytic graphite electrode.[117] Building on this model, Vincent and coworkers developed a heterogeneous NADH cofactor regeneration catalyst by

immobilising the diaphorase subunit along with an *E. coli* hydrogenase, Hyd2, and used it to supply NADH for an NADH-dependent lactate dehydrogenase, catalysing the conversion of pyruvate to lactate.[117] All results were analysed spectroscopically using UV-visible and IR spectroscopy. This was the first proof-of-concept of this technique, already showing NADH reducing activity that was comparable to that of the traditional FDH system.[117] Overall, this strategy of immobilising different enzyme moieties on electronically conducting particles offers the advantage of coupling relevant enzymes to suit reactions over a varied range of reaction conditions, without compromising catalyst activity. Moreover, the heterogeneous nature of the catalyst enables easy product separation and catalyst reusability.

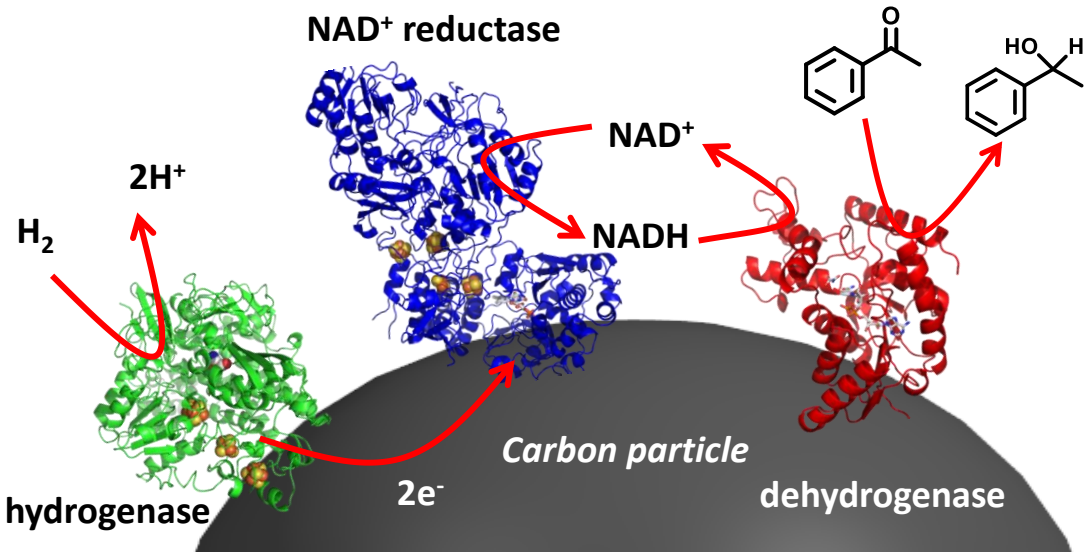


Figure 1. 13. Schematic representation of the HydRegen system showing NADH-regeneration used for dehydrogenase catalysed reduction of acetophenone to phenylethanol. Figure adapted from reference 118.[118]

This system was further expanded for operation with an alcohol dehydrogenases (ADH-105) from Johnson Matthey (JM), for the reduction of acetophenone to phenylethanol. A detailed study of various reaction parameters like enzyme and cofactor loading, and the effect of immobilised ADH vs ADH in solution, on initial enzyme activity, turnover frequency and total turnover numbers were determined. An impressive turnover number of 655 moles of product per mole of NAD^+ was recorded

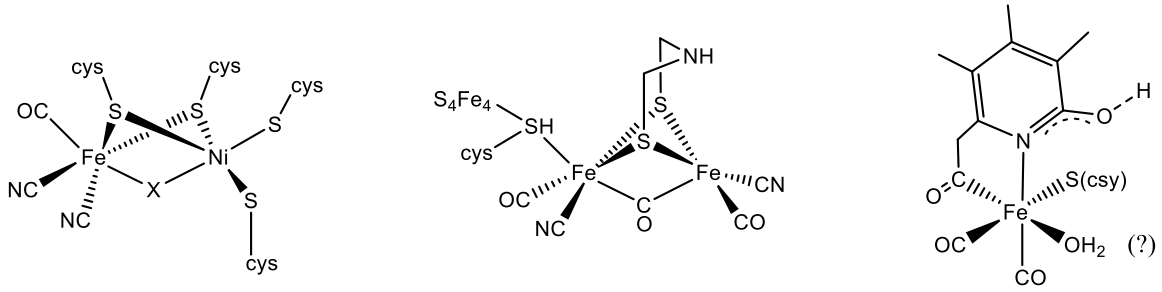
by using as little as 0.01 mM NAD^+. Nicotinamide cofactors, particularly the reduced forms tend to become unstable under certain reaction conditions like high pH.[119] As a result, a sufficient quantity of the cofactor is required to run a biocatalytic reaction. In this respect, the ability to use as low as 0.01 mM NAD^+ highlights the enhanced stability this system confers on the cofactor. The cofactor concentration will also depend on the K_M of the recycling enzyme for the cofactor. For instance, a lower k_M value indicates that the enzyme has a higher affinity for the cofactor, and so, a high enzyme activity can be achieved with lower concentrations of the cofactor. The highest TTN was recorded to be in the order of 130,000 when 1 mM of NAD^+ was used. Interestingly, reactions performed using particles with all three enzymes immobilised showed a two fold increase in reaction rate (0.74 vs 1.41 s^{-1}) when compared to the reaction in which only the hydrogenase and diaphorase moieties were immobilised. This was hypothesised to be the result of a high concentration of NADH in close proximity to the production enzyme, ADH. The reusability of the catalyst was also tested, showing *c.a.* 90% conversion to the product during the second cycle.

This brings us to the discussion on different hydrogenases

1.5. Hydrogenases and their classification

Hydrogenases are metalloenzymes that catalyse the reversible oxidation of molecular hydrogen to protons and electrons and vice versa. They are considered to be among the oldest enzymes thriving on earth which enabled microorganisms to exploit H_2 as their energy source from the H_2 rich atmosphere of the early Earth. Although most isolated hydrogenases have been able to function in both directions, their activity is usually biased to a certain extent depending on their physiological functions. There are three phylogenetically distinct classes of hydrogenases – [NiFe], [FeFe] and [Fe] hydrogenases, that are classified based on the composition of their catalytic metal centres. Among them, [NiFe] hydrogenases are the most widespread and the best investigated class of hydrogenases

so far.[120,121] [FeFe] hydrogenases are a slightly smaller class with only three well-defined groups. Both NiFe and FeFe hydrogenases share some common features despite their convergent evolution and different amino acid sequences. Both enzyme classes possess a unique bimetallic centre, either NiFe or FeFe, respectively, with non-protein ligands, CO and CN^- bound to the iron atom. This type of coordination results in a large crystal field splitting, generating the low spin Fe(II).[122] There are two bridging sulfur atoms, and a free coordination site on one of the metal atoms. Figure 1. 14. shows the active sites of the three classes of hydrogenases. These active sites remain buried within the enzyme and are connected to the protein surface through iron-sulphur (FeS) clusters that act as channels for transporting substrates and products. NiFe hydrogenases show better H_2 oxidation characteristics whereas FeFe hydrogenases are efficient at H_2 evolution.[123] [Fe] hydrogenases are the most recently discovered, and perhaps the most enigmatic among the three classes of hydrogenases. They are restricted only to methanogenic archaea and vary in structure and mechanism from that of the [NiFe] and [FeFe] hydrogenases. The catalytic cycle of [Fe] hydrogenases involves heterolytic cleavage of H_2, followed by direct hydride transfer to methenyl-H4MPT$^+$ to yield methylene-H4MPT, facilitating CO_2 reduction to methane. The reaction mechanism proceeds without any electron transfers, which justifies the lack of FeS clusters in these enzymes.[124–127]



[NiFe] hydrogenase [FeFe] hydrogenase [Fe] hydrogenase

Figure 1. 14. Chemical structure of the active sites of the three classes of hydrogenases.

1.5.1. NiFe hydrogenases

[NiFe] hydrogenases are broadly divided into four groups that are subdivided into a further 22 different subgroups. Group 1 includes membrane-bound H_2-uptake [NiFe] hydrogenases, while group 2 consists of cytosolic H_2-uptake [NiFe] hydrogenases. Group 3 covers cytosolic bidirectional hydrogenases, and all membrane-bound H_2-evolving hydrogenases belong to group 4.[120,121,128] [NiFe] hydrogenases from group 1d are particularly attractive due to their O_2-tolerance trait compared to the standard, O_2-sensitive [NiFe] hydrogenases.[129] For this reason, extensive efforts have been invested in understanding the specific differences in their structures that set them apart from standard O_2-sensitive [NiFe] hydrogenases.[130] Some well-known examples of O_2-tolerant hydrogenases include, the soluble hydrogenase (SH) from *Rasltonia eutropha* H16 and the membrane bound hydrogenase, Hyd1 from *E. coli*. Such O_2-tolerant enzymes hold remarkable advantages for biotechnological applications when it comes to reaction conditions as well as reactor design making enzymatic reactions more industrially viable. This DPhil project predominantly involved the exploitation of Hyd1 to uncover new reactivities that eventually led to the development of a new flavin-regeneration system. Alongside this, other robust hydrogenases were also tested for flavin-reduction activity. A brief description of the structure and function of these hydrogenases will be discussed in this chapter.

1.5.2. General features of NiFe hydrogenases

The NiFe hydrogenase typically contain two subunits – a large subunit (α-subunit) that incorporates the NiFe active centre where hydrogen cycling takes place. The small subunit harbours at least three FeS clusters that engage in electron transport. On the whole, this assembly remains identical for both O_2-tolerant and O_2-sensitive hydrogenases, with slight differences that confer them with strikingly distinct properties. Substrate/ inhibitor access to the deeply buried active sites is facilitated by

hydrophobic gas channels while electron transfer happens through a series of FeS clusters located in the small subunit.

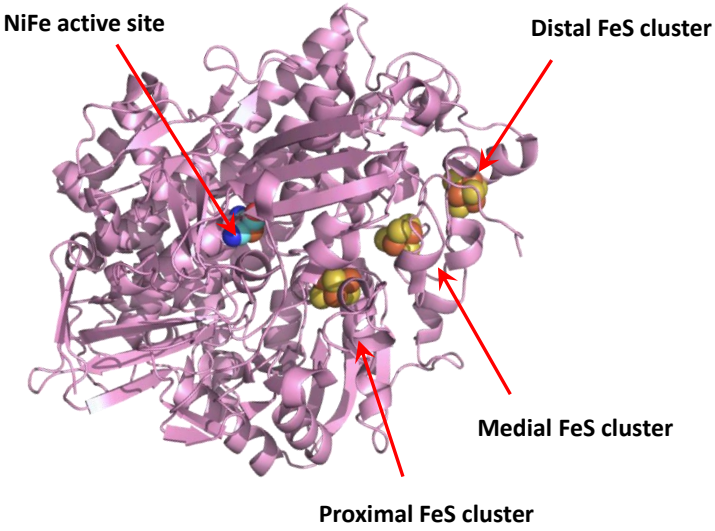


Figure 1. 15. Crystal structure of the NiFe hydrogenase, Hydrogenase 1 (monomer) from *E. coli* (PDB: 3USE).

1.5.3. Metal Active centre

The metal active centre located in the large subunit is bimetallic, comprising of a Ni and Fe atom. The active site is anchored to the main protein structure through 4 thiolate linkages provided by four cysteine residues. Two of the four cysteines appear as bridging ligands between Ni and Fe while the remaining two cysteines are coordinated to Nickel alone in a terminal fashion. In [NiFeSe] hydrogenase, one of these terminal cysteine thiolates is replaced by a selenocysteine.[131] The Fe is coordinated to one CO and two CN^- ligands whose IR bands act as a sensitive probe to observe changes relating to the different redox states of active site. The Ni atom changes its oxidation state to I, II or III during different stages of catalysis, while Fe remains in a constant low spin (II) state, and is likely to be stabilised by CO and CN^- ligands which exhibit π accepting and σ bonding characteristics.[132] There may be a fifth ligand bridging Ni and Fe, whose identity changes during the

different stages of the catalytic cycle.[133] Figure 1. 15. shows the structure of the active site of a NiFe hydrogenase.

1.5.4. FeS clusters

There are three FeS clusters in a NiFe type hydrogenase, that are named as proximal, medial and distal based on their distance from the active site (Figure 1. 16). They act as electron relay channels shuttling electrons from the buried active site to the outer protein surface. The proximal cluster can be a standard [4Fe-4S] cluster or an unusual [4Fe-3S] cluster which influences the enzyme's behaviour towards O_2.[134] The medial [3Fe-4S] cluster and the distal [4Fe-4S] clusters are generally preserved across all types of [NiFe] hydrogenases.[135]

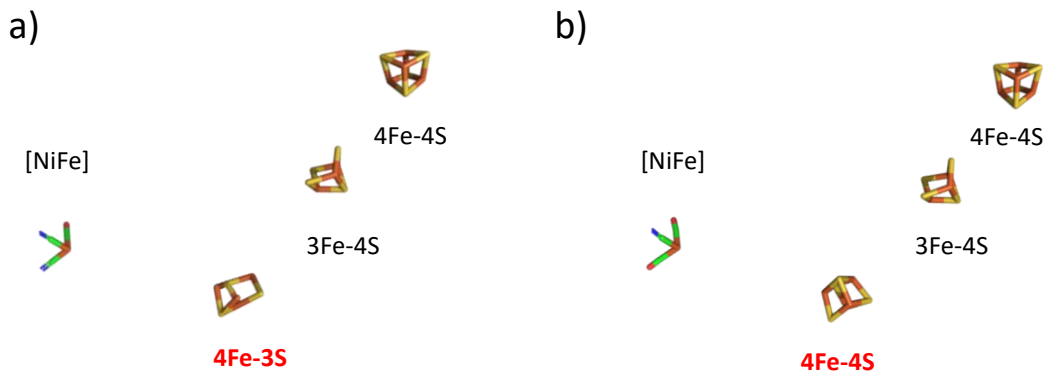


Figure 1. 16. A comparison of the proximal FeS cluster present in the crystal structure of the a) O_2 tolerant Hyd1 [NiFe] hydrogenase from *E. coli* and b) the standard O_2 sensitive [NiFe] hydrogenase from DvMF.

1.5.5. Hydrogenases from *E. coli*

E. coli produces a total of four [NiFe] hydrogenases, Hyd1-4. Both Hyd1 and Hyd2 are membrane associated hydrogenases that are located in the periplasm and function as H_2-uptake hydrogenases coupling H_2-oxidation to quinone reduction through different electron acceptor moieties. They take part in the bacterial respiratory chain engaging in energy conversion. Hyd3 and Hyd4 are non-energy

converting enzymes and are part of a formate hydrogenlyase complex, which couples formate oxidation by formate dehydrogenase to the reduction of protons by Hyd3 or Hyd4.[128,136,137]

1.6. Hydrogenase 1 from *E. coli* (Hyd1)

Hyd1 is a membrane bound O_2-tolerant NiFe hydrogenase from *E. coli* that preferably catalyses H_2-oxidation under neutral pH. It is an increasingly investigated enzyme type due its high levels of tolerance to O_2. Like a typical NiFe hydrogenase, Hyd1 contains a large and a small subunit, containing the NiFe active site and three FeS clusters. It is generally isolated as a dimer, i.e. it contains two identical large and small subunits. Crystal structures of Hyd1 in its oxidised, reduced and inhibited state are also available in the literature.[138]

1.6.1. The crystal structure of Hyd1

Hyd1 is encoded by the first three genes HyaABC within a six gene operon HyaABCDEF. HyaA and HyaB encode the small and the large subunits, respectively and HyaC, an integral membrane b-type cytochrome.[122] Hyd1 was first crystallised by Volbeda *et al*. in 2012, as a dimeric complex containing two small subunits and two large subunits.[138] Interestingly this crystal structure did not possess the transmembrane α helix nor the cytochrome b subunit. However, in 2013, a Hyd1 variant containing a 4Fe4S medial cluster was purified and crystallised with the transmembrane domains and a single cytochrome subunit (Figure 1. 17.).[139] An insight into the crystal structure was key for a greater understanding of the catalytic mechanism of the enzyme. The proximal clusters in the as isolated crystal reveals a mixture of two conformations for the proximal 4Fe-3S cluster.[138] One that is similar to that which appears in all standard hydrogenases, and a second conformation in which the iron is pentacoordinated forming additional bonds to a nearby amide N of the Cys 20 and the oxygen atom of a nearby glutamic acid residue, besides three sulphur linkages. This forms a distorted trigonal bypyramidal shape, generating a highly oxidised iron.[138] The distal clusters on the two monomers

were only 10 Å apart, which was postulated to permit electron tunnelling from one active site to the other being able to protect it from O_2 attack.[140] That is, under O_2 attack, if the active site in one of the monomers has used up all its electrons to reduce O_2 to water, it can be reductively reactivated using electrons from H_2 oxidation at the active site of the other monomer.[139] A membrane anchoring α helix is present in the small subunit in both Hyd1 and Hyd2.[141]

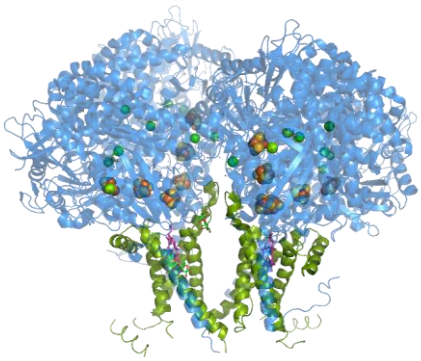


Figure 1. 17. Heterodimeric crystal structure of Hyd1 from *E. coli* in complex with cytochrome *b* (4GD3) obtained from a sample with mutationally generated medial cluster 4Fe4S.[139] The helical cytochrome *b* is shown in green.

1.6.2. Oxygen tolerance

O_2-tolerant hydrogenases prominently display an unusual [4Fe-3S] proximal cluster that is thought to play a major role in conferring O_2-tolerance to these enzymes.[134] Standard NiFe hydrogenases possess the typical 4Fe-4S cubane centre that is coordinated by four cysteine ligands. In addition to these four cysteine ligands that are conserved in all NiFe hydrogenases, O_2-tolerant hydrogenases display two additional cysteine ligands. One bridging sulphide is replaced by the sulphur atom of one of the two additional cysteines, and the second cysteine is found coordinated to the 4Fe-3S cluster as a terminal ligand. This coordination of additional cysteines results in a more open and distorted conformation rather than the typical cuboidal structure. This allows the 4Fe-3S cluster to access three redox states, as well attain a higher redox potential capable of making two redox transitions that enable an

immediate delivery of two of the four electrons and protons required to reduce O_2 to harmless water and OH^- at the active site.[134,135,142,143] The two sequential redox transitions are as follows: $[4Fe\text{-}3S]^{3+} \rightleftharpoons [4Fe\text{-}3S]^{4+} \rightleftharpoons [4Fe\text{-}3S]^{5+}$, the latter super-oxidized state has an unusual Fe−N(amide) bond that stabilizes a valence-localized Fe^{3+} subsite.[144]

The third electron is supplied by the oxidation of Ni^{II} to Ni^{III}. The final, fourth electron is supplied by the high potential medial cluster which was later confirmed to be as important as the proximal cluster for O_2-tolerance.[144] The water produced as a result of O_2 reduction is likely transported to the solvent through specialised hydrophilic channels formed by highly conserved residues not found in the O_2-sensitive counterparts.[142] Further experiments, where the two additional cysteine ligands were exchanged for glycine, resulted in the loss of O_2-tolerance traits. More specifically, Cys19 was crucial for this character and the other cysteine residue Cys120 had rather less impact.[130] Further, Armstrong and coworkers have found that quaternary structures of Hyd1 exhibited better O_2 tolerance than their monomer counterparts. It has been hypothesised that the short distance of just 12 Å between the distal clusters of two monomers can allow for fast electron tunnelling, which can permit electrons from H_2-oxidation at one active site to be transferred to the other active site during O_2 attack.[140] In some hydrogenases, specifically regulatory hydrogenases, access to the active site by O_2 is prevented by a narrow hydrophobic access that allows only H_2, and filters the bulkier O_2.[145]

1.6.3. Redox states of the NiFe active site in Hyd1

During H_2 cycling, the bimetallic NiFe centre cycles through a series of active site redox states acquired through protonation and electron-transfer processes. These redox states can be represented in a catalytic cycle as shown in Figure 1. 18. Aided by spectroscopy, particularly IR spectroscopy, three predominant redox states were first characterised – Ni-SI, Ni-R and Ni-C states. Isolated Hyd1 generally exists as a mixture of predominantly two states – Ni-B, also called the ready

state and the Ni-SI state. Oxygen sensitive hydrogenases have an additional Ni-A state, also called the unready state. The inactive/ unready Ni-A state is collectively represented by an oxygenated species, although a clear picture of this complex is still under debate.[144] The Ni-B state is predicted to carry a bridging OH^- ligand that is determined through DFT calculations.[146] The two states vary significantly in their rates of reductive reactivation (from a few minutes to hours of activation under H_2). The formation of Ni-A or Ni-B relies on the number of electrons, either two or four that are available to reduce the O_2 present in the active site.[147] While the Ni-B state is activated within a few seconds by electrons or H_2, the Ni-A state takes a longer time with the rate varying depending on the enzyme and other conditions.[122]

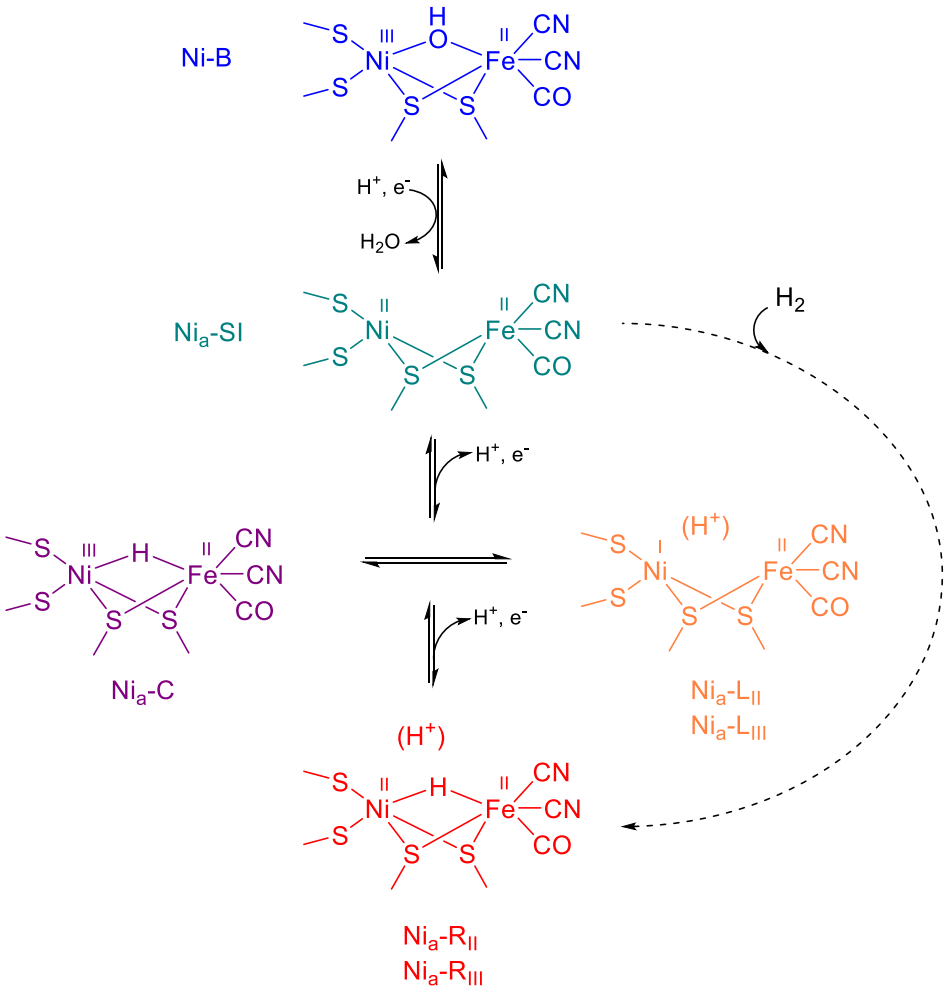


Figure 1. 18. A schematic representation of the different redox states of NiFe hydrogenases during H_2 cycling adapted from reference 148 with permission from Royal Society of chemistry publisher: *Chemical Science*, **2021**, *12*, 12959-12970.[148] License id: 1189781-1.

The first step in the H_2-cycle is the interaction of H_2 with Ni-SI (the most oxidised active state) that leads to the heterolytic cleavage of H_2, forming the Ni_a-R state, which contains a bridging hydride between Ni and Fe. The hydride bridge in this state is unsymmetrical with the H^- forming a stronger coordination with Ni rather than with Fe.[149,150] This is in contrast to the usual man-made organometallic catalysts where the H^- is displaced towards Fe.[151] The transition from Ni_a-SI to Ni_a-R is postulated to occur via an initial H_2 bonding with Ni forming a Kubas-complex like arrangement (see Figure 1. 19.) and the proton released has been proposed to be abstracted by a thiolate on the nearby terminal cysteine residue.[152] Another model was proposed by Armstrong and coworkers,

where a strictly conserved arginine residue promoted H_2-oxidation at the active site. The conserved arginine suspends a guanidine N atom just above the active site generating a frustrated Lewis-pair type arrangement (Figure 1. 19.). The guanidine group then acts as a base aiding in proton abstraction.[153] Hyd1 displays two forms of Ni_a-R states as indicated by two ν_{CO} bands.[152,154] The Ni_a-R sub-states are designated as Ni_a-R_{II} and Ni_a-R_{III} based on their relative ν(CO) wavenumber positions in comparison to that observed in other hydrogenases. *E. coli* Hyd1 does not display any Ni_a-R_I state, however, this sub-state tends to be the dominating species in many O_2-sensitive hydrogenases. These sub-states have been suggested to differ in the location of the proton near the active site. [152]

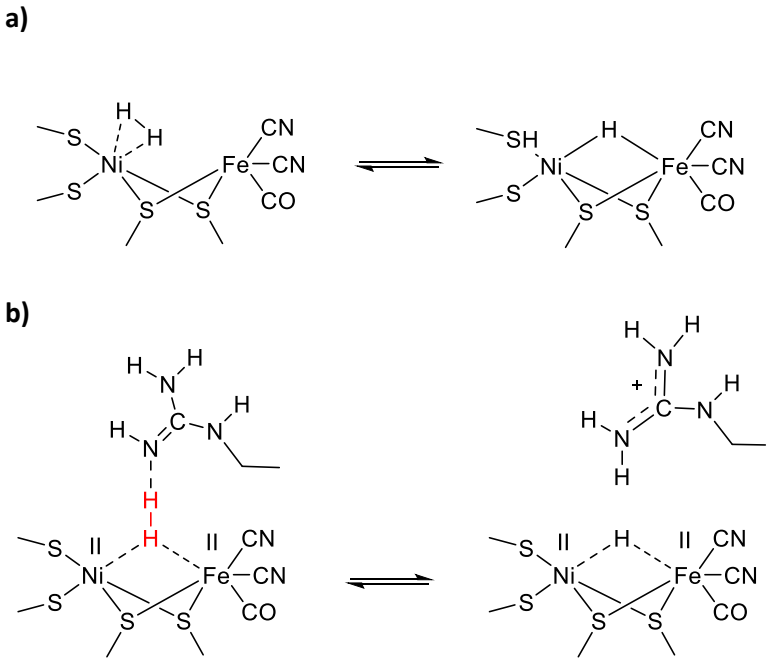


Figure 1. 19. Proposed mode of H_2 activation based on the a) Kubas-type complex and b) frustrated Lewis pair mechanism. The state on the right would be one of the Ni_a-R sub-states.

The resulting proton from heterolytic cleavage is estimated to reside on a nearby base, however, this assumption is still uncertain due to the challenges of locating a small H atom within the large protein body.

From Ni_a-R state, an electron transfer to the FeS cluster generates the Ni_a-C state, which still has a bridging hydride ion, but Ni is oxidised from Ni^{II} to Ni^{III}. The bridging hydride is then lost as a proton to a nearby base forming Ni_a-L state where Ni^{III} is reduced to Ni^{I}. The Ni_a-L state was initially observed only under cryogenic conditions in the presence of light and only involves the relocation of a proton and electron density. Hence, the two states are shown at the same redox level in the catalytic cycle.[122,132] Moreover the Ni_a-L and Ni_a-C states seemed to have been equally populated suggesting an equilibrium between the two states. [154]

A structural insight into Hyd1 using protein film infrared electrochemistry (PFIRE) devised by Vincent and co-workers resulted in a finding that the Ni_a-L state can also be accessed under dark conditions at ambient conditions in this hydrogenase. This finding suggests that the Ni_a-L state is formed as an intermediate between Ni_a-C and Ni_a-SI states, in contrast to early assumptions where Ni_a-C to Ni_a-SI transition was believed to be concerted. pH-dependent studies on the Ni_a-L states support the hypothesis that these sub-states occur either as a result of different positions of the proton released from Ni_a-C or from two different conformations arising from pH changes.[152] While *E. coli* hydrogenase displays two Ni_a-L sub-states, most O_2 sensitive hydrogenases display only one Ni_a-L state at a high wavenumber and for the O_2 sensitive enzymes, this Ni_a-L state is only stabilised at cryogenic temperatures when Ni_a-C is photolysed.

The starting Ni_a-SI state is reformed from the Ni_a-L state, after the loss of another electron to the FeS cluster and is accompanied by the oxidation of Ni^{I} to Ni^{II}. Thus a new H_2-cycle is initiated.

1.6.4. Predicted mechanism of flavin reduction by Hyd1

A confirmed mechanism for flavin reduction by Hyd1 was not explored in this thesis. Hyd1 has been well characterised in the literature and this information was helpful in predicting a plausible mechanism for flavin reduction.[138,153] Oxidation of H_2 takes place at the NiFe active site as discussed

above and the oxidation activity is often measured using the artificial electron acceptor, benzyl viologen as an external electron acceptor in the solution. Electrons resulting from H_2 oxidation are relayed through FeS clusters to the surface of the protein, where flavin reduction is expected to occur, similar to the reduction of benzyl viologen. This prediction arises from a previous observation with benzyl viologen, where studies show that the reduction of this electron acceptor takes place only in the presence of the small subunit, indicating that substrate reduction occurs at the FeS cluster rather than at the NiFe active site. Small molecules such as H_2 or O_2 access the active site via hydrophobic gas channels which are suitable in size for these small diatomic molecules, but are highly unlikely to allow flavin to access the active site cavity.[138]

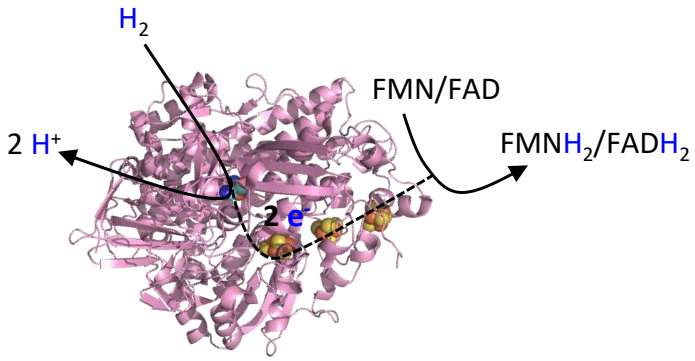


Figure 1. 20. Enzyme crystal structure and predicted reaction mechanism for H_2 oxidation and flavin reduction in Hyd1 from *E. coli* (PDB code: 3USE)

1.7. Hyd2 from *E. coli*

Hyd2 is from a group 1c NiFe hydrogenase encoded by the genes hybOABC in the hybOABCDEFG operon.[155] Like Hyd1, Hyd2 is also a membrane bound periplasmic hydrogenase, however, it is not O_2-tolerant and therefore, it is classed as a standard O_2 sensitive NiFe hydrogenase. The physiological role of Hyd2 in *E. coli* is to couple H_2-oxidation to the production of succinate by a fumarate reductase.[141] It is bidirectional in behaviour and hence efficient in both H_2 oxidation and evolution as opposed to the O_2-tolerant Hyd1 which is predominantly a H_2-oxidiser. The active centre housed in

the hybC (large) subunit is structurally identical to that of Hyd1. The HybO subunit possesses three FeS clusters, where the proximal cluster is a conventional 4Fe-4S, likely explaining the enzyme's sensitivity towards O_2.[156] The HybA subunit consists of four FeS clusters essential for mediating electron transfer between the enzyme and quinone pool.[157] The HybB is an integral membrane protein that contacts HybA to the quinone pool. Hyd2 was crystallised as a heterodimer using a new overexpression system developed by Beaton *et al*.[155] High resolution X-ray diffraction studies on the enzyme crystal revealed that the two distal clusters are separated by 12.3 Å, a distance, too large for rapid electron transfer to take place. This also explains why Hyd2 cannot tolerate molecular oxygen since it cannot accumulate sufficient electrons for O_2 reduction to water.[155] A significant difference observed for Hyd1 and Hyd2 is their over potential requirement for H_2 oxidation. While Hyd2 shows no over potential requirement for H_2 oxidation/ evolution, Hyd1 requires a slight over potential of about 50-100 mV before the onset of H_2 oxidation.[158] The other difference is the population of Ni-B and Ni-A states formed upon exposure to O_2, where the ratio of Ni-B:Ni-A states for Hyd1 is far greater than in Hyd1. This suggests that Hyd2 is more than twice as likely as Hyd1 to form the Ni-A states, and hence takes a longer time to reactivate.[159]

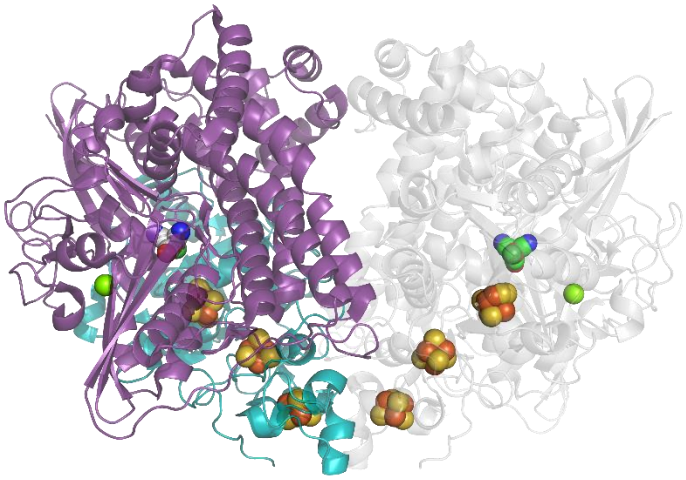


Figure 1. 21. Crystal structure of Hyd2 present (PDB: 6EHQ) as a dimer of heterodimers ([HybOC]$_2$) containing two large subunits (purple) and two small subunits (blue). The other monomer is shown in grey to highlight the FeS clusters and NiFe centre

1.8. DvMF (*Desulfovibrio vulgaris* Miyazaki F) hydrogenase

The DvMF hydrogenase is a NiFe type standard hydrogenase from *Desulfovibiro vulgaris* Miyazaki F, a sulphate reducing anaerobic bacterium. It is a periplasmic membrane bound hydrogenase, capable of H_2 oxidation as well as evolution.[160] The DvMF hydrogenase is also the first successfully crystallised hydrogenase with a structure attained by Higuchi *et al*. in 1987.[161,162] As usual, there is a large and small subunit, accommodating a NiFe active centre and three FeS clusters (one 3Fe4S cluster and two 4Fe4S) respectively. Electrons released as a result of H_2 oxidation are transferred through the FeS clusters to the cytochrome c_3, the physiological electron acceptor.[160] This hydrogenase undergoes the usual redox cycle like any other standard hydrogenase and corresponding results from crystallographic and spectroscopic studies are reviewed in detail in the literature.[160,163,164]

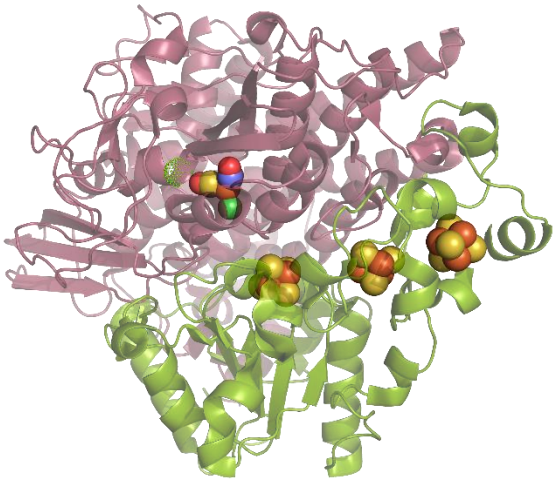


Figure 1. 22. Crystal structure of the standard DvMF hydrogenase (PDB: 1H2R) showing the NiFe active centre, [4Fe4S] proximal and distal clusters, and [3Fe4S] medial cluster.

1.9. The concept of this project

The primary aim of the project is to explore the possibility of developing a H_2-driven, Hyd1 catalysed system for the reduction of flavins, FAD and FMN. Previous reports of a H_2-driven system for flavin reduction was demonstrated by Herr *et al*., using the NAD^+ reducing soluble hydrogenase from *Ralstonia eutropha* H16. As previously described in this chapter, the application of SH for biotechnology is limited due to the poor stability of the enzyme.[104] Moreover the complex procedure to express and purify the enzyme is unattractive.[99] In contrast, Hyd1 is natively expressed in *E. coli* and is shown to exhibit extraordinary selectivity that can be relevant for applications in biocatalysis. This feature has also been showcased in a number of experiments in this project, like temperature tolerance and stability towards O_2, over extended durations.

This project then explores the opportunity to utilise the newly developed, H_2-driven flavin regeneration system to supply reduced flavins to enzymes such as ene-reductases and nitro reductases to perform valuable biotransformations. These enzymes are mostly operated with

NAD(P)H which is regenerated by a regenerating enzyme like glucose dehydrogenase and formate dehydrogenase, that rely on sacrificial, carbon-based reductants, glucose and formate, respectively. Such carbon intensive regeneration methods are not viable and suffer from poor atom economy. Certain enzymes like halogenases are operated with an NADH:flavin reductase that ensures a steady supply of reduced flavins at the expense of NAD(P)H. The oxidised $NAD(P)^+$ is reduced following the same methods as discussed above. Despite the mild reaction conditions, such multi-enzymatic systems are complex to implement. This project was conceived on the hypothesis that the hydrogenase enzyme can be used to harness the reducing power of H_2, the ultimate clean reductant for the reduction of flavins, thus achieving 100% atom efficiency.

Chapter 5 discusses the results obtained for demonstrating the Hyd1/ flavin regeneration system with FMN-dependent nitro reductases for the production of chiral amines. The production of amines is a highly desirable chemical transformation in the pharmaceutical industries, with over 90% of drugs containing at least one amine functionality. The application of enzymatic methods for their synthesis is increasingly becoming popular in industry.[165,166] For e.g. an evolved ω-transaminase obtained from several rounds of mutagenesis catalysed the synthesis of Sitagliptin (an antidiabetic drug developed by Merck & Co.)[167] Until recently, factors like low availability of active transaminases and unfavourable reaction equilibria remained problematic in this field.[168–170] Similarly, nitroreductases that reduce nitro groups to amines present another useful synthetic route. However, operating these enzymes with the typical glucose/ GDH system would lead to a highly carbon-intensive reaction. For every nitro group being converted to the amine, three equivalents of glucose molecules are consumed making the cost of glucose a significant component of the reaction economics.[36] Imine reductases are another class of enzymes that will synthesise amines, however they are strictly NADPH dependent, meaning they need the more expensive cofactor, for which cofactor regeneration is less well developed.[76,171]

The last chapter discusses the early attempts for reducing the less commonly researched cofactor – deazaflavin, F_{420}, using a range of hydrogenase enzymes. The interesting structural and electrochemical properties of this cofactor, its laboratory synthesis, and its potential for application in biotechnology are briefly discussed.

2

Chapter 2 Methods

This chapter throws light on the various techniques and materials used in this project to accomplish and analyse flavin reduction reactions and their application with suitable enzymes. Typical experimental procedures and essential concepts for understanding enzymatic catalysis are discussed here.

2.1. Enzyme sources and preparation

This section contains information about the sources of enzymes used in this project and the molecular biology procedures for their preparation and purification. All enzymes used in the project were either prepared by members within the Vincent group, provided by collaborators or were purchased from commercial sources.

2.1.1. Hydrogenases

2.1.1.1. Hydrogenase 1 from *E. coli* (Hyd1)

Hyd1 was prepared in house and kindly provided by Dr Miguel Ramirez in the Vincent group using the following procedure:

Hdy1 was produced by homologous over-expression of the genes encoding the structural subunits of the enzyme and key maturases. After overexpression under anaerobic growth, the Hyd1 enzyme was purified by Metal Affinity Chromatography in a Nickel-NTA prepacked column. After elution with imidazole containing buffer, the protein was further purified by Size Exclusion Chromatography using a HiLoad 16/600 Superdex 200 pg gel-filtration column (GE Healthcare, UK). Subsequently, the enzyme was buffer-exchanged into Tris HCl buffer (20 mM Tris-HCl, pH 7.2, 350 mM NaCl, 0.02% Triton X, 1 mM dithiothreitol (DTT)), concentrated and stored at −80 °C.[172]

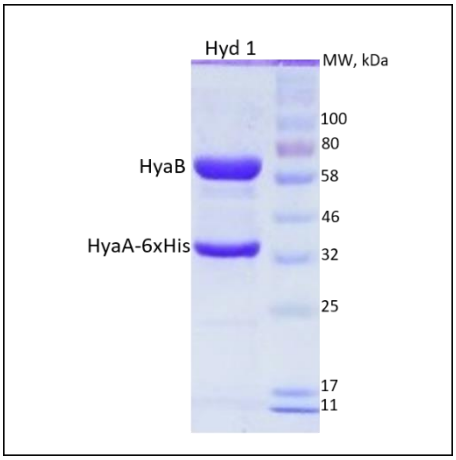


Figure 2. 1. SDS-PAGE (sodium dodecyl sulfate polyacrylamide gel electrophoresis) analysis of purified Hyd1

As discussed in the introduction, Hyd1 preparations were predominantly hetero-dimers (HyaAB) and lacked the cytochrome subunit.[140] Hyd1 samples with cytochrome subunits were prepared and provided by Wangzhe Li and Sophie Kendall-Price, DPhil students in the Vincent group, and those that lacked the cytochrome subunits were provided by Dr Rhiannon Evans from the Vincent Group.

Hyd1 without cytochrome was produced from previously established procedure using an FTH2014 strain where a delta TM (transmembrane) enzyme was isolated from the supernatant. This strain has a modified hya operon (hyaA) that removes the transmembrane domain which is required for anchoring Hyd1 to the membrane. [173,174]

Flavin reduction by a given volume of Hyd1 varied across different batches of Hyd1. This is due to the difference in concentrations of the enzyme being isolated during every preparation. For this purpose, the activity of Hyd1 for flavin reduction from a freshly prepared batch was always evaluated using a colorimetric assay and the volume was adjusted accordingly to give consistent units of activity in further experiments. In some cases, it was required to evaluate the concentrations of the Hyd1 samples in order to calculate the enzyme turnover numbers and turnover frequencies. This was done by the Bradford assay which is detailed in section 2.2.5.1.

2.1.1.2. Hydrogenase 2 from *E. coli* (Hyd2)

Hyd2 samples used for this project were provided by Dr Rhiannon Evans from the Vincent group. All Hyd2 samples were purified using a previously established procedure and had a concentration of 3.5 mg mL^{-1}.[175,176] Hyd2 containing its catalytic core HybOC was produced from an overexpression plasmid (pQE-80-ΔTMΔTat hybO, simply known as pO^C) which lacks the C-terminal transmembrane helix domain and the N terminal Twin Arginine Translocation (Tat) system of hybO. This overexpression plasmid was used on an *E. coli* strain called 'HJ001-hyp'. A preculture was prepared from a single colony in 5 mL Luria Broth (LB), with ampicillin (100 μg mL^{-1}) at 37 °C for 7 hours with 200 rpm. Inoculation was prepared in a 5 L LB media that was supplemented with glycerol (0.5% (v/v)), sodium fumarate (0.4% (w/v)) and ampicillin (100 μg mL^{-1}). This was further topped up to the brim and allowed to inoculate at 37 °C without shaking. Expression of pO^C was induced using isopropyl β-D-1-thiogalactopyranoside (IPTG, final concentration 1 mM) at an $OD_{600\ nm}$ (optical density measured at 600 nm) of 0.25. After 9 hours of induction, cells were harvested by centrifugation at 4 °C, and were resuspended in Tris buffer (100 mM) with EDTA 1 mM, NaCl 50 mM, DNAse (0.003% (w/v)), and lysozyme (0.012% (w/v)), pH 7.5 and frozen at -80 °C. Purification was carried out by adding protease inhibitor tablets (cOmplete, mini EDTA-free protease inhibitor cocktail, Roche, 1 tablet per 30 L culture) to thawed cells followed by stirring at 4 °C for 20 min. Cells were then lysed at 1380 bar by two passes through a cell disruptor system (Constant Systems). Debris was pelleted by ultracentrifugation at 45,000 rpm for 30 min at 4 °C. The resulting supernatant solution was added with Imidazole (50 mM) and DTT (1 mM) and loaded to a Ni-affinity column (5 mL column volume, His-trap FF Crude, GE Healthcare) pre-equilibrated with Tris buffer (50 mM, pH 7.2), NaCl (350 mM), imidazole (50 mM) and DTT (1 mM). Unbound protein was washed from the column using 20 column volumes. Hyd2 was eluted over an imidazole gradient of 50 – 500 mM over 16 – 20 column volumes and the fractions were collected. The purity of each fraction was evaluated by measuring

absorbances at 280 and 420 nm and by SDS-PAGE. The pure fractions were then pooled and concentrated through centrifugation by using centrifugal concentrators with a 50,000 molecular mass cut off (Vivaspin). Concentrated protein was buffer exchanged into Tris buffer (50 mM, pH 7.2), NaCl (350 mM), glycerol (10% v/v), and DTT (1 mM) using PD-10 desalting columns from GE Healthcare, and aliquots were finally snap frozen and stored in liquid N_2.

2.1.1.3. NiFe Hydrogenase from *Desulfovibrio vulgaris* Miyazaki F (DvMF)

DvMF hydrogenase were obtained through a collaboration with Dr Patricia Rodriguez Macia (University of Oxford) and Prof Wolfgang Lubitz (Max Planck Institute for Chemical Energy Conversion). DvMF hydrogenase was produced and purified at the Max Planck Institute for Chemical Energy Conversion, by Ms Patricia Malkowski and Ms Nina Breuer following already published procedure[177] and were posted to Oxford on dry ice.

2.1.2. Glucose dehydrogenase

2.1.2.1. GDH-101

A part of this project investigated recycling nicotinamide cofactors, NAD^+ and $NADP^+$ using traditional glucose dehydrogenase (GDH) in order to compare and evaluate the effect of the flavin regeneration system and the glucose dehydrogenase system when they were coupled to an ene-reductase. Commercially available glucose dehydrogenase, GDH-101 was used for this project and was supplied by Johnson Matthey.

2.1.3. Old Yellow Enzyme ene-reductases

2.1.3.1. Old Yellow Enzyme from *Thermus scotoductus* (*Ts*OYE)

The selective reduction of ketoisophorone (**1**) to (*R*)-levodione (**2**) was accomplished using *Ts*OYE, kindly provided by our collaborator, Dr Caroline Paul from TU Delft and it was prepared using

established protocols. The *Thermus scotoductus* ene-reductase of the Old Yellow Enzyme family (*Ts*OYE)[3,4] was produced by heterologous expression in *E. coli*. The gene encoding for *Ts*OYE was previously cloned in a pET-22b(+) vector, transformed into *E. coli* BL21(DE3) competent cells, which were spread on Lysogeny Broth (LB) agar plates containing ampicillin (100 μg mL^{-1}) and left to grow at 37 °C overnight. A pre-culture was started in LB medium supplemented with ampicillin (100 μg mL^{-1}) by picking one isolated colony, and shaken at 37 °C overnight. After inoculation of 1 L Terrific Broth (TB) medium (supplemented with 100 μg mL^{-1} ampicillin) with 10 mL of pre-culture, the 5-L flask was shaken in an incubator at 37 °C until the optical density at 600 nm ($OD_{600\ nm}$) reached an absorbance of 0.6, then was cooled to 30 °C. Expression was induced by addition of isopropyl β-D-1-thiogalactopyranoside (IPTG, 0.5 mM). After 20 h at 30 °C, cells were harvested by centrifugation at 10,000 rpm for 20 min at 4 °C, resuspended and washed with MOPS-NaOH buffer (20 mM, pH 7.0) and centrifuged again. The cell pellet was frozen at -80 °C overnight. The cell pellet was then thawed and resuspended in the same buffer, with DNaseI, $MgCl_2$ and a cOmplete™ EDTA-free protease inhibitor cocktail tablet, to be passed through a Multi Shot Cell Disruption System once, and centrifuged at 10,000 rpm for 20 min at 4 °C. The resulting supernatant was heated at 70 °C for 90 min, and centrifuged at 6,000 rpm for 30 min at 4 °C. The resulting yellow supernatant was analysed by UV-visible spectroscopy (Cary 60 spectrophotometer) to determine flavin content (in a UV cuvette, by denaturing the enzyme sample with 0.2% sodium dodecyl sulfate, SDS) and the Bicinchoninic acid (BCA) assay was used to determine overall protein content. Flavin mononucleotide (FMN) was supplemented based on these measurements and the enzyme solution was left on ice for 30 min. The enzyme solution was then passed through a desalting column (PD-10) to remove excess FMN with MOPS-NaOH buffer (20 mM, pH 7.0), and further concentrated in an Amicon ultra centrifugal filter with a cut-off of 10 kDa, also ensuring the removal of any excess FMN. The resulting *Ts*OYE was

observed to be >95% pure by SDS-PAGE, frozen with liquid nitrogen and stored at −20 °C (−80 °C for long-term) as a 200 µM solution in MOPS-NaOH buffer (20 mM, pH 7.0).

2.1.3.2. Commercial ene-reductases

Commercial samples of ene-reductases (ENE-101, ENE-102, ENE-103, ENE-107, ENE-108 and ENE-109) were provided by Johnson Matthey in lyophilised form and used without further purification.

2.2. UV-visible spectroscopy

Throughout this project, UV-visible spectroscopy remained a highly exploited spectroscopic technique for determining enzyme activity via colourimetric assays and, protein concentration. Additionally, a range of experiments such as temperature study, control experiments and K_M studies were also performed using UV-vis spectroscopy.

2.2.1. Theory of UV-visible spectroscopy[178,179]

When a continuous radiation of light is passed through a transparent substance, a portion of light may be absorbed by the substance resulting in an absorption spectrum. The UV-visible region in the electromagnetic spectrum spans between 200 and 800 nm and absorption of light in this region stimulates the excitation of electrons from lower to higher energy levels. The difference in energy between the two levels is given by

$$\Delta E = h\nu = \frac{hc}{\lambda}$$

Where

ΔE is the energy difference

h is the Planck's constant (6.626 x 10^{-34} m^2 Kg s^{-1})

c is the velocity of light (3×10^8 m s^{-1})

The most probable electronic transition is generally from the highest occupied molecular orbital (HOMO) to the lowest unoccupied molecular orbital (LUMO). The energy gap between different electronic levels vary giving rise to transitions of varying energies as shown in Figure 2. 2.

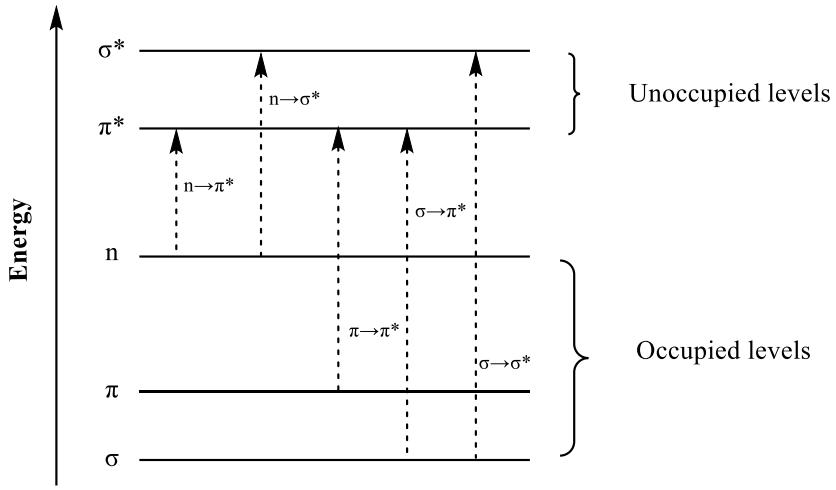


Figure 2. 2. Electronic energy levels and possible electronic transitions between them.

2.2.2. Electronic transitions in cofactor molecules

The highest-energy transition is from the σ to σ* orbital which absorbs UV light of very short wavelength often around 150 nm and is quite difficult to access using conventional spectrophotometers. This type of transition is commonly observed in alkanes. n→π* transitions become important in unsaturated compounds containing heteroatoms such as oxygen and nitrogen. π→π* transitions are observed in unsaturated molecules, whereas the n→σ* transitions become important in saturated molecules that contain nonbonding electron pairs e.g. heteroatoms like N, O and S. The possible electronic transitions and their corresponding UV-visible spectrum for nicotinamide and flavin cofactors are discussed next.

2.2.2.1. Nicotinamides - NAD^+ and NADH

NAD^+ and NADH contain heterocyclic aromatic rings, adenine and nicotinamide that can exhibit transitions into the π* orbital when illuminated by UV-visible light. NAD^+ shows an absorption maxima at λ_{max} = 260 nm due to a combination of π – π* transitions in both the adenine and nicotinamide rings. When NAD^+ is reduced to NADH, a hydride is added into the nicotinamide ring, converting it into a dihydronicotinamide moiety as shown in Figure 2. 3. This leads to a slight decrease in absorbance at λ_{max} = 260 nm and a new absorbance peak occurs at λ_{max} = 340 nm which is characteristic of NADH. The formation of this new peak occurs as a result of a bathochromic shift caused by an n→π* transition from the nitrogen atom to the nearby conjugated amide group in the dihydronicotinamide ring.

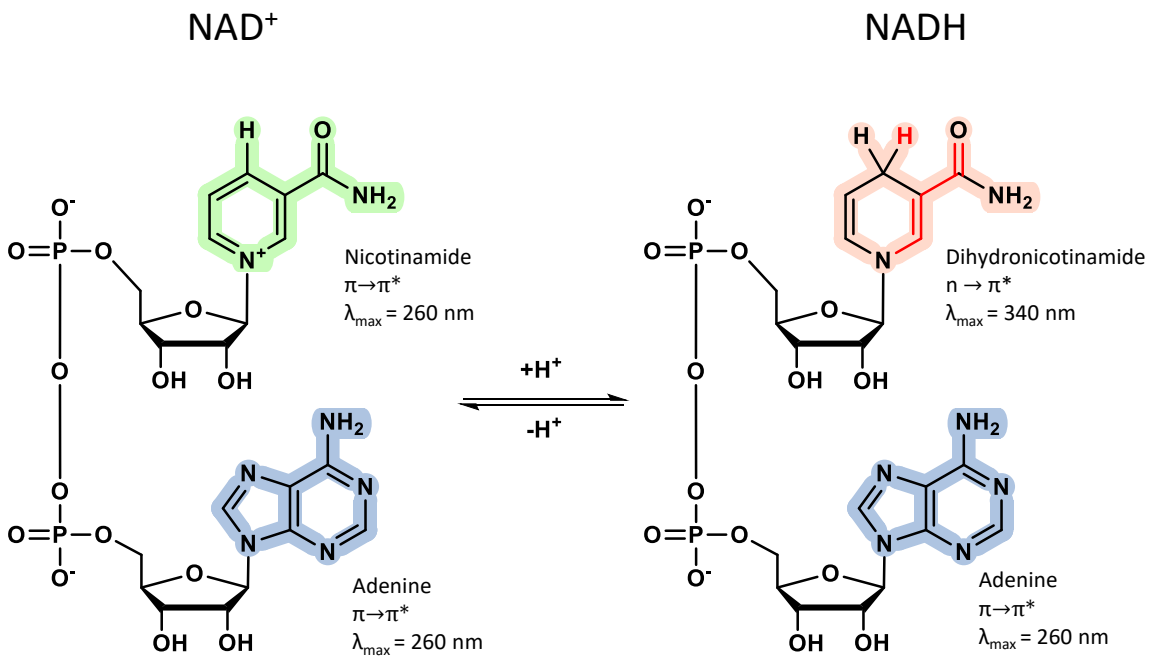


Figure 2. 3. Chemical structures of NAD^+ and NADH highlighting the guanine (blue), nicotinamide (green) and dihydronicotinamide (orange) rings that that are responsible for UV-vis activity.

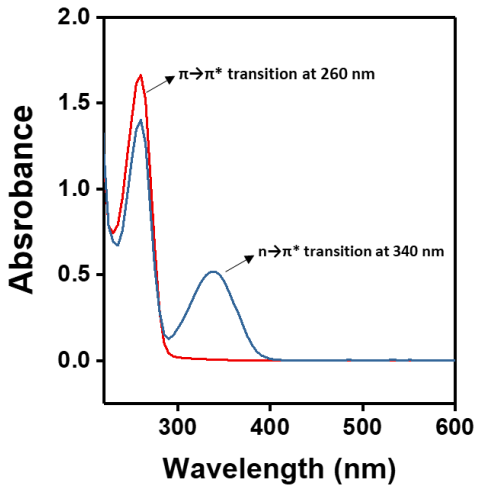


Figure 2. 4. UV-visible spectra of NAD^+ (red) and NADH (blue) recorded in Tris buffer (pH 8, 100 mM) at room temperature.

2.2.2.2. Flavins - FAD, FMN and $FADH_2$, $FMNH_2$[180–182]

The isoalloxazine moiety in flavins is the chromophore core where electronic transitions occur giving rise to a characteristic UV absorption spectrum.[183] Since the isoalloxazine ring is also the centre for oxidation-reduction catalysis, (as discussed in Chapter 1), spectral changes recorded during enzymatic reactions become important for understanding reaction mechanisms. Flavins can exist in different redox and protonation states (Scheme 2. 1.) and the stability of each state is largely dictated by the protein moiety encapsulating the flavin cofactor. Oxidised flavin can be directly reduced to its two electron reduced (hydroquinone) state or to its one electron reduced (semiquinone) state. The semiquinone species can remain in two spectroscopically distinguishable protonation states — neutral or anionic semiquinone states absorbing at 580–620 nm and around 380 nm respectively (see Figure 2. 8.).[183] Similarly the flavin hydroquinone also exists as the anionic or neutral form.

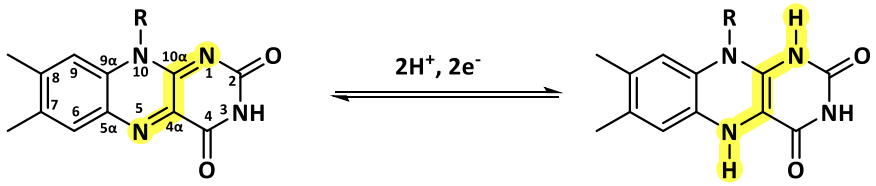
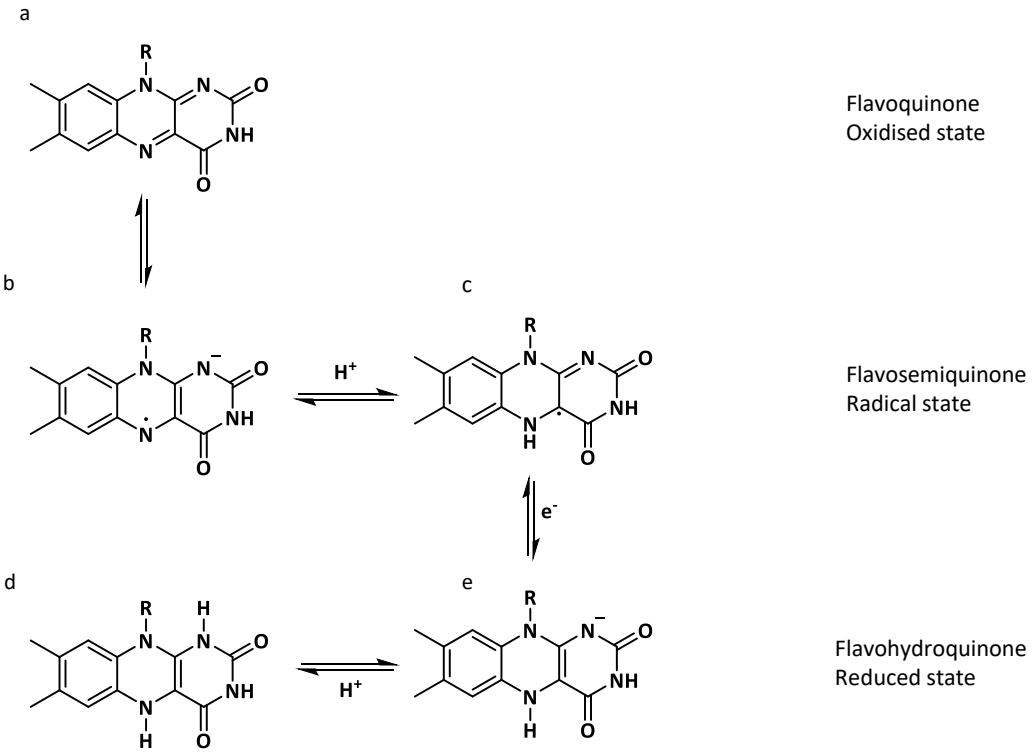


Figure 2. 5. Two electron, two proton reduction of oxidised flavin to give the fully reduced dihydroquinone state. The diimine moiety undergoing reduction is highlighted in yellow

Thus, in total flavins can exist in 3 different redox states as shown in Scheme 2. 1. This includes the oxidised flavin which after one electron reduction forms the radical anion semiquinone containing a radical electron on $C_{4\alpha}$ and a negative charge on N_5. This can be followed by a proton transfer reaction that stabilises the negative charge and forms a neutral radical semiquinone. Another subsequent electron reduction forms the reduced anionic hydroquinone which can eventually accept another proton leading to the neutral hydroquinone. The redox states of flavins and their redox transitions are shown in Scheme 2. 1.



Scheme 2. 1. The different redox states of flavin: a) oxidised flavin, b) anionic flavin semiquinone, c) neutral flavin semiquinone, d) anionic flavin hydroquinone and, e) neutral flavin hydroquinone

The spectroscopic behaviour of flavins can be understood by considering the structural and electronic transitions happening in the isoalloxazine ring. The oxidised state remains to be the most extensively studied flavin form both experimentally and theoretically due to the ease of access of this state. In contrast, the semiquinone and hydroquinone redox states are quite unstable, therefore spectral reports for such states are available only for flavins contained within protein environments that offer them a stabilising environment.[184] Moreover, the exact positions of absorption peaks of flavins depend on their surrounding protein or solvent environment that fine tune their redox properties.[185–187]

However, in a recent study, Mondal *et al*.[181] have used DFT (Density functional Theory) calculations to relate the electron density distribution in the isoalloxazine ring of different redox states to its photophysical properties and interpret the possible electronic transitions that can take place by

means of a Walsh diagram. A Walsh diagram is a plot of orbital binding energy and the bond angles in a molecule that gives insight into changes in the geometry of the molecule when it undergoes redox changes. The distinct spectral features of each redox state are primarily attributed to bond order changes of the α-diimine bond (N_1=$C_{10\alpha}$-$C_{4\alpha}$=N_5) which transforms to an ethane 1,2 diamine (N_1-$C_{10\alpha}$=$C_{4\alpha}$-N_5) upon reduction[188] (see Figure 2. 5. highlighted in yellow).

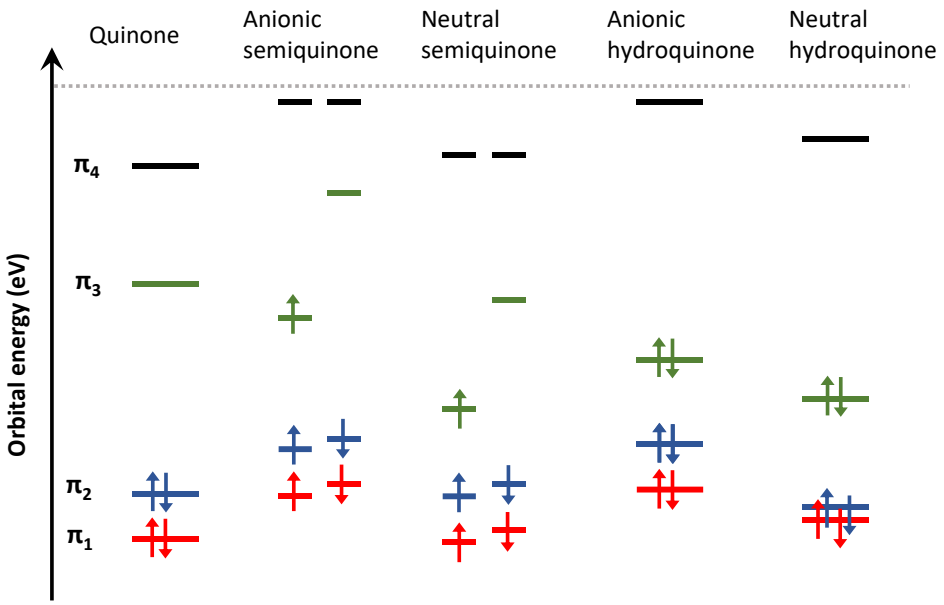


Figure 2. 6. A Walsh diagram showing the molecular orbitals of different redox states of the isoalloxazine ring in flavins, adapted from reference 181 with permission from Elsevier publisher: *Journal of Photochemistry and Photobiology A: Chemistry*, **2020**, *387*, 112164.[181] (License number: 5253550544021)

Figure 2. 6. displays the Walsh diagram showing different molecular orbitals of the various redox states of flavin. Most of these molecular orbitals are similar in shape and are typical π type orbitals delocalised over the pyrimidine ring. Among all other orbitals, the π_3 orbital deserves special attention. This orbital remains bonding at $C_{4\alpha}$-$C_{10\alpha}$ and antibonding at N_1=$C_{10\alpha}$ and plays a significant role due to substantial difference in its occupancy during the reduction process which is also the reason for distinct absorption pattern. In the oxidised state, it remains empty and is the lowest occupied molecular orbital (LUMO). Upon single electron addition, this LUMO accepts an electron and becomes a singly occupied orbital (SOMO) which further receives another electron to become

the highest occupied molecular orbital (HOMO) corresponding to the fully reduced hydroquinone state.

Oxidised state

If we look closely at the UV-visible spectra of oxidised, free FAD and FMN in aqueous solution, there are four absorbance peaks at *c.a.* 220, 265, 375 and 450 nm. Among them, the lower energy transitions at *c.a.* 450 nm and 375 nm have been significantly explored for spectroscopic studies. Absorbance at 450 nm is attributed to a lower energy $\pi \rightarrow \pi^*$ transition which is indicative of the high molar extinction coefficient ($>10^4$ M^{-1} cm^{-1}). Complete Neglect of Differential Overlap (CNDO) calculations suggest that the absorbance peak at 375 nm is an overlap of two transitions: $\pi \rightarrow \pi^*$ and $n \rightarrow \pi^*$ where the $n \rightarrow \pi^*$ transition, is predicted to be as a result of non-bonding electron pairs in N_1.[182] Later DFT calculations have shown this transition to correspond to the excitation of electrons from $\pi_2 \rightarrow \pi_3$ orbital and $n \rightarrow \pi_3$ orbital. It is also worth noting that the UV-visible spectra of flavins buried within protein structures may or may not resemble the spectra of free flavins and sometimes possess slight variations in their spectra depending on their environment (polarity) or their orientation with the protein.

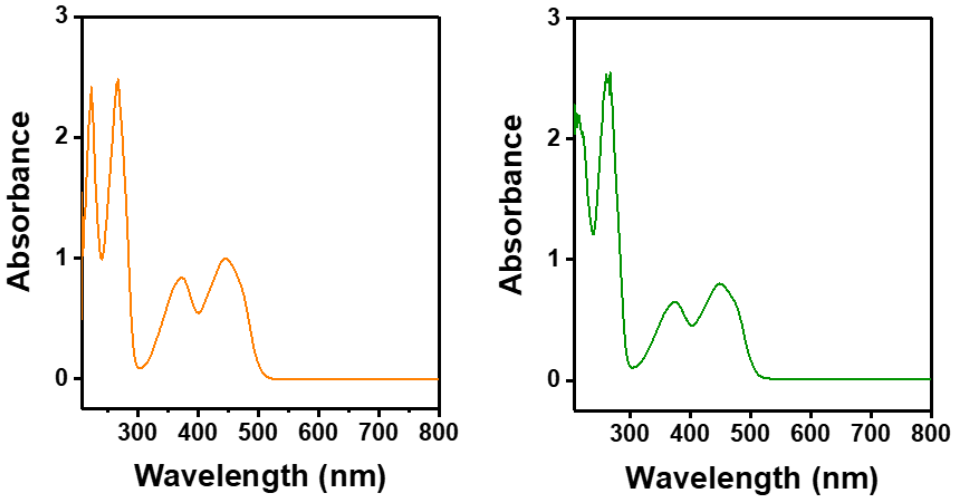


Figure 2. 7. UV-visible spectrum of oxidized FMN (orange) and FAD (green) recorded at 0.1 mM concentration, in Tris buffer (pH 8, 50 mM) at 25 °C.

Semiquinone states

The radical semiquinone states also exhibit a bright $\pi_2 \rightarrow \pi_3$ transition around 450–650 nm that gets red shifted in the order quinone → anionic semiquinone → neutral semiquinone due to decreasing energy gap between the orbitals caused by reduction. However, the most bright transition for the radical forms, is the transition from SOMO π_3 to a vacant π_5^* orbital occurring at *c.a.* 340–360 nm.

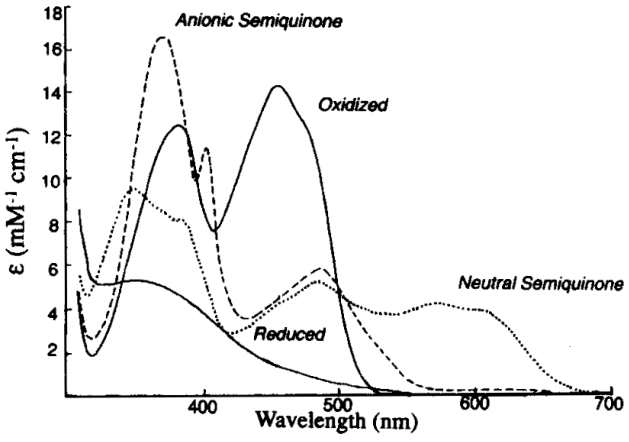


Figure 2. 8. UV-visible spectrum of the different redox states of FAD in glucose oxidase. This spectrum was taken from an article by Prof. Vincent Massey with permission from Biochemical Society publisher: *Biochem. Soc. Trans.*, 2000, **28**, 283–296.[189,190] (License ID: 1182387-1)

Hydroquinone states

The anionic and neutral hydroquinone states have very similar absorption spectra. These states show no transition into the π_3 orbital because this orbital is already fully occupied. Therefore there is no absorption at 450 nm. This was also observed in all of the flavin reduction assays performed in this project. A $\pi_3 \rightarrow \pi_5^*$ transition is observed around the near UV region at 320–340 nm and a second peak appears at *c.a.* 200–300 nm corresponding to $\pi_3 \rightarrow \pi_6^*$ transition.

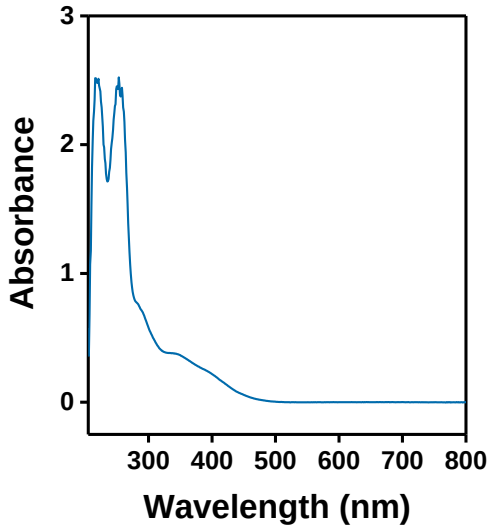


Figure 2. 9. UV-visible spectrum of fully reduced FMN ($FMNH_2$) obtained after a biocatalysed reduction in Tris buffer (pH 8, 50 mM) at 25 °C.[191]

2.2.2.3. Deazaflavins

Deazaflavins have a similar structure to that of flavin cofactors but differ in that they have a carbon atom substituted for N-5 in the isoalloxazine ring. The two commonly known biological forms of deazaflavins are F_o and F_{420}, although early biomimetic studies have reported the synthesis of nearly 20 variations of the deazaflavin structure. The structures and functions of F_o and F_{420} are discussed in chapter 6, while this section will focus on their UV-visible spectroscopic properties.

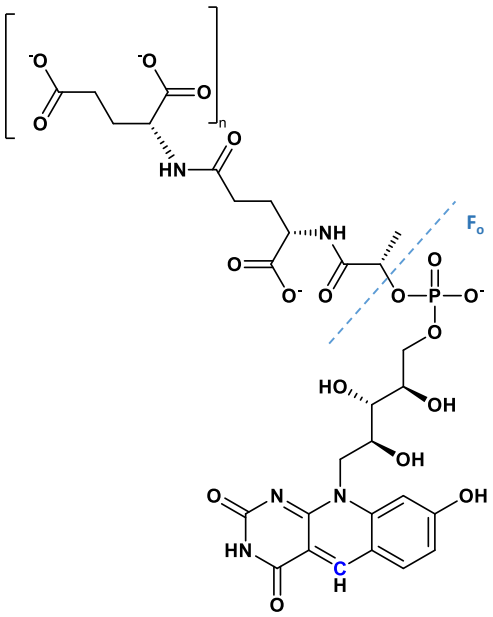


Figure 2. 10. Structure of F_o and F_{420}.

In the oxidised state, F_{420} shows two absorption peaks at 420 nm (ε = 40,000 M^{-1} cm^{-1})[192] and 247 nm which shift to lower wavelengths of up to 375 nm and 230 nm respectively with decreasing pH. At low pHs their intensity also decreases. This absorbance is due to π→π* transitions of electrons delocalised in the isoalloxazine ring. Upon reduction to $F_{420}H_2$, the 420 nm peak is lost and a new peak at 320 nm appears. This peak however has a lower molar absorptivity in comparison to the value observed for oxidised F_{420}.

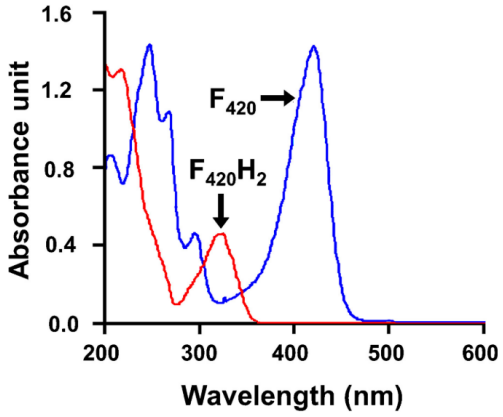


Figure 2. 11. UV-visible spectrum of F_{420} (blue) and $F_{420}H_2$ (red) taken from reference 63.[63]

The absorption spectra of F_{420} are blue shifted to about 50 nm compared to the absorption spectra of flavins.[63,193] The UV-visible spectrum of 5-deazariboflavin is quite similar to that of the riboflavin and shows a blue shift of about 50–60 nm.

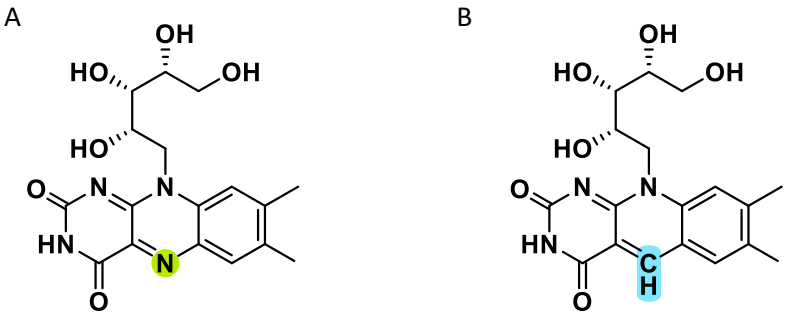


Figure 2. 12. Structures of A) riboflavin and B) 5-deazariboflavin.

Similar to FMN, 5-deazaflavin also shows an isosbestic point at *c.a.* 333 nm (whereas in FMN, it is *c.a.* 330 nm)[194]. Figure 2. 13. shows the UV-visible spectrum of 5-deazariboflavin and F_{420},.

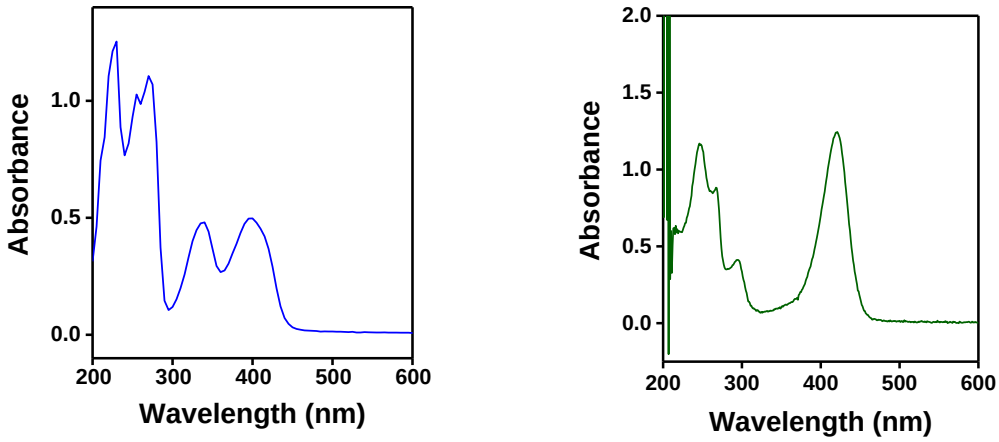


Figure 2. 13. UV-visible spectrum of 5-deazariboflavin (blue), F_{420} (green).

2.2.3. The Beer-Lambert law

The Beer-Lambert law gives the relation between the absorbance of a molecule at a particular wavelength and its extinction coefficient according to the following equation:

$$A = \varepsilon c l \text{ where,}$$

A is the absorbance

ε is the molar extinction coefficient, M^{-1} cm^{-1}

c is the concentration, M, and

l is the length of the sample cell (cuvette), cm

The extinction coefficient values for flavins and nicotinamides are available in the literature and are tabulated in Table 2. 1.

Table 2. 1. Extinction coefficient values for different cofactors

Cofactor	**λ_{max} (nm)**	**Extinction coefficient ε (mM^{-1} cm^{-1})**
FAD	375	9.3
	450	11.30
FMN[183]	373	10.4
	445	12.5
NAD^+	260	17.4
NADH[195]	260	14.1
	340	6.22
$NADP^+$	260	17.8
NADPH[196]	260	-
	340	6.22

2.2.4. Calculating enzyme activities

Using the extinction coefficient values, and the absorbance recorded during UV-visible spectroscopy, the concentration of oxidised and reduced forms of a cofactor can be calculated using the Beer-Lambert law. In the case of flavin cofactors, oxidised FAD and FMN absorb at λ_{max} = 450 and 445 nm respectively. When FAD and FMN are reduced using a suitable reductant, the formation of $FADH_2$ or $FMNH_2$ does not show any new absorption peak, as one would observe in the case of NADH or

NADPH. However, the intensity of absorbance at 450 and 445 nm decreases with the formation of $FADH_2$ and $FMNH_2$ which is used to determine the concentration of the reduced flavin and hence enzyme activity. This is done by determining the rate at which the absorbance at either 450 or 445 nm (in the case of FAD and FMN respectively) deceases. For this, UV-visible activity assays, were performed, where the reaction mixture was scanned every 30 seconds over 30 minutes. The concentration of oxidised flavin ($flavin_{ox}$) was calculated for every scan and the slope value for decreasing [$flavin_{ox}$] vs time (panel b in Figure 2. 14) was used to determine the activity of Hyd1 in terms of mM min^{-1} or nmol min^{-1}. Specific enzyme activity could also be calculated using the concentration of Hyd1 as mM min^{-1} mg^{-1} of Hyd1 used. A typical reduction activity assay for FMN and the corresponding plot of [$flavin_{ox}$] vs time is shown in Figure 2. 14. The slope value corresponding to the linear portion of the curve is generally used for calculating enzyme activity. The initial lag phase observed at the beginning of the assay is due to a characteristic H_2 dependent activation phase for aerobically purified Hyd1.[197]

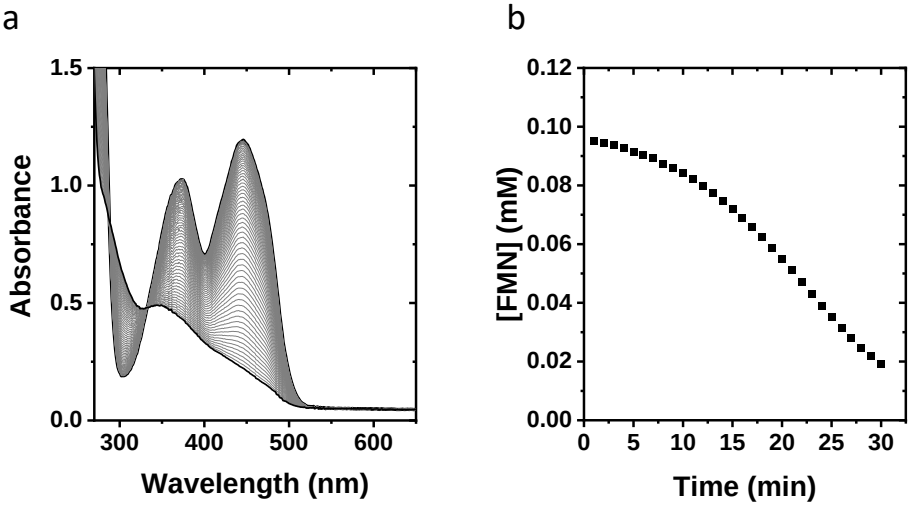


Figure 2. 14. A) A typical activity assay for FMN reduction catalysed by Hyd1 performed under H_2 atmosphere. b) A plot of [FMN] vs time showing a negative slope indicating the formation of $FMNH_2$. FMN concentration was calculated from the absorbance recorded at λ = 445 nm.

Experimental setup and procedure for the biocatalysed reduction of flavins under H_2 are given in section 2.3.2

2.2.5. Plate reader

A plate reader works on the principle of UV-vis spectroscopy. Unlike a conventional UV-vis spectrophotometer, it enables scanning of multiple samples simultaneously. This is particularly useful when large number of samples need to be scanned, for instance screening of a large library of enzymes. A plate reader was used to conduct Bradford assays that required scanning serial dilutions of Hyd1 samples in order to determine their concentrations. All Bradford assays were done on a SpectroSTAR Nano absorbance plate reader using 96-well clear plastic plates from ThermoFischer.

2.2.5.1. Bradford assay

The Bradford assay is an easy, quick and reliable method used for the quantitation of microgram quantities of proteins with molecular weights greater than 3,000. The general protocol involves using the Bradford reagent, which is a dye called Coomassie Brilliant Blue G-250 shown in Figure 2. 15 This dye is capable of producing a distinct colour upon binding with a protein[198] and can exist in three different forms—anionic (blue), neutral (green) and cationic (red). The dye reagent predominantly exists in the cationic form under acidic conditions showing absorption at λ_{max} = 470 nm. Upon binding with the protein, it is converted to a stable anionic form absorbing at λ_{max} = 595 nm. The absorption at 595 nm is due to the protein bound dye which is used to calculate the concentration of the protein. It is thought that the presence of a macromolecular form along with active basic (arginine) and aromatic functional groups facilitate dye binding to the protein.[199]

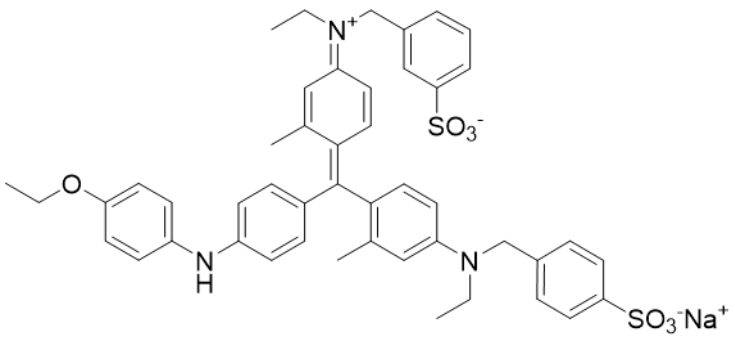


Figure 2. 15. Chemical structure of Coomassie Brilliant Blue G-250.

Protein concentrations were determined using the Bradford Protein Assay kit from Thermo Scientific and the manufacturer's instructions were followed without any modification for this experiment. Bovine Serum Albumin (BSA) ampules contained within this kit were used a relative standard. A detailed protocol followed for conducting the Bradford assay is given in the appendix.

2.3. Reaction set-up

2.3.1. Pressure vessel

A pressure vessel reactor can conduct chemical reactions under pressures greater than atmospheric pressure. In this project, all ene-reductase and nitro reductase catalysed reduction reactions that used the flavin regeneration system were performed in a Büchi Tinyclave pressure vessel (Figure 2. 16).[200] Using a pressure vessel helped minimise the loss of volatile substrates and products due to evaporation and also facilitated a constant pressure of H_2 throughout the reaction. The Büchi Tinyclave pressure vessel can withstand pressures of up to 10 bar and temperatures of up to 200 °C. The total volume of the glass container is 25 mL which can accommodate five centrifuge tubes containing reactions mixtures (Eppendorf, 1.5 mL).



Figure 2. 16. An image of the Büchi Tinyclave pressure vessel used to perform small scale H_2-pressurized reactions.

2.3.2. Procedure for setting up a pressure vessel reaction for alkene hydrogenation reactions

Using a syringe and needle, 600 µL of H_2-saturated Tris-HCl buffer (50 mM, 25 °C) was transferred to a centrifuge tube (Eppendorf, 1.5 mL) that contained the required quantities of flavin and the alkene substrate in DMSO. A total concentration of 1 vol% DMSO in the reaction mixture was used unless otherwise stated. A portion of this solution (approx. 0.2 mL) was used to transfer the designated quantity of Hyd1 (activated under H_2 for 3–15 h) and *Ts*OYE or other ene-reductase into the reaction tube in sequence *via* a needle and syringe. The lid of the centrifuge tube was pierced once with a needle, capped, and placed in the Büchi Tinyclave pressure vessel which was then charged to the designated pressure of H_2. The pressure vessel was then removed from the glovebox and wrapped in aluminium foil to exclude light in order to prevent photodecomposition or photochemical side

reactions of flavin, flavoenzyme, or both.[201] The vessel was placed on a Stuart® mini see-saw rocker set to 30 oscillations/min to ensure adequate mixing of the reaction mixture.

2.3.3. *In situ* UV-visible reactions in UV cuvettes

UV-visible spectra were recorded on a Cary 60 spectrophotometer with a cell holder (Agilent) and a Peltier accessory for temperature control using a quartz cuvette (path length 1 cm, cell volume 1 mL, Hellma). The indicated buffer was used to take a baseline scan. In some of the experiments, there was a uniform shift of the baseline across the entire spectral region (200–800 nm), which was corrected for during data processing in Origin 2017. The concentration of FMN was directly calculated based on the absorbance at λ_{max} = 445 nm (ε = 12.50 mM^{-1} cm^{-1}) and FAD based on the absorbance at λ_{max} = 450 nm (ε = 11.30 mM^{-1} cm^{-1}). A typical activity assay involved adding the required volume of buffer into a UV-visible quartz cuvette, which was then placed in the cell holder and allowed to warm to the indicated temperature (pre-set on the Peltier accessory) for 5 min. A baseline was recorded using the UV-visible spectrophotometer. A solution of 0.1 mM flavin (unless otherwise noted) in the designated buffer was next prepared in the cuvette, which was then capped with a rubber septum that was pierced with two needles to provide a gas inlet and outlet. An H_2-line was then connected and H_2 was bubbled through the flavin solution via the inlet needle for *c.a.* 10 minutes. The needle was then moved up to the headspace through which a continuous flow of H_2 was supplied. About 0.3 mL of the flavin solution was then used to transfer a designated quantity of Hyd1 into the cuvette using a syringe and needle, and the needle and syringe rinsed by drawing solution in and out of the cuvette. The assay was carried out by taking one scan (200–800 nm) every 30 seconds over 30 minutes. A typical setup is illustrated in Figure 2. 17.

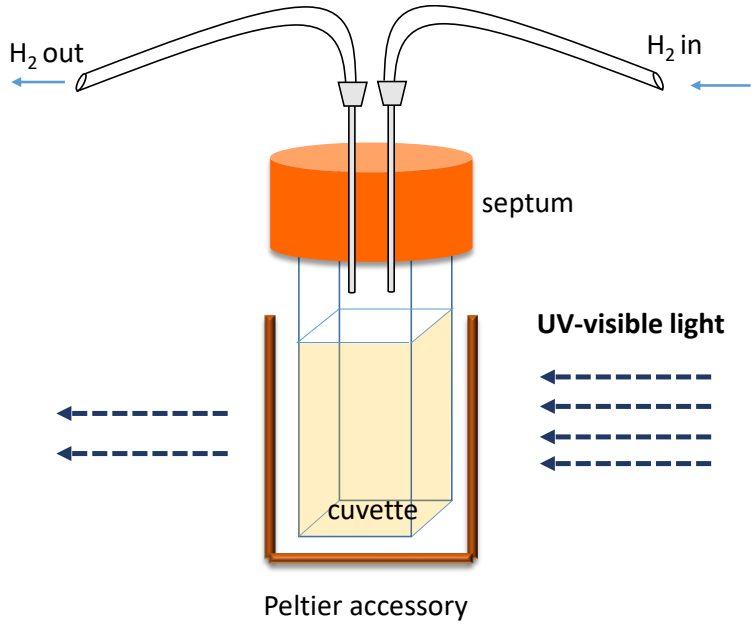


Figure 2. 17. Figure showing the experimental setup used for UV-visible activity assay for the H_2-driven reduction of flavins cofactors using Hyd1.

2.4. Analytical methods

2.4.1. NMR spectroscopy

Proton (^{1}H) NMR spectroscopy was used predominantly to characterise and confirm products from synthetic experiments and analyse preliminary results from nitroreductase reactions. NMR samples from synthetic procedures were prepared using solvents as indicated in the literature. For analysing samples from nitroreductase reactions, a certain volume of the reaction mixture was drawn and mixed with deuterated water (D_2O) to give 10% D_2O and 90% H_2O in the final sample used for analysis. This mixture was then taken for ^{1}H NMR analysis using the water suppression mode. All analyses were carried out on a 400 MHz Bruker Avance III HD nanobay NMR spectrometer equipped with a 9.4 T magnet. All spectra were obtained at room temperature and processed using MestreNova®14.2.0.

2.4.2. Gas Chromatography

The progress of alkene reduction reactions was monitored by taking time points of the reaction mixture and analysing them by gas chromatography. Two different gas chromatographs were used for different substrates and products based on the quality of separation. All analyses were performed on a ThermoScientific Trace 1310 GC except for dimethyl itaconate and its corresponding products which were analysed on a ThermoFinnigan Trace GC instead. Sample preparation consisted of drawing aliquots (15 or 25 µL) of reaction mixture at the required time points. The reaction mixture was then extracted into 200 µL ethyl acetate (EtOAc), then 150 µL of the EtOAc layer was removed, dried over Na_2SO_4 and 75 µL of the solution was taken for GC analysis. Conversion to the corresponding products and the enantiomeric excess (%*ee*) were calculated based on the peak area of their respective peaks.

2.4.3. GC method and parameters

Instrument: ThermoScientific Trace 1310 GC

Column: CP-Chirasil-Dex CB (Agilent), 25 m length, 0.25 mm diameter, 0.25 µm (film thickness), fitted with a guard of 10 m undeactivated fused silica of the same diameter

Carrier: He (CP grade), 170 kPa (constant pressure)

Inlet temperature: 200 °C

Injection conditions: Splitless with split flow 60 mL min^{-1}, splitless time 0.8 min, purge 5 mL min^{-1}.

Injection volume = 0.1 µL.

Detection: FID (H_2 = 35 mL min^{-1}, air = 350 mL min^{-1}, makeup N_2 = 40 mL min^{-1}, temp = 200 °C)

Reduction of ketoisophorone and 4-phenyl-3-buten-2-one

Oven heating profile:

Time (minutes)	Temperature
0 → 5	Hold at 70 °C
5 → 14.5	Ramp to 165 °C at 10 °C/min
14.5 → 20.2	Ramp to 200 °C at 50 °C/min

Compound retention times (reduction of ketoisophorone):

Time (minutes)	Compound
12.27	Ketoisophorone
12.68	(*R*)-levodione
12.80	(*S*)-levodione

Compound retention times (reduction of 4-phenyl-3-buten-2-one):

Time (minutes)	Compound
14.48	4-Phenyl-3-buten-2-one
12.86	4-Phenyl-2-butanone

Reduction of 2-methyl-5-nitropyridine

Oven heating profile:

Time (minutes)	Temperature
0 → 5	Hold at 70 °C
5 → 24	Ramp to 165 °C at 5 °C/min
24 → 29.7	Ramp to 200 °C at 50 °C/min

Compound retention times (reduction of 2-methyl-5-nitropyridine)

Time (minutes)	Compound
18.2	5-amino-2-methylpyridine
18.4	2-methyl-5-nitropyridine

Instrument: ThermoFinnigan Trace GC

Reduction of dimethyl itaconate

Instrument: ThermoFinnigan Trace GC

Column: Cyclosil-B (Agilent), 30 m length, 0.25 mm diameter, 0.25 µm (film thickness)

Carrier: He (CP grade), 100 kPa (constant pressure)

Inlet temperature: 220 °C

Injection volume: 2 µL

Detection: FID (H_2 = 35 mL min^{-1}, air = 350 mL min^{-1}, N_2 = 30 mL min^{-1}, temp = 250 °C)

Oven heating profile:

Time (minutes)	Temperature
0 → 160	Hold at 70 °C
160 → 170	Ramp to 180 °C at 20 °C/min

Compound retention times (reduction of dimethyl itaconate)

Time (minutes)	Compound
83.67	dimethyl itaconate
58.50	(*R*)-dimethyl methyl succinate
60.76	(*S*)-dimethyl methyl succinate

The chiral phase GC-FID chromatograms of all substrates and products are shown in Figure 2. 18 to Figure 2. 20.

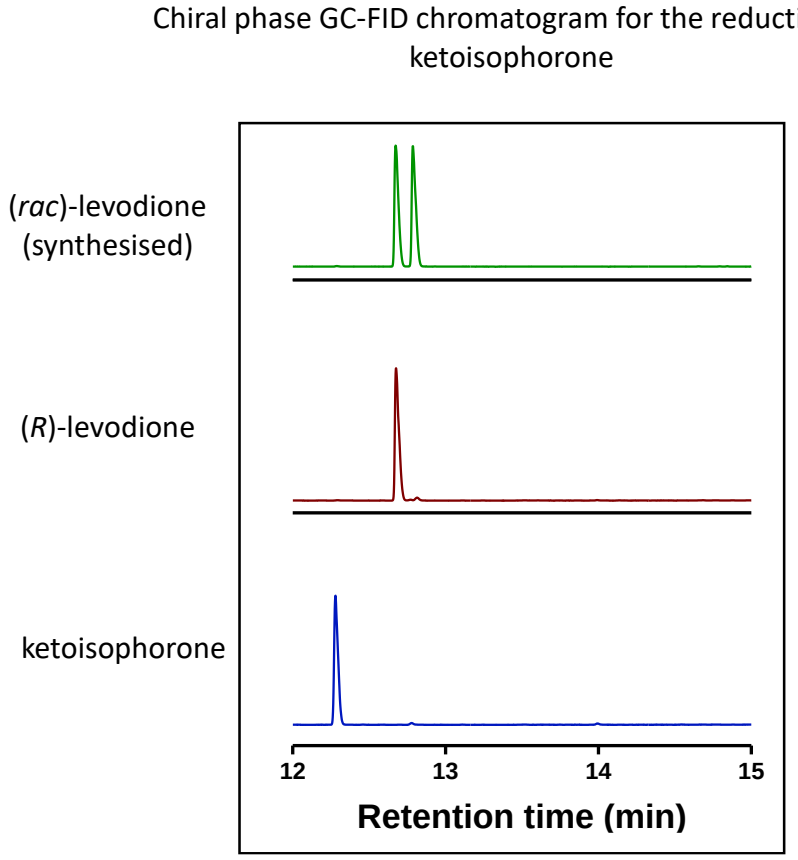


Figure 2. 18. GC-FID results of ketoisophorone (blue, commercially available in ≥98% purity), (*R*)-levodione (brown, was obtained from Baker's yeast fermentation and was a gift from Dr. Adrie Straathof from the Delft University of Technology) and (*rac*)-levodione (green, synthesised following literature procedure)[22] standards.

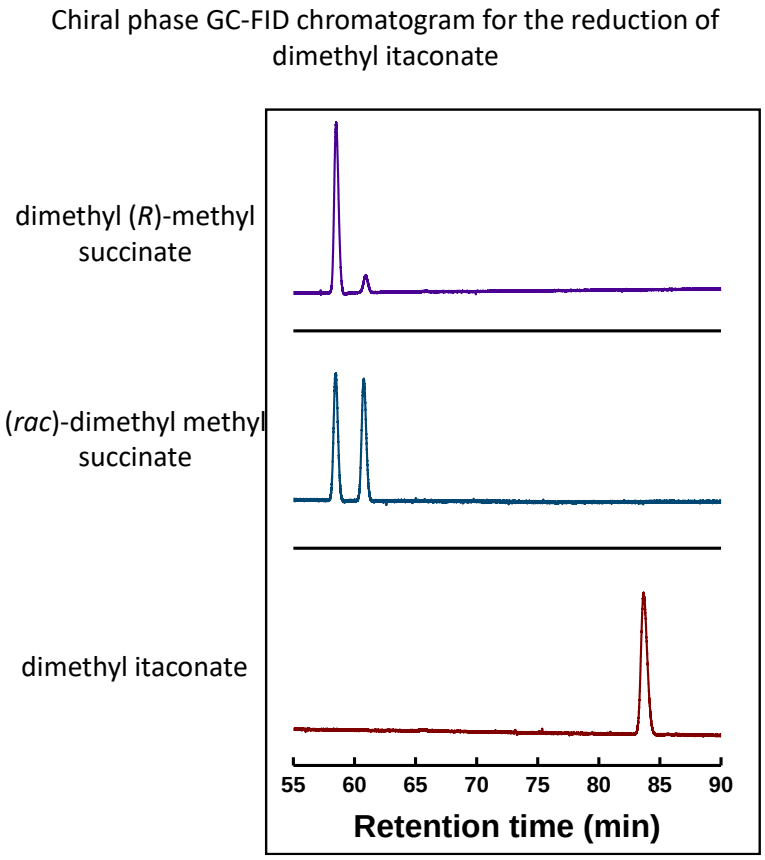


Figure 2. 19. GC-FID chromatogram of dimethyl itaconate (brown, commercially available, 98%), (*rac*)-dimethyl methyl succinate (dark blue, commercially available, 98%) and dimethyl (*R*)-methyl succinate (purple, commercially available, 99%) standards.

Chiral phase GC-FID chromatogram for the reduction of 4-phenyl-3-buten-2-one

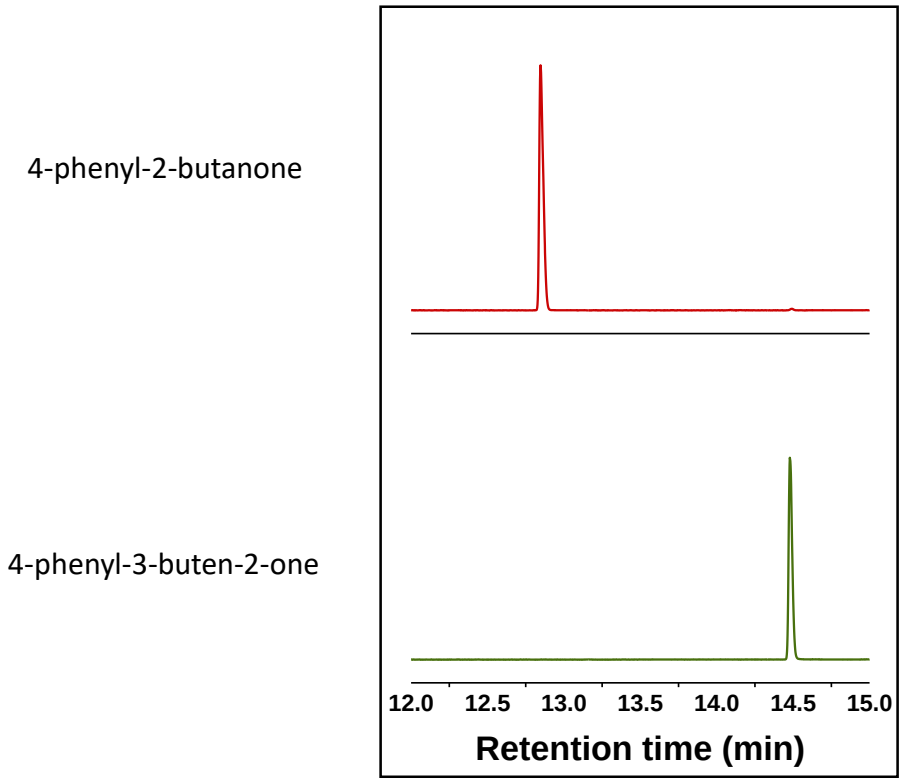


Figure 2. 20. GC-FID chromatogram of 4-phenyl-3-buten-2-one (green, commercially available, 99%) and 4-phenyl-2-butanone (red, commercially available, 98%) standards.

2.4.4. Mass spectrometry

Mass spectrometry was used for analysing reaction samples from nitro reduction reactions, discussed in chapter 5. Analysis by mass spectrometry helped to ensure that no unwanted side products were present in the reaction mixture as they could not be detected by gas chromatography. All analyses were performed on an Agilent 6120 bench-top single quadrupole analyser which was connected to an Agilent 1260 IsoPump and a CTC Analytics 2777 Sample Manager. Sample preparation involved diluting a small aliquot of the reaction mixture in acetonitrile such that the total concentration of the sample was 100 μg mL^{-1}.

2.5. Enzyme Kinetics and Measurements[202,203]

Enzyme kinetics involve examining the rates of an enzyme catalysed reaction and have been practised widely from the early half of the 20th century to study enzymes. Investigating the kinetics of an enzymatic reaction gives insight into the specificities of an enzyme and its reaction pathways, as well as informing design and optimisation of biotransformation reactions. Kinetic measurements will be particularly useful in this project for investigating the newly discovered flavin reduction reaction by hydrogenase enzymes.

Enzymatic reactions proceed via the formation of an enzyme-substrate complex, ES which exists transiently before formation of the product. A simple reaction can then be represented as

$$E + S \rightleftharpoons ES \rightarrow P + E \qquad 1$$

Where E is the enzyme, S is the substrate, P is the product and ES is the enzyme-substrate complex

This reaction takes place in two steps: formation of the enzyme substrate complex, ES that is fast and reversible, followed by a slow product formation step accompanied by the dissociation of the enzyme and product. Assigning rate constants for the above reaction, and assuming the reaction is in the initial stage, we can write the equation as follows:

$$E + S \underset{k_{-1}}{\overset{k_1}{\rightleftharpoons}} ES \xrightarrow{k_2} P + E \qquad 2$$

Under these conditions, the reverse reaction of P and E to form S can be ignored. The rate constants k_1 and k_{-1} denote the rate of formation of the ES complex and rate of dissociation of the ES complex

respectively. The formation and dissociation of ES is very rapid because it only involves the forming and breaking of non-covalent bonds.

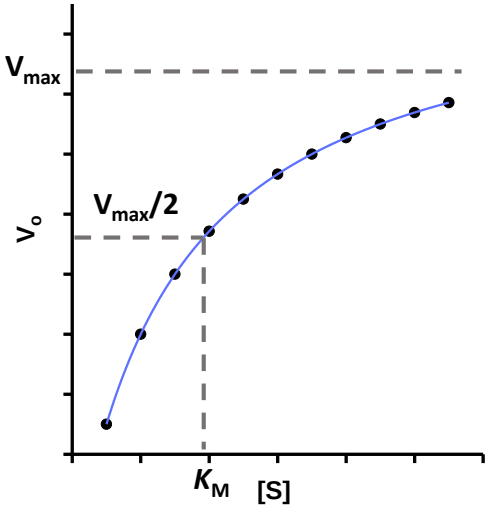


Figure 2. 21. A typical plot of velocity vs substrate concentration for an enzyme catalysed reaction that obeys the Michaelis-Menten equation.

2.5.1. Michaelis-Menten equation

The Michaelis-Menten equation gives an algebraic expression that relates reaction velocity and substrate concentration of an enzymatic reaction according to equation 4. A typical plot of initial velocity, V_o vs substrate concentration [S] is shown in Figure 2. 21. From the graph, it can be seen that at a high substrate concentration, there is negligible change in the initial velocity and hence, at this stage the amount of enzyme becomes rate limiting. At lower substrate concentration however, initial velocity varies greatly with changes in the substrate concentration. Thus the curve obtained for V_o vs [S] is a rectangular hyperbola of the equation:

$$y = \frac{ax}{b+x} \qquad 3$$

Where,

a is the asymptote of the curve,

b is a point on the x axis corresponding to the value of a/2

In an enzymatic reaction, y would denote the initial velocity, V_o and x, the substrate concentration. The value of the asymptote would denote V_{max}, the maximum velocity of the reaction. b denotes the Michaelis-Menten constant which can be defined as the concentration of the substrate at which V_o is equal to ½ V_{max}, giving the following equation:

$$V_o = \frac{V_{max}\,[S]}{K_M + [S]} \qquad 4$$

This is the Michaelis Menten constant proposed by Leonor Michaelis and Maud Menten which forms the basis for any enzyme kinetic study.

2.5.2. Derivation of the Michaelis-Menten constant

The Michaelis-Menten equation can be derived in two ways:

I. Rapid equilibrium assumption, which assumes the association and dissociation of the ES complex is very fast, such that at any given time, this reaction is in equilibrium.
II. The steady state assumption where ES reaches a steady state immediately after the substrate is added to the enzyme. This is also the widely accepted derivation and will be discussed next.

The steady state derivation assumes a period of time during which the rates of formation and decomposition of the enzyme substrate complex, ES is equal such that the concentration of the enzyme substrate complex is constant. If we assume a constant steady state concentration of ES, then the rate limiting step is

$$ES \rightarrow E + P \qquad 5$$

And the velocity can be written as

$$V_o = k_2[ES] \quad (6)$$

Since the formation and dissociation of ES occurs at equal rates, we can apply the steady state approximation to ES, that leads to

$$\frac{d[ES]}{dt} = k_1[E][S] - k_2[ES] - k_3[ES] = 0 \quad (7)$$

$$k_1[E][S] - k_2[ES] - k_3[ES] = 0 \quad (8)$$

Upon rearranging,

$$k_1[E][S] = (k_2 + k_3)[ES] \quad (9)$$

$$\frac{k_2+k_3}{k_1} = \frac{[E][S]}{[ES]} = K_M \quad (10)$$

$$[ES] = \frac{[E][S]}{K_M} \quad (11)$$

The total enzyme concentration can be expressed as E_{total} which includes the free enzyme, E and the substrate bound enzyme ES.

Therefore,

$$E_{total} = E + ES \quad (12)$$

Substituting these values in equation (11), we get

$$[\mathrm{ES}] = \frac{([\mathrm{E_{total}}]-[\mathrm{ES}])[\mathrm{S}]}{K_\mathrm{M}} \quad 13$$

Further rearranging,

$$[\mathrm{ES}] = \frac{[\mathrm{E_{total}}][\mathrm{S}]}{K_\mathrm{M}+[\mathrm{S}]} \quad 14$$

At the maximum reaction rate, V_{max}, all the enzyme would remain bound to the substrate and so [ES] will be equal to $[E_{total}]$

$$\mathrm{V_{max}} = k_2[\mathrm{E_{total}}] \quad 15$$

Substituting the expression for [ES] from the equation 14, into equation 6, and combining it with equation 15, we get the Michaelis-Menten equation as shown below:

$$\mathrm{V_o} = \frac{\mathrm{V_{max}}[\mathrm{S}]}{[\mathrm{S}]+K_\mathrm{M}} \quad 16$$

In equation 16, when K_M becomes equal to [S], then V_o can be written as

$$\mathrm{V_o} = 0.5\mathrm{V_{max}} \quad 17$$

Thus, K_M can be defined the substrate concentration at which an enzyme catalyses a reaction at half its maximum rate (V_{max}). Generally, a lower K_M value indicates greater affinity of an enzyme to its substrate and vice versa. Determination of K_M for the Hyd1 catalysed reduction of flavins were done using UV-visible spectroscopy and are discussed in detail in chapter 3.

2.5.3. Enzyme inhibition[202,203]

An enzymatic reaction can sometime be slowed down or completely terminated by the presence of molecules called inhibitors (I) that interfere with enzyme activity. Enzyme inhibitors are already present in cells and are important components that aid in regulating metabolism. Based on the type and mechanism of action, enzyme inhibition can happen in two ways:

I. Reversible inhibition – competitive, uncompetitive and non-competitive binding
II. Irreversible inhibition

Consider an enzyme (E) and inhibitor (I), forming an equilibrium with the enzyme-inhibitor complex (EI), then their dissociation constant K_i (in this case, inhibition constant) can be given by the following equation:

$$\mathrm{E} + \mathrm{I} \rightleftharpoons \mathrm{EI} \qquad 17$$

$$K_\mathrm{d} = K_\mathrm{i} = \frac{[\mathrm{E}][\mathrm{I}]}{[\mathrm{EI}]} \qquad 18$$

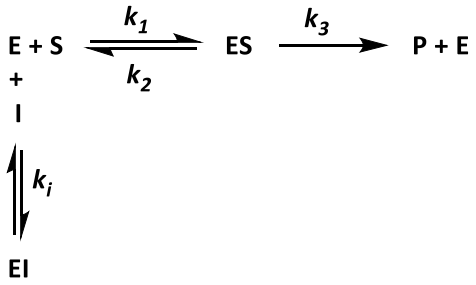
2.5.3.1. Reversible inhibition

Reversible inhibitors bind to the enzyme through weak, non-covalent forces that also bind the substrate and product. Reversible inhibitors can further be categorised as competitive, uncompetitive and non-competitive inhibitors.

Competitive inhibition

The most common type of inhibition in biochemistry is the competitive inhibition, where the inhibitor binds to a free enzyme forming an EI complex. Since the active site in the enzyme is now occupied by the inhibitor, the substrate can no longer bind to the enzyme and the EI complex cannot participate in catalysis. This type of inhibition is called the classical competitive inhibition. In some cases, the

inhibitor can bind at a different site in the enzyme, altering the substrate binding site such that the enzyme can no longer bind to the substrate. This type of inhibition is called a non-classical competitive binding and is commonly observed in allosteric enzymes. In the presence of both substrate and inhibitor, the ratio of ES and EI complexes in the reaction depends on the concentration of the substrate and inhibitor and their affinities for the enzyme. Thus, the proportion of EI can be lowered by introducing more substrate, and it is possible to saturate the enzyme by adding suitably high concentrations of the substrate. From this understanding, two conclusions can be drawn for competitive inhibition: a) the maximum velocity, V_{max} is the same in the presence or absence of inhibitor because by adding more substrate it is possible to saturate the enzyme active; b) Since more substrate would be required to achieve half the enzyme population to be saturated with the substrate, K_M would appear to increase with increasing concentrations of a competitive inhibitor. The newly obtained K_M is called an 'apparent K_M' and the relevant kinetic scheme can be illustrated as below:

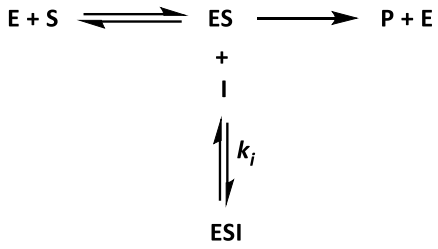


Scheme 1. A simple equation representing competitive inhibition.

Uncompetitive inhibition:

An uncompetitive inhibitor does not bind to the free enzyme, but only to the ES complex at a site different from where the substrate binds the enzyme. This results in an ESI complex, that is rather inactive and does not lead to catalysis. As a result, this type of inhibition alters the reaction rate

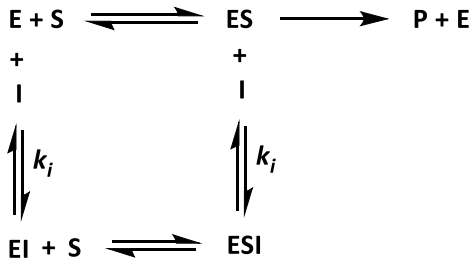
constant in the following ways: a) V_{max} is decreased due to the formation of inactive ESI complex. b) K_M also appears to decrease because the [S] required to achieve ½ V_{max} decreases. A kinetic scheme for this is shown below:



Scheme 2. A simple equation representing uncompetitive inhibition.

Non-competitive inhibition:

Non-competitive inhibitors can bind in two ways, either to the free enzyme or to the enzyme substrate complex, forming an ES or ESI complex respectively, albeit at a site different from the enzyme binding site. In a classic non-competitive inhibition, we observe an apparent decrease in V_{max}, but no change in K_M is detected. However this type of inhibition is uncommon among enzymes, and in most cases a change on V_{max} as well as K_M are observed. This is referred to as mixed inhibition.



Scheme 3. An equation representing the non-competitive mode of inhibition.

Table 2. 2. The effect of reversible inhibitors on apparent V_{max} and apparent K_M

Type of inhibitor	**Apparent V_{max}**	**Apparent K_M**
Competitive	No change	Increases
Uncompetitive	Decreases	Decreases
Non-competitive	Decreases	No change

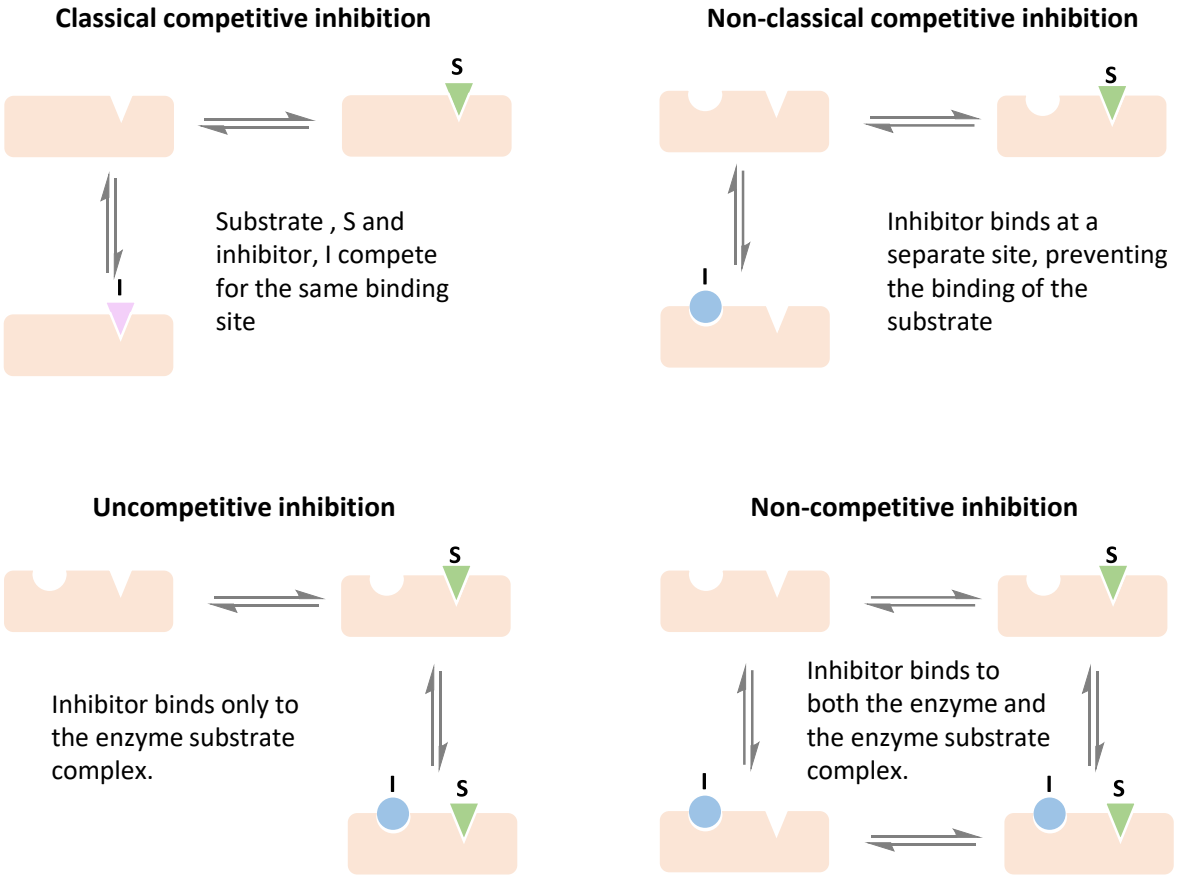


Figure 2. 22. Illustration of the different types of inhibition to enzyme catalysed reactions adapted from reference 202.[202]

2.5.3.2. Irreversible enzyme inhibition

During irreversible enzyme inhibition, an inhibitor forms strong covalent bonds with specific functional groups at an enzyme active site (and sometime also causes damage) which is vital for catalytic activity. Irreversible inhibitors are helpful in understanding reaction pathways. For instance,

if an irreversible inhibitor that can specifically bind to an amino acid residue is added to an enzyme, loss of enzyme activity after inhibitor addition can help identify amino acids with significant catalytic functions.

2.6. Chemicals and reagents

2.6.1. Gases

H_2 gas used during the experiments were supplied in high purity from compressed gas cylinders from BOC. Prior to using, all solvents and DI water were degassed to remove any dissolved oxygen by flushing them with nitrogen gas overnight.

2.6.2. Buffers

All experiments in this project were performed using buffered solutions. This was to facilitate enzyme activity because different enzymes function optimally at specific pHs. Almost all experiments were performed using 50 mM Tris-HCl buffer. Temperature dependent studies were done using phosphate buffers which provided more pH stability to the wide temperature range. Additionally, a mixed buffer was used to study enzyme behaviours at a broad of range of pH (pH 4–9). The pH values of buffers were monitored using a Mettler Toledo Seven Compact^{TM} pH meter.

All buffers were prepared by dissolving a required mass of the buffer salt in the required amount of deionised water to obtain desired concentrations. Tris buffers were prepared using Trizma Base purchased from Sigma Aldrich and their pHs were adjusted by adding dropwise solutions of 3 M HCl. All buffers were degassed with nitrogen gas before use in reactions. Phosphate buffers were prepared from Dipotassium hydrogen phosphate and potassium dihydrogen phosphate salts from Fisher Scientific. A required concentration of both the solutions were prepared and one solution was titrated against the other until the desired pH was attained.

Mixed buffers were prepared by dissolving the following salts. The solutions were then titrated with either HCl or KOH solutions to reach the desired pH's.

Table 2. 3. A list of all the components and their respective quantities used to prepare the mixed buffer

Component	**Commercial source**	**Concentration (mM)**	**MW (g/mol)**	**Mass required for 100 mL volume (g)**
NaCl	Sigma	100	58.44	0.5844
MES hydrate	Sigma Aldrich	15	213.24	0.3198
HEPES	Free acid, Melford	15	238.3	0.3575
TAPS	Sigma Aldrich	15	243.3	0.3650
CHES	Sigma Aldrich	15	207.3	0.3110
sodium acetate	Anhydrous, Fisher	15	82.03	0.1230

2.6.3. Cofactors

FAD (disodium salt, ≥98%, Cayman Chemical Company), and FMN (monosodium salt dihydrate, Applichem Panreac), NAD^+ (β-Nicotinamide adenine dinucleotide, anhydrous, 97.5%, Prozomix), NADH (β-Nicotinamide adenine dinucleotide, reduced disodium salt hydrate, 99.8%, Prozomix) and $NADP^+$ (98.8%, Prozomix) were purchased and used as received.

2.6.4. Glovebox

Unless otherwise stated, all experiments were either setup or carried out in a glovebox (Glove Box Technology Ltd) under a protective N_2 atmosphere (O_2 < 3 ppm).

2.6.5. Substrates and standards

Ketoisophorone (2,6,6-trimethyl-2-cyclohexene-1,4-dione, ≥98%), dimethyl (*R*)-(+)-methylsuccinate, (*rac*)-dimethyl-methylsuccinate (98%), 4-phenyl-3-buten-2-one (99%) and 4-phenyl-2-butanone (98%), 1-acetyl-1-cyclohexene (97%) were purchased from Sigma-Aldrich. Cyclohexyl methyl ketone (95%) was purchased from Alfa Aesar. Dimethyl itaconate (98%) was purchased from Fluorochem. (6*R*)-levodione was obtained by Baker's yeast fermentation and was a gift from Dr. Adrie Straathof from the Delft University of Technology. GC standard (*rac*)-levodione was prepared following literature procedure[22]. All aqueous solutions were prepared with deoxygenated MilliQ water (Millipore, 18 MΩ cm). 2-Methyl-5-nitropyridine (95%) and 5-amino-2-methylpyridine (97%) were purchased from Alfa Aesar.

3

Chapter 3 Developing methods for H_2-driven flavin reduction

This chapter describes experiments to test whether NiFe hydrogenases can directly reduce flavin cofactors – FAD and FMN. The surprising observation that several hydrogenases can reduce flavin cofactors under H_2 is discussed in detail. Flavin reduction activity measured under different reaction conditions shows interesting results that help in understanding the mechanism of this reaction. Results from these reactions also demonstrate the robustness of this system showcasing hydrogenases as a promising and potential flavin recycling catalyst.

3.1. Reduction of FMN and FAD by Hyd1

Figure 3. 1. presents the results of the UV-visible activity assay designed to test whether Hyd1 can reduce flavin cofactors – FMN and FAD under H_2. The UV-visible spectroscopy of flavins in their oxidized and reduced states is discussed in the previous chapter and this reduction reaction can be followed spectrophotometrically.

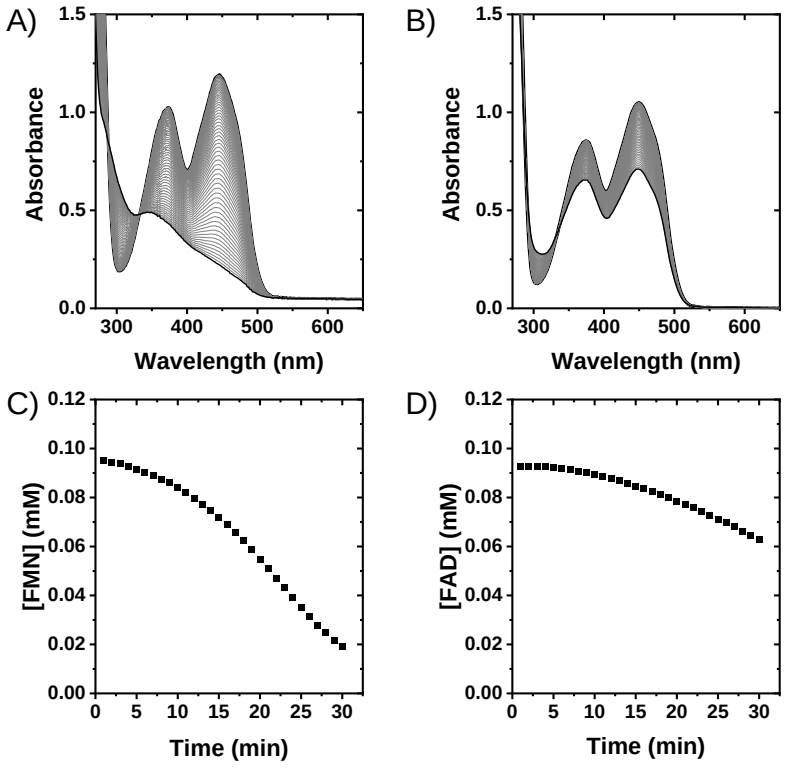


Figure 3. 1. Activity assay for H_2-driven Hyd1 reduction of flavins measured by *in situ* UV-visible spectroscopy. A) Hyd1 reducing FMN. B) Hyd1 reducing FAD. C) Calculated [FMN] based on λ_{max} = 445 nm (ε = 12.50 mM^{-1} cm^{-1}). D) Calculated [FAD] based on λ_{max} = 450 nm (ε = 11.30 mM^{-1} cm^{-1}). [FMN] and [FAD] were calculated from Beer-Lambert law using the absorbance value obtained during the activity assay. The linear phase of the slope of [flavin] vs time was used for calculating initial enzyme activity.

Reaction conditions: 800 µl scale, 0.1 mM flavin, 38 µg Hyd1 in Tris-HCl buffer (50 mM, pH 8.0, 25 °C) under a flow of H_2 in the cuvette headspace.

Experimental procedure for the activity assay performed is described in chapter 2, section 2.3.3. Reduction of the cofactors is monitored by the decrease in absorbance over time at λ_{max}=445 nm and λ_{max}=450 nm for FMN and FAD respectively. From panels A and B in Figure 3. 1., it is immediately clear that Hyd1 can reduce both FMN and FAD. The presence of clear isosbestic points at 330 nm can indicate the lack of side products. The reduction of flavins by Hyd1 is an unexpected observation because Hyd1 does not have a flavin catalytic site itself. The decrease in absorbance at 445 and 450 nm, indicates that the concentration of FMN and FAD respectively decreases, and that their reduced forms are being generated. Since there are no new peaks formed by the reduced flavin forms, unlike

in nicotinamide cofactors, a plot of [flavin] vs time was drawn with the obtained absorbance values using the Beer-Lambert law. The slope of the linear phase of this plot was used to calculate enzyme activity.

The discovery of this non-native activity is essentially the most important finding in this thesis that has resulted in the project taking exciting directions and its applications for several biocatalytic transformations. Panels C and D in Figure 3. 1. show the plot of flavin concentration vs time - a lag phase is generally observed at the beginning of the assay which is attributed to the well-characterised H_2-dependent activation phase for aerobically purified hyd1.[197] For this reason, Hyd1 was always activated under H_2 atmosphere before using it in the later reactions. The slope corresponding to the linear phase of the reaction was used to calculate the activity and specific activity of the enzyme.

Table 3. 1. Activity and specific activity calculated for flavin reduction by Hyd1

Entry	Cofactor	Activity (nmol min^{-1})	Specific activity (nmol min^{-1} mg^{-1})
1	FMN	2.9	76
2	FAD	1.2	32

The rate of reduction of FAD was slower when compared to that of FMN. This could not be explained by the difference in the thermodynamic driving force, because both FAD and FMN have similar reduction potentials.[204] It is hypothesised that this can be due the differences in the interaction of FAD and FMN at the protein surface. Clear explanations for this behaviour has not been studied in detail. Perhaps, crystal studies with the enzyme infused with the respective cofactor can yield interesting information. However, this exploration was beyond the scope of this thesis and has led to new research interests for further investigation within the group.

3.2. Control experiments for Hyd1 catalysed flavin reduction

The next set of experiments were focused on performing various control reactions. Similar procedures described for flavin reduction in the previous section were done without one or more components of the reaction mixture. This is helpful to confirm that both Hyd1 and H_2 are essential for efficient flavin reduction to take place.

3.2.1. Flavin reduction in the absence of molecular hydrogen

Figure 3. 2. presents the UV-visible spectra of the activity assay for the reduction of FAD and FMN using Hyd1 in the absence of H_2.

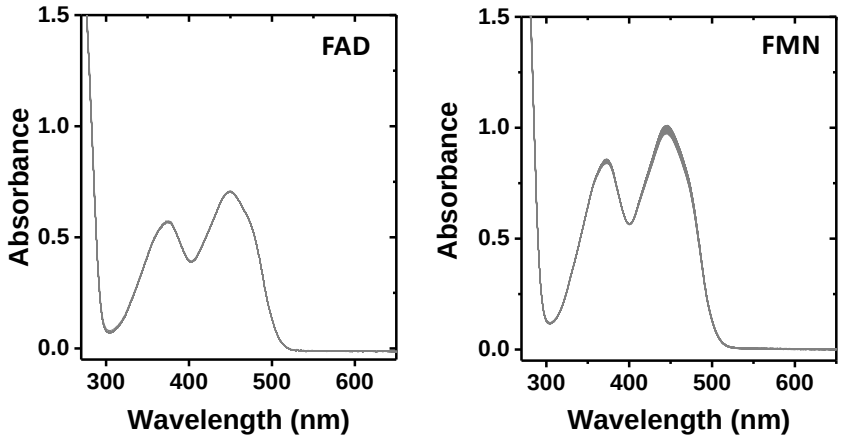


Figure 3. 2. UV—visible spectrum obtained for the background flavin reduction with Hyd1 present but no H_2. Reaction conditions: 800 µL scale, 0.1 mM flavin in Tris-HCl buffer (50 mM, pH 8, 25 °C), 40 µg Hyd1 at 25 °C.

The absence of any spectral change is indicative that no reduction has occurred, because no reductant was supplied to the reaction. Negligible specific activities of 0.06 nmol min^{-1} mg^{-1} and 2.08 nmol min^{-1} mg^{-1} for FAD and FMN respectively were measured.

3.2.2. Flavin reduction in the absence of Hyd1

Figure 3. 3. displays the UV-visible spectra obtained for the reduction of FMN and FAD in the absence of Hyd1 while it was still supplied with H_2.

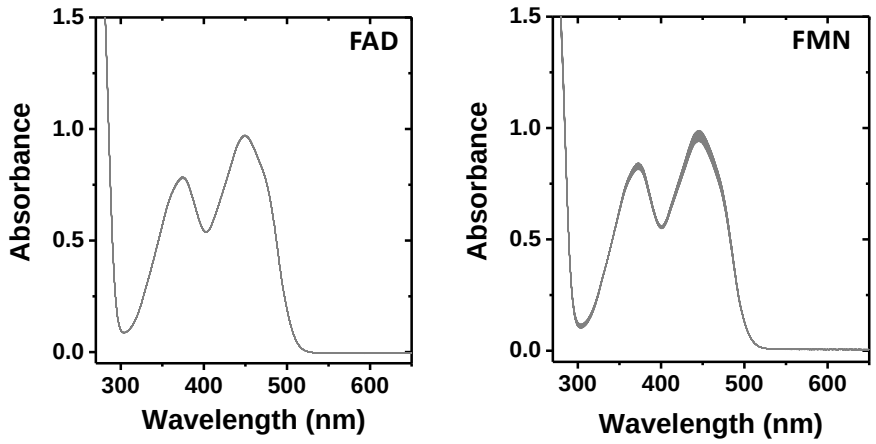


Figure 3. 3. UV-visible spectrum obtain for the background flavin reduction in absence of Hyd1, under H_2.

Reaction conditions: 800 µL scale, 0.1 mM flavin in Tris-HCl buffer (50 mM, pH 8, 25 °C), H_2 flow in cuvette head space, at 25 °C.

Results from this experiment indicate that Hyd1 is essential for flavin reduction to happen, because Hyd1 is required to catalyse the oxidation of H_2 in order to provide reducing equivalents for the reaction. The overall decrease in [FAD] and [FMN] amounts to 0.0 mM and 0.005 mM after 30 minutes respectively which is indeed negligible.

3.2.3. Flavin reduction in the absence of H_2 and Hyd1

Figure 3. 4. presents the UV-visible spectra obtained for the activity assays performed using reaction mixtures that contained neither H_2 nor the Hyd1, but just FMN or FAD.

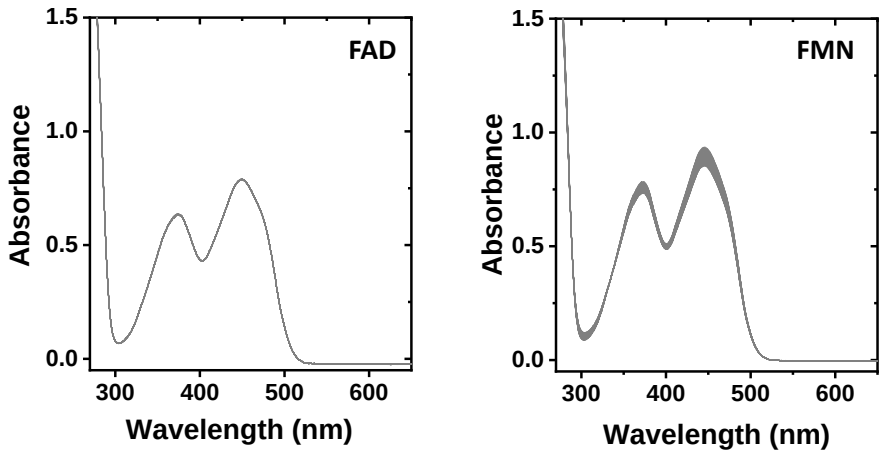


Figure 3. 4. UV-visible spectrum obtained for the background flavin reduction in the absence of both H_2 and Hyd1

Reaction conditions: 800 µL scale, 0.1 mM flavin in Tris-HCl buffer (50 mM, pH 8, 25 °C), at 25 °C.

The aim of this experiment was to test if factors like temperature or light (from the UV spectrophotometer) could lead to changes in absorbance that can potentially contribute to background activity for the duration of the assay (30 minutes). At 25 °C, the overall decrease in [FAD] and [FMN] at 25 °C amounts to 0.00 mM and 0.08 mM after 30 minutes respectively. Thus, there was no appreciable change in the absorbance as seen from Figure 3. 4.

In order to ensure that the flavins were also stable at elevated temperatures (50 °C to 70 °C) such that there was no unwanted change in absorbance from cofactor decomposition, a similar experiment was performed at 50 °C, 60 °C and 70 °C. The change in absorbance at the respective wavelengths measured for each reaction at that particular temperature was also negligible, implying that there was no appreciable decomposition of flavins upon exposure to light of 200–800 nm from the UV-visible spectrophotometer for the given duration of the assay and at that given elevated temperature. A clear picture that compares this result is shown in Figure 3. 6.

3.3. Effect of temperature on flavin reduction by Hyd1

Figure 3. 5. shows the results obtained for the reduction of flavins by Hyd1 at different temperatures ranging from 25° C to 70° C. All reaction mixtures were allowed to warm to the indicated temperature (pre-set on the Peltier accessory) at least for 5 minutes before beginning the experiment. Each assay was carried out by taking one scan (200–800 nm) every 30 seconds over 30 minutes. However, reactions times for the flavin reduction activity at different temperatures were not extended beyond 30 min.

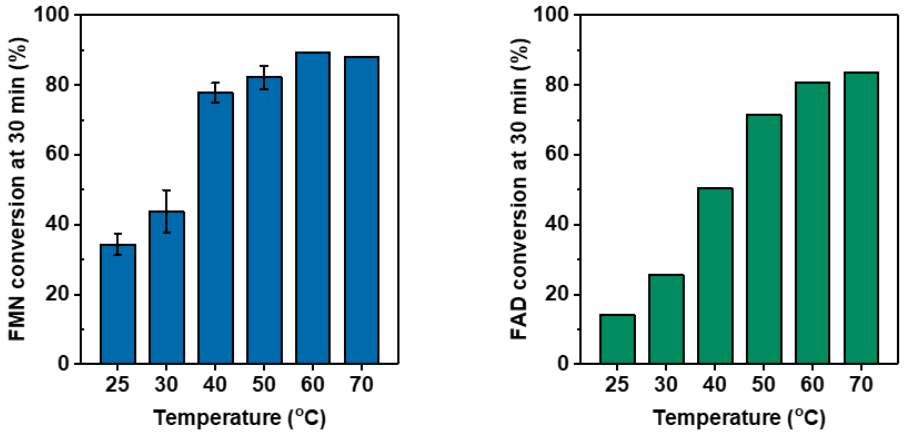


Figure 3. 5. Bar graph showing the %conversion of FAD (green) and FMN (blue) to $FADH_2$ and $FMNH_2$ respectively at various temperatures

Reaction conditions: 800 µL scale, 0.1 mM flavin, 0.0012 U Hyd1 under H_2-flow in phosphate buffer (50 mM, pH 8.0) at various temperatures. Conversions were calculated after 30 min using UV-visible spectroscopy.

An increasing trend in the activity with increasing temperature was seen with both the FMN and FAD, with FMN showing a higher activity at all temperatures compared to that observed in FAD. Flavin reduction activity beyond 70 °C was not explored, although this is technically possible. The chances of mild evaporation of the reaction mixture above 70 °C, might require careful handling of the experimental setup in order to obtain a clear UV-vis spectrum. Reactions for FMN were done in duplicate with the bar graph representing the average conversion values and the error bars indicating

the standard deviation. A similar reproducibility in results is expected to extend to the reduction with FAD. Experiments for FAD reduction at different temperatures, and for FMN reduction at 60 and 70 °C were not repeated due to time constraints caused by COVID-19 restrictions.

This temperature dependent activity data demonstrates the robustness of this system and validates the potential to couple this flavin recycling system to a broader range of enzymes including thermophilic enzymes.

Figure 3. 6. shows a graph comparing the conversion values obtained for the H_2-driven reduction of FAD and FMN with Hyd1 at different temperatures and the conversion values obtained for control reactions (no Hyd1, no H_2) that were also performed at elevated temperatures (25 °C, 50 °C–70 °C). These results showed that no appreciable background reduction occurs for reactions performed at elevated temperatures.

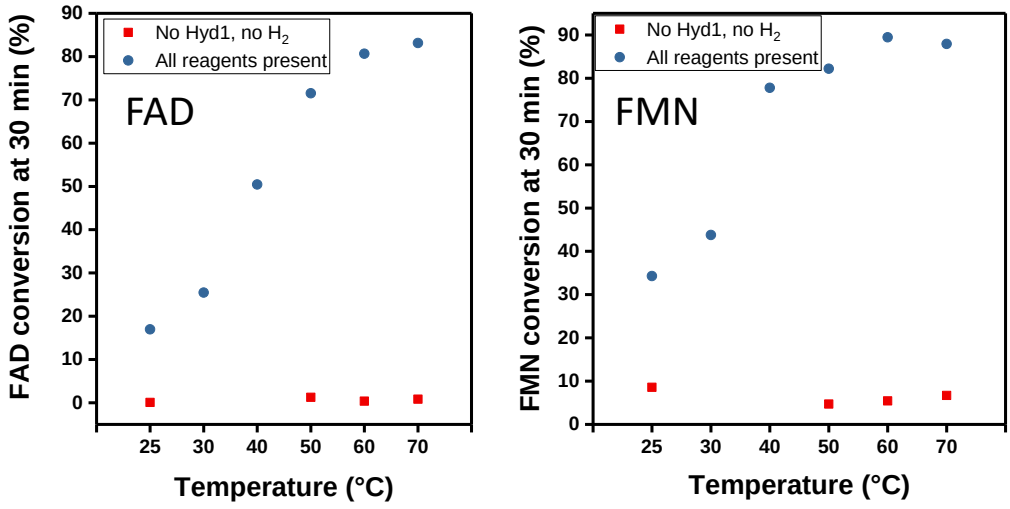


Figure 3. 6. Graphs showing %conversion of FAD and FMN to $FADH_2$ and $FMNH_2$ respectively at various temperatures for reactions with all reaction components present (blue circles) and control reactions (red squares) with no Hyd1 and no H_2.

3.4. Hyd1 samples with and without the cytochrome subunit

Hyd1 is a membrane bound periplasmic hydrogenase and in the cell, the enzyme is anchored to the cytoplasmic membrane by an integral membrane *b*-type cytochrome and a C-terminal transmembrane α helix. Once removed from the cytoplasmic membrane, the cytochrome *b* complex becomes unstable and is not usually observed in Hyd1 crystals.[138] However, the crystal structure of a Hyd1 variant complexed with its transmembrane domains and a single cytochrome subunit was obtained by Volbeda *et al*. (Figure 3. 7.).[139]

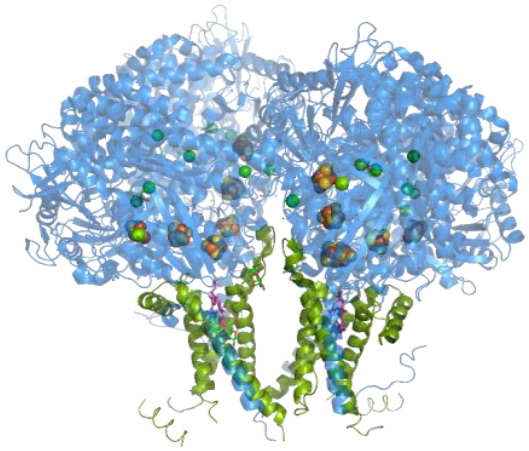


Figure 3. 7. Heterodimeric crystal structure of Hyd1 from *E. coli* in complex with cytochrome *b* (PDB code: 4GD3) obtained from a sample with mutationally generated medial cluster 4Fe4S.[139] The helical cytochrome *b* is shown in green.

It is expected that the cytochrome *b* has two haems, however only one haem proximal to the small subunit could be identified. Cytochrome *b* was initially considered as a physiological redox partner that was involved in sending electrons to the respiratory chain.[205] However, some studies also suggest that the main role of cytochrome *b* would be to anchor the hydrogenase to the membrane, if the function of Hyd1 itself was to provide aerobic shock protection rather than to engage in energy conversion.[139]

Hyd1 samples used throughout this project lacked the cytochrome *b* subunit. However, it was important to verify that the absence of cytochrome in the Hyd1 samples did not lead to drastic changes in the flavin reduction activity.

3.4.1. Reduction of FMN using Hyd1 enzyme that contains or lacks the cytochrome

Figure 3. 8. shows the UV-visible spectrum of the activity assay for FMN reduction under H_2 by the two forms of Hyd1 – with and without cytochrome, in order to determine whether the presence of the partner cytochrome, HyaC, impacts the flavin reduction activity. The rate of FMN reduction was not affected significantly by the presence or absence of cytochrome.

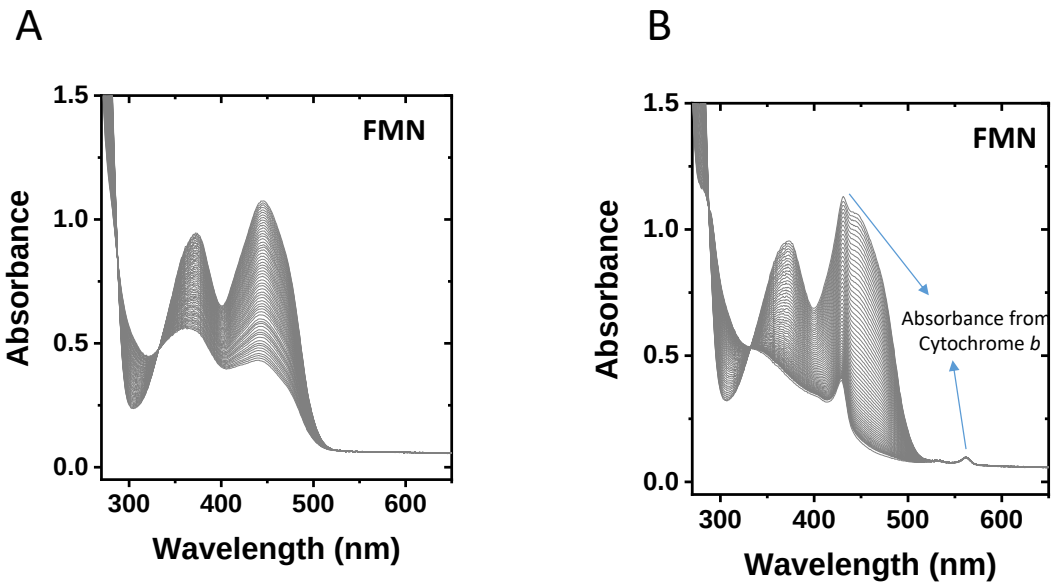


Figure 3. 8. FMN reduction under H_2 using a Hyd1 sample that A) does not contain the cytochrome and B) does contain cytochrome.

Reaction conditions: 800 µL scale, 0.1 mM FMN in Tris-HCl buffer (50 mM, pH 8, 25 °C), 40 µg Hyd1 expressed without the cytochrome gene (activated for 16 h under H_2) or 60 µg Hyd1 containing the cytochrome subunit (activated for 17 h under H_2) at 25 °C.

The two versions of Hyd1 for these experiments was provided by Wangzhe Li and Sophie Kendall-Price, with advice from Dr Rhiannon Evans (University of Oxford). Hyd1 with cytochrome was separated by gel filtration. Hyd1 without cytochrome was prepared from a strain lacking the hyaC

gene. The specific activity observed for FMN reduction by Hyd1 with and without cytochrome was determined to be 51.6 nmol min^{-1} mg^{-1} and 47.5 nmol min^{-1} mg^{-1} respectively. An absorbance change for oxidised vs reduced cytochrome is overlaid on the spectral changes from the FMN cofactor in panel B of Figure 3. 8. giving rise to a sharp peak at around 425 nm. Figure 3. 9 shows the absorption spectrum of Hyd1 purified with its cytochrome subunit. The blue spectrum is that of the anaerobically purified enzyme. The red spectrum is obtained after exposure of the Hyd1 sample to air for 4 h. Upon reduction of the same sample under 100% H_2 for 1 h, gives the spectrum in green.

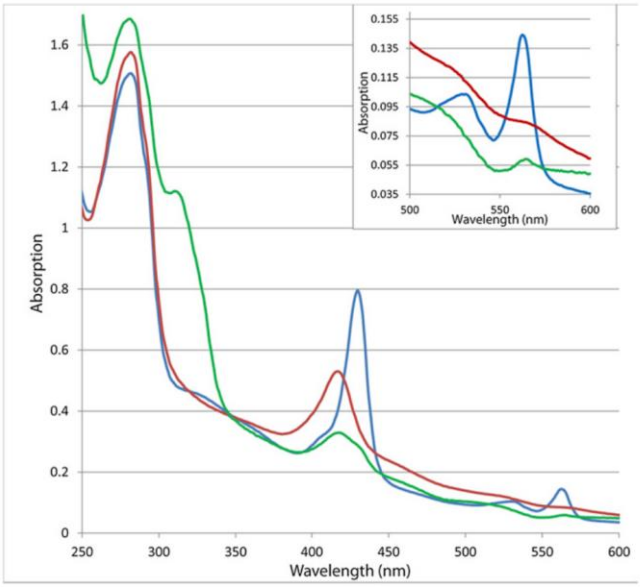


Figure 3. 9. UV-visible spectrum of *E. coli* Hyd1 with cytochrome *b* used for crystallisation. The sample after anaerobic purification showed an absorption peak at 429 nm and 562 nm (blue). The figure is taken from reference 139 with permission from Elsevier publisher: *Structure* **2013**, *21*, 184–190.[139] license number: 5240220838001.

3.5. Effect of pH on the reduction activity of Hyd1

The FMN reduction activity by Hyd1 was tested at various pHs ranging from pH 4–9. Reduction activity in terms of nmol flavin reduced per minute was calculated from UV-vis activity assays. To keep the buffer components the same for all the reactions, a mixed buffer was prepared and used for this reaction. Reactions at pH 4, 5, 7 and 9 were done twice to make sure the results are

reproducible. The highest activity for flavin reduction was observed at pH 4 and there was a significant decrease in activity at pH 8 and pH 9. The results from these experiments are shown in Figure 3. 10. with the bar graph representing the average activity for FMN reduction and the error bars representing the standard deviation.

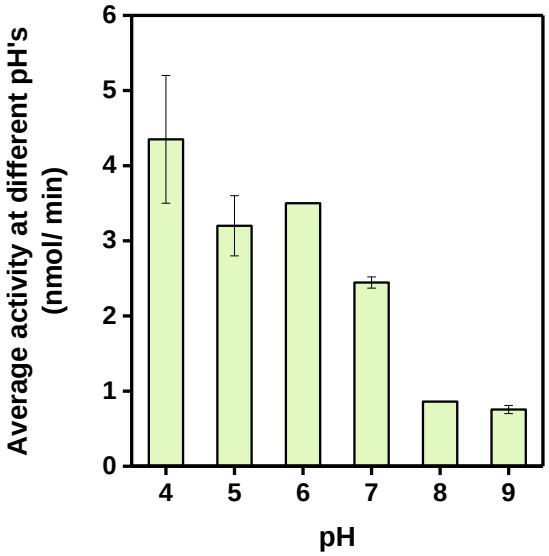


Figure 3. 10. Effect of pH on the FMN reduction activity by Hyd1.

This change in activity could not be attributed to thermodynamic effect because the $FMN/FMNH_2$ and the H^+/H_2 couples should change the same way with pH. Perhaps this behavior may arise from pH effects on hydrogenase activity due to the pK_a values of the residues involved in the proton transfer pathway. Alternatively, it could result from pH-related changes in surface protonation which affects the interaction between hydrogenase and FMN. The theoretical isoelectric point of Hyd1 is 6.04 (calculated using https://web.expasy.org/cgi-bin/compute_pi/pi_tool). The initial site in the proton transfer pathway in NiFe hydrogenases has been proposed to be a glutamic acid residue, as determined from experimental and computational studies. A complete picture of the proton transfer pathways in hydrogenases has however not been acquired so far.[206,207] The pK_a of the acid chain of

glutamic acid is 4.1, indicating that above a pH of 4.1, the acid side chain remains in its negatively charged deprotonated carboxylate form.

3.6. Flavin reduction by other hydrogenases

The reduction of flavin cofactors, FAD and FMN by other hydrogenases, other than Hyd1 was investigated. Flavin reduction activity was explored for two hydrogenases: Hydrogenase-2 (Hyd2) from *E. coli* and the NiFe hydrogenase from *Desulfovibrio vulgaris* Miyazaki F (DvMF)

3.6.1. Reduction of FMN and FAD by Hyd2

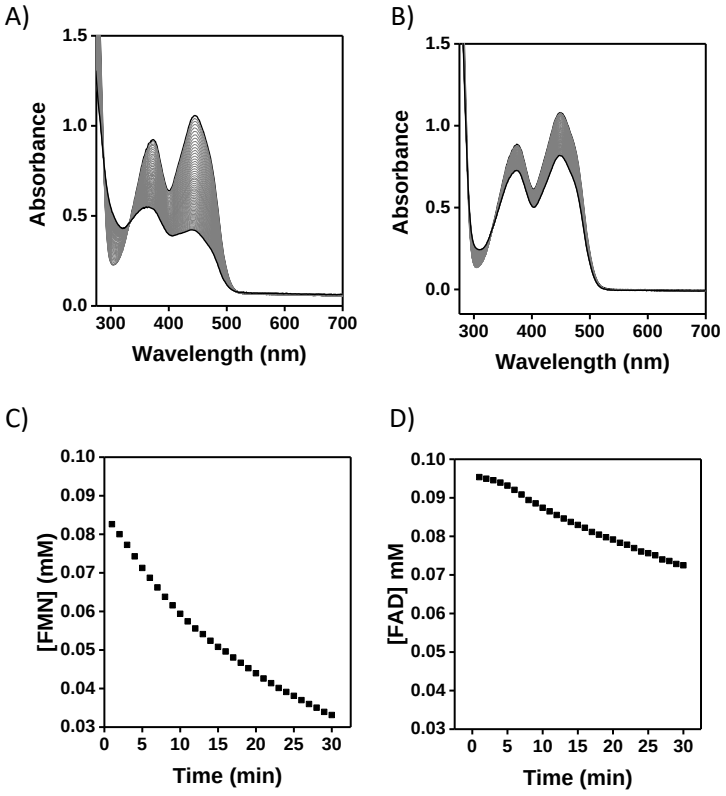


Figure 3. 11. Activity assay for Hyd2 catalysed reduction of A) FMN and B) FAD measured by *in situ* UV-vis spectroscopy, C) calculated [FMN] based on λ_{max} = 445 nm (ε = 12.50 mM^{-1} cm^{-1}), D) calculated [FAD] based on λ_{max} = 450 nm (ε = 11.30 mM^{-1} cm^{-1}).

Reaction conditions: 800 µL scale, 0.1 mM flavin, 0.044 mg mL^{-1} Hyd2 (activated under 1 bar H_2 for 20 h), Tris-HCl buffer (pH 8, 50 mM), at 25 °C.

Panels A and B in Figure 3. 11. show the UV-visible spectra of the activity assay performed for the reduction of FMN and FAD using Hyd2. The spectral changes show that Hyd2 is also capable of catalysing flavin reduction.

Hyd2 is relatively more O_2 sensitive and functions reversibly catalysing both H_2 oxidation and evolution efficiently. Like Hyd1, the slope corresponding to the linear phase of the reaction was used to calculate flavin reduction by Hyd2 (Table 3. 2).

Table 3. 2. Activity and specific activity calculated for flavin reduction by Hyd2

Entry	Cofactor	Activity (nmol min^{-1})	Specific activity (nmol min^{-1} mg^{-1})
1	FMN	1.1	31
2	FAD	0.6	17

3.6.2. Reduction of FMN and FAD by DvMF hydrogenase

Similarly, reduction of flavins by DvMF NiFe hydrogenase was also observed and their activities calculated as shown in Table 3. 3

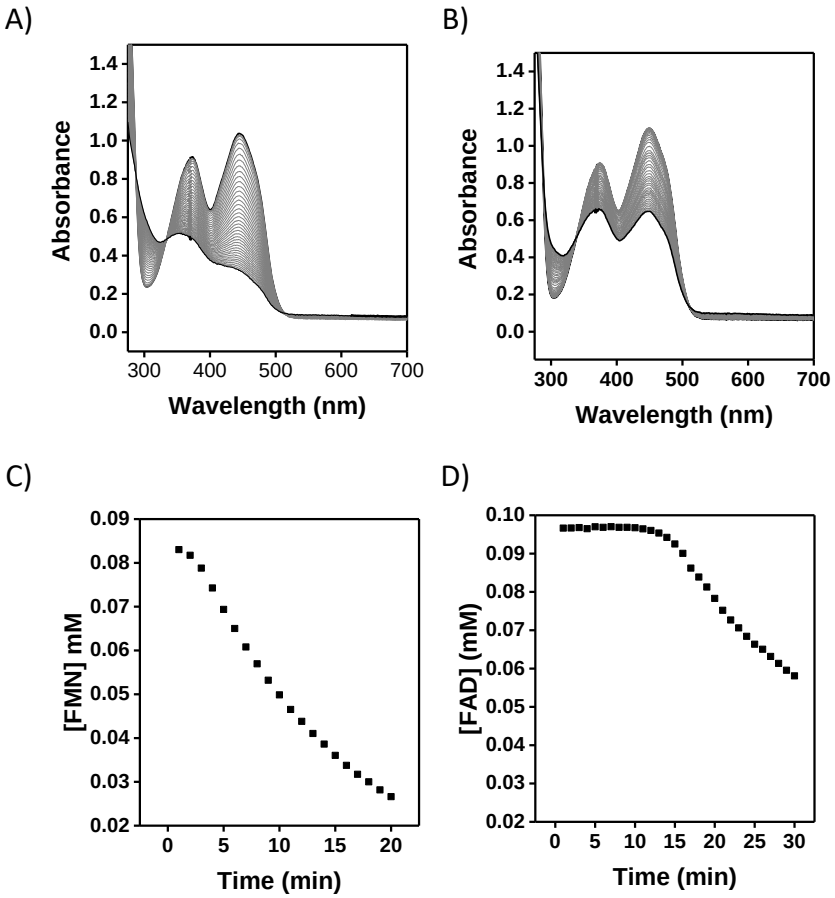


Figure 3. 12. Activity assay for DvMF catalysed reduction of A) FMN and B) FAD measured by *in situ* UV-vis spectroscopy, C) calculated [FMN] based on λ_{max} = 445 nm (ε = 12.50 mM^{-1} cm^{-1}), D) calculated [FAD] based on λ_{max} = 450 nm (ε = 11.30 mM^{-1} cm^{-1}).

Reaction conditions: 800 µL scale, 0.1 mM flavin, 0.045 mg mL^{-1} DvMF (activated under a flow of H_2 for 45 min), Tris-HCl buffer (pH 8, 50 mM), at 25 °C.

Table 3. 3. Activity and specific activity calculated for flavin reduction by DvMF hydrogenase

Entry	Cofactor	Activity (nmol min^{-1})	Specific activity (nmol min^{-1} mg^{-1})
1	FMN	2.5	70
2	FAD	1.8	51

For FMN, only a 20 minute activity assay was performed, however, nearly full conversion of FMN to $FMNH_2$ was observed during this reaction time.

Similar to Hyd1, the flavin reduction activity was higher for FMN when compared to that of FAD during reduction reactions by both the enzymes.

A direct comparison of the reduction activities by the two enzymes against the reduction activity by Hyd1 would not be fair due to differences in techniques used for enzyme activation under H_2. Alongside, there is uncertainty with regard to the activation states and purities of the enzymes. However, the experiments have helped confirm that a few other hydrogenases, apart from Hyd1 are also able to reduce oxidised flavins.

3.7. Kinetic studies to determine the K_M (Michaelis-Menten constant) of Hyd1 for FAD

K_M (or apparent K_M) values are helpful in determining an optimal substrate concentration to use for an enzyme catalysed reaction. In order to find a K_M value for the reduction of FAD by Hyd1, the reduction activity of Hyd1 for FAD reduction was measured at various concentrations of FAD and a plot of activity vs concentration would be expected to give a Michaelis-Menten curve from which the Michaelis-Menten constant can be calculated. FAD concentrations ranging from 0.025 to 5.5 mM were used for this reaction.

Absorbance values of FAD at 450 nm and 360 nm were too high to measure for the higher concentrations, but the absorbance at 512 nm could be used to calculate the concentration of FAD in accordance with Beer-Lambert Law. The calibration curve (Figure 3. 13 A) provided an extinction coefficient of $\varepsilon = 460\ M^{-1}\ cm^{-1}$ for FAD at 512 nm. Using this, the initial activity of Hyd1 for varying concentrations of FAD was recorded. However, there was a decrease in enzyme activity at higher FAD concentrations (≥ 3.5 mM) suggestive of inhibition or other adverse effect on the enzyme. In order to determine an effective or apparent K_M for the enzyme functioning at low flavin concentrations, only the first five data points were fitted to a hyperbolic function to determine an apparent K_M at low

flavin concentration. Figure 3. 13 B shows the Michaelis-Menten plot obtained for Hyd1 catalysed reduction of FAD under H_2. The data points corresponding to the blue circles and red squares each represent experiments performed on two different days under comparable conditions. The decrease in activity after 2.5 mM was observed during both the experiments, indicating a reproducible drop in activity at higher FAD concentrations. The observed decrease in activity at higher flavin concentrations could be due to substrate or product inhibition. New or abnormal precipitation indicative of protein denaturation was not observed indicating that high concentrations of flavin do not induce damage to the protein. Attempts have not been made to explain this effect, but the apparent K_M gives a useful working value to aid in the planning of biotechnology experiments designed to exploit the flavin recycling system.

Flavin concentrations in the later experiments were generally decided such that a biocatalytic reaction is accomplished in a suitably acceptable time frame (usually within 24 h) because increasing flavin concentrations can help speed up a reaction until a certain elevated concentration. On the other hand, working with lesser flavin concentration can result in higher flavin turnover numbers which becomes advantageous while performing reactions on large scale, because cofactors are expensive. So, investigating ways to minimise flavin concentration while not drastically compensating with reaction conversion and reaction time appeared important.

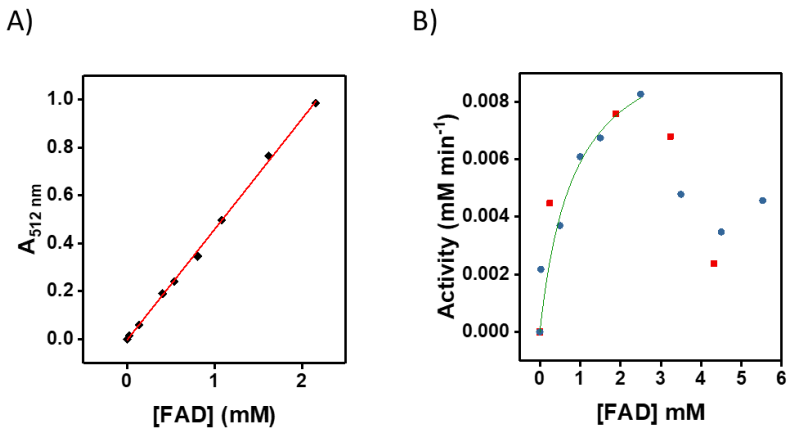


Figure 3. 13. A) Calculating the extinction coefficient for FAD at 512 nm. B) Michaelis-Menten plot to determine an apparent K_M = 0.9 ± 0.5 mM for Hyd1 catalysed reduction of FAD. The data points corresponding to the blue circles and red squares each represent experiments performed on two different days under comparable conditions. The Michalis-Menten curve was fitted only to the data represented by the blue circles.

3.8. Complete reduction of FMN to $FMNH_2$

Figure 3. 14 shows the UV-visible spectra of FMN (red) and $FMNH_2$ obtained upon reduction by Hyd1 under H_2 (yellow) and sodium dithionite (blue). A comparison of the two spectra from biocatalytic and chemical reduction is presented.

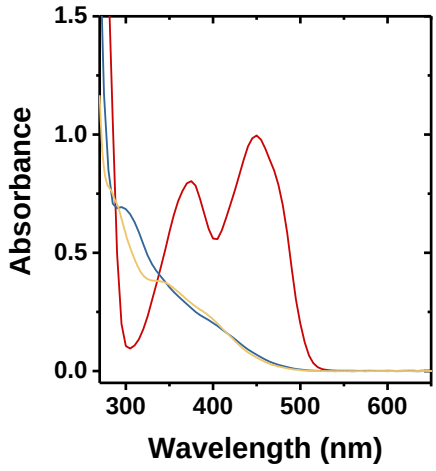


Figure 3. 14. UV-visible spectra of FMN (red) and $FMNH_2$ produced by Hyd1 under H_2 (yellow) or sodium dithionite (blue).
Reaction conditions for FMN reduction by Hyd1 (yellow): 800 µL scale, 0.08 mM FMN in Tris-HCl buffer (50 mM, pH 8, 25 °C), H_2 flow in cuvette head space, 57 µg Hyd1, at 25 °C. The full reduction of FMN by Hyd1 was completed during the experiment designed to test the stability of Hyd1 over time (>5 days).
Reaction conditions for FMN reduction by sodium dithionite (blue): 800 µL scale, 0.08 mM FMN in Tris-HCl buffer (50 mM, pH 8, 25 °C), 0.15 mM sodium dithionite, 25 °C.

Reduction with the Hyd1/flavin system showed the stability of this catalyst for extended reaction time. About 57 µg Hyd1 was activated under H_2 at *c.a.* 22 °C for 58 h, then incubated in 0.08 mM FMN under H_2 (1 bar) in a sealed vessel for 62 h. Upon release of H_2, $FMNH_2$ partially oxidised under the N_2 atmosphere to 0.05 mM FMN (determined using UV-visible spectroscopy). The Hyd1 and FMN/$FMNH_2$ solution was placed back under H_2, and full reduction to $FMNH_2$ was noticed after 3.5 h (Figure 3. 14, spectrum in yellow). Thus, following a 58 h activation period under H_2, plus 62 h of incubation with FMN and a 3.5 h of further FMN reduction experiment, shows that the Hyd1 was active for a total of 123 h at room temperature which is about 5 days. It must be noted that a 58 h activation time for Hyd1 might not be necessary based on previous information from literature, where an exhaustive activation of the enzyme was achieved by continuous saturation with H_2 for nearly 12-32 h under anaerobic conditions.[133,153]

The difference in absorbance at 315 nm is due to the background absorbance of sodium dithionite at this wavelength. Figure 3. 15 shows the UV Vis spectrum of 0.1 mM and 0.2 mM sodium dithionite in Tris-HCl buffer at pH 8.

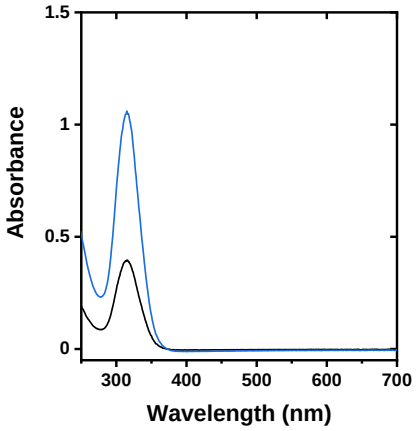


Figure 3. 15. UV-visible spectrum of 0.1 mM (black) and 0.2 mM (blue) sodium dithionite in Tris-HCl buffer (50 mM, pH 8)

3.9. Overview

Hyd1 has shown promising results for flavin reduction under varied experimental conditions. These results pave the way for exploring this system as a clean and straightforward flavin regeneration technique that can supply reduced flavins for enzymes that rely on them for catalysing valuable reactions. Determining flavin reduction activity under different experimental conditions has revealed the robustness of this system as a potential flavin regeneration catalyst. For instance, the increased activity for flavin reduction by Hyd1 at elevated temperatures is an exciting observation that expands the scope of combining this system with a broad range of enzymes. The ability of Hyd1 to stay active for nearly 123 h at room temperature demonstrate its high stability.

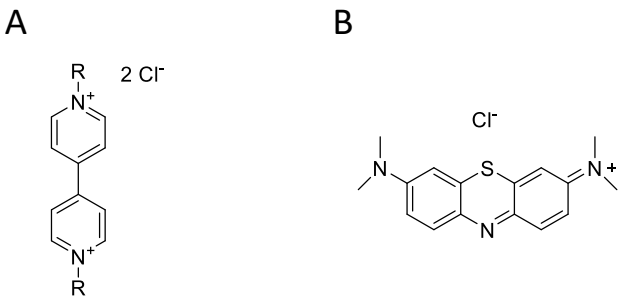


Figure 3. 16. Chemical structures of A) methyl or benzyl viologen and B) methylene blue

The mechanism by which flavin reduction takes place is however still unclear. The H_2 oxidation activity by Hyd1 is usually measured spectrophotometrically using artificial electron acceptors like methyl viologen and methylene blue whose chemical structures are shown in Figure 3. 16.[208] Similarly, the rate of H_2 production by hydrogenases is measured by the rate of oxidation of reduced methyl viologen.[197,209] Electrons from H_2 oxidation are relayed through FeS clusters where evidence suggests that benzyl viologen reduction happens rather than at the NiFe active centre.[210] With information from preliminary studies, it could be hypothesised that flavin reduction also happens

with electrons transferred via the FeS clusters. Following on from these primary results, the discovery of this new reactivity is expected to lead to interesting research explorations both in fundamental studies and applications in biotechnology.

4

Chapter 4 Coupling flavin regeneration to ene-reductases

The previous chapter discussed results relating to the application of various hydrogenases, in particular the Hyd1 enzyme, for effective and clean reduction of flavin cofactors, FAD and FMN. The stability of Hyd1 for prolonged durations and the ability to sustain catalysis at elevated temperatures led to further research to explore its potential as a cofactor recycling system to support catalysis by Old Yellow enzyme (OYE) ene-reductases. The significance of OYE ene-reductases in industrial applications and biotransformations are discussed in Chapter 1. This chapter will elaborate on the experimental procedures, reaction optimisation and outcomes for the application of Hyd1 as a flavin regeneration system to supply reduced flavins to two OYE ene-reductases: *Ts*OYE (provided by our collaborator, Dr Caroline Paul from TU Delft) and commercially sourced ene-reductases from Johnson Matthey to perform selective hydrogenation reactions.

4.1. Introduction

The reduction of unsaturated alkenes has remained a fundamental reaction type essential for synthetic procedures to prepare valuable chemical products. The chiral centres introduced through asymmetric alkene reductions are highly useful in pharmaceutical chemistry. However, as previously discussed in this thesis, the well-established conventional methods used for these chemical transformations have become unattractive due to many reasons such as high costs, exploitation of precious metals, high H_2 pressure, high catalyst loading and extensive separation techniques required for product purification. Therefore, it is critical to invent alternative methodologies that can circumvent such problems alongside fulfilling the environmental and economic needs of current industrial synthetic processes.[211] In this respect, ene-reductase enzymes have become particularly valuable in the fine chemical sectors for yielding highly selective products through the reduction of activated alkenes. Among many families of ene-reductase enzymes, those that belong to the Old Yellow Enzyme family are the most predominantly studied and used for asymmetric reduction reactions.[41,46,212]

4.2. Old Yellow Enzyme ene-reductases (OYE)

Old Yellow Enzyme (OYE) ene-reductases contain a tight, but non-covalently bound FMN cofactor which plays a central role in catalysis.[50] These enzymes are typically used with nicotinamide cofactors NAD(P)H as their hydride source which enables the reduction of the FMN cofactor present within the enzyme. The reduced FMN then transfers a hydride moiety to an activated alkene bringing about the asymmetric hydrogenation reaction. The cost of reduced nicotinamides NAD(P)H required for the functioning of such enzymes is prohibitively expensive necessitating the need for cost-effective hydride donors for viable industrial applications. A traditional method is to use a cofactor recycling system where $NAD(P)^+$ is continually reduced by a recycling enzyme that in turn depends on a sacrificial reductant. A typical example is the GDH/glucose system that uses a glucose dehydrogenase (GDH) enzyme which can reduce $NAD(P)^+$ to NAD(P)H by converting glucose into gluconolactone (Figure 4. 1.).

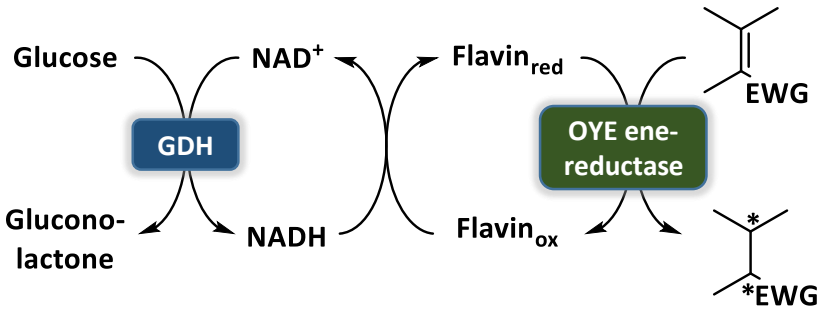


Figure 4. 1. Conventional enzymatic alkene reduction by OYE ene-reductase that employs a GDH/glucose recycling system for NAD(P)H regeneration. EWG stands for an electron withdrawing group.

Other known systems that work on the same principle include formate dehydrogenase/formate phosphite dehydrogenase/phosphite systems. This projects shows how the newly developed Hyd1/ flavin recycling system can be coupled to OYE ene-reductases for selective reduction of activated alkenes employing H_2 as the reductant. The use of H_2 as a clean reductant leaves no waste making this process atom-economical.

The application of Hyd1 for flavin regeneration was demonstrated for two categories of OYE ene-reductases:

I. *Ts*OYE from *Thermus scotoductus*

II. Commercial samples of numerous ene-reductases provided by Johnson Matthey

4.2.1. *Ts*OYE ene-reductase

*Ts*OYE ene-reductase is a cytoplasmic reductase found in the thermophilic bacterium, *Thermus scotoductus* SA-1 initially isolated from a gold mine in South Africa. This bacterium is known to possess two NAD(P)H dependent Fe(III) reductases – a membrane associated and a soluble Fe(III) reductase that can reduce Fe(III) to Fe(II).[213,214] Apart from Fe(III), several metals such as Mn(IV), Co(III)-EDTA, Cr(VI) and U(VI) also served as electron acceptors.[213] Amongst this diverse activity, the reduction of Cr(VI) by *Thermus scotoductus* gained much attention for potential application in chromate reduction. Cr(VI) is a carcinogen and a common environmental metal contaminant due to its unregulated release by industrial activity. By using bacterial chromate reductase, Cr(VI) can be reduced to the more harmless Cr(III) and this has hence stimulated interests in investigating this enzyme.[214,215] Later research revealed that the cytoplasmic chromate reductase (*Ts*OYE) from *Thermus scotoductus* SA-1 was homologous to the OYE ene-reductase, YqjM from *Bacillus subtilis* (50%) and XenA from *Pseudomonas putida* 86 (45%) which typically catalyse the reduction of C=C activated double bonds.[215,216] This finding led to the exploration of *Ts*OYE as an ene-reductase and it has been shown that it can selectively reduce α, β-unsaturated compounds covering a broad substrate scope with a preference for cyclic substrates. *Ts*OYE possesses a TIM (triose-phosphate isomerase) Barrel shape and exists as a homodimer in solution. The name triose-phosphate isomerase comes from the first enzyme containing this fold to be crystallised.

Tim barrel is a type of stable protein folding pattern, also called as the α/β barrel where the β sheet is folded and closed to form a barrel shape. α helix is a helical secondary structure whose stability arises from internal hydrogen bonds formed between their amino acids residues. β Strands on the other hand have a zig zag arrangement and often form β sheets through hydrogen bonding with nearby strands.[203] Nearly 10% of all known enzymes exhibit this TIM barrel shape and catalyse numerous reactions.[217] In a TIM barrel, there are eight parallel β strands each of which is attached to the other by an α helical segment. The β helices remain on the interior of the protein and covered by a total of 8 α helices.[202,218]

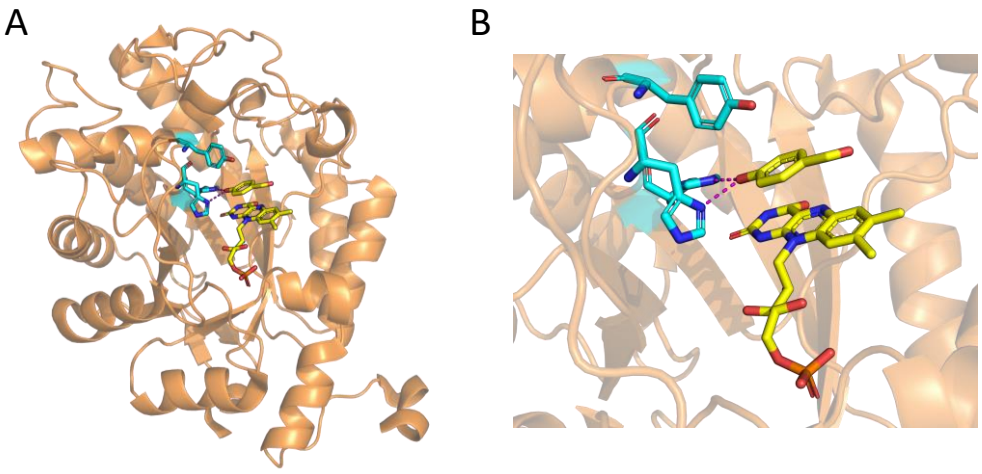


Figure 4. 2. A) Crystal structure of *Ts*OYE in complex with one of its accepted substrates *p*-hydroxybenzaldehyde (PDB code: 3HGJ). Stick figures in yellow represent the substrate stacked on top of FMN. Stick figures in blue show the nearby active site residues B) A close up of the active site showing the carbonyl interaction of *p*-hydroxybenzaldehyde with the nearby histidine residues during alkene reduction.

The molecular mass of the *Ts*OYE monomer is *c.a.* 36 kDa as observed in SDS-PAGE and the molecular mass of the native homodimer was found to be 72.4 kDa as determined from size exclusion chromatography.[215] As a thermostable enzyme, *Ts*OYE shows optimal activity at 65 °C which is attributed to additional proline residues, a characteristic of enzymes from the *Thermus* species. The presence of proline residues facilitate structural stabilisation at higher temperatures imparting thermostability to the protein framework. The reaction mechanism for alkene hydrogenation is

similar to that of any other OYE ene-reductase and is illustrated in Figure 4. 3. The carbonyl oxygen in the substrate forms hydrogen bonds with the active site histidine residues (His 172 and His 175) and the substrate lies in a parallel fashion above the *si*-face of the FMN cofactor.[219–222] As a result of hydrogen bonding, the C=C double bond gets polarised followed by nucleophilic attack at the β-carbon by a hydride from the FMN N_5 atom. A simultaneous trans- addition of a proton to the α-carbon takes place presumably from the Tyr177, thus saturating the α, β-unsaturated double bond.

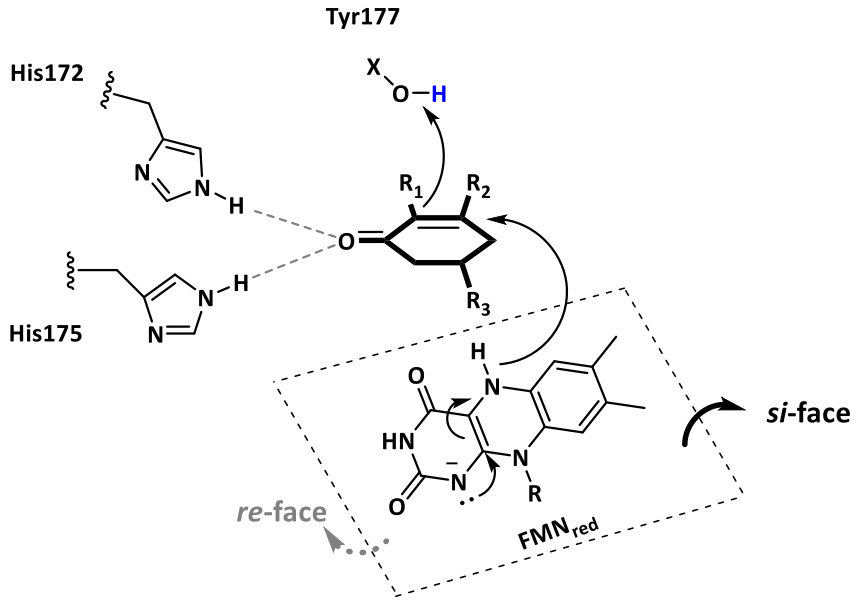


Figure 4. 3. An illustration of the hypothesised mechanism for OYE ene-reductase catalysed alkene reduction adapted from reference 223.[223]

4.2.1.1. Developing a H_2-driven system for the reduction of ketoisophorone (1) to (*R*)-levodione (2) using *Ts*OYE and the Hyd1 recycling system for flavins

*Ts*OYE enzymes require the continuous supply of reducing equivalents to catalyse alkene reductions, as discussed previously. Therefore it was investigated whether the Hyd1 flavin recycling system could be coupled to *Ts*OYE to supply reduced flavins for alkene hydrogenation catalysis. *Ts*OYE is already known to accept a varied range of activated alkenes. Ketoisophorone is among its well-known accepted substrates and previous reports are available, where this reaction was explored for the

application of different flavin regeneration catalysts.[103,224] This offered a benchmark to evaluate the Hyd1 flavin recycling catalyst during later stages. A simple reaction scheme for this reaction is shown in

Figure 4. 4.

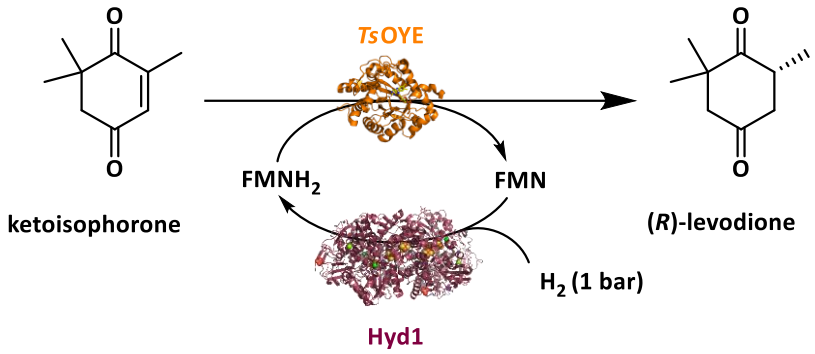


Figure 4. 4. Hyd1 flavin recycling system coupled to *Ts*OYE catalysed reduction of ketoisophorone to (*R*)-levodione.

4.2.1.2. Reaction setup and optimisation for the reduction of 1

All reduction reactions were done in a pressure vessel following experimental procedure outlined in Chapter 2, section 2.3.1. Using the pressure vessel prevented unnecessary loss of volatile substrates and products due to evaporation and facilitated accurate measurements of reaction conversions by gas chromatography (GC). *Ts*OYE has been shown to remain active over a broad pH range with more than 50% of its maximal activity retained over pH 5–9.[224] Since flavin reductions by Hyd1 were predominantly studied at pH 8, initial reactions for alkene hydrogenations were also conducted at pH 8 using Tris buffer (pH 8, 50 mM). As well as being pH tolerant, *Ts*OYE is also known to tolerate several organic solvents such as DMSO, methanol, 2-propanol, ethanol and acetonitrile at varying solvent ratios showing activity up to 40 vol% of the organic solvent. However, with increasing co-solvent concentration, varying degrees of activity loss were observed for different solvents, with the best tolerance recorded for DMSO which showed good activity retention at 40 vol%.[224] Therefore, reactions with *Ts*OYE in this project were done with just 1 vol% DMSO in the total reaction mixture.

Reactions were usually 600 µL in volume which was ideal for monitoring conversions of multiple reactions within centrifuge tubes placed inside a pressure vessel for reaction optimisation. A standard volume of 10 µL *Ts*OYE was used for all reactions, and this parameter remained unaltered for most reactions, as the aim was to assess the Hyd1 system for flavin recycling. A volume of 10 µL enzyme, gave a total *Ts*OYE concentration of 3.3 µM in the reaction mixture which is an optimal concentration used for biotransformations of up to 10 mM ketoisophorone.[224] This concentration corresponded to a total of 72 µg *Ts*OYE in the reaction mixture. Reactions were allowed to run for a minimum of 24 h and at least 3 time points were taken for each reaction at 1, 15 and 24 h. After charging with H_2, the pressure vessel was taken out of the glovebox and placed on a see-saw rocker to ensure adequate mixing of the reaction contents. All reactions were done at room temperature that varied between 20-22 °C. Conversions recorded for reaction optimisation are shown in Table 4.1

Table 4. 1. Optimising reaction conditions for the reduction of **1** to **2** using the Hyd1/flavin recycling system and *Ts*OYE

Entry	[**1**] (mM)	[FMN] (mM)	Conv. to **2** (%)[a]	Hyd1 TOF at 60 min (min^{-1})[b]	Hyd1 TTN[c]	FMN TN[d]
1	2	0.5	100	20.4	2,100	4
2	2	0.1	100	7.8	2,100	20
3	5	0.1	95 {100}	4.8	5,200	50
4	10	0.1	62 {97}	5.4	10,200	97
5	20	0.1	24 {37}	5.4	7,800	74
6[e]	20	0.1	{44}	8.4	9,300	88
7[f]	10	0.1	{94}	9.6	9,900	94
8[g]	20 then 24.2[h]	0.1	{29} then >99[i]	3.0	20,200[i]	240[i]

Reaction conditions: In accord with procedure outlined in chapter 2, section 2.3.1., using 57 µg Hyd1, 72 µg *Ts*OYE in Tris-HCl buffer (50 mM, pH 8), 1 vol% DMSO at room temperature (20 °C–22 °C). [a] GC conversion to **2** at 15 h {and 24 h}. [b] Hyd 1 turnover frequency (mol **2** per mol Hyd1 per min) was calculated after 60 minutes. [c] Hyd1 total turnover number (mol **2** per mol Hyd1) and [d] FMN turnover number (mol **2** per mol FMN) were determined at the end of the reaction. [e]4 bar H_2. [f]35 °C; some evaporation of **1** and **2** was observed from GC-FID. [g]71 µg Hyd1 was used. [h]Reaction was fed with additional 72 µg *Ts*OYE and 4.2 mM **1** at 66 h and 71 h, respectively. [i]Conversion, Hyd1 TTN and FMN TN were determined at 134 hours, additional time point data in Figure 4. 6.

Turnover number (TN) or total turnover number (TTN) corresponds to the moles of substrate converted into the product by one mole of Hyd1. Turnover frequency (TOF) is equal to the moles of substrate converted into the product by one mole of Hyd1 per minute. As a benchmark, the highest known turnover number recorded for an enzyme is that of the catalase, which is 4×10^7 s^{-1} and many enzymes relevant for biotechnology have shown to exhibit turnover numbers between 1 s^{-1} and 10^4 s^{-1}.

The first reaction (entry 1 in Table 4.1) was started with the lowest substrate concentration of 2 mM and a high cofactor concentration of 0.5 mM. High cofactor concentrations promote favourable conditions for product formation as the cofactor is essential for the ene-reductase to function. However, the drawback of using more cofactor, at least on an industrial scale is its relatively high cost

and hence it is ideal to keep the cofactor concentrations suitably low while optimising reaction conditions. This can also result in increased cofactor turnover number. Hence another reaction with the same substrate concentration (2 mM), but with a lower cofactor concentration of 0.1 mM FMN (see entry 2, Table 4.1.) was evaluated. Both entries 1 and 2 showed 100 % conversion after a 15 h reaction time, however the Hyd1 turnover frequency (calculated at 60 min) in entry 1, that received a higher FMN loading, was nearly 3 times higher than that observed for entry 2, which received 5 times less FMN. Since the concentration of Hyd1 was constant in both the reactions, the Hyd1 total turnover number remained the same.

Subsequent reactions with higher substrate concentrations and 0.1 mM FMN, were performed next, to examine the effect of substrate concentration on reaction performance. Conversions of 100% and 97% were achieved for 5 and 10 mM substrate concentrations after a 24 reaction time, and a maximum Hyd1 total turnover number of 10,200 was recorded. Conversion of 20 mM **1**, however showed a drastically low conversion of 37% which may be due to substrate or product inhibition issues. To test this, a series of reactions with varying concentrations of the substrate could be performed. With regard to product inhibition, perhaps a way to remove the excessive amount of product in the mixture can be a solution. This conversion later improved to 44% when the reaction was performed at 4 bar H_2 (compare entries 5 and 6 in Table 4.1.) which also showed increased Hyd1 turnover frequency (TOF) from 5.4 to 8.4 min^{-1}.

Chiral phase GC-FID chromatogram for the reduction of ketoisophorone

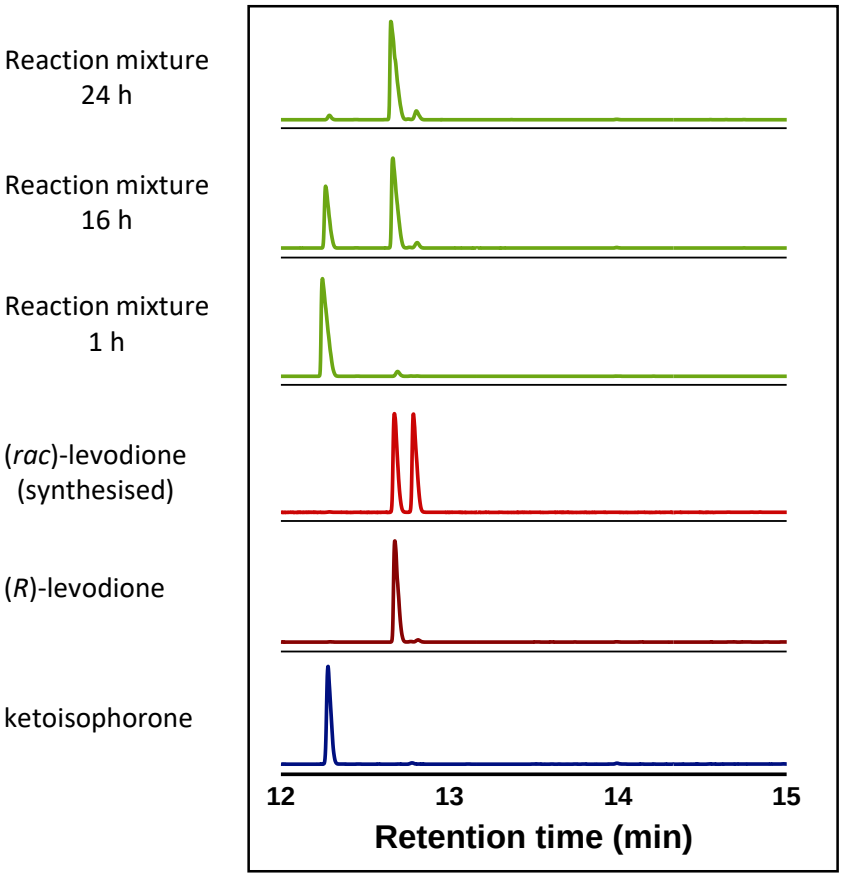


Figure 4. 5. Exemplary GC-FID results of ketoisophorone reduction (green) - ketoisophorone (purple, commercially available in ≥98% purity), (*rac*)-levodione (red, synthesised following literature procedure)[22] and (*R*)-levodione (burgundy, obtained from Baker's yeast fermentation and was a gift from Dr Adrie Straathof from the Delft University of Technology) standards.

All reaction mixtures were analysed using chiral GC-FID following the procedure outlined in chapter 2, section 2.4.2. Conversions and enantiomeric excess (*ee*%) were calculated based on the peak area of substrate and products appearing on the GC chromatogram. Samples for GC-FID analysis were prepared following procedure in chapter 2, section 2.4.2 and their chromatograms are attached in the appendix.

Both Hyd1 and *Ts*OYE are capable of sustaining catalysis at higher temperatures, so entry 4 was repeated at 35 °C (see entry 7) to test the effect of temperature on substrate conversion. A

conversion of 94% and nearly twice the TOF as that observed at room temp. (4.8 and 9.6 min^{-1} at room temp. and 35 °C respectively) were recorded. However, this result was not fully reliable, as GC-FID showed that some substrate and product evaporated due to elevated temperature. Ketoisophorone and (*R*)-levodione are volatile compounds having boiling points of *c.a.* 222 °C and 236 °C respectively. They may undergo evaporation at elevated temperatures leading to a different substrate-product ratio in the reaction mixture. The extent to which the substrate and the product has evaporated is also difficult to measure. This would affect the conversions determined from GC analysis, as they are calculated based on the ratio of substrate and product peak areas which has now been altered due to evaporation.

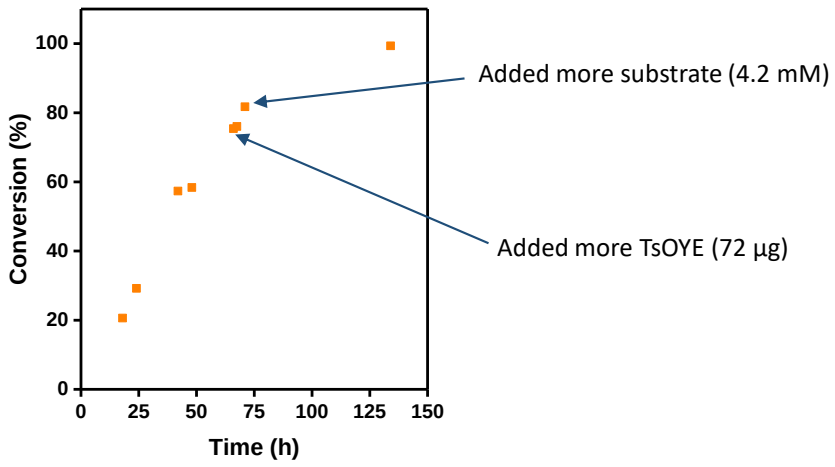


Figure 4. 6. Catalytic stability of Hyd1 for FMN recycling in the conversion of ketoisophorone to (*R*)-levodione over 134 h. This reaction corresponds to entry 8 in Table 4.1.

Entry 8 was a replica of entry 5, but focussed on monitoring the stability of the alkene reduction system over prolonged duration of time. The reaction received a higher Hyd1 loading of 71 µg. Reaction progress was monitored by taking multiple time points as shown in Figure 4. 6. At 66 h, more *Ts*OYE (72 µg) was added to check whether additional ene-reductase can influence reaction rate, however, no prominent change in conversion was observed. As the reaction neared completion at 77 h, an additional 4.2 mM ketoisophorone was added and allowed to continue catalysis. At 134 h,

the reaction was stopped for analysis although there was room to prolong the reaction by adding more substrate. GC-FID showed >99% conversion and the highest Hyd1 TTN of 20,200 and FMN turnover number of 240 were recorded. This experiment showed that Hyd1 flavin recycling system can sustain catalysis for 134 h (~ 5.5 days) with a steady reaction progression as shown in Figure 4. 6. This highest TTN of 20,200 is in the order of magnitude appropriate for use as a catalyst in pharmaceutical and fine chemical industries[225] and is comparable to values exhibited by commercial grade enzymes.[226]

Turnover frequencies for all reactions in Table 4.1. were calculated at 60 min. The highest TOF was 20.4 min^{-1} observed for entry 1 in Table 1.4. This reaction had only 2 mM substrate and showed nearly 50% conversion at 60 min which accounts for the high TOF. An elevated reaction temperature also showed higher TOF as inferred from comparing data in entry 4 and 7.

Enantioselectivity for all reactions was always >99% at the first time point at 60 min, however this decreased with increasing reaction time. At 15 h and 24 h, *ee* dropped to an average of approximately 93% and 88% respectively, due to a non-enzymatic racemisation of (*R*)-levodione in alkaline medium. This has been confirmed from a previous study that encountered a similar problem for the desired product.[223] Further investigation on the effect of pH and enzyme concentration on enantiopurity concluded that neutral pH (7) yielded better enantioselectivity. The racemisation of (*R*)-levodione occurs through enolisation because the molecule possesses an achiral α-carbon with an H atom. It is already known that enolisation is catalysed by either an acid or a base. Thus it is reasonable to observe that neutral reaction medium minimised racemisation and improved enantioselectivity.[223] This racemisation was also more pronounced for longer reactions due to a time dependent racemisation of (*R*)-levodione.[223] This was true for reactions in this project too where the lowest *ee* of 27% was recorded at 134 h for entry 8. Additionally it was noted that increasing temperature also leads to increased racemisation as seen in entry 7 that has an *ee* of 68%. Moving

forward, this undesirable product racemisation can be addressed using two useful strategies: a) *Ts*OYE has a broad pH activity range between pH 5 and 9 which makes it possible to run reactions at lower pH that can improve enantiopurity; b) the more time the product spends in the aqueous medium, the more racemisation occurs, so, shorter reaction times where possible can help to prevent unnecessary racemisation. Taking multiple time points for a reaction provides an estimated end-time for the reaction and helps to prevent longer reactions that lead to the unwanted racemisation.

4.2.1.3. Control experiments

Following reaction optimisation, the next set of reactions concentrated on control experiments where one or more reaction components were deliberately omitted from the reaction mixture. This is to ensure that there are no other side/ additional reactions contributing to product formation other than just the postulated reaction. Reaction conditions, enzyme and substrate loading for all control experiments were similar to the reaction in entry 4 in Table 4.1. and time points taken for analysis were at least 15 h or more. Reactions with only Hyd1 or *Ts*OYE did not lead to product formation indicating the two enzymes depend on one another to generate the product. In the presence of both the enzymes, but zero FMN, there was no conversion too. This shows that Hyd1 cannot reduce *Ts*OYE directly, and requires free soluble flavin for electron transfer. Likewise, reactions with just FMN with no enzyme also resulted in zero conversion, confirming that free FMN in solution does not have background ene reduction activity and also cannot react directly with H_2. The table below summarises the various combinations of enzyme and cofactor used for the control reactions.

Table 4. 2. Control experiments for H_2-driven ketoisophorone reduction

Entry	FMN	*Ts*OYE	Hyd1	Conversion to **2** (%)
1	✓	-	✓	0
2	✓	✓	-	0
3	-	✓	✓	0
4	✓	-	-	0

Reaction conditions: 600 µL scale, 0.1 mM FMN, 57 µg Hyd1, 72 µg *Ts*OYE , 10 mM **1**, Tris-HCl buffer (50 mM, pH 8.0, 25 °C), 1 vol% DMSO at room temperature (20–22°C) in a pressure vessel (1 bar H_2), 24 h.

4.2.1.4. Reproducibility

After control experiments, the alkene reduction system was tested for reproducibility as it is important to ensure that the system is reliable and enables smooth transitions for scale up and enzyme/ substrate scope expansion. For this experiment, three identical reactions were done, each in a centrifuge tube placed within the same pressure vessel to avoid differences in H_2 pressure. Time points were taken at 1 and 3 h and reaction mixtures were analysed by GC to determine their respective conversions. The results are tabulated in Table 4. 3.

Table 4. 3. Results from a triplicate reaction to prove the reproducibility of the reduction reaction of ketoisophorone.

Entry	**Conversion (%)**	
	1 h	**3 h**
1	17	44
2	17	48
3	19	53
Standard deviation	1	4
Standard error	0.6	2.5

Reaction conditions: 300 µL scale, 0.1 mM FMN, 71 µg Hyd1, 72 µg *Ts*OYE, 10 mM ketoisophorone, Tris-HCl buffer (50 mM, pH 8.0, 25 °C), 1 vol% DMSO at room temperature (20–30 °C) in a pressure vessel (1 bar H_2).

From the table it can be seen that standard deviations and standard error values calculated are within accepted values.

4.2.1.5. Comparison to other similar systems in the literature

In search of better flavin regeneration systems, numerous methods have been reported and their application with useful enzymes explored. A comparison of the Hyd1 recycling system with these

techniques is important to appreciate its advantages and disadvantages, and identify key factors for further improvement.

Hollmann and co-workers[227] coupled a direct photochemical regeneration of reduced FAD to a styrene monooxygenase, *Pseudomonas* sp. VLB120 (StyA) for the epoxidation of styrene. This system relied on the light driven reduction of FAD where the reaction mixture was illuminated using a light source and EDTA (ethylenediamine tetraacetic acid) was employed as the electron donor. It was interesting to note that this system could function only with FAD concentrations of *c.a.* >0.2 mM. At 0.1 mM FAD or less, there was no conversion. This behaviour was attributed to the inability of StyA to utilise such low concentrations of $FADH_2$. Above all, the intensity of light supplied significantly influenced the reaction rate – brighter light favoured higher conversion, however, beyond a certain intensity, more intense light lead to lower conversion owing to the photo decomposition of FAD when exposed to light for prolonged durations. A major downside of this system was the photo instability of FAD due to which the reaction did not progress after *c.a.* 1 h and the reaction yield did not exceed past 62%, although, the enantioselectivity for most reactions was >99%. A similar approach was followed in another study where OYE ene-reductase, YqjM from *Bacillus subtilis* was used *to* convert 2-methylcyclohexenone to (*R*)-2-methylcyclohexanone. [201] FMN was regenerated using commercial LED's as the light source and EDTA as the electron donor. This system had similar complaints of photodegradation of both the YqjM bound and free FMN. Under such conditions, a maximum FMN turnover number of 30–40 was recorded.[201]

Some photochemical regeneration techniques employed Rh(II) and Ir(III) based photosensitisers to regenerate OYE ene reductases.[228] The applicability of this system was demonstrated for two ene-reductases – TOYE from *Thermoanaerobacter pseudethanolicus* E39 and pentaerythritol tetranitrate reductase (PETNR) from *Enterobacter cloacae* PB2. Reactions were performed in a Triethanolamine

(TEA) buffer which also served as the sacrificial electron donor and methyl viologen was employed as the electron transfer mediator. All reactions were performed anaerobically and were illuminated using a 150 W halogen lamp. Minor side reactions from non-enzymatic activity were observed as a result of direct reduction of the substrate by the photosensitiser. Control reactions in the absence of the electron mediator, methyl viologen gave *c.a*. 4–8% conversion which could be due to a direct electron transfer from the photosensitiser to the enzyme bound FMN. The presence of several possible non-enzymatic side reactions necessitate laborious optimisation procedures, although most reaction yields and selectivity remained comparable to that obtained for traditional nicotinamide cofactors.

Lauterbach and co-workers[103] devised an enzymatic regeneration system for flavins using the NAD^+ reducing soluble hydrogenase (SH) from *Ralstonia eutropha* that couples H_2 oxidation to flavin reduction. Its application was demonstrated with three enzymes – *Ts*OYE, StyA and a recombinant peroxygenase from *Agrocybe aegerita* (rAaeUPO), each catalysing different biotransformations. Although this system uses H_2 like the Hyd1 system, the two enzyme systems engage in distinct reaction mechanisms making it interesting to study them as two separate systems. An illustration of flavin reduction by both the enzymes is shown in Figure 4. 7. In the SH from *Ralstonia eutropha*, flavin reduction is hypothesised to happen at the NAD^+ binding site, where the natively present FMN-b is temporarily substituted by free flavin and later released upon reduction by electrons mediated through the FeS clusters present within the enzyme framework.[103] Hyd1 on the other side, has a more simple composition, containing just the NiFe active site and a chain of FeS clusters (see chapter 1, for full structure description). Flavin reduction in Hyd1 is presumed to happen through electrons relayed through the FeS clusters rather than at the NiFe active site itself. This assumption is based on a previous report that investigated the reduction of benzyl viologen by Hyd1 which showed that benzyl viologen reduction is not possible when Hyd1 does not possess the small subunit which

accommodates the FeS clusters. This possibility has been ruled out in the SH, because the FeS clusters remain deeply buried inside the enzyme and hence only negligibly contributes to flavin reduction.[103] Nevertheless, both systems have showed a lower activity for FAD reduction in comparison to FMN which could be due to the differences in the structure of FAD and FMN and hence their mode of interaction with the protein. A striking contrast between the two systems was found in their respective control reactions. As discussed earlier, when the enzymes were present and with no flavin, the Hyd1 recycling system shows no conversion to the product. However, when SH is used for flavin recycling, detectable conversion was observed which, the authors of the paper attribute to direct electron transfer from SH to the flavin of OYE. [103] But, an alternative explanation is that electron transfer in solution could be facilitated by free FMN which has dissolved from the FMN-b site of the SH under reducing conditions.

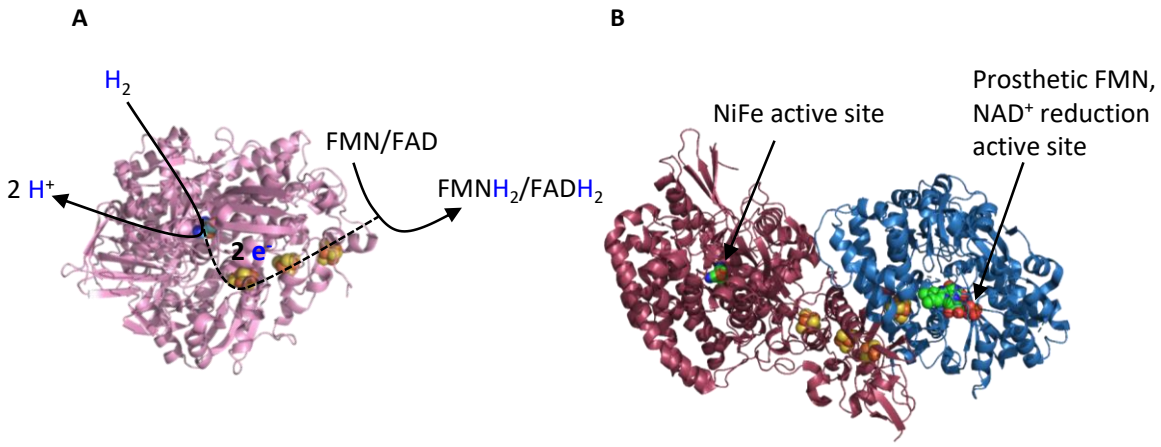


Figure 4. 7. Enzyme crystal structure and predicted reaction mechanism for H_2 oxidation and flavin reduction in A) Hyd1 from *E. coli* (PDB code: 3USE) and B) SH from *Ralstonia eutropha* (PDB code: 5XF9)

Table 4. 4. A summary of the total SH and flavin turnover numbers observed with each enzyme in the work of Lauterbach and co-workers[103]

Entry	Enzyme	Cofactor	SH TTN	Flavin TN
1	*Ts*OYE	FMN	8400	105
3	UPO	FMN	750	225
			46000 (immobilised)	
2	StyA	FAD	333	3.3

Entry 1 in Table 4.4. shows the highest flavin TN of 105 for ketoisophorone reduction by *Ts*OYE for a 16 h reaction. A direct comparison of the SH and Hyd1 systems could not be made due to differences in reaction conditions and catalyst loading of the two reactions. For instance, the SH recycling system received a higher catalyst loading of 0.2 mM FMN and 2.5 µM SH when compared to the Hyd1 flavin system where most experiments were performed using 0.1 mM FMN and only 0.95 µM Hyd1. Similarly, Lauterbach and co-workers performed these reactions at 30 °C using 8 µM *Ts*OYE whereas ketoisophorone reduction reactions by the Hyd1/flavin recycling system were conducted at ambient temperature that varied between 20–22 °C and using 3.33 µM *Ts*OYE. The Hyd1/flavin system was explored for a variety of reactions that led to improved Hyd1 and FMN total turnover numbers of 20,200 and 240 respectively. The unusual stability of Hyd1 offered a great advantage.

When the SH recycling system is coupled to a recombinant peroxygenase (rAaeUPO) for H_2-driven hydroxylation reaction, an initial SH total turnover number of 750 was observed (entry 2 in Table 4.4.). Immobilising the SH on Amberlite FPA54 improved its stability which subsequently increased the SH and FMN turnover number to 46,000 and 225 respectively. Combining the SH flavin recycling system with the styrene monooxygenase, StyA showed the least SH and FAD turnover number. This is due to the requirement for both H_2 and O_2 in this reaction. While H_2 and O_2 are needed for the formation C_4-hydroperoxyflavin that is in turn used by the StyA, the high reactivity of $FADH_2$ with O_2 also leads to the formation of H_2O_2 which is an undesired side product resulting in lower conversions.

*Ts*OYE has also been shown to accept a range of synthetic nicotinamides (mNADHs) as reducing agents to perform catalysis. Reduction rates (k_{red}) of up to 770 s^{-1}, surpassing that exhibited by natural coenzyme NAD(P)H has been observed. Application of this system for reducing ketoisophorone to (*R*)-levodione resulted in quantitative conversions closely comparable to that obtained for NADH and NADPH.[31] Nevertheless, this system relies on stoichiometric amounts of mNADHs due to lack of well-established regeneration techniques. A common method for their regeneration is the use of a rhodium based complex $[Cp^*Rh(bpy)(H_2O)]^{2+}$ that can reduce two among the five different mNADHs synthesised and makes use of formate as a sacrificial reductant. However this system suffers from mutual inactivation of the organometallic complex and the enzyme in addition to producing unwanted end-waste product. [229]

Another approach involves a chemoenzymatic method that employs an organometallic complex, pentamethylcyclopentadienyl rhodium bipyridine ($[Cp^*Rh(bpy)(H_2O)]^{2+}$)[224] for regenerating flavins in OYE ene-reductase, *Ts*OYE. A model reaction consisted of the organometallic complex, catalytic amounts of FMN, *Ts*OYE, and sodium formate as the electron donor. This system required careful adjustment of the reaction components and their concentrations which significantly influenced the overall conversion and enantioselectivity. For instance, higher concentrations of the electron donor, sodium formate lead to higher conversion rates, however, increasing its concentration also deactivated *Ts*OYE which led to poor enantioselectivity. The regeneration catalyst exhibited an overall turnover number of 100 and an FMN turnover number of 40. This system also suffered from the previously reported mutual inactivation of the complex and enzyme requiring improvements for their preparative applicability.[229]

Electrochemical methods for flavin regeneration are also widely reported for their applications with monooxygenases like P450 monooxygenase and styrene monooxygenases, however there are not

many examples of their application with ene-reductases. A primary advantage with electrochemical regeneration is the use of reagent-free electrons instead of chemical reducing equivalents to reduce cofactors. Electrochemical regeneration can be accomplished either by

- a direct regeneration of the enzyme at the electrode or
- an indirect electrochemical regeneration of the enzyme using mediators, or
- an electrochemical regeneration of the cofactors required by the enzyme[230]

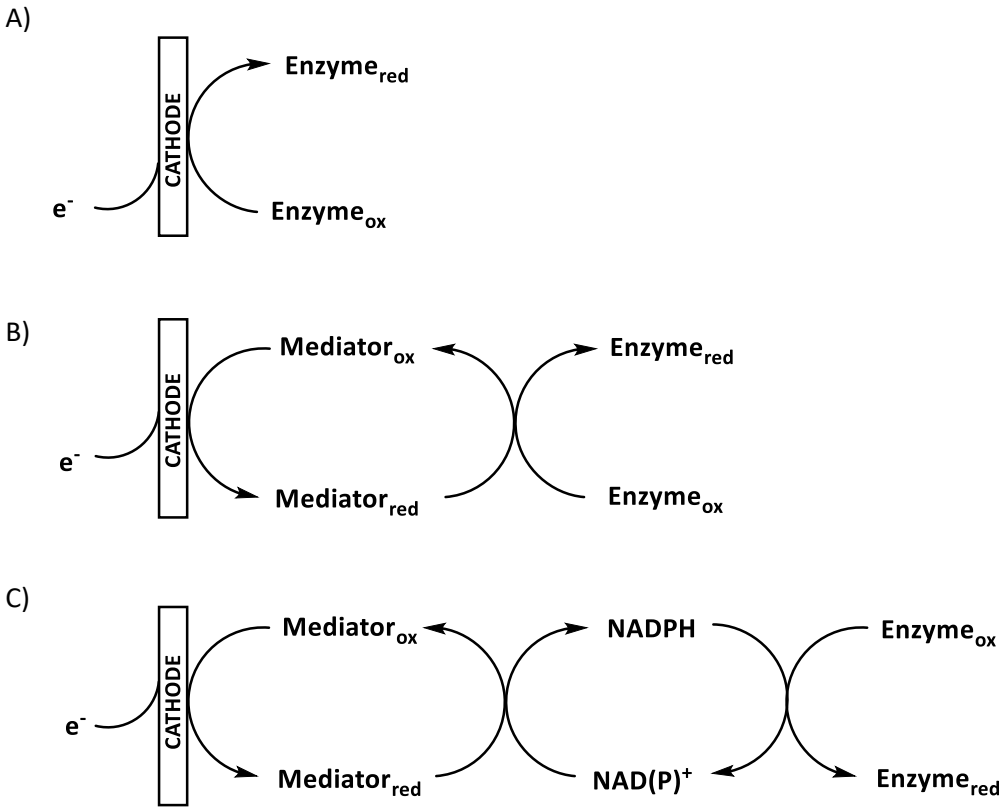


Figure 4. 8. Electrochemical regeneration of enzymes by A) direct electrochemical regeneration, B) indirect electrochemical regeneration using a mediator, C) electrochemical regeneration of cofactors used by the enzyme. Figure adapted with permission from Elsevier publisher: *Journal of Molecular Catalysis B: Enzymatic*, **2008**, *51*, 57-72.[230] License number: 5236920926484

Hollmann *et al*. devised a direct cathodic reduction of styrene monooxygenase using a cylindrical carbon felt as the cathode and a Pt wire as the anode for the stereospecific *S*-epoxidation of a range of styrene substituents with >98% *ee*. The enzyme bound FAD was directly reduced to $FADH_2$ at the

electrode substituting for Styb, the NADH-dependent flavin reductase component and NAD^+ cofactor, resulting in a highly simplified system. Nevertheless, reaction rates recorded for this method were rather low compared to that observed for a native reaction which was largely due to the low stability of StyA, the $FADH_2$-dependent styrene monooxygenase component. Although this system is not exploited for alkene reductions by ene-reductases, the authors foresee that it can be applicable to any enzymatic reaction that involves reduced flavins as cofactors.[231] An improved version of the same system focussing on improved enzyme (StyA) stability and cofactor regeneration rates was proposed by Ruinatscha *et al*., where a microporous, three-dimensional reticulated vitreous carbon (RVC) electrode was employed. The improved mass transfer delivered by this system did lead to improved product production rates even under a flavin concentration of just 0.01 mM. However, the system encountered unwanted by-products, acetophenone and phenylacetaldehyde formed by a possible radical attack of the flavin semiquinone on the reaction product, styrene oxide.[232] More cases of the direct electrochemical regeneration of a range of monooxygenases on different types of electrodes have been investigated and reported in the literature.[233]

The second method employs a mediator to accomplish the electrochemical regeneration of flavin cofactor (Figure 4. 8.). Fisher *et al*. investigated the use of methyl viologen to supply electrons to the enzyme active site, substituting for the expensive nicotinamide cofactors. This was then demonstrated for the reduction of a range of alkene substrates, using pentaerythritol tetranitrate reductase (PETNR). Reaction rates were calculated to range between 15–70% of the those reactions supplemented with stoichiometric amounts of NADPH.[234] Several other mediators compatible with other enzymes have also been reported. For instance, Cobalt sepulchrate is a known mediator used with P450 monooxygenase[235]

Electrochemical reduction of some cofactors has also been observed and several examples,

particularly for the nicotinamide cofactors are reported in the literature. Hollmann and co-workers developed a rhodium based complex, [Cp*Rh(bpy)Cl]Cl, (Cp=C_5Me_5; bpy=2,2'-bipyridine) that was found to reduce NAD(P)$^+$ to NAD(P)H. The oxidised metal complex was continually regenerated by cathodic reduction. This system was coupled with a flavin-dependent monooxygenase called 2-hydroxybiphenyl-3-monooxygenase to carry out *ortho*-hydroxylation of α-substituted phenol derivatives. Productivity of this system was at about 50% of a typical enzymatic regeneration processes under non-optimised reaction conditions.[236] The decreased productivity rates were due to the formation of hydrogen peroxide formed by the reaction of molecular oxygen and the complex as well as the reduction of O_2 at the carbon-felt cathode. Hydrogen peroxide is an oxidising agent that can oxidise amino acid side chains present in the protein backbone leading to its fragmentation. This may lead to enzyme denaturation and inactivation.[237] Enzymes that are prone to oxidative damage by H_2O_2 are often operated with the enzyme, catalase that decomposes H_2O_2 to harmless water and O_2.

A major reason for poor or relatively lower turnover numbers recorded in most electrochemical regenerations has been due to the oxygen dilemma associated with mechanism of monooxygenases. While O_2 is essential for the enzyme to form the C_4-peroxyflavin, the high reactivity of flavins towards O_2 also lead to a spontaneous and wasteful oxidation of the reduced flavins being formed in the reaction.[238]

Hence, Tosstorff and co-workers looked into exploring electrochemical cofactor regenerations for oxygen-independent enzymes such as *Ts*OYE (an OYE ene-reductase). After an initial screening of several mediators, [Cp∗Rh(bpy)(H_2O)]$^{2+}$ was found to reduce both NAD(P)$^+$ and FMN at good rates, with NADP$^+$ showing the highest conversion when coupled to *Ts*OYE for the reduction of (-)-carvone to (+)-dihydrocarvone.[239] The highest mediator TOF for these reactions was recorded as 45 h^{-1} which equals about 0.75 min^{-1}. As a comparison, the highest Hyd1 TOF recorded for reactions with *Ts*OYE

using the Hyd1 recycling system is 20.4 min^{-1}.[239]

4.2.2. Commercial ene-reductases from Johnson Matthey

Following initial success with *Ts*OYE, the Hyd1 system was next expanded to a range of ene-reductases from Johnson Matthey (JM) and more alkene substrates. Typically, JM ene-reductases are operated with a GDH/glucose or FDH/formate recycling system that continually reduces $NAD(P)^+$ to NAD(P)H. The Hyd1 system helps to avoid the formation of unnecessary end-waste product (gluconolactone or carbon dioxide respectively) offering a more atom-economical alternative.

4.2.2.1. Preliminary screening of various substrates and ene-reductases

A preliminary screening of numerous ene-reductases (ENE-101, 102, 103, 107, 108 and 109) against three substrates 1-acetyl-1-cyclohexene (**3**), dimethyl itaconate (**5**) and 4-phenyl-3-buten-2-one (**7**) for their reduction to cyclohexyl methyl ketone (**4**), dimethyl (*R*)-methyl succinate (**6**) and 4-phenyl-2-butanone (**8**) respectively was performed.

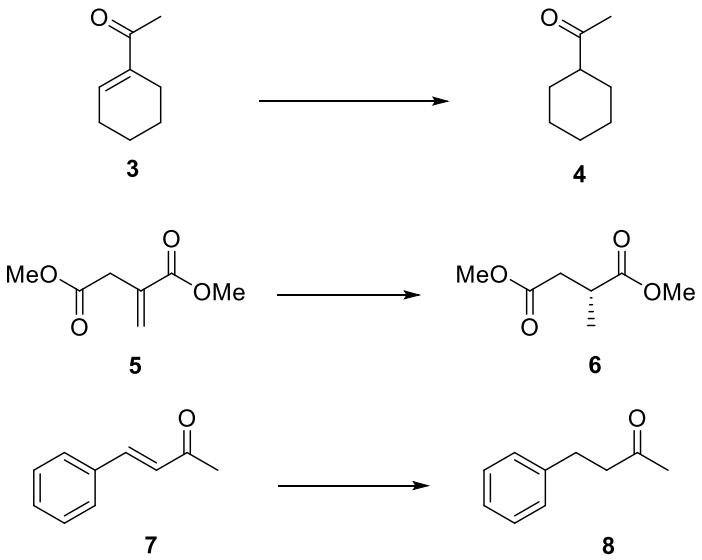


Figure 4. 9. Structures of substrates and their respective reduced products used with ene-reductases

Each reaction mixture was of 300 µL scale, and received the same catalyst and substrate loading. All reactions were evaluated for both FAD and FMN cofactors. Reaction setup followed the procedure in chapter 2, 2.3.1. Two Time points at 1 and 17 h were taken for analysis by GC. Conversions obtained for each reaction are shown in Table 4.5.

Table 4. 5. Preliminary screening of various ene-reductases against three substrates using Hyd1 catalysed FAD or FMN recycling systems.

%conversion calculated from GC at 1 h and {17 h}							
		1-acetyl-1-cyclohexene (**3**)		4-phenyl-3-buten-2-one (**7**)		dimethyl itaconate (**5**)	
Entry	Ene-reductase	**FMN**	**FAD**	**FMN**	**FAD**	**FMN**	**FAD**
1	ENE-101	9.6 {99}	8.6 {74}	3.7 {23}	2.7 {29}	6.6 {75}	0 {78}
2	ENE-102	0 {0}	0 {0}	1.3 {9}	0 {0}	0 {0}	0 {0}
3	ENE-103	22.3 {100}	11.8 {100}	24.9 {100}	6.3 {100}	7.4 {96}	0 {100}
4	ENE-107	9.1 {70}	13.9 {100}	7.5 {48}	2.8 {75}	23.3 {97}	0 {100}
5	ENE-108	50.6 {100}	13.2 {100}	36.8 {100}	8.8 {100}	38.1 {99}	9.9 {100}
6	ENE-109	51.3 {100}	26.6 {100}	51.3 {100}	17.5 {100}	24.5 {100}	0 {100}

Reaction conditions: 300 µL scale, 5 mM substrate (1 vol% DMSO), 0.5 mM FMN, 19.5 µL Hyd1, 1.5 mg ene reductase, Tris HCl buffer (pH 8), 1 bar H_2. Reaction temperature in the case of FMN: 21–24 °C and FAD: 26–32 °C

ENE-101 gave a maximum conversion of 99% for **3** at 17 h using FMN as the cofactor. Low conversions of 23% and 29% with FAD and FMN respectively was observed for **7**. ENE-102 gave no or very negligible conversion for all reactions and will not be explored for further optimisation. ENE-103 showed full conversion for almost all reactions at 17 h. However, analysis of conversions at 1 h indicated that substrates **3** and **7** were the most preferable substrates, offering better conversions. ENE-108 and ENE-109 gave full conversion of all substrates at 17 h when either FMN or FAD were used as cofactors. A quantitative comparison of all reactions is not possible because the limited volume in the pressure vessel did not allow for all reaction tubes to be placed together at the same time. Therefore entries 1, 2, 3 and entries 4, 5, 6 containing FAD as the cofactor were placed in two

different pressure vessels and run on the same day. Similarly, the next set of reactions with FMN cofactor was done another day. Slight temperature differences on both the days (see Table 4.5 footnotes) for the FMN and FAD systems could not be directly compared and this prevented identification of the better cofactor for these reactions. Nevertheless, it was useful to know that the JM ene-reductases can function using either FAD or FMN. Further, ENE-103 and ENE-107 for **5** and **7** reductions respectively were considered for investigating the effect of flavin concentration in the reaction. Table 4. 6. shows the results from these reactions and these data have now been published.[191] Comparing entries 1 and 2, a slight improvement in conversion when the flavin concentration was increased from 0.1 to 0.5 mM was observed. This was in agreement with the results obtained for *Ts*OYE. However, it was interesting to note that there was a distinct improvement in conversion (from 35% to 100%) upon increasing flavin concentration in entries 3 and 4. This can be related to the apparent K_M (0.9 ± 0.5 mM) which means that the operational flavin concentrations are in a range where the enzyme rate is still sensitive to flavin concentration.

Table 4. 6. Effect of varying flavin concentrations during reduction reaction catalysed by ene-reductase and the flavin recycling system

Entry	Alkene	[FMN] (mM)	OYE	Time (h)	Conv. (%)[a]	*ee* (%)
1	dimethyl itaconate	0.1	ENE-103	42	81	>99
2	dimethyl itaconate	0.5	ENE-103	42	98	>99
3	4-phenyl-3-buten-2-one	0.1	ENE-107	40	35	n.a.[b]
4	4-phenyl-3-buten-2-one	0.5	ENE-107	40	100	n.a.[b]

Reaction conditions: 142 µg Hyd1, 3 mg OYE and 5 mM alkene substrate in Tris-HCl (50 mM, pH 8), 1 vol% DMSO, 1 bar H_2, at room temperature (20–30 °C). [a]Chiral-phase GC conversions to **6** and **8**. [b]Not applicable.

A set of control reactions were also done for the above reactions to ensure that all reaction components were required. The results from the control reactions are shown in Table 4.7. and Table 4.8. These results confirm that zero or very low conversion is achieved if FMN, Hyd1 or ene-reductase are not present in the reaction mixture.

Table 4. 7. Control experiments for H_2-driven reduction of **5**

Entry	FMN	Ene-103	Hyd1	Conversion to 6 (%)
1	✓	-	✓	0
2	✓	✓	-	0
3[a]	-	✓	✓	0
4	✓	-	-	0

Reaction conditions: 300 µL scale, 0.5 mM FMN, 71 µg Hyd1, ENE-103 (3 mg), 5 mM **3**, Tris-HCl buffer (50 mM, pH 8.0, 25 °C), 1 vol% DMSO at room temperature (20–26 °C) in pressure vessel (1 bar H_2), 18 h.
[a]Reaction conditions: 600 µL scale, 142 µg Hyd1, ENE-103 (1.2 mg), 5 mM dimethyl itaconate, Tris-HCl buffer (50 mM. pH 8.0, 25 °C), 1 vol% DMSO at room temperature (18–20 °C) in pressure vessel (1 bar H_2), 18 h.

Table 4. 8. Control experiments for H_2-driven reduction of **7**

Entry	FMN	Ene-107	Hyd1	Conversion to 8 (%)
1	✓	-	✓	0
2	✓	✓	-	2
3	-	✓	✓	6
4	✓	-	-	0

Reaction conditions: 300 µL scale, 0.5 mM FMN, 7.5 µL (0.003 U) Hyd1, ENE-107 (3 mg), 5 mM **5**, Tris-HCl buffer (50 mM, pH 8.0, 25 °C), 1 vol% DMSO at room temperature (20–26 °C) in pressure vessel (1 bar H_2), 18 h.

4.2.2.2. Reaction optimisation

The Hyd1 + JM ene-reductase system was explored further to study the effect of factors like temperature, H_2 pressure, enzyme and cofactor loading on the overall conversion. Optimising reaction conditions for all reaction combinations (18 different reactions shown in Table 4.5) appeared time consuming and laborious. So reaction optimisation was restricted to only 4 combinations of ene-reductases and substrates as shown in Table 4. 9. These 4 combinations were chosen such that they yielded moderate conversions during the preliminary screen shown in (Table 4.5) and that they are diverse enough to make a reasonable representation of all the other reactions.

Table 4. 9. Ene-reductase and substrate combinations chosen for reaction optimisation.

Entry	Substrate	Ene-reductase
1	1-acetyl-1-cyclohexene	ENE-103
2	dimethyl itaconate	ENE-103
3	1-acetyl-cyclohexene	ENE-107
4	4-phenyl-3-buten-2-one	ENE-109

As a starting point, reaction parameters were chosen based on an article published by JM presenting results from ene-reductase catalysed alkene reductions.[35] Using similar reaction conditions helps in comparing the efficiencies of the two systems during later experiments. In this article, reactions were performed in a 250 mM potassium phosphate buffer at pH 7 that contained 20 mM substrate in toluene. A total concentration of 1.1 mM NAD^+, 30 mM D-glucose, 10 U mL^{-1} GDH and 100 mg mL^{-1} ene-reductase were used for each reaction.[35]

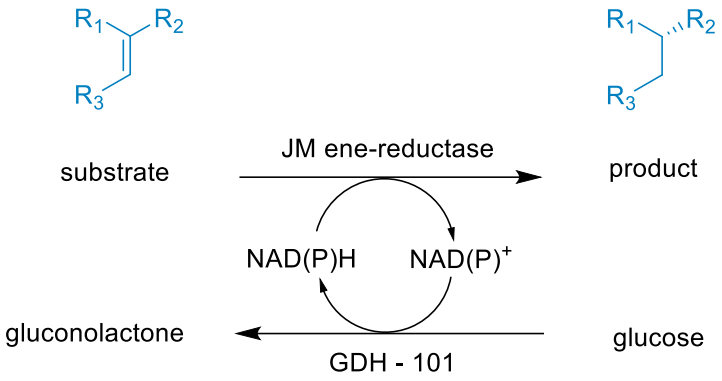


Figure 4. 10. Ene-reductase catalysed alkene reduction using the GDH/glucose system as regenerating catalyst for NAD(P)H

A high buffer concentration was essential for their reactions to maintain the desired pH that would otherwise get altered over time due to by-product accumulation. The use of GDH/glucose system to recycle NAD(P)H results in the gluconolactone by-product remaining in the reaction mixture, which leads to an decrease in the pH of the reaction which is in turn adjusted by adding a base. This is not the case with the Hyd1/flavin system because there is no waste generated from H_2 oxidation.

Next, it was necessary to understand the choice of toluene as a co-solvent for these reactions. The reason to explore toluene as a cosolvent was primarily to find out if it exhibits any distinct results on conversions or enzyme activity compared to DMSO that was widely used in this project. This was because of the fact that previously reported experiments done on an industrial scale have been carried out with toluene.[240] So two reactions differing only in their co-solvents – DMSO or toluene

were investigated (entries 1 and 3 in Table 4. 10.). Both solvents showed similar substrate conversion at 18 h. When this reaction was fed with more substrate and the reaction time extended (+20 mM at 45 h and +20 mM at 68 h), varying conversion rates were observed for the two reactions. Comparing entries 1 and 3 in Table 4. 10., it can be seen that over time, the reaction containing DMSO as the co-solvent gave 100% conversion at 97 h compared to that with toluene (51% conversion at 97 h). The decrease in conversion at the later time point (97 h) could be due to a low tolerance exhibited by ene-reductase or Hyd1 towards increasing concentrations of toluene as adding more substrate during the fed-batch reaction increases the vol% of the co-solvent from 1 vol% to 3 vol%. Comparing entries 1 and 2 in Table 4. 10 it was seen that higher Hyd1 concentrations lead to complete conversion at 97 h despite its low tolerance to toluene initially. However, using DMSO is rather a favourable option from an environmental and safety perspective, due to its relatively low toxicity when compared to toluene which may be more harmful .[241] Moreover, there is more data on enzyme tolerance and enhanced enzyme activity when DMSO is used as a co-solvent in the reaction medium.[242–245]

Table 4. 10. Effect of co-solvent (toluene/ DMSO) on conversion

Entry	**Co-solvent[a]**	**Hyd1**	**Conversion %**	
		µg	**18 h**	**97 h**
1	Toluene	230	99	51
2	Toluene	470	100	100
3	DMSO	230	100	100

Reaction conditions: 600 µL reaction scale, 20 mM 1-acetyl-1-cyclohexene (added +20 mM in fed-batch at 45 h and +20 mM at 68 h), 1.1 mM FMN, 3 mg ENE-109, 250 mM phosphate buffer, pH 7 in pressure vessel under 1 bar H_2, temp: 16–20 °C. [a]1 vol% co-solvent at the start of the reaction, which increased to 3% at 97 h due to more substrate being added.

Information about optimum pH for each ene-reductase was also available in the manual from JM's C=C double bond reduction kit as tabulated below.

Table 4. 11. Optimum operational pH values of ene-reductases available in Johnson Matthey's C=C double bond reduction kit

Ene-reductase	**Optimum pH**
ENE-101	6.5 – 8.0
ENE-102	7.0 – 7.5
ENE-103	7.0 – 7.5
ENE-107	6.0 – 9.5
ENE-108	6.5 – 9.0
ENE-109	6.0 – 8.5

All of these ene-reductases appear to show good activity at pH 7 and this was chosen for the next work.[35] With information from the existing individual test experiments and already published results, a suitable set of reaction conditions was finalised for taking this system forward for reaction optimisation. Reaction optimisation focused on investigating variations in conversion arising from differences in reaction temperature, pressure and Hyd1 loading.

Table 4. 12. GC-FID conversions for the reduction of selected alkenes with JM ene-reductases at two different temperatures and pressures using the Hyd1/flavin system for cofactor regeneration.

Entry	Ene-reductase	Substrate	% conv. at 1 bar H_2								% conv. at 4 bar H_2		
			25 °C					35 °C			25 °C		
			5.4 mU Hyd1		10.8 mU Hyd1			10.8 mU Hyd1			10.8 mU Hyd1		
			22 h	27 h	3 h	18 h	24 h	3 h	18 h	24 h	3 h	18 h	24 h
1	103	**3**	58	70	10	75	92	24	100	100	13	72	92
2	103	**5**	72	82	20	80	90	32	100	100	19	87	97
3	107	**3**	12	16	3	10	12	4	12.4	14.7	3	11	11
4	109	**7**	95	100	24	91	100	46	100	100	25	100	100

Reaction conditions*:* 600 µL reaction scale, 20 mM substrate, 1.1 mM FMN, 5 mg mL^{-1} ene-reductase, 250 mM potassium phosphate buffer, pH 7 in pressure vessel. Hyd1 was activated under H_2 for at least 15 h.

From Table 4.12., entries in green received 5.4 mU Hyd1, whereas entries in orange received 10.8 mU Hyd1. Both batches showed comparable conversions, however it is important to note that the conversions for the two batches were calculated at slightly different time points. In particular, with phenyl butenone, 100% conversion was observed in both the reactions. Thus, suitably lower Hyd1 concentrations are sufficient to yield fairly high conversions provided the reaction time is extended accordingly. Entries in orange and blue show the effect of temperature on reaction conversions. Over a 24 h reaction time, reactions in entry 4 showed full conversion to the product at both 25 °C and 35 °C. However, reactions at 35 °C appear to proceed faster than the reactions conducted at 25 °C, as shown by slightly higher conversions. Earlier time points taken at 3 h, revealed that conversions were nearly twice for the reactions conducted at 35 °C when compared to those that were performed at 25 °C. Thus, an elevated reaction temp. shortens the reaction time, which is preferable for tricky products like (*R*)-levodione that racemises in the aqueous reaction mixture with increasing time. On

the other hand, it is worth noting that industrial enzymatic transformations are typically performed as overnight reactions and hence the longer reaction times of up to 24 h should not be seen as a significant limitation to this system. The energy savings for room temp. reactions may outweigh the rate advantages of increasing temperature.

Comparing experiments conducted at 1 and 4 bar H_2 reveal that the supplied H_2 pressure does not significantly affect conversions as evident from the results in Table 4.12. (compare entries in orange and yellow). Hence, a minimum pressure of 1 bar H_2 appears sufficient for these reactions so far. A general observation from entry 3 in Table 4.12. is that **3** is not the best compatible substrate for ENE-107 due to the very poor conversions observed. However, with ENE-103, good conversions were observed. The reason for this difference in activity was not explored in detail, but this could be due to poor compatibility between the substrate and enzyme active site.

4.2.2.3. Comparison of the Hyd1 recycling system with the GDH/glucose recycling system for alkene reductions using ene-reductase from JM

Optimising reaction conditions was helpful to understand the effect of numerous reaction parameters on conversion. Following this, it was important to evaluate how the newly developed Hyd1 system compares with the conventionally used GDH/glucose recycling system that is used to recycle NAD^+ to NADH, which is then used by the ene-reductase. This assessment is crucial to identify key areas for further improvement in the Hyd1 recycling system simultaneously allowing to appreciate its existing advantages. Therefore all reactions from Table 4.12. were repeated with GDH-101, glucose and NAD^+ instead of Hyd1 and flavin using the same reaction conditions. Firstly, NAD^+ reduction activity by GDH-101 was determined by UV-vis activity assay as shown in Figure 4. 11. This helped in estimating the amount of GDH-101 that would be required to attain an NAD^+ reduction

activity of 10.8 mU which is also the FMN reduction activity for the amount of Hyd1 used for previous reactions.

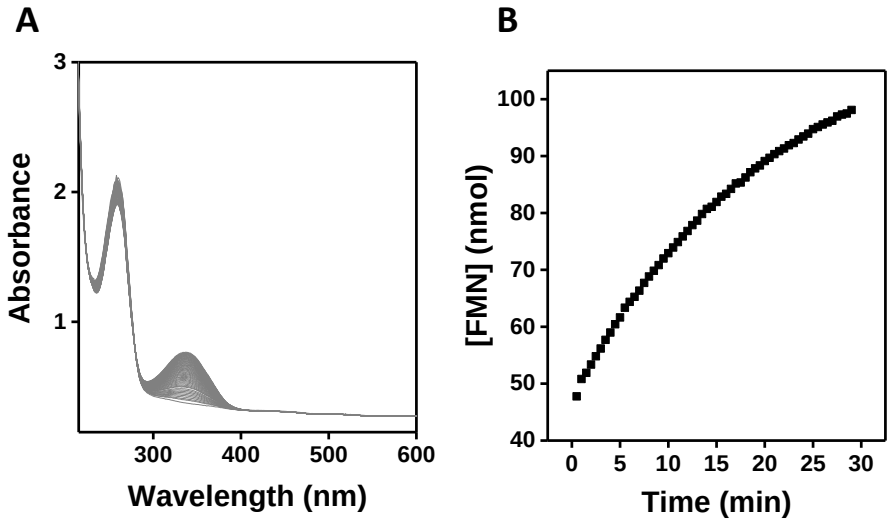


Figure 4. 11. UV-vis activity assay showing the reduction of NAD^+ to NADH catalysed by GDH-101 and using glucose as the reductant. A) UV-visible spectrum of GDH-101 reducing NAD^+. B) Calculated [NADH] based on λ_{max} = 340 nm (ε = 6.22 mM^{-1} cm^{-1}).
Reaction conditions: 800 µl scale, 0.1 mM NAD^+, 5 µg GDH-101, 3 mM D-glucose (anhydrous) in potassium phosphate buffer (250 mM, pH 7.0, 25 °C).

All reactions were done under N_2 atmosphere to prevent any possible side reactions by O_2-dependent NADH oxidase which could be present as a possible contaminant in ene-reductases.[53,215] Moreover, molecular oxygen has been found to reoxidise OYE ene-reductases in certain studies.[45,246,247] GC conversions for these reactions are tabulated in Table 4.13.

Table 4. 13. Conversions obtained for the reduction of various alkene substrates using ene-reductases from JM and GDH-101 as the recycling system for NAD^+ cofactor.

Entry	Ene-reductase	Substrate	%conversion					
			25 °C			35 °C		
			1.5 h	3 h	6 h	0.5 h	1.5 h	3 h
1	103	**3**	55	92	100	42	73	100
2	103	**5**	40	62	75	31	55	76
3	107	**3**	80	100	100	82	100	100
4	109	**7**	78	98	97	79	98	99

Reaction conditions*:* 600 µL reaction scale, 20 mM substrate, 1.1 mM NAD^+, 30 mM glucose, 26 µg GDH-101 equivalent to 10.8 mU reduction activity, 5 mg mL^{-1} ene-reductase in potassium phosphate buffer (250 mM, pH 7) under N_2 atmosphere.

A comparison of results from Table 4.12. and Table 4.13. showed the clear distinction in the reaction time required for complete conversion of the alkene by the two different recycling systems. While the GDH-101 recycling system showed full conversion of almost all the substrates at 6 h, the Hyd1 system required longer reactions time of *c. a.* 18-24 h as shown in Table 4.12.

Similar to the results observed for the Hyd1 recycling system, reactions at elevated temperature showed higher conversions at a given time point. At 25 °C, all reactions proceeded to full conversion at 6 h except for entry 2 which was slower than all other reactions. At 35 °C, all reactants were completely converted to the product at 3 h except for entry 2. Interestingly, the two recycling systems displayed contrasting results for entry 3 that contained 1-acetly-1-cyclohexene and ENE-107. In the case of Hyd1 recycling system, entry 3 had the least conversion, however this reaction showed some of the best conversions when operated with GDH-101 and glucose. The slowest reaction with the GDH recycling system was entry 2 involving ENE-103 and dimethyl itaconate, however this was

not the case with the Hyd1 recycling system where it showed good conversions of up to 97%. The type of cofactor employed can also influence the yield and stereoselectivity of a biocatalytic reaction.[47] Although a clear explanation for this behaviour has not been discussed explicitly, it could be hypothesised that this variation in reaction rates could be based on how readily an enzyme is able to accept electrons from the cofactor.

4.2.2.4. Reproducibility of results for alkene reduction using GDH-101 and glucose recycling system

Reactions in entries 4 and 1 from Table 4.13. were done as duplicates at 25 °C and 35 °C respectively and their corresponding standard deviation and standard errors were calculated and found to be within reasonable degree of error.

Entry 1 from Table 4.13.			**Entry 4 from Table 4.13.**	
Sample	% conversion		% conversion	
	0.5 h	1.5 h	1.5 h	3 h
1	42	73	78	98
2	37	89	89	100
Std deviation	**2.4**	**7.9**	**5.6**	**1.1**
Std error	**1.7**	**5.6**	**4.0**	**0.8**

Reaction conditions*:* 600 µL reaction scale, 20 mM substrate, 1.1 mM NAD^+, 30 mM glucose, 26 µg GDH-101 equivalent to 10.8 mU reduction activity, 5 mg mL^{-1} ene-reductase in potassium phosphate buffer (250 mM, pH 7) under N_2 atmosphere.

Thus the application of Hyd1 as a clean and straight-forward recycling system for the flavin cofactor was demonstrated with *Ts*OYE and a range of commercial ene-reductases from Johnson Matthey for the selective reduction of various activated alkenes. The Hyd1 and FMN turnover numbers recorded so far approach values suitable for use in industry, however, there is not sufficient information to accurately benchmark the results obtained. An acceptable turnover number for a specific cofactor is decided based on the cost of the cofactor and the value of the chemical synthesised.[248] Since, flavins are not as commonly used in industry as the nicotinamide cofactors, a proper price for the flavin cofactors on an industrial scale is not easy to obtain. Flavins are employed as reductants by a diverse

range of enzymes like halogenases, monooxygenases and dehalogenases, and hence the Hyd1 recycling system can be explored for a wide range of valuable transformations in the future and has potential applications in industry. The Hyd1/flavin system offers an atom economical process that is ideal for industries as they try to accomplish a net zero economy. The simple and robust system that can easily be coupled to several enzymes makes it an attractive choice for industrial application. The high turnover numbers achieved during the first round of optimisation already shows the high relevance of this system for industrial application.

5

Chapter 5 Coupling Hyd1 to nitroreductases for the synthesis of amines

In the previous chapter, Hyd1 was demonstrated as a clean flavin recycling system for a range of ene-reductases accomplishing highly selective alkene reductions. It is indeed important to show the compatibility of this system with other enzymes too, in order to validate its broad utility for synthetic purposes. This chapter focusses on expanding the Hyd1/flavin system to flavin-dependent nitroreductases to selectively reduce nitroarenes to their corresponding anilines using commercial, NAD(P)H-dependent nitroreductases from Johnson Matthey. This chapter elaborates on the experimental methods adapted for this experiment and the results from these biocatalysed nitro reductions are discussed.

5.1. Amines

Amines are nitrogen containing chemical compounds where an sp^3 hybridised nitrogen atom is bonded to three other elements. Ammonia (NH_3) containing three hydrogen atoms bonded to a nitrogen atom is the simplest amine. Organic amines are formed when one or more hydrogen atoms are replaced with one or more alkyl or aryl functional groups. Replacement with one, two and three alkyl groups give rise to primary, secondary and tertiary amines respectively as shown in Figure 5. 1.

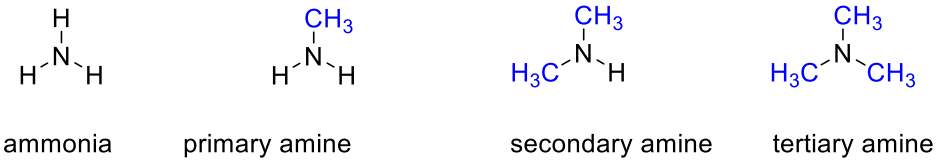


Figure 5. 1. Classification of amines based on the number of carbon atoms attached to the nitrogen atom

Several alkaloids like quinine, morphine, coniine and nicotine possess amine functional groups. Many established drugs like ephedrine and phenylephrine that are used as decongestants, and the well-known paracetamol are also amines. Amines are the building blocks of DNA and RNA, the biomolecules essential for most life-forms on earth. They are an integral part of many Active Pharmaceutical Ingredients (APIs) as they help to tune the physicochemical properties of a drug

molecule and sometimes play a vital role in enhancing receptor affinity.[249] The increasing application of amines, especially aniline and its derivatives, as intermediates in dyestuffs, agrochemicals and APIs in the chemical industry has led to a great deal of research focussing on the development of efficient synthetic routes and methodologies for preparing amines. For instance, anilines and their application for dyestuff remained the foundations of the synthetic dye industries, leading to the establishment of the well-known industries: BASF and BAYER. The versatility of anilines have also led to their expansion into pharmaceuticals.

5.2. Synthesis of amines

Amines can be accessed by numerous methods from a variety of starting materials, due to the plethora of synthetic routes that have been reported up to now.[250] The method of synthesis is usually decided based on the type of substrate, reaction scale and the cost involved.

Literature data suggests that an increased interest in research for efficient and selective amine synthesis after 2000, led to the discovery of many diverse synthetic methods that eventually enabled its growth from a small topic to a widely researched subject.[251] Since then, many reviews consolidating the different synthetic routes were published among which the reduction of nitro compounds is of interest to this chapter.[251–254] The reduction of nitro compounds to amines is useful in two scenarios – (i) for chemoselective reduction to amines in synthetic applications and (ii) to metabolise hazardous nitro compound pollutants released into the environment through industrial, agricultural and pharmaceutical activities.[255]

5.2.1. Catalytic hydrogenation

Traditional industrial syntheses of amines from nitro compounds predominantly employed stoichiometric reducing agents such as sodium hydrosulfite, iron, tin or zinc in ammonium hydroxide for the reduction of nitro groups.[256] The Bechcamp reaction is an ideal example for this case, where

aromatic nitro compounds were reduced with iron and a dilute acid to obtain their aniline derivatives. Such reactions have been on the decline in many industries due to the excess waste that is generated in the end. In this respect, catalytic hydrogenation in the presence active metals proves highly efficient and several catalytic systems have been adapted in industry for large scale hydrogenation processes.[257] The catalysts employed are either metals or a combination of metals like Ni, Cu, Mn, Fe, Pd, Al, Pt and C used under varying reaction conditions. A major drawback in these type of nitro reductions is chemoselectivity when other functional groups like C-C multiple bonds, halogen atoms and carbonyl groups are present (C=C, C≡C, C=N, C=O, and C-X). Moreover, it was often difficult to selectively reduce only one nitro functional group in di- or poly-nitrated aromatic compounds. Nevertheless, the selectivity of some catalysts could be enhanced by making targeted modifications, for instance, when PbO or H_3PO_2 was added to supported Pt catalysts, there was improved selectivity for nitro reduction, however this reaction also suffered from low yields.[258]

In the last few decades, many research groups reported the design and application of several supported metal nanoparticles that showed improved selectivity for nitro reduction reactions as well as allowed for easy recovery of the catalyst. Corma *et al*. achieved a breakthrough in this area, by designing gold nanoparticles supported on TiO_2 that facilitated nitro reductions, exhibiting up to 98% selectivity on a range of functionalised substrates under mild reaction conditions.[259,260] Nanoparticles made from Fe, Pt, Pd and Rh on a range of supports like carbon nanofibers (CNFs), dendrimer matrices and organosilica matrices were later reported.[261] Most catalysts were able to tolerate a wide range of functional groups like carbonyls, amides, esters, nitriles, and even halogens. The sole problem of using precious metal catalysts is their high cost. In the recent years a plethora of non-noble metal catalysts based on Fe, Co, Ni and Cu have been reported to accomplish nitro reduction reactions. In addition to being employed for direct hydrogenation with H_2, these metals have also demonstrated their catalytic performance utilising a range of reductants like $NaBH_4$, hydrazine, CO/

H_2O (water gas reaction), alcohols and formic acid.[257] Homogeneous catalytic systems for chemoselective nitro reductions are also found in the literature. Recent research has been concentrated on the usage of biphasic systems, consisting of a water soluble catalyst. This enables easy recycling of the catalyst as the water-immiscible nitro and amine compounds remain in the organic phase.

Apart from catalytic hydrogenation, reduction of nitro compounds are also accomplished via other methods like catalytic transfer hydrogenation, hydride transfer reductions, metal dissolving reductions and metal-free reductions which are discussed extensively in the literature and briefly discussed in this chapter.[261]

5.2.2. Mechanism for the hydrogenation of nitro group to amine

The classical and most accepted mechanism for nitro reduction is the one proposed by Haber (Figure 5. 2.).[258] The reduction of a nitro group to an amine takes place via a number of intermediates and through the consecutive addition of three hydrogen molecules or in other words, six reducing equivalents. The intermediates formed in sequence from RNO_2 are nitroso (R-N=O) and hydroxylamine (RNHOH) compounds with each step requiring two equivalents of the reductant. Further reduction of the hydroxylamine intermediate results in the final amine product.[262] Usually this transformation is characterised by only trace amounts of the nitroso compound, whereas the concentration of the hydroxylamine intermediate is dependent on several factors like the nature of the reaction itself, like temperature, pressure, solvent and catalyst. This indeed corresponds to the reaction profiles that show a fast reduction of the nitro group to the nitroso compound followed by a quick hydrogenation to the hydroxylamine intermediate. The conversion of hydroxylamine to the amine is the slow process and hence is the rate-determining step in the reaction.[256] Apart from these sequential steps, in rare cases, certain parallel reactions can also occur depending on the

concentrations of the intermediates present in the reaction mixture. A condensation reaction between the nitroso and hydroxyl intermediates could occur, leading to an azoxy compound. This, on further hydrogenation gives the azo, hydrazo and finally the amine compound as shown in Figure 5. 2.[263]

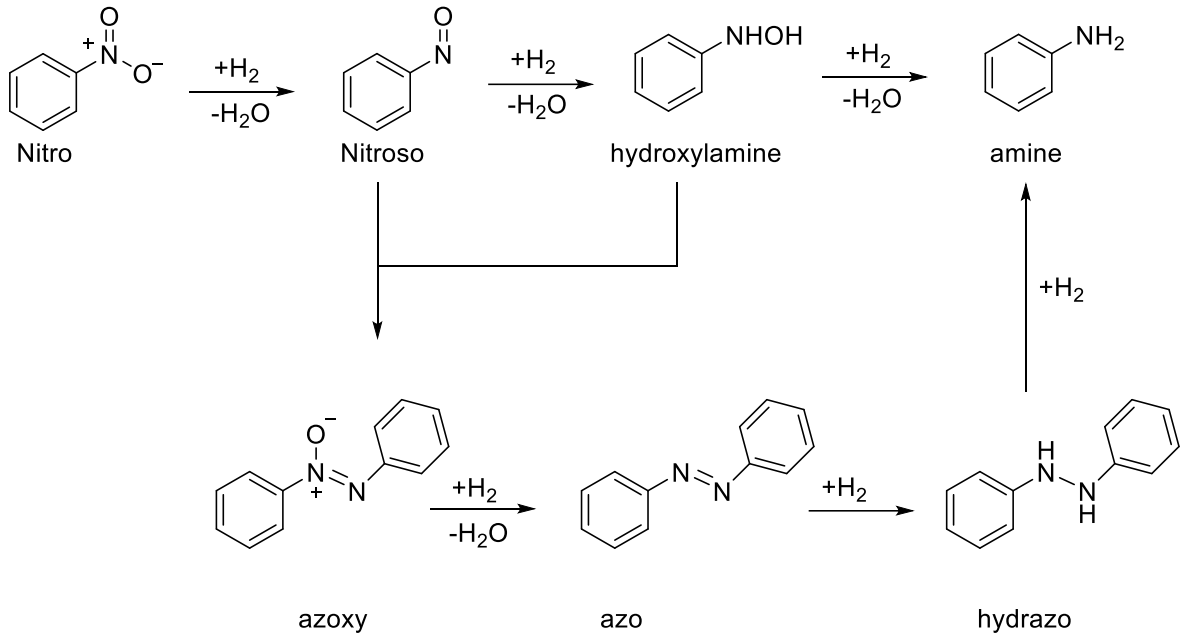


Figure 5. 2. Nitro hydrogenation route proposed by Haber[258]

The reduction of nitro functional groups (-NO_2) to amines (-NH_2) is the most common reductive transformation among all other reduction reactions used in small scale drug synthesis and is an important route for the synthesis of amines.[258,264–266] These reduction reactions are largely explored for the readily available aromatic nitro substrates which are expected to occur quite quickly compared to aliphatic substrates that on the other hand, require relatively longer reaction times, higher catalyst loadings and generate unwanted by-products.

5.2.3. Catalytic transfer hydrogenation

Catalytic transfer hydrogenation is another popular alternative for catalytic hydrogenation, where easily accessible reagents like HCOOH, $HCOONH_4$, *i*PrOH, and $NH_2NH_2{\cdot}H_2O$ are used for hydrogen source. This helps in the convenient control of hydrogen evolution within the reaction as opposed to the use of high-pressure reactors.[256] Nitro reduction by catalytic transfer hydrogenation is generally carried out either by using heterogeneous metal nanoparticles or organometallic complexes as catalysts. Additionally, transfer hydrogenation methods are frequently reported to occur in milder and greener solvents like ethanol and iPA.[267] For instance, Cao and co-workers used gold nanoparticles supported on TiO_2 in combination with $HCOONH_4$ as hydrogen source for the reduction of nitrobenzene. Despite the high selectivity (99%), this reaction was also feasible in water and at room temperature. Further this system was extended to aliphatic amines showing >99% yields. Beller *et al*., proposed an iron based complex generated *in situ* in the reaction mixture from $Fe(BF_4)_2.6\ H_2O$ and a tetraphos ligand, tris[(2-diphenylphosphino)-ethyl]phosphine $[P(CH_2CH_2PPh_2)_3$; $(PP_3)]$. It is worth noting that this reaction was the first base-free transfer hydrogenation in the synthesis of amines and showed the highest conversion when formic acid was used as the reducing agent, when compared to other formates which yielded negligible conversion. Overall, this reaction showed good to excellent yields, chemoselectivity, and was able to operate at room temperature.[268]

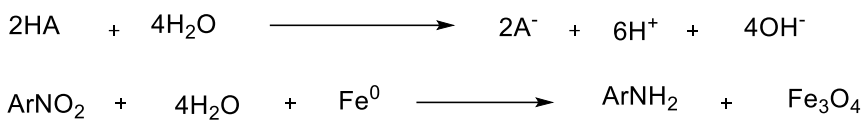
5.2.4. Hydride transfer reductions

These reactions involve a direct transfer of hydride from a reducing agent to the nitro substrate with or without the help of a catalyst. Some of the commonly employed reducing agents include $LiAlH_4$, $NaBH_4$, silane and siloxane. The finding that many metal catalysts, both from transition and main group metals can efficiently enhance these reactions has resulted in widespread research lately – especially in the application of noble nanoparticles. One of the best examples is the use of

magnetically active Au nanoparticles designed by S. Park *et al*.[269] They highlight a simple and highly reliable synthetic route for the preparation of the gold nanoparticles, which are then immobilized on an easily separable iron oxide core. The reactions showed quantitative conversion at room temperature as well as exhibited excellent selectivity tolerating alcohols, carbonyls, acids, nitriles and alkenes.[269] Comparing the various catalytic transfer hydrogenation (C.T.H) reactions and the hydride transfer reactions reported in the literature, the number of highly selective reactions achieved with C.T.H are higher than those recorded for the hydride transfer reactions.[261]

5.2.5. Metal dissolving reductions

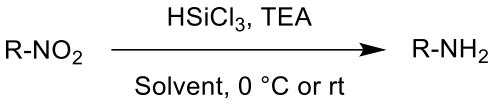
Metal dissolving reductions are a classic method known to facilitate nitro reductions for a long time. The best example here is the Bechamp process (1854) – one of the oldest commercial processes used in the manufacture of amines. It was the first reduction of nitro functional group to amines performed using iron $(Fe)^0$ and HCl. [270] The mechanism involves the adsorption of an aromatic nitro compound on Fe^0 surface, where it reacts with the protons produced by the reaction between acid and water leading to the formation the respective aromatic amine.[270] Scheme 5. 1. shows this reaction. Other common metals used for this reaction are Al, Fe, Zn, In, Sn, and Sm used with proton sources such as H_2O, AcOH, HCl and NH_4Cl. Recent advances in this methodology include the introduction of a phase transfer catalysis and the use of ultrasound irradiation that have proven to speed up the reduction processes.[261] Kelly and Lipshutz achieved a highly selective and mild reduction of nitro compounds to primary amines using Zn dust (metal) and ammonium chloride (proton source) and a commercially available surfactant as an additive that forms micelles enabling this transformation in water.[271] Since metal dissolving reactions require excessive amounts of metals, such reactions are quite unsustainable and require extensive separation methods in the end.



Scheme 5. 1. Simple reaction scheme of the Bechamp reduction process

5.2.6. Metal free reductions

Metal free reductions reactions are attractive because they help to avoid metal contaminations, and hence offer a simpler downstream processing. Following the first reduction of this type, reported by Bruce and Perez-Medina,[272] this technique has been revisited by many research groups who showed that several reducing agents can be applied in a similar manner to accomplish nitro reductions. Some of the reagents include sodium dithionite, elemental sulphur and dihydroanthracene. A common drawback encountered in many metal free reduction reactions was the moderate conversions achieved despite the often harsh reaction conditions like high temperatures, long reaction times and excessive reducing agents. Nevertheless, widespread research in this field has led to advancements in the past that include improved selectivity and greener reaction conditions. Lately, Orlandi *et al*., have shown that nitro compounds can be reduced to their corresponding amines in the presence of trichlorosilane and tertiary amines. Excellent selectivity, broad substrate scope and quantitative yields were observed under mild reaction conditions (0 °C to r.t.). Further this system has also been demonstrated for commercial applicability for the synthesis of Aliskiren.[273]



Scheme 5. 2. Reduction of nitro compound using trichlorosilane and tertiary amines at 0 °C or at room temperature.[273]

5.3. Biocatalytic synthesis of amines

Advancements in the discovery of new enzymes, genetic engineering and directed evolution have expanded the toolbox of enzymatic amine synthesis. Many enzyme families catalysing different kinds of reactions to yield amines have been reported in the recent years. Biocatalytic approach to amine synthesis offers an environmental friendly and highly selective synthetic route under milder reaction conditions. Some of the most well-known enzymes are explained in detail below. Figure 5. 3. shows an overview of the important enzyme catalysed reactions.

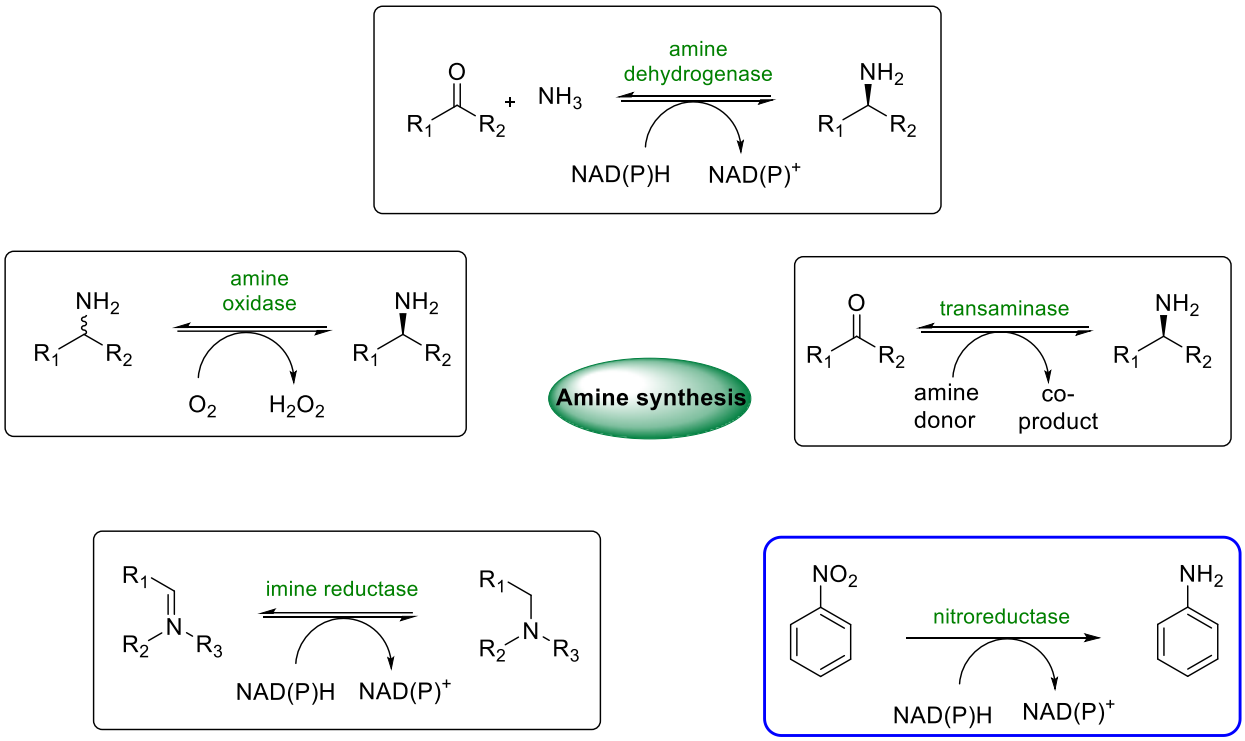


Figure 5. 3. Different reactions catalyzed by various enzymes to prepare amines.

5.3.1. Transaminases

Transaminases are group of pyridoxal 5'-phosphate-dependent enzymes that catalyse the reversible transfer of an amine group from a primary amine to a suitable carbonyl compound such as an aldehyde or a ketone. Since the reaction is reversible, the conversions and product yields are therefore determined by the reactant which is in excess during the reaction. In a typical reaction,

pyridoxal 5'-phosphate gets converted to pyridoxamine phosphate which in turn relies on a sacrificial amine donor that gets converted to an end waste product (ketone).[65,168] Transaminases can be divided into several types based on the substrates they act on. α-transaminases only accept substrates that contain a carboxylic acid group at the α position of the carbonyl moiety, whereas ω-transaminases are compatible with ketones containing carboxylic acid groups both at the α and distal positions. A small portion of ω-transaminases also accept substrates even without a carboxylate group and are called amine transaminases.[65,168] For this wide substrate compatibility, amine transaminases have received increasing interest lately for synthetic applications.[165,166,274,275]

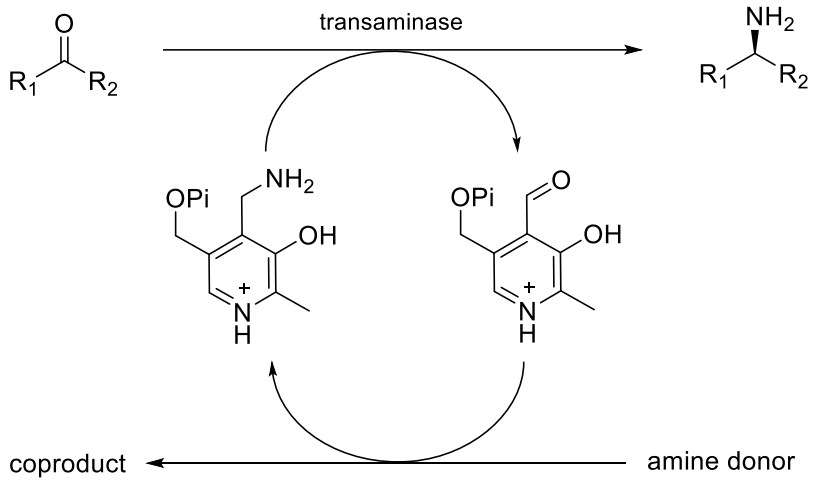


Figure 5. 4. A general reaction scheme for transamination reaction catalysed by pyridoxal 5'-phosphate-dependent transaminase.[65]

The applicability of transaminases in the past was limited by factors like narrow substrate scope of wild-type enzymes, lack of methodologies to monitor and favourably shift reaction equilibrium to improve conversions, enzyme inhibition by ketone by-product, access to only primary amines and requirement of the complex sacrificial amine donor, pyridoxal 5'-phosphate.[65,168] The back reaction to ketone has been addressed by strategic methodologies recently that focus on ways to remove the inhibiting ketone by-product that is generated during the reaction. For instance, using isopropylamine (*i*PrNH$_2$) as the donor, generates acetone as the ketone end product which can be

removed easily under reduced pressure due to its high volatility. Other strategies to shift the equilibrium of the transaminase reactions towards desirable conversion include the introduction of a second chemical or catalytic reaction or precipitation that prevents product inhibition.[65,168] Despite such modifications, new ways to achieve favourable reaction equilibria are still a commonly researched topic in this field. The expansion of enzyme engineering techniques has facilitated access to transaminases with broader substrates scopes and that can be used for industrially relevant applications. The best example of this result, is the application of an evolved ω-transaminase obtained from several rounds of mutagenesis, for the synthesis of Sitagliptin (an antidiabetic drug) with excellent selectivity, and yield (Figure 5. 5)[167]

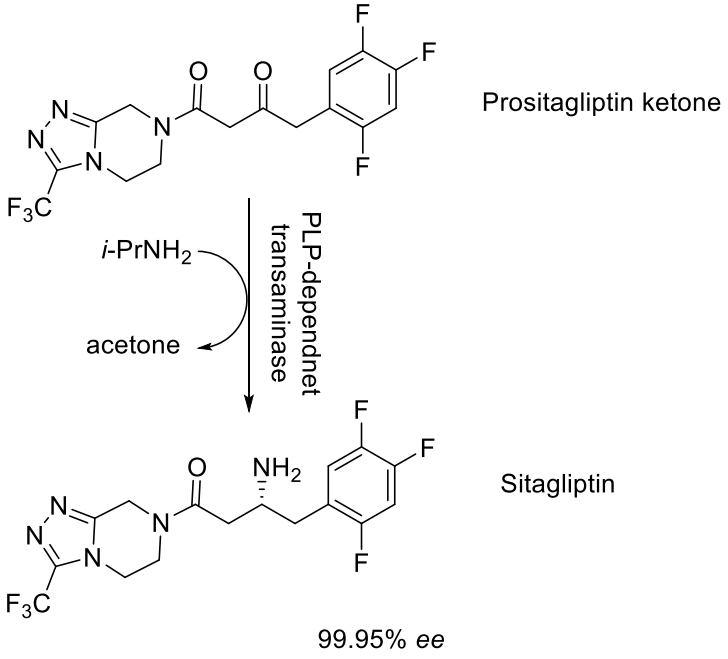


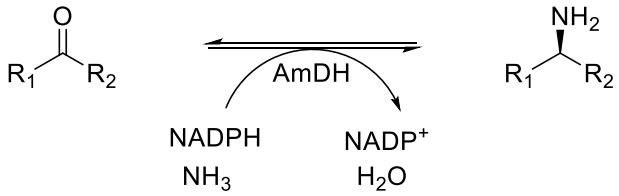
Figure 5. 5. Biocatalytic transamination of Prositagliptin ketone to the enantiopure Sitagliptin catalysed by the (*R*)-selective transaminase ATA-117, a homolog of an enzyme from *Arthrobacter sp*.[167]

In addition to the application for asymmetric synthesis, transaminases also catalyse kinetic resolution, where amine transfer takes place selectively, from only one enantiomer of a racemic mixture of amines, resulting in the corresponding ketone, leaving the desirable amine enantiomer

intact. These reactions also come with a drawback of lesser yield when compared to asymmetric synthesis that can give a 100% theoretical yield.[276]

5.3.2. Amine dehydrogenases

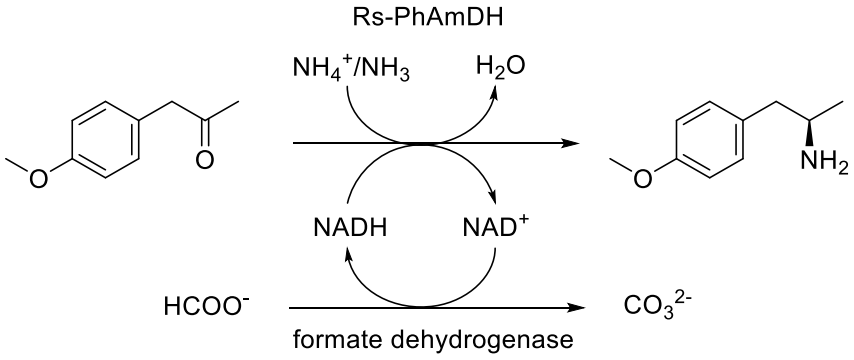
Following transaminases, amine dehydrogenases (AmDH) stand next in terms of synthetic utility, enzyme availability and scalability.[276] These enzymes typically catalyse the reversible reductive amination of carbonyl compounds (such as ketones, aldehydes and keto acids) to amines using ammonia as the amine donor and nicotinamide cofactor, NAD(P)H as the hydride source.[168] The nicotinamide cofactors are further recycled by a suitable cofactor regeneration system e.g. glucose/ GDH or formate/FDH.[277]



Scheme 5. 3. A typical reductive amination of a carbonyl compound catalysed by amine dehydrogenase (AmDH).

These enzymes are advantageous in that they utilise a cheaper amine source, ammonia and also lead to water as the waste product showing better atom economy. As a general fact, not many amine dehydrogenases have been identified in nature, and moreover, the present wild type enzymes offer limited substrate scope. As a result, developments in protein engineering techniques, have resulted in new amine dehydrogenases showcasing improved substrate scope and stability.[168] Literature reports have several examples of successful applications of amine dehydrogenases used for preparing pharmaceutically relevant amines or amino acids. Mutti and co-workers accomplished a highly stereo selective conversion of aliphatic and aromatic aldehydes and ketones using three different AmDHs, among which a variant of L-phenyl alanine dehydrogenase from *Rhodococcus sp.* M4 (Rs-PhAmDH)

was demonstrated for preparative scale enzymatic synthesis (Scheme 5. 4.). These reactions were conducted in ammonium formate buffer which both acted as the nitrogen source as well as the reducing equivalent for the nicotinamide cofactor (Scheme 5. 4.).[278] Formate dehydrogenase utilises formate, the counter ion of ammonium, and forms carbon dioxide. Free ammonia or ammonium ions are utilised by the enzyme for catalysing the reductive amination. The by-products observed in the end are only water and carbonate.



Scheme 5. 4. Reduction of *para*-methoxy phenyl acetone to its corresponding amine using Rs-PhAmDH on a preparative scale (208 mg). [278]

In an attempt to address problems pertaining to substrate scope expansion and process development for bulk synthetic applications, Groger and co-workers used a variant amine dehydrogenase, EsLeuDH-DM, a leucine dehydrogenase obtained from *Exigobacterium sibiricum*. The enzyme accommodated a range of aryl ketones including aryl-aliphatic ketones, diketones, α/β keto acids/ esters, aromatic bicyclic ketones, and exhibited full conversion even at higher substrate concentrations of 50 mM. Possibilities to immobilise the enzyme were further explored resulting in successful immobilisation of EsLeuDH-DM on commercially available carriers.[279]

5.3.3. Amine oxidases

Amine oxidases (AO) are enzymes that belong to the oxidoreductase family that typically catalyse redox reactions. AOs catalyse the oxidation of amines to imines accompanied by the simultaneous

reduction of O_2 to hydrogen peroxide. In aqueous media, the resulting imine is hydrolysed to the corresponding ketone.

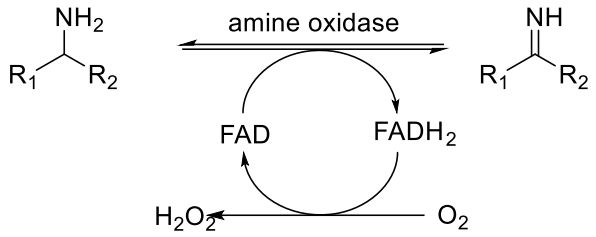
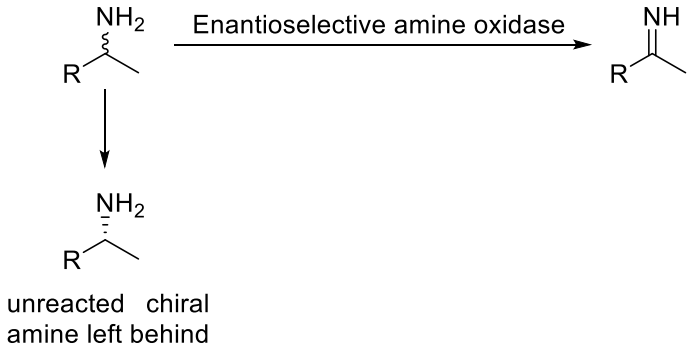


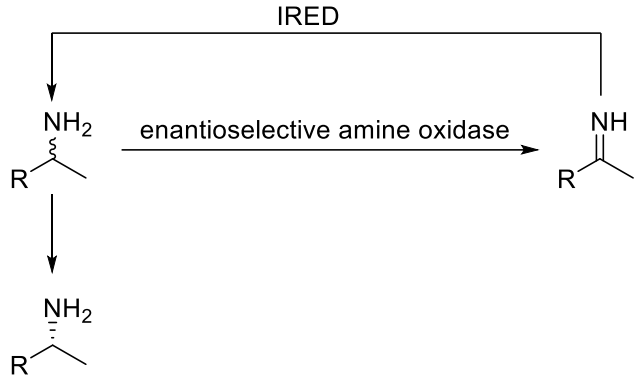
Figure 5. 6. A general reaction scheme showing the oxidation of an amine to imine catalysed by amine oxidase with the simultaneous reduction of FAD to $FADH_2$ and the formation of H_2O_2.

Based on their cofactor dependence, amine oxidases are classified as type I and type II: type I AOs are copper-dependent enzymes containing copper and pyrroloquinoline quinone (PQQ) cofactors. Type II AOs are flavin dependent enzymes, predominantly comprising monoamine oxidases (MAO).[65] Although imine formation is catalysed by both enzymes, only flavin-dependent enzymes allow the release of the formed imines from the active site, whereas in copper-dependent enzymes, the imine intermediate is covalently bonded to the enzyme active site.[168] For this reason, type I copper-dependent enzymes are considered unsuitable for biocatalytic applications.[65] With regard to biocatalysis, amine oxidases are most extensively used for the resolution of racemic amines through dynamic kinetic resolution or deracemisation of a racemic amine substrate. Amine oxidases can be highly selective, oxidising only one enantiomeric form of a racemic mixture of amine to its corresponding imine and then to its ketone (Scheme 5. 5)



Scheme 5. 5. Amine deracemisation via selective oxidation of only one enantiomer of a racemic mixture of amine to its corresponding imine.

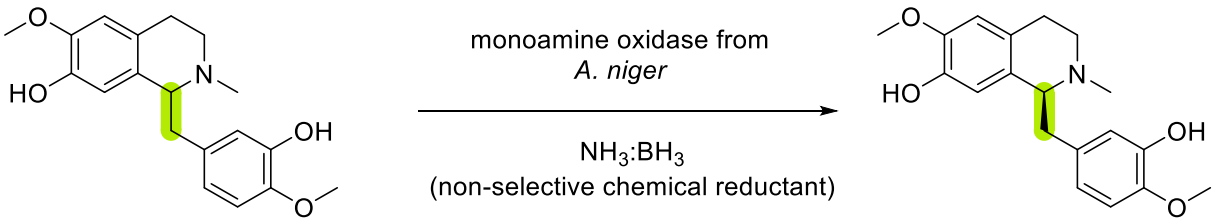
This leaves behind the other slow reacting enantiomer in an optically pure form, whereas the fast reacting amine is converted to the ketone. Thus ideally, only one enantiomer is left at the end. Rather than allowing the imine intermediate to hydrolyse into ketone, Turner and co-workers came up with the idea of adding a simple reducing agent that can reduce the remaining imine back to the racemic amine that would then undergo another round of selective oxidation to the imine (Scheme 5. 6). After multiple cycles of imine reduction and selective amine oxidation, a complete deracemisation would result in a 100% optically pure enantiomer.[280]



Scheme 5. 6. Cyclic deracemisation of racemic amines achieved by coupling amine oxidation by amine oxidase to imine reduction by a non-selective simple reducing agent.

Despite such excellent utility, amine oxidases also suffer from certain limitations. The main disadvantages with these enzymes are their narrow substrate scope, access to only (*S*)-selective

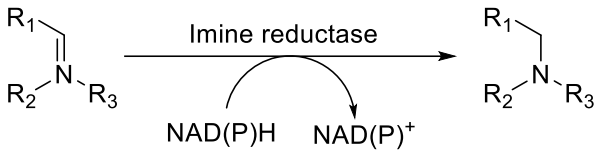
enzymes and long reaction times due to the slow oxidation of the enzyme bound FAD moiety.[168] However, with the help of directed evolution and rational design, a tool box of new AOs aimed at resolving such problems have been reported. Several monoamine oxidases from *A. niger* have been demonstrated for preparative scale synthesis. For example, the natural product (*S*)-reticuline was prepared on 150 g scale, by biocatalytic deracemisation of its corresponding benzylisoquinoline substrate by MAO variants from *A. niger* developed by Turner *et al*. with 80% yield (Scheme 5. 7).[281–284]



Scheme 5. 7. Preparative scale deracemisation of (*rac*)-benzylisoquinoline alkaloid to synthesise (*S*)-reticuline using a monoamine oxidase variant from *Aspergillus niger* in the presence of ammonia borane as the chemical reducing agent.[283]

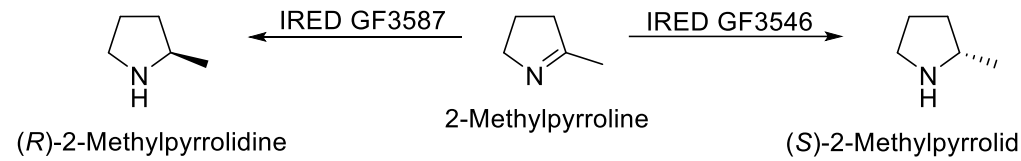
5.3.4. Imine reductases

Similar to amine oxidases, imine reductases (IREDs) are also members of the oxidoreductase family. They are NAD(P)H-dependent enzymes that catalyse the stereo selective reduction of prochiral imines to their corresponding amines. Imine reduction is a commonly observed reaction in biosynthetic pathways as a tool to generate chiral amines and is also the only class of enzymes that perform chemo selective imine reduction in nature.[76,285]



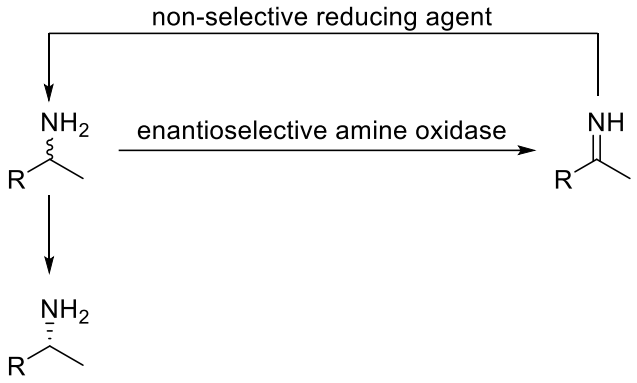
Scheme 5. 8. A typical reaction showing the NAD(P)H-dependent reduction of imine to amine catalysed by imine reductase.

An example for this case is the reduction of dihydrofolate catalysed by dihydrofolate reductase to give 5,6,7,8-tetrahydrofolate, an important cofactor in the synthesis of purine bases in most life forms. Despite this significance, the application of imine reductases for biocatalysis remained underexplored primarily due to their narrow substrate scope.[285] A major contribution to this field was made by Mitsukura *et al*., who, after screening a huge collection of microorganisms, identified two enantiocomplementary IRED's from *Streptomyces sp.* – (*R*)-IRED from *Streptomyces sp.* GF3587 and (*S*)-IRED from *Streptomyces sp.* GF3546 that reduced 2-methyl-1-pyrroline to the corresponding pyrrolidine compound (Scheme 5. 9.). Although these enzymes showed good activity with 2-methyl-1-pyrroline, similar activity could not be extended to other related substrates.[69]



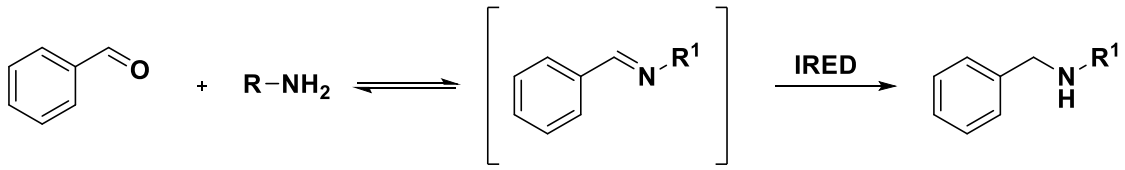
Scheme 5. 9. Two enantiocomplementary IREDs from GF3587 and GF3546 catalysing *R* and *S* selective reduction of 2-methylpyrroline to 2-methylpyrrolidine adapted from reference 284.[284]

Leipold *et al*., then expressed (*S*)-IRED from *Streptomyces sp.* GF3546 in *E. coli* and used the whole cells as biocatalysts for a wider range of substrates like dihydroisoquinolines, iminium ions and other five-, six-, and seven- membered rings.[286] Following this, they also demonstrated a gram scale preparation of (*R*)-coniine, from its corresponding imine, γ-coniceine, with 90% isolated yield and >99% *ee*, using the (*R*)-selective IRED from *Streptomyces sp.* GF3587.[287] Sometimes, the imine reductase is coupled with an amine oxidase for application in kinetic resolution. The enantioselective amine oxidase, would oxidise one of the enantiomers of a mixture of amines into their corresponding imine. The other amine enantiomer is left behind in its optically pure form. The imine formed is non selectively reduced back to its amine by a chemical reducing agent, or an imine reductase can be employed here to perform the entire reaction without any chemical reducing agent.[76,288]



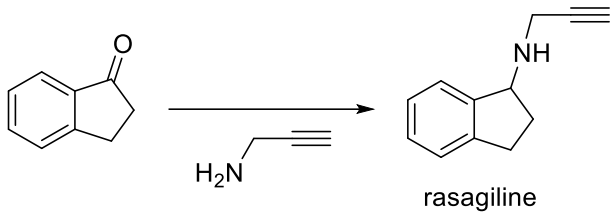
Scheme 5. 10. Deracemisation of amines using amine oxidase coupled to the imine reduction by imine reductase to accomplish a 'cyclic deracemisation' adapted from reference 282.[282]

Despite much research involved in imine reductases, the full mechanism of this enzymatic conversion is not yet known. Imine reductases offer the unique advantage of accessing primary, secondary and tertiary amines, unlike the transaminases, which are used for primary amine synthesis.[168]



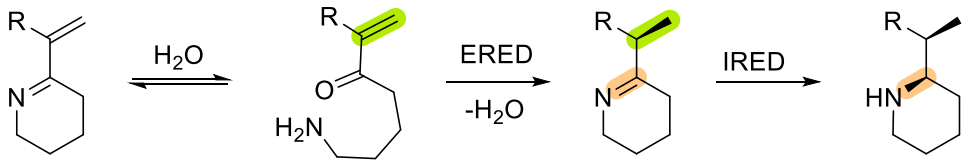
Scheme 5. 11. IRED or RedAm catalysed reductive amination forming secondary amines from their respective carbonyls adapted from reference 287.[287]

It is also worth noting that certain IREDs were also observed to catalyse reductive amination of carbonyl compounds leading to amines. This sub class of IREDs with reductive amination activity were observed by a few scientists who then named them as reductive aminases (RedAm).[289,290] For instance, RedAm have been useful in the important synthesis of rasagiline, a secondary amine used in the treatment of Parkinson's disease (Scheme 5. 12).[291]



Scheme 5. 12. Reductive amination of 1-indanone with propargylamine catalysed by an imine reductase from *Kribbella flavida* DSM 17836 (*R*-selective) or *Streptomyces ipomoeae* 91-03 (*S*-selective) to give rasagiline.[291]

The challenge associated with reductive amination by IREDs is the requirement of large quantities of the enzyme as well as excess amines, to achieve good conversions.[290] The increasing interest in the application of imine reductases in synthesis is also becoming apparent in the number of cascade reactions that are being reported. For instance, very recently, Turner and co-workers designed a cascade reaction with ene-reductases and IREDs for the preparation of branched amine heterocycles from enimines as shown in Scheme 5. 13.[292]

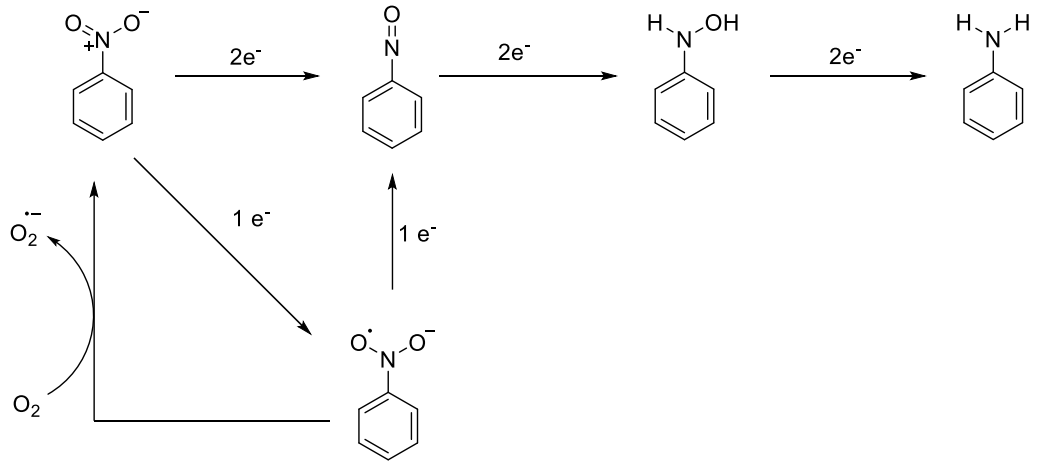


Scheme 5. 13. Selective one-pot synthesis of asymmetric heterocycles using ERED and IRED catalysed cascade reaction adapted from reference 289.[289]

5.4. Nitroreductase

Nitroreductases (NR) are flavin (FAD or FMN) containing, nicotinamide cofactor NAD(P)H-dependent enzymes mostly found in bacteria and in some archaea and eukaryotes. Their function in biology is not yet known, however, these enzymes have gained increasing interest in the last decades due to their ability to metabolise a range of nitro-compounds, thereby finding applications in bioremediation, prodrug activation in cancer therapy to facilitate enzyme mediated selective cell death,[293,294] live cell imaging, antibiotic resistance as well as for nitro reduction reactions in biotransformation, which is of interest to this project. Based on their ability to resist O_2 and their

electron transfer mechanism, nitroreductases are divided into two types: type I nitroreductases are oxygen insensitive enzymes and reduce nitro compounds by the successive transfer of two electrons obtained from NAD(P)H. This group of enzymes exhibit a broad substrate scope that includes nitro aromatic and nitro heterocyclic compounds. Type I nitroreductases have been further classified based on their cofactor dependence as NfsA and NfsB. NfsA is the major group and utilises NADH as the cofactor, whereas NfsB accepts both NADH and NADPH cofactors. Type II nitro reductases are O_2-sensitive and perform nitro reduction through a series of stepwise one-electron transfers. Under aerobic conditions, the one-electron transfer mechanism leads to the formation of a highly unstable nitro-anion radical which reoxidises quickly back to the original state accompanied by the formation of a superoxide that creates oxidative stress. Interestingly, type II enzymes can also perform two electron reductions under anaerobic conditions.[255] Scheme 5. 14. shows this process.



Scheme 5. 14. Electron transfer pathway of oxygen sensitive and oxygen insensitive nitroreductases.[295]

Type I nitroreductases are similar to ene-reductases in that they also follow a bi-bi ping pong mechanism, where a hydride is transferred from NADH to the enzyme bound flavin to generate a reduced anionic flavin. Hydride transfer from the reduced flavin to the aromatic substrate takes place subsequently. Despite the similar reaction mechanism, ene-reductases and NRs share no structural

similarity: nitroreductases are often homodimeric enzymes containing an FMN cofactor bound at their interface, and the active site is made up of residues from both the monomers.[296,297] Ene-reductases in contrast, exist as both monomers and dimers, and consist of TIM barrel structures, with the FMN cofactor bound independently to each monomer. Certain reports have shown that the activities of the two enzymes have some overlap for the two reactions – ene reduction and nitroreduction.[298] Moreover, exploration through site-directed mutagenesis have resulted in the creation of a new NR from an ene-reductase, ER KYE1 from *Kluyveromyces lactis* by Park *et al*.[49]

5.4.1. Model crystal structure of a nitroreductase

The crystal structures of several nitroreductases have been reported in the literature, and this information has contributed to better insight into the structure and binding interactions in NRs. Structural and functional knowledge of the protein framework is an important criterion for exploring site directed mutagenesis and engineering of the enzymes to further their applicability. Nitroreductases generally exist as homodimers, with two molecules of FMN held between their dimeric interface (Figure 5. 7.). The *re* face of FMN is exposed and solvent-accessible while the *si* face remains buried as observed in other similar homologous enzymes. The FMN cofactor is tightly held in position by hydrogen bonds to one monomer and by hydrophobic interactions with both the monomers, and is seen in a slightly bent 'butterfly conformation'. The substrate binding pocket containing the bound flavin is V-shaped and limits access to the *re* face of the flavin cofactor to only planar substrates.[296] Access to the active site is primarily controlled by two residues - Phe^{70} and Phe^{124}. In a later study, when NR was crystallised with a substrate nitrofurazone, it was observed that the Phe^{124} side chain undergoes displacement from its original position in the free protein to aid in substrate accommodation at the active site.[299]

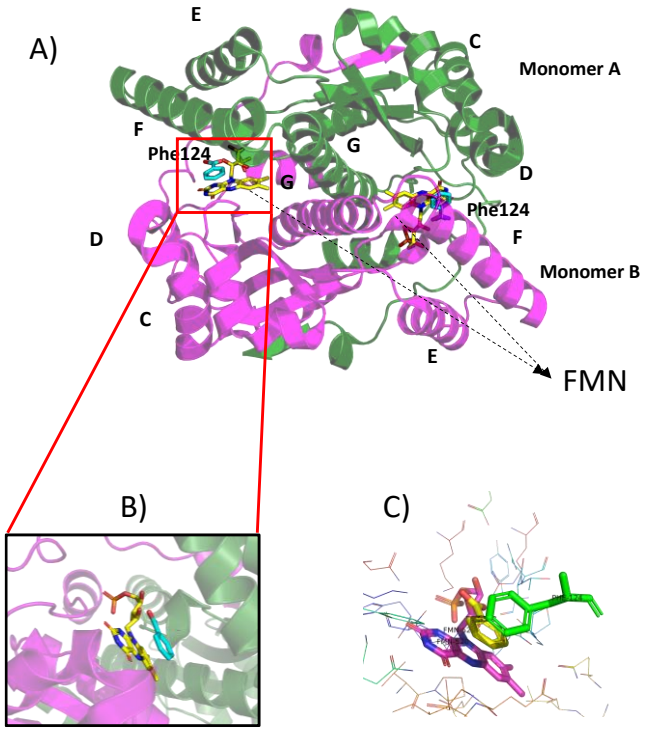


Figure 5. 7. A) Crystal structure of nitroreductase from *Enterobacter cloacae* bound with a benzoate substrate analogue. (PDB code: 1KQB, image generated using Pymol). The alphabet letters indicate the different helices. The two monomers are shown in two colours, magenta and green. The FMN bound (shown in yellow sticks) is found between the two monomers and a zoomed in version is shown in panel B. The benzoate substrate is shown as sticks in cyan.[300,301] The benzoate molecule sandwiched between FMN and Phe^{124} is shown in panel C.

Reports suggest that most substrate analogues are observed as a hydrophobic sandwich between the flavin isoalloxazine ring and the Phe^{124} ring (see panel C in Figure 5. 7.). This ring stacking could be indicative of the preference for aromatic substrates than to aliphatic substrates. Alterations to helix F have been shown to improve reactivity over 100-fold indicating that small amino acid modifications to the FMN binding site can lead to significant effects on substrate specificity and reaction kinetics[296] These arrangements indicate that redox reactions occur at the *re* face of the FMN, as the *si* face is buried within the enzyme. As a result, simultaneous accommodation of two substrates at the active site is impossible, i.e. the NADH cofactor as well as the substrate cannot be present in the active site at the same time, showing that the reaction proceeds in a ping-pong fashion with a substituted enzyme mechanism. Race *et al*. obtained crystals of *E. coli* nitroreductase bound to their

nitrofurazone substrate. In the oxidised state, the substrate was oriented towards the FMN with its amine group rather than its nitro group. The fact that substrate is sandwiched between the Phe[124] and isoalloxazine rings by Van der Waals and dipole-dipole interactions have led to a conclusion that changes in electron distribution in the flavin ring in its oxidised and reduced states is instrumental for substrate orientation and reactivity.[299]

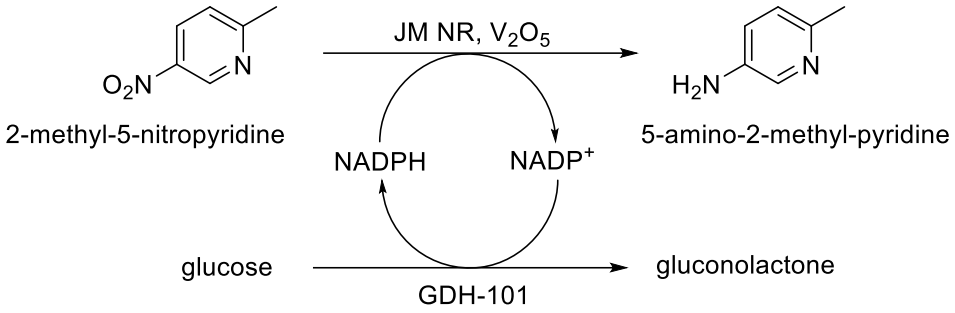
Although, ideally all NR's are expected to produce amines from their respective nitro compounds, it is important to learn that, in literature not all enzymes are reported to exhibit complete conversion to the final amines. Perhaps, most enzymes could only catalyse the reduction to the hydroxylamine product and not the final amine. For example, the oxygen-insensitive nitroreductase from *Enterobacter cloacae* catalyses the reduction of a broad range of nitro compounds to their corresponding hydroxylamine product, and not the expected amine product.[301,302] Examples of nitroreductases catalysing the complete conversion to amines is often very rare. In 2010, nitroreduction by NR from *Salmonella typhimurium* was reported and this was the first single enzyme catalysed reduction of nitrobenzene that reduced it all the way to aniline. Examples of reactions employing both NADH and NADPH as electron donors were demonstrated for a broad range of substrates.[303,304] It is important to note that for the reduction for each nitro group, three equivalents of NAD(P)H would be needed. Miller *et al*. investigated the role of substrate properties and the type of NR on nitro reduction rate as well as their ability to yield amines. The study was conducted on nitroreductases from four different super families. Firstly, they compared the reduction activities of two NR subclasses - NfsB from *S. typhimurium* and PnbA from *M. smegmatis* for a range of substrates to investigate the effect of substrate structure on reduction activity. It was concluded that substrates with a larger π system or with electron withdrawing groups showed improved activity and also facilitated progression to the final amine product.[302,305,306] Nitro reductions by nitroreductases are usually difficult to control because of the incomplete reduction to nitroso and hydroxylamine

intermediates. This is often not ideal, due to their high reactivity and toxicity. Additionally, the hydroxylamine and ntiroso products could condense to form azoxy products, all of which are reasons for the observed low yields of amine in most biocatalytic nitro reduction reactions. On the whole, the overall outcome of reactions not only depends on the enzyme activity, but also on the stability of the intermediates formed under the given conditions of pH, temperature and reaction concentrations.[303] Despite the valuable reactivity exhibited by nitroreductases, their usefulness in synthesis is often hindered by incomplete reduction to reactive intermediates that is the primary cause for low yields and unwanted side products.

5.5. Nitro reductions at Johnson Matthey (JM)

Recently, scientists at Johnson Matthey, achieved the selective reduction of several nitro aromatic compounds to their final amine products employing a combination of nitroreductase (biocatalyst) and a vanadium pentoxide catalyst that acts as the disproportionation agent to give high yields and scalability. The hydroxylamine intermediate is generated as a result of incomplete nitro reduction by the nitroreductase. This intermediate then undergoes a disproportionation cycle in the presence of V_2O_5 yielding the nitroso intermediate and the amine product. Eventually the final amine product gets accumulated over time. This finding was investigated for numerous nitroreductases against several nitroaromatic compounds and the results were patented.[307] Following this, the applicability of this reaction was demonstrated for the synthesis of 5-amino-2-methyl-nitropyridine. In particular, reaction design and enzyme engineering techniques were explored showing their importance to overcome scale-up problems and improve productivity.[36] The researchers found that moving from batch to a fed-batch reaction prevented the accumulation of intermediates to a great extent, which lowered the formation of undesired side-products. Following this, they showed the successful conversion of 500 mM 2-methly-5-nitropyridine with 95% yield in 26 h. Through rational enzyme engineering, new variants of nitroreductases were created to overcome problems of stability and

reactivity associated with the wild type enzymes. The new variant, NR-5 showed improved productivities by reducing reaction time and enzyme loading for such conversions.[36] A typical scheme for this nitro reduction is shown in Scheme 5. 15. It can be seen that the reaction is driven by nicotinamide cofactors NAD(P)H that rely on glucose and GDH-101 (Glucose Dehydrogenase-101) for their continual reduction.



Scheme 5. 15. JM nitroreductase catalyzed reduction of 2-methyl-5-nitropyridine to 5-amino-2-methyl-pyridine using NADPH and the glucose/ GDH recycling system.[36]

Employing a glucose/GDH system for cofactor recycling resulted in a few problems.[36] Firstly, nitroreductions to amines require 6 reducing equivalents which means three glucose molecules would be consumed to generate 3 NADH for every amine molecule produced. This led to an accumulation of excess gluconolactone waste that alters the reaction pH over time. For this reason, the above reactions were monitored using an automated pH STAT indicator that fed the required amount of NaOH to maintain a constant reaction pH. The unwanted waste and the constant addition of base to maintain reaction pH makes this system less attractive despite the good yields. Secondly, glucose in the reaction mixture has shown to undergo condensation with the primary amine, forming a Schiff base as an additional side product. Interestingly, compared to the various side products observed for a typical nitro reduction reaction, the glucose derived Schiff base seemed more difficult to avoid during the reaction and it remained as a major side product in most reactions, even in those reactions where the other side products were completely absent. The requirement for excessive

amounts of glucose combined with the cost of purified glucose (three equivalents for every nitro group reduced) required for this reaction results in a carbon inefficient biocatalytic system. In this respect, it was anticipated that the H_2 driven flavin recycling system can be an excellent recycling system for nitroreductases, aiding a cleaner and more sustainable reduction reaction.

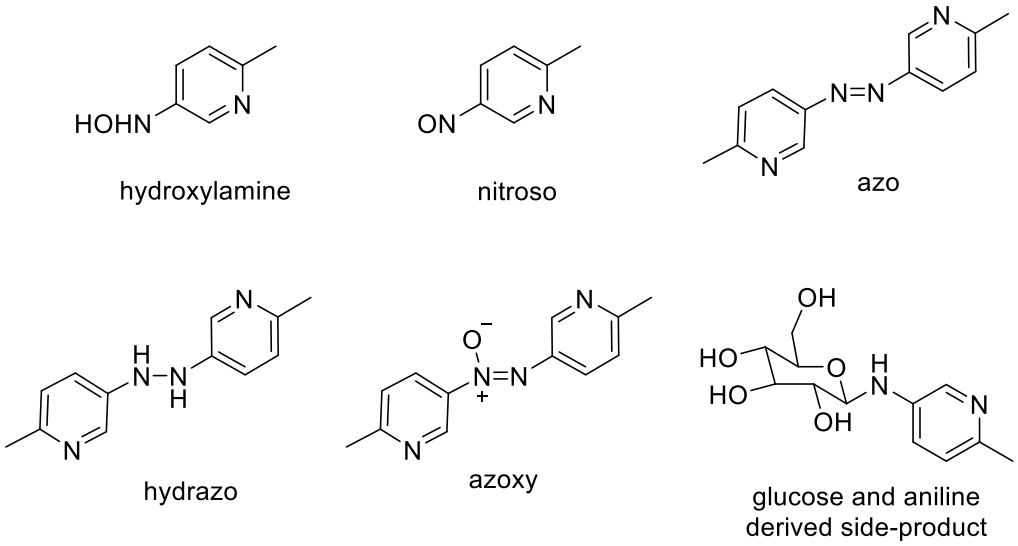
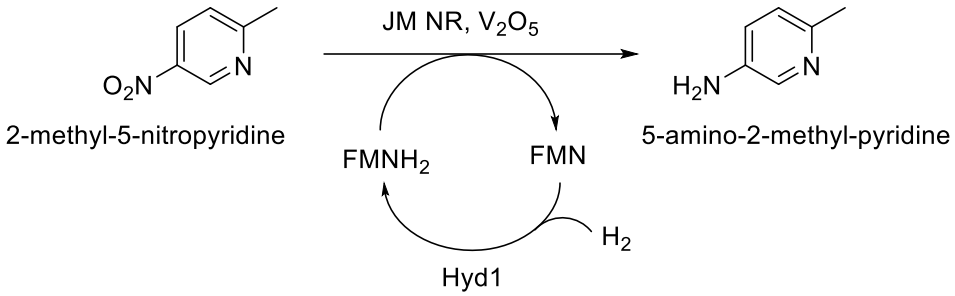


Figure 5. 8. Side products observed by JM during the reduction of 2-methyl-5-nitropyridine using nitroreductase, NADPH cofactor and the glucose/GDH-101 as the cofactor recycling system. [36]

5.6. H_2-driven flavin catalysed reduction of 2-methyl-5-nitropyridine using commercial nitroreductases from Johnson Matthey

As a starting point for evaluating the Hyd1/flavin system with nitroreductases, preliminary experiments were performed with reaction conditions similar to that published in the literature.[36] The choice of 2-methyl-5-nitropyridine as the substrate was also based on the fact that it was extensively used by the authors to perform screening studies.[36]



Scheme 5. 16. Reduction of 2-methyl-5-nitropyridine to 5-amino-2-methylpyridine using NR from Johnson Matthey, and the H_2/ flavin recycling system

The goal was to demonstrate the versatility of the flavin system with an enzyme of different reactivity other than ene-reductases, rather than comparing the performance of the two systems (H_2 driven vs $NADP^+$/glucose system). Due to time constraints and limited access to analytical facilities, a vigorous optimisation of the Hyd1/flavin for application with nitroreductases could not be performed.

5.6.1. Reaction setup and enzyme screening

Five nitroreductases, NR-4, NR-5, NR-14, NR-17 and NR-25 were initially screened to determine the most compatible enzyme for the Hyd1/flavin system. All reduction reactions were done in a pressure vessel following the experimental procedure outlined in Chapter 2, section 2.3.1. In the previous experiments with ene-reductases, using the pressure vessel was ideal to prevent the evaporation of volatile substrates and products. Although, this is not the case with the 2-methyl-5-nitropyridine and 5-amino-2-methylpyridine, it was convenient to translate the same protocol to the new reaction, helping to avoid working on a new reaction design. The reaction pH was maintained at pH 7 using a potassium phosphate buffer (100 mM). A rigorous monitoring of reaction pH is however not necessary for this reaction as no pH change occurs when H_2 is used as the reductant, because all six protons from H_2 are incorporated into the amine product or water molecules. The solid substrates

were dissolved in DMSO and introduced into the reaction mixture, such that the total DMSO vol% did not exceed 5 vol%.

Reactions were usually 300 µL in volume which was ideal for monitoring conversions of multiple reactions within centrifuge tubes placed inside a pressure vessel for reaction optimisation. A standard amount of 1 mg mL^{-1} of NR and 2 mM V_2O_5 was used for all reactions as adapted from the screening conditions found in literature.[36] All reactions were performed with 10 mM substrate in the reaction mixture, and received 10 µL of Hyd1 that corresponded to 3.95 mU activity. Reactions were allowed to run for 8 h and 3 time points were taken for each reaction at 3, 6 and 8 h. After charging with H_2, the pressure vessel was taken out of the glovebox and placed on a water bath that maintained a stable temperature of 35 °C. Reaction progress and conversions were calculated using data observed from GC, NMR and Mass spectrometry as follows.

5.6.2. Analysis in GC

Analysis of reaction mixture from nitro reduction was not straightforward due to differences in the response factor of the gas chromatograph for the 2-methyl-5-nitropyridine and 5-amino-2-methylpyridine. This could perhaps be due to the relatively low and different volatility of the nitro and amino compounds when compared to the previous alkene substrates and their hydrogenated products, for which the raw percentages of peak areas were directly used for calculating conversions.[308] Figure 5. 9. shows an exemplary chromatograph of a sample containing equal concentrations of 2-methyl-5-nitropyridine and 5-amino-2-methlypyridine.

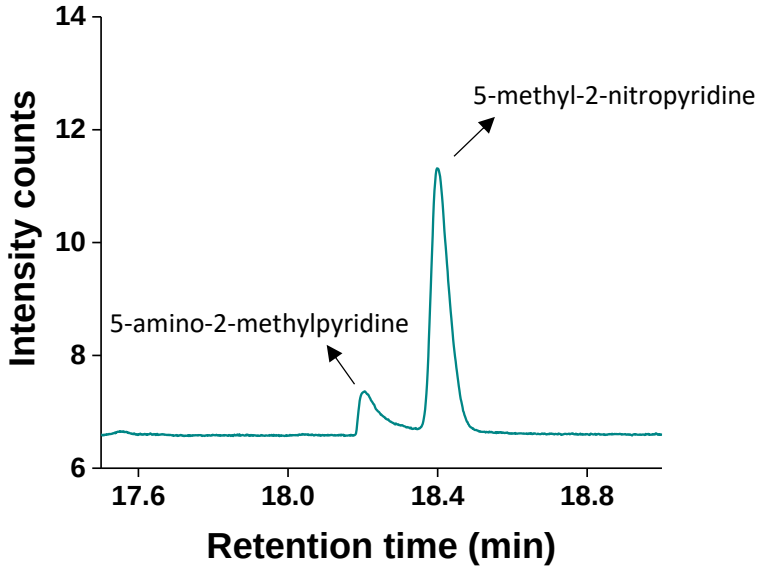


Figure 5. 9. GC chromatogram of a sample containing equal concentration of 2-methyl-5-nitropyridine and 5 amino-2-methylpyridine

Under ideal conditions the peak areas of 2-methyl-5-nitropyridine and 5-amino-2-methlypyridine should be similar or ideally the same, but the substrate at 18.4 minutes gives significantly greater counts compared to the product. In other words, it can be said that the GC detects the substrate better than the product by a certain value. A ratio of the peak area counts for the substrate and product is helpful to determine a corrected area for the product which then gives the actual concentration of the product in the reaction mixture.

To resolve this issue, a standard solution containing equimolar concentrations of the substrate and product was prepared to calculate a valid ratio that can reflect the original amounts of compounds in the chromatogram. A GC analysis sample was prepared exactly how a reaction mixture sample would be prepared for analysis i.e. 10 mM stock solutions of the substrate and the product were made in buffered solution of 300 µL total volume. Then equal quantities of the two stock solutions (5 µL substrate + 5 µL product) were mixed with 200 µL EtOAc, and the resulting mixture was vortexed for 10 seconds. Then, 150 µL of the organic layer was removed, dried over anhydrous sodium sulphate,

and 100 µL of this sample used for analysis by GC. This procedure was repeated thrice to determine an average value of the required ratio of corrected areas. This value was used throughout to correct the peak areas of the product obtained and hence the conversions. This is illustrated by the following sample calculation.

The peak area recorded for an equimolar solution of the product and substrate in the above chromatogram is 0.0635 and 0.2977 respectively. Ratio of corrected area is given by

$$Ratio\ of\ corrected\ area = \frac{0.0635\ area\ counts\ for\ amine}{0.2977\ area\ counts\ for\ nitro} = 0.21$$

For a sample displaying a 30:70 ratio of raw nitro:amine peaks in the GC chromatogram, the real ratio of the compounds will be calculated as given below.

$$\frac{70\ area\ counts\ for\ amine}{30\ area\ counts\ for\ nitro} \rightarrow \frac{70/0.21\ (amine)}{30\ (nitro)} = \frac{333\ (amine)}{30\ (nitro)}$$

These areas can then be converted to the percentage of each compound as

$$\%\ amine = \frac{333}{333 + 30} * 100 = 92\%\ amine$$

Thus the sample is actually a mixture having 8%/92% of the nitro and amine compound respectively.

This calculation is based on the assumption that the amine is the only product in the reaction mixture, because other possible side products were not detected in GC.

Following the above calculation, all reaction conversions were calculated. The following table shows the conversion values from GC, obtained for an initial screening of the different nitroreductases under the exact same reaction conditions.

Table 5. 1. Conversion of 2-methyl-5-nitropyridine to 5-amino-2-methylpyridine calculated from GC chromatogram values, corrected for the different counts observed for substrate and product

Entry	**Nitroreductase**	**%Conversion to 5-amino-2-methylpyridine[a]**		
		3 h	**5 h**	**8 h**
1	NR-4	10	43	70
2	NR-5	9	46	73
3	NR-14	10	45	74
4	NR-17	13	51	75
5	NR-24	12	50	77

Reaction conditions: 300 µL scale, 3.95 mU Hyd1, 1 mg mL^{-1} NR, 1 mM FMN, 10 mM 2-methyl-5-nitropyridine in potassium phosphate buffer (100 mM, pH 7), 5 vol% DMSO at 35 °C in pressure vessel (under 1 atm H_2). [a]GC conversion to 5-amino-2-methylpyridine.

The conversion values to 5-amino-2-methly-pyridine by the different NRs were quite similar indicating that the H_2/flavin recycling system was compatible and performed equally well with all the nitro reductases. However, conversion values for reactions that employed the GDH/glucose system varied for different nitroreductases. While NR-4 performed better than NR-14, the engineered enzyme, NR-5 showed the best activity and conversion with a maximum yield of 13.7 g 5-amino-2-methly-pyridine per g of NR used.[36]

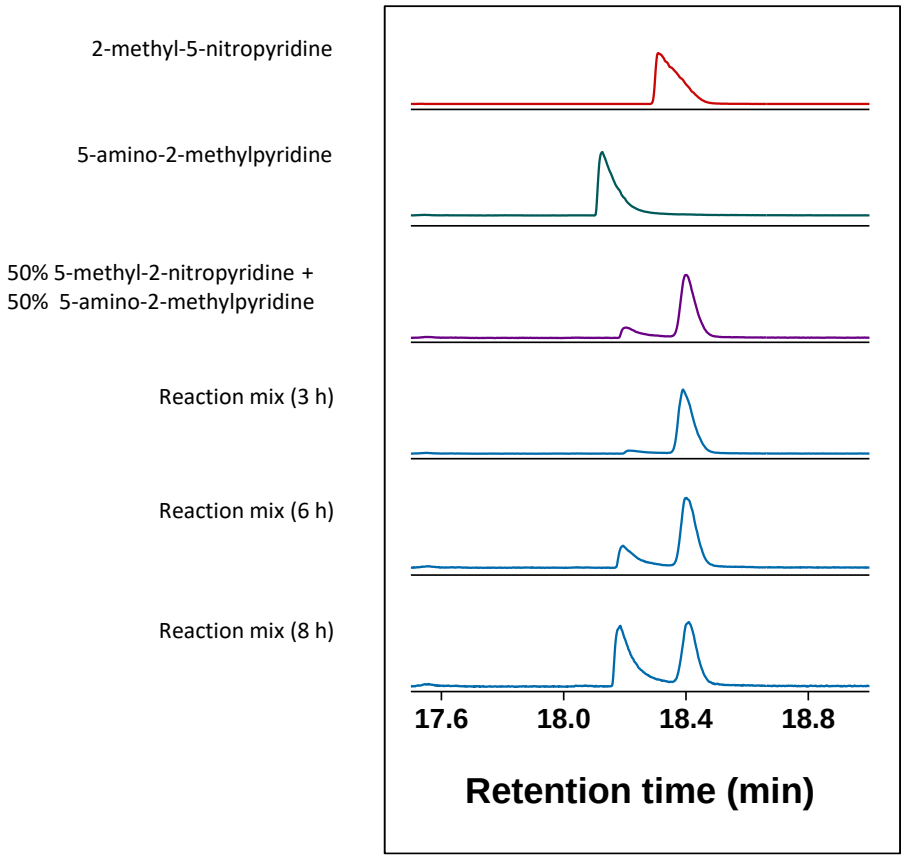


Figure 5. 10. GC chromatogram of 2-methyl-5-nitropyridine (red), 5 amino-2-methylpyridine (green), 50:50 ratio of 2-methyl-5-nitropyridine and 5 amino-2-methylpyridine (violet), and 3, 6 and 8 h time pints of the reaction mixture corresponding to entry 5 in Table 5. 1.

Additionally the reaction mixtures from nitro reduction reactions were also analysed by NMR to ensure the absence of any side products. Reaction mixtures used for analysis in GC and in NMR differed in substrate concentrations and time points, because higher substrate concentrations (at least 20 mM) were required for an NMR spectrum with good resolution. Therefore, these reactions were performed with a substrate concentration of 20 mM and analysed by NMR at 20 h.

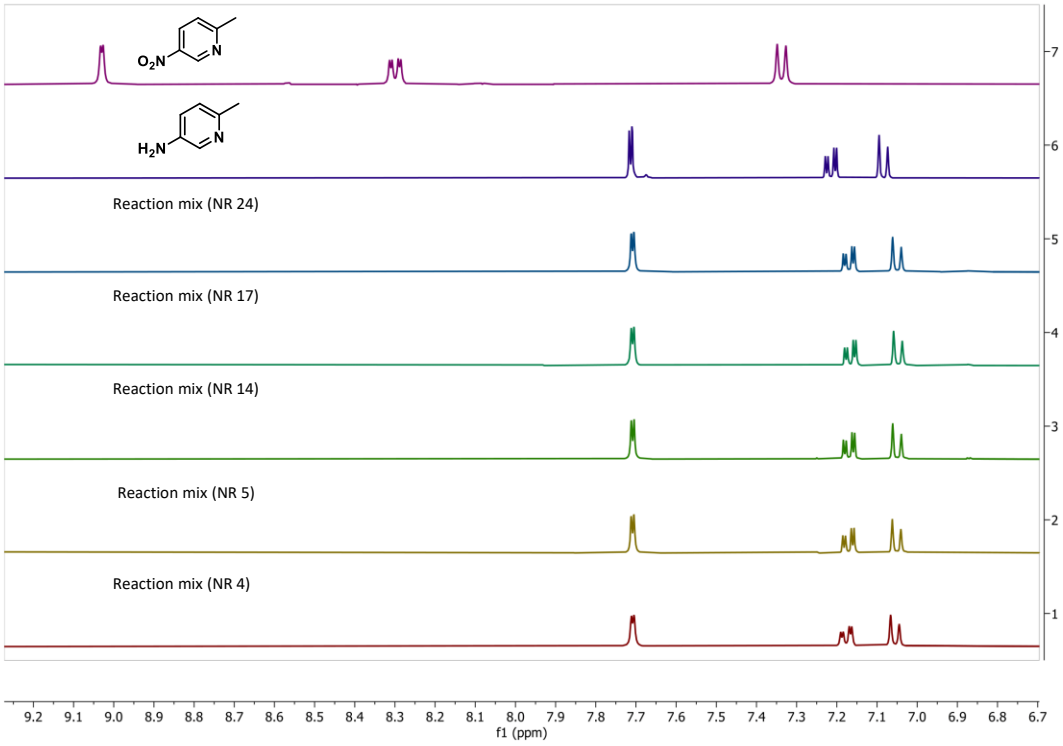


Figure 5. 11. ^{1}H NMR spectra of all the reactions used for screening the activity of the different NRs with the H_2/flavin recycling system.
Reaction conditions: 500 µL scale, 3.95 mU Hyd1, 1 mg mL^{-1} NR, 1 mM FMN, 20 mM 2-methyl-5-nitropyridine in potassium phosphate buffer (100 mM, pH 7), 5 vol% DMSO at 35 °C in pressure vessel (under 1 atm H_2).

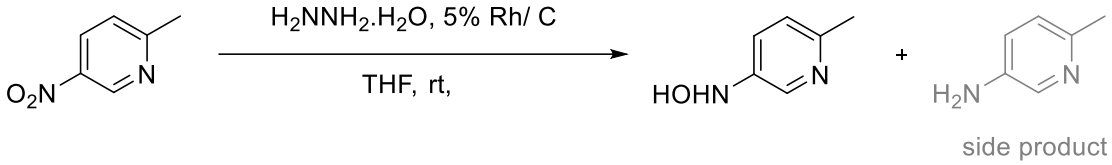
The NMR spectra of reaction mixtures with various NRs (Figure 5. 11.) showed no peaks that corresponded to the hydroxylamine intermediate, confirming the absence of any side products. This is also an indication that all nitroreductases catalyse the reaction almost equally well.

Simultaneously, the hydroxylamine product was also synthesised to compare the NMRs of the reaction mixtures.

5.6.3. Synthesis of *N*-(6-methylpyridin-3-yl)hydroxylamine

In accord with Feng *et al.*[309], 200 mg of 2-methyl-5-nitropyridine (1.4 mmol) and 24 mg of Rh/C (5%) were stirred in THF (7.5 mL) under an N_2 atmosphere at 23 °C. To this suspension, 0.1 mL of hydrazine monohydrate (2.0 mmol) was added dropwise and the reaction was allowed to stir at room

temperature. After 2 h 45 min, the suspension was filtered through a pad of celite, then the filtrate was extracted into EtOAc, concentrated *in vacuo* to obtain 20.7 mg (11% yield) of a mixture of amine and hydroxylamine as a yellow solid.



Scheme 5. 17. Laboratory synthesis of *N*-(6-Methylpyridin-3-yl)hydroxylamine to be used for comparing the NMRs from the nitro reduction reactions. The side product (in grey) was obtained as a result of over reduction of the hydroxylamine product.

The unusually low yield was due to excessive product loss during filtration through the celite. However, this was enough to analyse the product by NMR. Figure 5. 12 shows the ^{1}H NMR spectrum of *N*-(6-methylpyridin-3-yl)hydroxylamine with the over-reduced amine impurity.

^{1}H NMR of hydroxylamine (400 MHz, 9:1 H_2O+D_2O) δ 7.93 (d, *J* = 3.5 Hz, 1H), 7.13 (dd, *J* = 8.7, 2.6 Hz, 1H), 7.02 (d, *J* = 8.4 Hz, 1H)

^{1}H NMR of amine (400 MHz, 9:1 H_2O+ D_2O) δ 7.72 (d, *J* = 3.5 Hz, 1H), 7.24 (dd, *J* = 8.4, 2.8 Hz, 1H), 7.07 (d, *J* = 8.4 Hz, 1H)

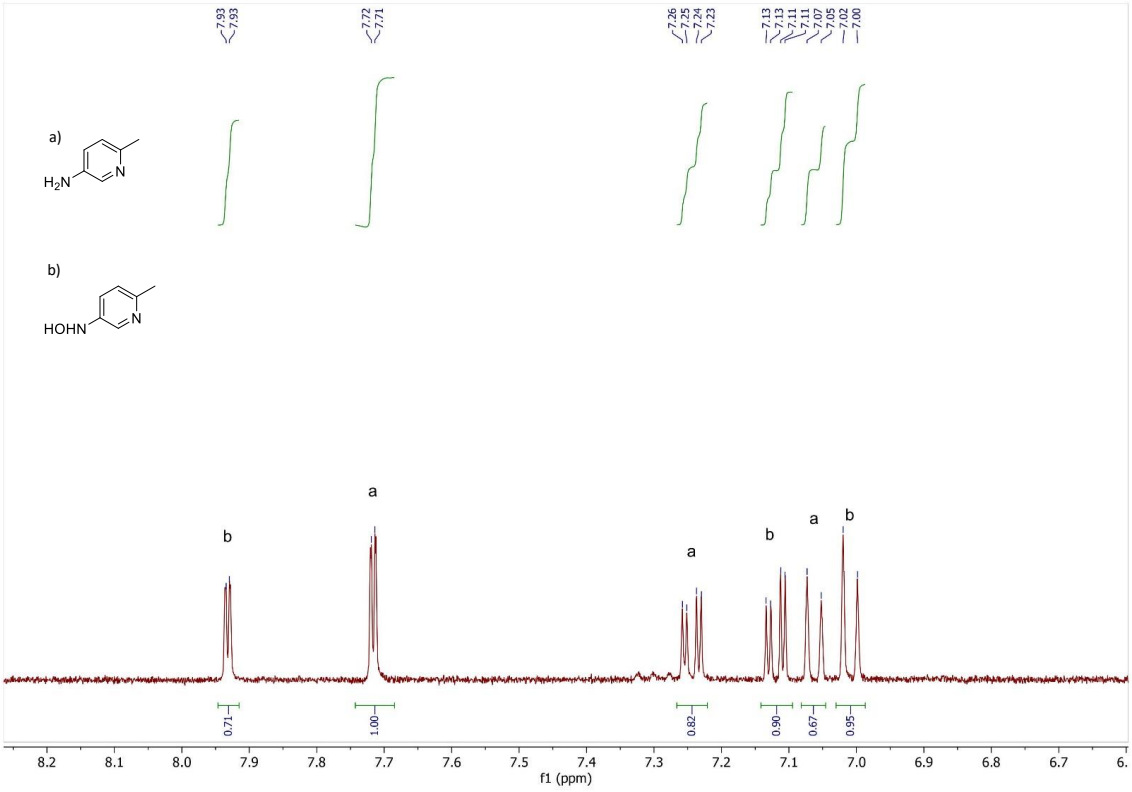


Figure 5. 12. ^{1}H NMR spectrum of *N*-(6-methylpyridin-3-yl)hydroxylamine with the over-reduced amine impurity

5.6.4. Reproducibility of nitro reduction reactions

To make sure that these values are reliable, it was next important to check the nitro reduction reactions were reproducible and that the conversions calculated for the reactions are within reasonable limits of experimental error.

So, two reaction tubes, each containing the same amount of substrate, enzyme loading (Hyd1 and NR-17) and total reaction volume were prepared and placed within the pressure vessel for the reaction. Time points were taken at 3 and 6 h, and the corresponding standard errors were calculated as shown in Table 5. 2 and it can be seen that the conversion values are within a reasonable value of error.

Table 5. 2. Results from a duplicate reaction to show reproducibility of the reaction

Entry	**%Conversion to 5-amino-2-methylpyridine**	
	3 h	**6 h**
1	8	49
2	6	46
Standard deviation	1	1.5
Standard error	0.7	1.1

Reaction conditions: 300 µL scale, 1 mM FMN, 3.95 mU Hyd1, 1 mg mL^{-1} NR-17, 10 mM 2-methyl-5-nitopyridine, potassium phosphate buffer (100 mM, pH 7.0), 5 vol% DMSO at 35°C) in a pressure vessel (1 bar H_2)

5.6.5. Control experiments

Control reactions are a useful way to ensure that the reaction proceeds in the expected route. Hence, various combinations of the reaction mixture, with and without the different catalysts and the FMN cofactor were performed. Time points for these reactions were taken at 3 h, 6 h and at 20 h and the conversions obtained are tabulated in Table 5. 3.

Table 5. 3. Results from the control experiments for the reduction of 2-methyl-5-nitropyridine

Entry	**Hyd1**	**NR-17**	**FMN**	**V_2O_5**	**Conversion to 5-amino-2-methylpyridine (%)**		
					3 h	**6 h**	**20 h**
Full reaction	✓	✓	✓	✓	**8**	**49**	**100**
5	✓	✓	-	✓	1	10	69
4	-	✓	✓	✓	0	0	0
3	✓	-	-	✓	1	13	63
1	✓	✓	✓	-	1	n.d.	99
2	✓	-	-	-	0	2	48

Interesting results were obtained from the control reactions. Conversions at the 3 and 6 h time points were indeed quite low for all the reactions that did not receive one or more reaction components. However, when the reactions were analysed at 20 h, considerable conversions could be seen for many entries in Table 5. 3.

Another important point to consider here is the formation of side products. Since the GC chromatograph is unable to separate and detect the expected hydroxylamine intermediate, these reactions were analysed by NMR. A clear result from the table, is that in the absence of Hyd1, no conversion was obtained at any time point. Entry 2 shows that Hyd1 alone is capable of reducing the nitro compound, presumably via a direct reduction by electrons released from H_2 oxidation. However, it is important to ensure that the substrate has been converted to the desired amine product and not the hydroxylamine intermediate.

5.6.6. Evaluating the efficacy of control reactions in generating the final amine product

Analysis of the reaction mixtures from control reactions by NMR is essential to ensure that the conversion of 2-methyl-5-nitro-pyridine has proceeded to the amine product and not the hydroxylamine intermediate, which were indistinguishable in analysis by GC. This is important to understand the key roles of various catalysts in the reaction, in particular, those that facilitate the complete conversion to the amine.

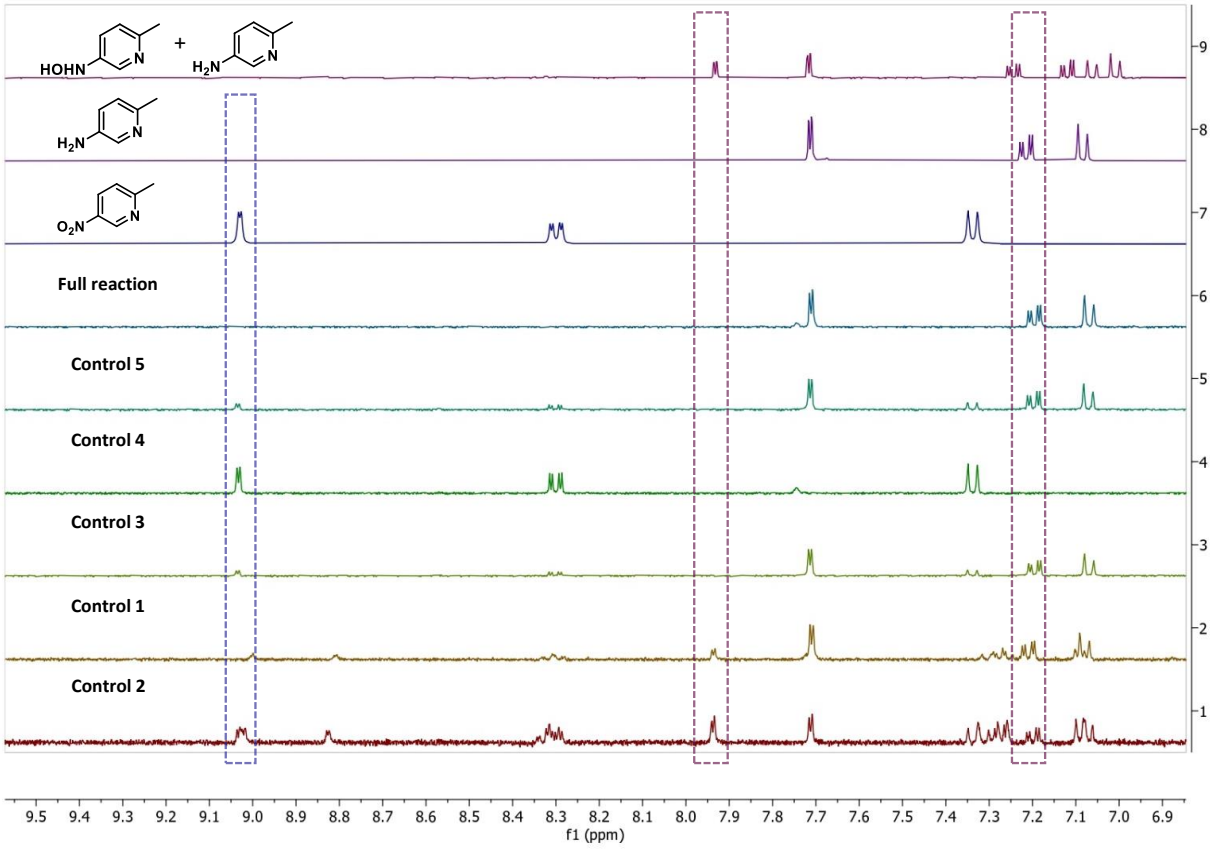


Figure 5. 13. ^{1}H NMR of all the control reactions, the nitro substrate, amine product and the hydroxylamine + amine mixture.

The full reaction showed a clean and complete conversion to the amine as we can see by comparing the NMR spectra of the substrate and the expected product. Control reactions 1 and 2 showed the presence of hydroxylamine as seen from the NMR above. These reactions were the only ones that did not contain V_2O_5 metal catalyst. This proves that the presence of V_2O_5 is key for driving the reduction of hydroxylamine to amine, with the H_2-driven flavin recycling system, just as it was found to be with GDH/glucose/NADPH system. Almost all control reactions showed at least trace amounts of the starting material. Control reaction 4 that did not have Hyd1 showed zero conversion. Control reaction 5 that did not have any FMN showed 69% conversion to the final amine. No hydroxylamine is detected from the NMR. This suggests that Hyd1 can reduce the enzyme bound FMN present in the nitroreductase, although it is possible that traces of free flavin released form the enzyme could carry

out an electron shuttle role. Control reaction 3 containing just Hyd1 and V_2O_5 also shows 63% conversion to the product which could indicate that Hyd1 alone (in the absence of NR) is capable of reducing the substrate to the final amine product, provided the V_2O_5 catalyst is also present. This requirement of V_2O_5 can be confirmed from the NMR of control reaction 2 which had only Hyd1 (and no V_2O_5). Although half the substrate has been reacted in this reaction, the NMR clearly shows the presence of a significant portion of the hydroxylamine. Thus it was inferred from these control reactions that the presence of V_2O_5 was key to achieve complete conversion of the nitro substrate to the amine. Comparing the conversion rates for the control reactions and the original reaction, it can be concluded that the reaction proceeds quickly and cleanly when all the reaction components are present. The addition of a catalytic quantity of FMN significantly contributed to faster conversion rates.

5.6.7. Reaction intensification

With the preliminary studies having been conducted, it was then important to explore the potentials of this system for larger scale reactions. For this, a more intensified reaction was performed with NR-14 where the reaction scale was increased from 300 to 500 µl and substrate concentration was increased to 20 mM. Full conversion to the product was recorded at 19 h. Analysis of this reaction mixture in NMR (Figure 5. 14.) showed no accumulation of the hydroxylamine side product. Further analysis of the reaction by mass spectrometry was performed to make sure that there were no side products (Figure 5. 15.). The molecular mass of 2-methyl-5-nitropyridine and 5-amino-2-methylpyridine are 138.13 and 108.14 respectively. Samples for analysis were prepared following the procedure outlined in chapter 2, section 2.4.4. Panels B and C in Figure 5. 15 show the mass spectra of the product and substrate standards that show a prominent peak at $[M+H]^+$ = 109.1 and 139.0 respectively. Panel A shows the mass spectrum of the reaction mixture which also shows a single prominent peak that corresponds to that of the amine product. The absence of additional peaks in

the mass spectrum of the reaction mixture indicates that no unwanted side products were generated.

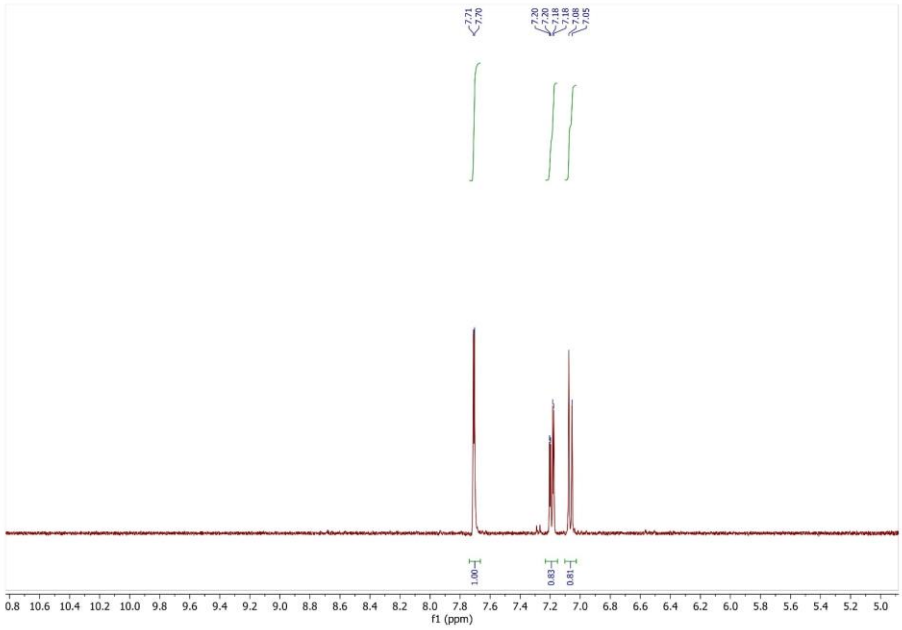


Figure 5. 14. ^{1}H NMR spectrum of reaction mixture used for reaction intensification with NR-14.

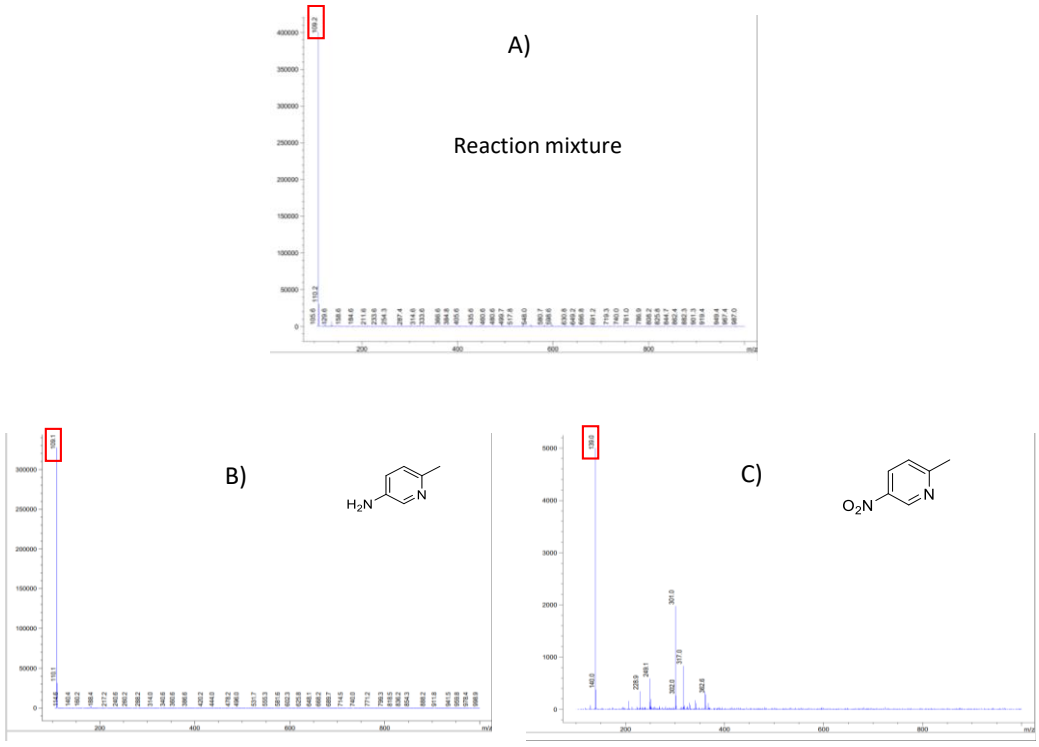


Figure 5. 15. Mass spectrum of A) the reaction mixture used for reaction intensification with NR-14 confirming the presence of the expected product and the absence of other side products, B) 5-amino-2-methylnitropyridine and C) 2-methyl-5-nitropyridine standards

5.7. Summary

A proof-of-concept that the H_2/flavin system can be extended to a different family of enzyme, nitroreductases, has been demonstrated. Under non-optimised conditions, good reaction conversions have been reported and several different commercial NRs have been screened. A vigorous exploration for reaction scale up for these reactions could not be performed due to time constraints, but the preliminary results obtained so far have shown good promise. In particular, using the H_2-driven flavin recycling for nitro reduction reactions can substantially lower the carbon based waste generated from using thrice the amount of glucose for every substrate molecule reduced. The addition of a base for monitoring reaction pH and the formation of unwanted side products from the reaction between reaction intermediates and glucose is also avoided. These advantages make the Hyd1 an attractive flavin regeneration catalyst for nitro reduction reactions.

6

Chapter 6 The Deazaflavin cofactor, F_{420}

Chapter 6 focuses on extending the application of hydrogenases as a regeneration catalyst for another cofactor – the F_{420}, a deazaflavin coenzyme that has gained attention lately due to the ability of F_{420} enzymes to catalyse chemical transformations for a broader range of substrates that were otherwise impossible to achieve using NAD(P)H or flavin-dependent enzymes. A brief background on deazaflavins, their laboratory synthesis, potential regeneration techniques and results obtained for preliminary attempts to reduce them with different hydrogenases are discussed here.

6.1. Deazaflavins

Up to now, enzymatic reduction of activated double bonds has been achieved largely with enzymes that employ nicotinamide cofactors, NADH or NADPH. Recently, there has been interest in a new class of cofactors – the deazaflavins, found in a range of useful enzymes.[64,310]

The most important form of deazaflavin cofactor, F_{420} was first discovered by Cheeseman *et al*. in 1972, as a fluorescent compound that was involved in the hydrogen metabolism of a methanobacterium strain M.o.H. The name F_{420} arises from the observed absorption maximum of the compound at 420 nm at pH 7 and 'F' here stands for 'factor'.[311] Eirich *et al*. later reported that this cofactor was a predominant constituent in anaerobic bacteria that generally biosynthesise methane, and considered it as a signature molecule of methanogenic bacteria.[192] As time passed, this cofactor was also identified in other species like the sulphate-reducing archaea, halobacteria, streptomycetes, mycobacteria and in the blue-green algae, *Anacystis nidulans*.[63,192] It has been proposed that these cofactors are a result of evolution by enzymes in search of cofactors with distinct electrochemical properties.[312] Perhaps, it could have also been an attempt to access a cofactor with properties hybrid between the nicotinamides and the flavins.[313]

6.1.1. Structure and chemistry of deazaflavins

Deazaflavins contain a 7, 8-didemethyl-8-hydroxy-5-deazariboflavin core closely resembling the isoalloxazine ring of flavins, but with a prominent difference at position 5, where the nitrogen atom (N-5) is substituted for a carbon atom (C-5) (Figure 6. 1).[63] Positions C-7 and C-8 in the ring are unsubstituted and hydroxylated respectively in F_O and F_{420}, unlike in flavins where the corresponding positions are methylated. Depending on the substitution at N-10, two important deazaflavins have been reported in biological systems – F_o, where N-10 contains a ribitol side chain, and F_{420} where the ribitol side chain is further ligated to 2 to 7 glutamate residues through a phospholactate moiety (Figure 6. 1). The number of glutamate residues present varies depending on the microorganism. Pioneering work by Walsh has shown that the substitution of N-5 in place of C-5 in the isoalloxazine ring has been the crucial determinant that renders F_{420}-dependent enzymes with distinct electrochemical properties — a redox potential as low as -380 mV, compared with riboflavin (-210 mV), FAD (-220 mV), FMN (-190 mV) and nicotinamides (-320 mV).[192,194] The thermodynamic potential for the $F_{420}/F_{420}H_2$ couple at pH 7, 25 °C is -340 mV[314,315] and that for the H^+/H_2 couple at pH 7 is -413 mV. This means, in theory, the reduction of F_{420} by H_2 is just feasible thermodynamically, provided the hydrogenase starts oxidising H_2 close to the H^+/H_2 potential. However, Hyd1 starts oxidising H_2 at about 80-100 mV above this potential, so the reaction might not occur with Hyd1 as the catalyst.[197] The unusual low redox potential helps F_{420}-dependent enzymes to reduce an even broad range of substrates that are otherwise quite recalcitrant.[22] Besides possessing a low redox potential, dihydro reduced forms of deazaflavin cofactors show an increased stability towards reoxidation by O_2 with a half-life in the order of hours, instead of seconds as that observed for flavins.[314]

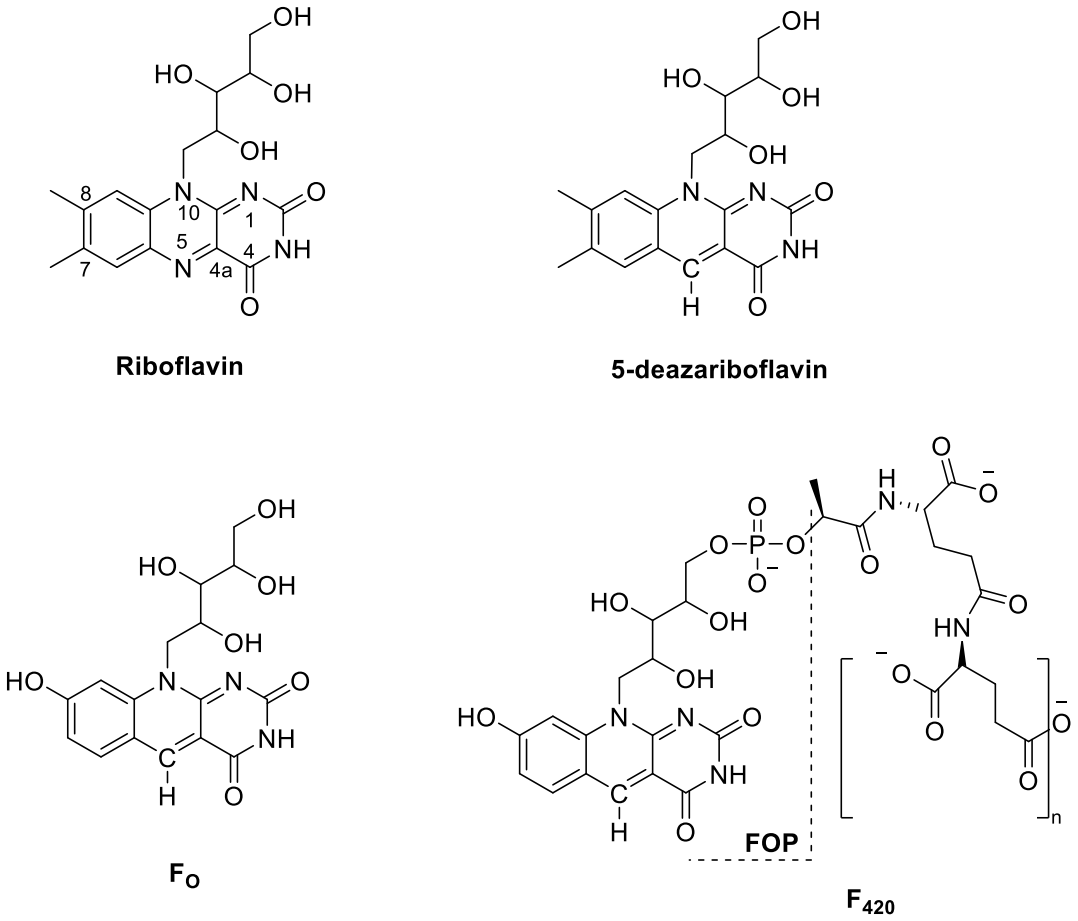


Figure 6. 1. Chemical structures of riboflavin, 5-deazariboflavin, F_O, FOP and F_{420}.

6.1.2. F_{420} and F_O

The two cofactors, F_O and F_{420} drastically differ from one another in terms of physiology and distribution. F_O is distributed widely in nature, but, only serves as a chromophore rather than a cofactor in biological systems. In contrast to F_O, the taxonomical distribution of F_{420} is limited to only to two phyla, Euryarchaeota and Actinobacteria.[63] It functions as a hydride donor/acceptor that is capable of mediating an array of challenging catalytic cycles. However, F_{420} is difficult to isolate in large quantities and laboratory synthesis of this cofactor is also tedious involving several unstable, highly reactive intermediates that can lower the overall reaction yield.[316,317] Fortunately, the more accessible F_O can act as an F_{420} mimetic in vitro, which makes it simpler to develop deazaflavin

mediated reactions on a practical scale.[22,314,318] The additional catalytically inactive side chain present in F_{420}, increases substrate affinity of the cofactor by several folds, but decreases the enzyme turnover rates. The increased substrate affinity is attributed to the formation of electrostatic interactions between the F_{420} oligoglutamate side chain and the conserved surface residues of the F_{420}-dependent enzymes. Thus, this results in a higher affinity and a diminished turnover rate. This difference in affinities with variable F_{420}-tail length (two glutamates compared to 5-8 glutamates) has been experimentally verified in literature.[319] In cases where only F_{420} is particularly required, the cofactor is harvested from sources that naturally produce it, especially from many species of *Mycobacteria*, albeit in very low yields. Recently, Shah *et al*., reported the production of F_{420} from the simple *E. coli* by heterologously expressing the biosynthetic genes from *Mycobacterium smegmatis* and *Methanosarcina mazei*. This biosynthesis of F_{420} in *E. coli* was optimised to produce the highest recorded yield of 3.0 µmol g^{-1} DCW (grams of dry cell weight).[320]

6.1.3. Deazaflavins – nicotinamide in a flavin's clothing[192]

Upon one electron reduction, both nicotinamides and deazaflavins form high energy pyridine radicals that prevent them from forming stable semiquinones. Flavins on the other hand form a relatively more stable central pyrazine radical allowing them to perform both one and two electron transfer processes.[192,314,321] As a result, deazaflavins behave as two electron carriers, similar to the nicotinamides, despite their structural similarity to flavins. This has led to a description of deazaflavins as a 'nicotinamide in a flavin's clothing'.[192]

The increasing number of isolated and characterised F_{420}-reducing dehydrogenases and F_{420}-dependent enzymes strengthen the possibility of exploiting them in biotechnology to achieve new reactions.[64,319,322–326] F_{420} recycling techniques are still underdeveloped like that of the flavins in terms of industrial applicability and economic needs.

6.1.4. UV-visible spectroscopy of F_{420}

Deazaflavin compounds are generally UV-active and fluorescent compounds. In the presence of UV light, the delocalised electrons in the isoalloxazine ring undergoes π→π* transition. In the oxidised state, F_{420} shows an absorption maximum at λ = 420 nm and the position of this peak changes depending on the pH of the sample.[193] Apart from the prominent peak at 420 nm, transitions of n→π* character display peaks at 344 and 292 nm of low strength.[327] Upon reduction, the peak at 420 nm is lost and $F_{420}H_2$ that is formed displays a new peak at 320 nm.[328]

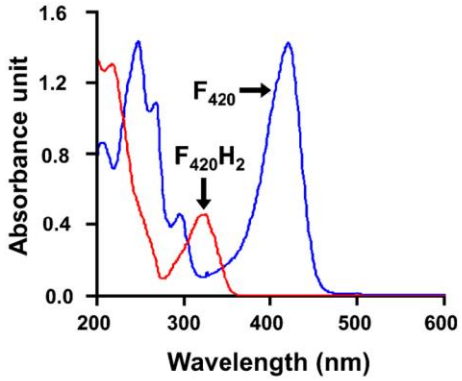


Figure 6. 2. UV-visible spectrum of F_{420} (blue) and $F_{420}H_2$ (red) reproduced from reference 63.[63]

6.2. Potential cofactor recycling methods for F_{420}

Similar to the well-known glucose dehydrogenase (GDH) that reduces $NAD(P)^+$ to NAD(P)H, by converting glucose to gluconolactone, F_{420} has also been found to be reduced to $F_{420}H_2$ by an enzyme called glucose-6-phosphate dehydrogenase (G6PD).[329] The reaction proceeds with the stoichiometric consumption of glucose-6-phosphate that gives 6-phosphogluconolactone. Glucose-6-phosphate dehydrogenase is essentially an $NADP^+$ reducing enzyme that participates in the pentose phosphate pathway, delivering reducing energy to the cells. However, later, another family of G6PDs, initially discovered in *Nocardia* and *Mycobacteria* showed exceptional F_{420} reducing properties and were hence called F_{420}-dependent glucose-6-phosphate dehydrogenases (FGDs).[329] Following this,

additional FGDs were identified in several microorganisms like *Methanoculleus thermophilus, Rhodococcus jostii* RHA1, *Nocardioidaceae and Cryptosporangium arvum*.[313,330] The latter two FGDs from *Nocardioidaceae* and *Cryptosporangium arvum*, are promiscuous towards other 6-phosphate sugars and are also named as F_{420} sugar-6-phosphate dehydrogenases (FSDs) for this reason. Nevertheless, their highest specificity is towards glucose-6-phosphate (G6P). Mycobacterial FGDs and the FGD from *Rhodococcus jostii* RHA1 are highly specific to G6P, and have shown to exhibit poor activity with other sugar-6-phosphates.[313,330] A good example for the application of FGD, was demonstrated by Mathew *et al*., where $F_{420}H_2$ was recycled using FGD from *Rhodococcus jostii* RHA1 to support enantio- and regioselective ene-reductions by $F_{420}H_2$-dependent reductases.[22]

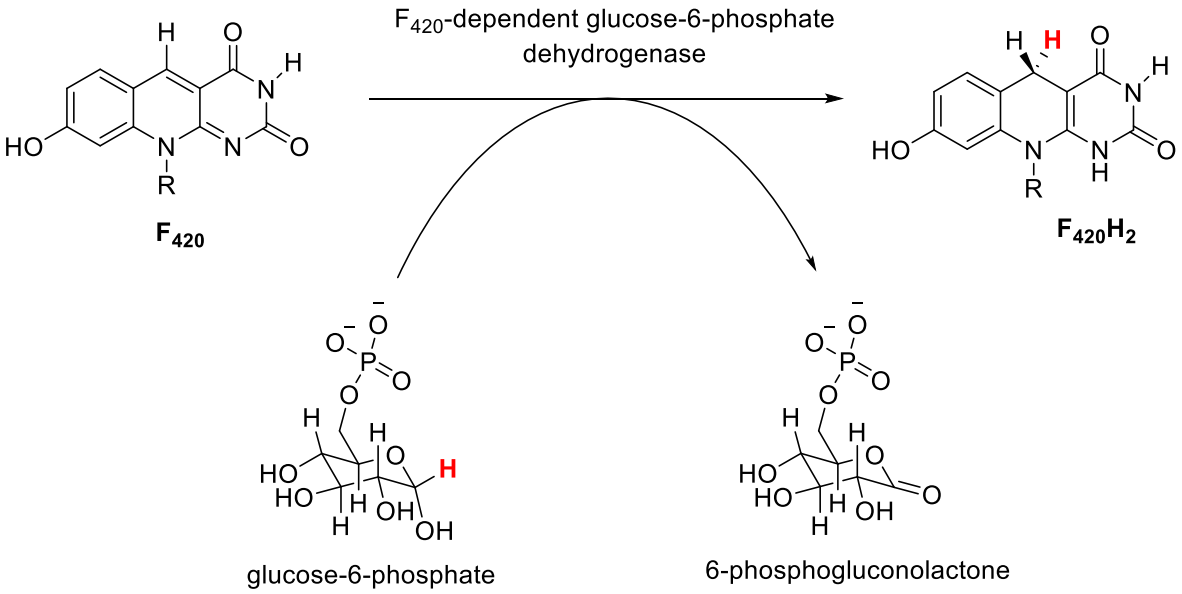


Figure 6. 3. An F_{420}-dependent glucose-6-phosphate dehydrogenase reduces F_{420} to $F_{420}H_2$ by converting glucose-6-phosphate to 6-phosphogluconolactone. The hydrogen atom in red denotes hydride transfer taking place from C-1 of glucose-6-phosphate to C-5 of F_{420} resulting in $F_{420}H_2$ and the side product, 6-phosphogluconolactone.

Formate dehydrogenase (FDH), employing formate as a reductant is also an attractive catalyst for F_{420} cofactor recycling as the end product is volatile CO_2. In the past, several methanogenic bacteria have shown to possess formate dehydrogenase linked to F_{420} reduction.[331–333] Their application for F_{420}

reduction in vitro is less explored at the moment, however these enzymes represent a promising system for F_{420} recycling for biocatalytic application.

F_{420}:NADPH oxidoreductase (Fno) which couples F_{420} reduction with NADPH oxidation and vice versa is another potential recycling system for F_{420} cofactor. In methanogens, Fno is involved in reducing $NADP^+$ i.e. it functions as an $F_{420}H_2$-dependent NADP reductase. This is also the thermodynamically feasible reaction considering the redox potentials of the two cofactors. While in bacteria, Fno acts in the reverse direction as an F_{420}-reducing NADPH dehydrogenase.[63,334–336] When employed for F_{420} regeneration in vitro, Fno needs to be coupled with an NADPH regenerating system which adds to the complexity of the reaction.[335]

Certain H_2 metabolising microorganisms including methanogens and sulphate reducing archaea, have shown to possess NiFe hydrogenase enzymes that couple H_2 oxidation to F_{420} reduction in vivo. However, their application for use in vitro is still unclear, due to their instability and sensitivity to O_2.[337] Figure 6. 4. shows an overview of the various potential F_{420} recycling systems that can be developed from the present data available in literature.

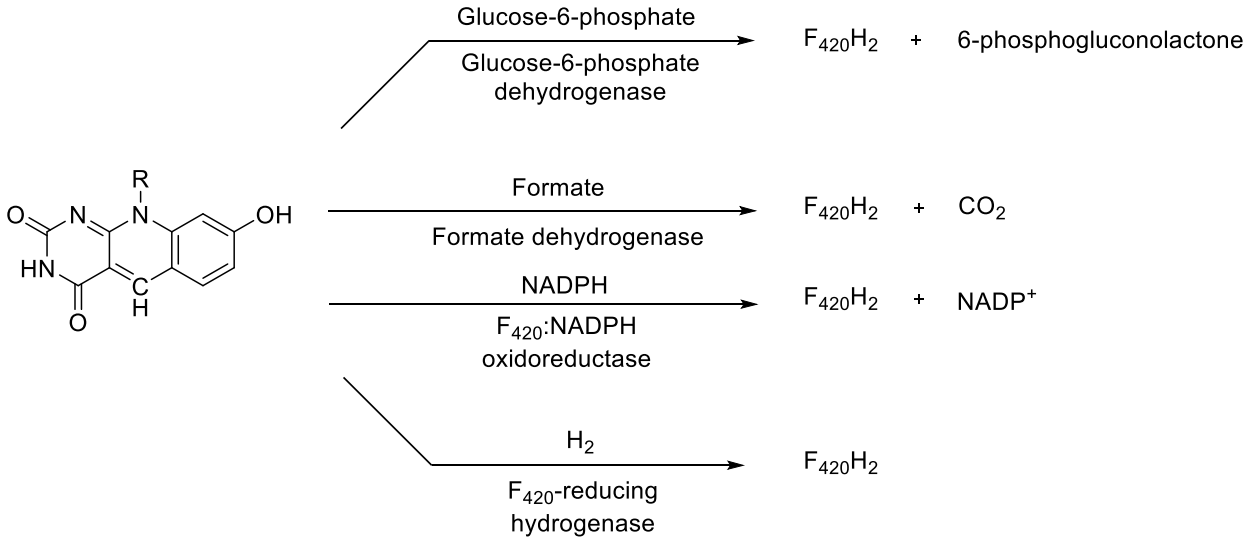


Figure 6. 4. Potential enzymatic methods that can be exploited to develop F_{420} cofactor recycling systems.

6.3. Classification of deazaflavoenzymes and their relevance for biotechnology applications

Cofactor F_{420}-dependent enzymes have remained under-explored for biocatalytic applications, perhaps due to their limited distribution in nature or poor activity or the lack of efficient F_{420} recycling techniques.[23,64] Literature reports discussing their potential in promoting new and novel reactions for biocatalysis have stimulated interest in this cofactor recently. The classification of deazaflavoenzymes into different families either based on their three-dimensional fold or evolutionary history shows an evolving trend as more and more deazaflavoenzymes are discovered. The most recent classification is reported by Mascotti *et al*., where the authors classify deazaflavoenzymes into five different classes based on their structural folds: Class I comprises TIM-barrel F_{420}-dependent enzymes; Class II includes the Rossmann fold F_{420}-dependent enzymes, Class III involves the β-roll F_{420}-dependent enzymes; Class IV exclusively encompasses the SH3 barrel F_{420}-dependent enzymes and Class V includes the three layer ββα sandwich F_{420}-dependent enzymes.[338] Among them, two families – luciferase like hydride transferases (LLHTs) and flavin/deazaflavin dependent oxidoreductases (FDORs) from Class I and Class III respectively show the greatest potential for biocatalysis.[310]

F_{420}-dependent enzymes have been reported to catalyse a number of key reduction reactions in biological systems like the reduction of enoates, ketones, imines and nitro-groups.

FDOR's catalyse enoate reduction reactions and are known to exhibit a broad substrate promiscuity, making them promising candidates for biocatalysis. The reaction mechanism involves both hydride and proton transfer from $F_{420}H_2$ to the same face of the activated double bond, resulting in cis hydrogenation, the opposite enantioselectivity obtained for products formed from flavin-mediated reactions – trans hydrogenation.[310] The first step involves the binding of $F_{420}H^-$ to the enzyme,

followed by the substrate binding to the adjacent pocket of the enzyme through hydrophobic interactions. Next, the nucleophilic C-5 centre of the cofactor aligns with the electrophilic alkene group of the substrate facilitating hydride transfer.[23] A comparison of the reaction mechanism occurring in flavin-dependent OYE ene-reductases and F_{420}-dependent reductases is shown in Figure 6. 5.

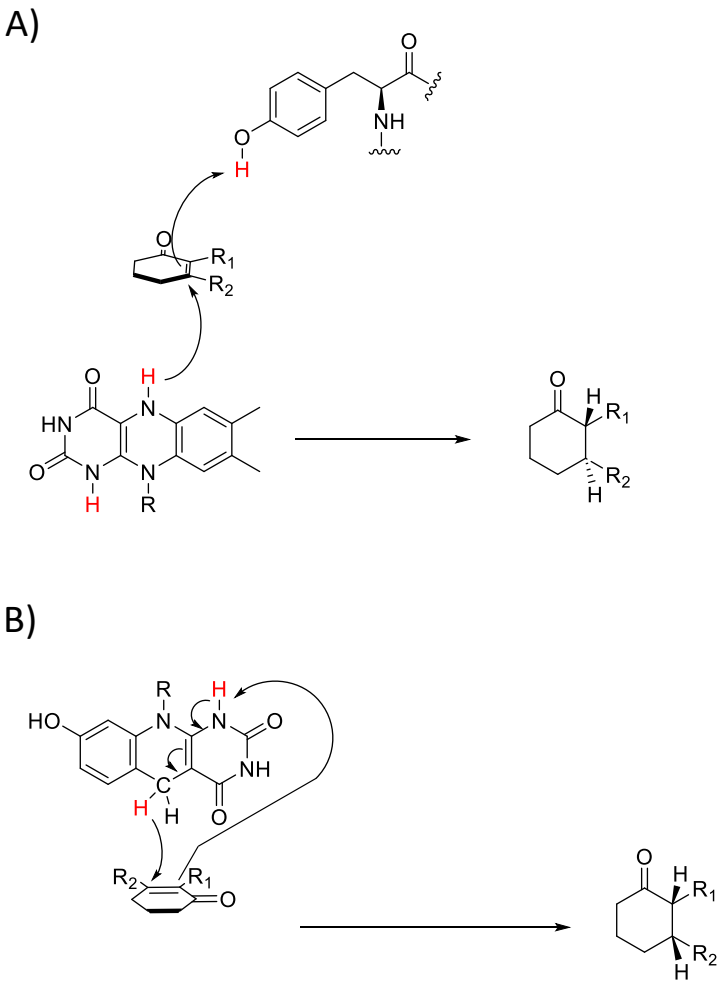


Figure 6. 5. Double bond reduction by a A) a flavin-dependent (Old Yellow Enzyme) ene-reductase and B) the proposed mechanism of reduction by an F_{420}-dependent reductase. Essentially the reduction facilitated by the OYE type enzyme results in trans-hydrogenation and the F_{420}-dependent reductase yields cis-hydrogenated product. This figure was adapted from reference 310.[310]

Mathew *et al*. demonstrated for the first time, that F_{420}-dependent enzymes can be exploited for enantioselective ene reductions.[22] In order to fully exploit the benefits of FDORs for biocatalysis, a

wider substrate scope is yet to be elucidated. Additionally, the so far reported low reaction rates may need attention — directed evolution and enzyme engineering approaches can often lead to enzymes with enhanced reactivity.[22,23]

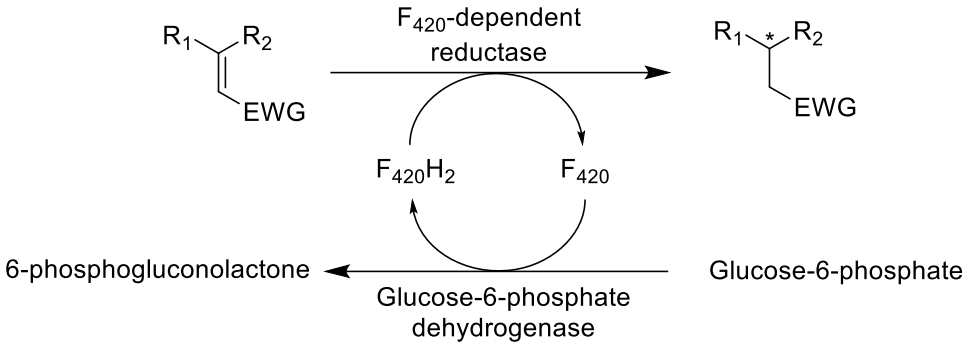


Figure 6. 6. C=C double bond reduction by an F_{420}-dependent reductase that utilises a glucose-6-phosphate dehydrogenase regenerating enzyme which converts glucose-6-phosphate to the end product, 6-phosphogluconate.[22]

In 2020, an F_{420}-dependent alcohol dehydrogenase (ADF) from *Methanoculleus thermophilicus* was shown to catalyse the reduction of prochiral ketones to their corresponding (*S*)-alcohols with excellent enantiopurity (> 99% *ee*). Interestingly, ADF was employed as a self-sufficient cofactor recycling system for $F_{420}H_2$ by using isopropanol as a cheap cosubstrate. An investigation into replacing F_{420} with FOP (cofactor FOP lacks the poly-γ-glutamate lactyl tail present in F_{420}), resulted in lower yields, but the enantioselectivity of the product remained unchanged.[339]

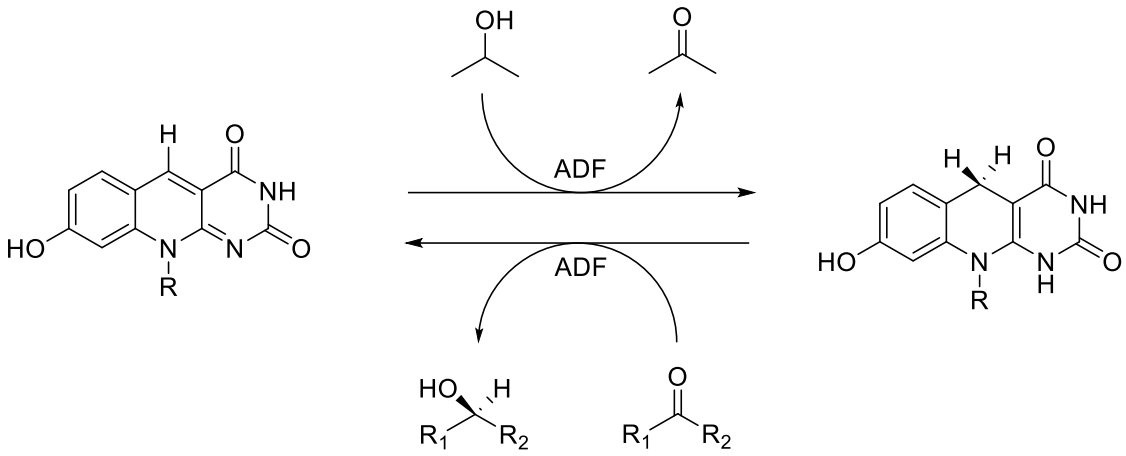


Figure 6. 7. F_{420}-dependent alcohol dehydrogenase (ADF) employed as a self-sufficient F_{420} cofactor recycling system for ketone reductions using isopropanol as a cheap cosubstrate.

A few F_{420}-dependent enzymes displaying imine reduction have also been detected, however their expansion to a biocatalytic chemical reaction is yet to be demonstrated. An FDOR from *Streptomyces tateyamensis* was identified as responsible for the reduction of dehydropiperidine in thiopeptide antibiotics produced in this bacterium.[340] Another F_{420}-dependent imine reductase from *Streptomyces achromogenes* has been found to reduce the imine in 4-ethylidene-3,4-dehydropyrrole-2-carboxylic acid during tomaymycin production, a compound with interesting pharmaceutical properties.[341]

Biocatalytic reactions performed with F_{420}-dependent nitroreductases have not been reported yet, however, nitro reduction activity by these enzymes have been described in a few microorganisms. One example is the reduction of NO_2 to NO by $F_{420}H_2$ in the presence of O_2, a reaction that protects mycobacteria from nitrosative damage. A detailed study into this reaction was conducted by Purwantini *et al*. in a mutant strain of *Mycobacterium smegmatis*, a non-pathogenic relative of *M. tuberculosis*.[324] Another F_{420}-dependent nitroreductase, Npd, from *Rhodococcus* has shown to facilitate hydride transfer to the nitro groups in picric acid, during the catabolism of TNT (trinitrophenol).[342]

6.4. Reducing deazaflavins with hydrogenases

The established hydrogenase based regeneration system for flavins (discussed in chapters 2-5) was extended to a few deazaflavin cofactors. Firstly, the readily available 5-deazariboflavin bought from Santa Cruz Biotechnology was tested with the soluble hydrogenase, SH from *Ralstonia eutropha*. A UV-visible activity assay following the procedure outlined in chapter 2, section 2.2.3 was performed. SH was added to a solution containing 0.1 mM 5-deazariboflavin (800 µL) in Tris-HCl buffer in a UV-cuvette to attempt the H_2-driven reduction of 5-deazariboflavin. This reduction reaction was unsuccessful as no changes were observed in the UV-vis spectrum as seen in Figure 6. 8. This could be a result of incompatibility between cofactor and enzyme binding sites. An accurate measurement of the H_2 concentration present in the cuvette solution could not be made. However, the experimental procedure involved saturating the reaction mixture by bubbling it with a steady flow of H_2 gas for *c.a* 10 minutes before introducing the hydrogenase enzyme. Throughout the reaction, the cuvette headspace was supplied with a constant flow of H_2 gas. In a study by de Poorter *et al*., the authors show that incubating F_{420} in the presence of cell extracts from *Methanothermobacter thermautotrophicus,* under increased H_2 concentrations resulted in the concomitant decrease of the absorbance at 420 nm, a characteristic result for F_{420} reduction. At about 80% H_2, the reaction mixture was bleached (turned colourless) completely due to the complete reduction of F_{420} to $F_{420}H_2$.[315] Hence insufficient H_2 can be ruled out as a possible reason for the failure of this reaction.

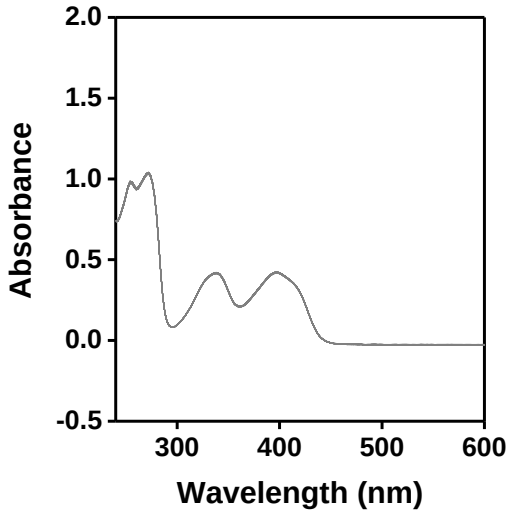


Figure 6. 8. UV-visible activity assay attempted for the reduction of 5-deazariboflavin by the soluble hydrogenase, SH from *Ralstonia eutropha* with H_2 flow present in the cuvette head space.

However, there are other known deazaflavin cofactors that have higher reported biocompatibility, and hence new experiments were planned with other forms of deazaflavin cofactors like F_{420} and F_O.[22] Additionally, there are also ways to genetically alter the active site within SH such that it can accommodate deazaflavin cofactors, or it may be possible to make use of the increasing number of F_{420}-dependent dehydrogenases being discovered.[322,323,330,337]

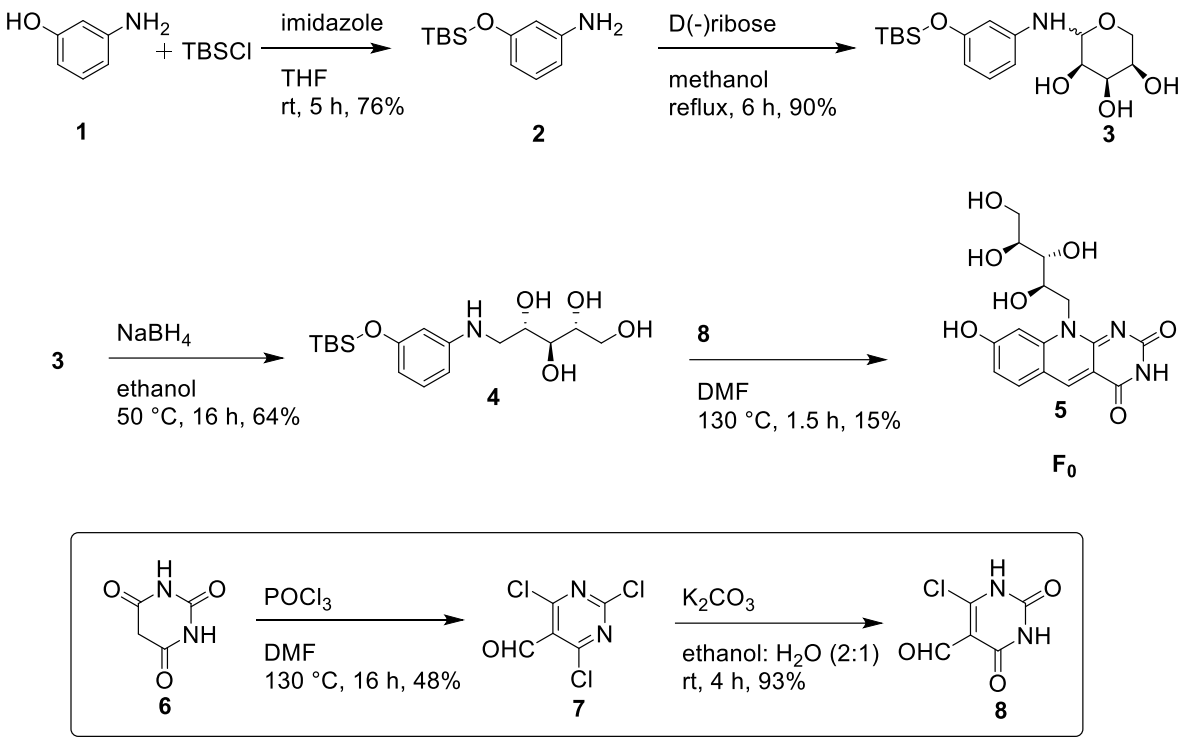
6.4.1. Synthesis of F_O

Access to commercial F_{420} and F_O is limited and the cofactors are very expensive, hence F_O was synthesised using a previously reported procedure such that the synthesised cofactor can be used for UV-visible activity assays.[317]

Selective *O*-protection of 3-aminophenol (**1**) was achieved in 76% yield using tert-butylchlorodimethylsilane (TBSCl) and imidazole. Protection of 3-aminophenol served various purposes like chemo selectivity in later steps, improved redox stability and simplified purification. Then, *N*-ribosylaniline (**3**) was generated from a condensation reaction between *O*-protected 3-

aminophenol (**2**) and ribose in dry methanol under reflux. The crude product was purified to give **3** as a mixture of isomers in 90% yield. Reduction of **3** with $NaBH_4$ in ethanol at 50 °C provided the corresponding N-ribitylaminophenol (**4**) in 64% yield after column purification. As suggested in the literature, this ribityl species developed brown stains due to apparent decomposition products upon exposure to air and light. Conducting experiments under dark and anaerobic conditions eliminated this phenomenon to a large extent. This intermediate product was stored at -20 °C to avoid any further decomposition.

In parallel, 6-chloro-5-formyluracil (**8**) was prepared for the final condensation step (Scheme 6. 1, inset). 2,4,6-Trichloro-5-formyluracil (**7**) was generated from barbituric acid (**6**) in 48% yield following Vilsmaier-Haack conditions. Pyrimidine **7** was then converted to **8** in 93% yield upon stirring under basic conditions. The condensation of **4** and **8** generated F_O (**5**) in 15% (35 mg) yield, of comparable purity to prior reports.[317,343] While all intermediates were achieved in appreciable yield, there was excessive product loss during the last step during purification attempts. However, 35 mg of F_O was enough for structure confirmation by ^{1}H NMR and for use in UV-vis spectroscopy experiments.



Scheme 6. 1. Reaction scheme for the laboratory synthesis of F_O following literature reported procedure[317]

6.4.2. Characterisation of synthesised F_O

F_O and F_{420} show similar UV-spectral properties as both of them bear the same photoactive deazaflavin ring.[63] The experimental UV-vis spectra of the synthesised F_O aligns with the reported values (Figure 6. 9 a and b).[324,328] The obtained ^{1}H NMR spectrum also matches well with published spectrum, except for a few DMF solvent peaks (7.75 ppm, 2.89 ppm and 2.73 ppm highlighted in Figure 6. 9, d) that were hard to eliminate because of its high boiling point (Figure 6. 9). Once F_O was characterised and reasonable purity confirmed, it was taken for the next stage of biocatalytic study.

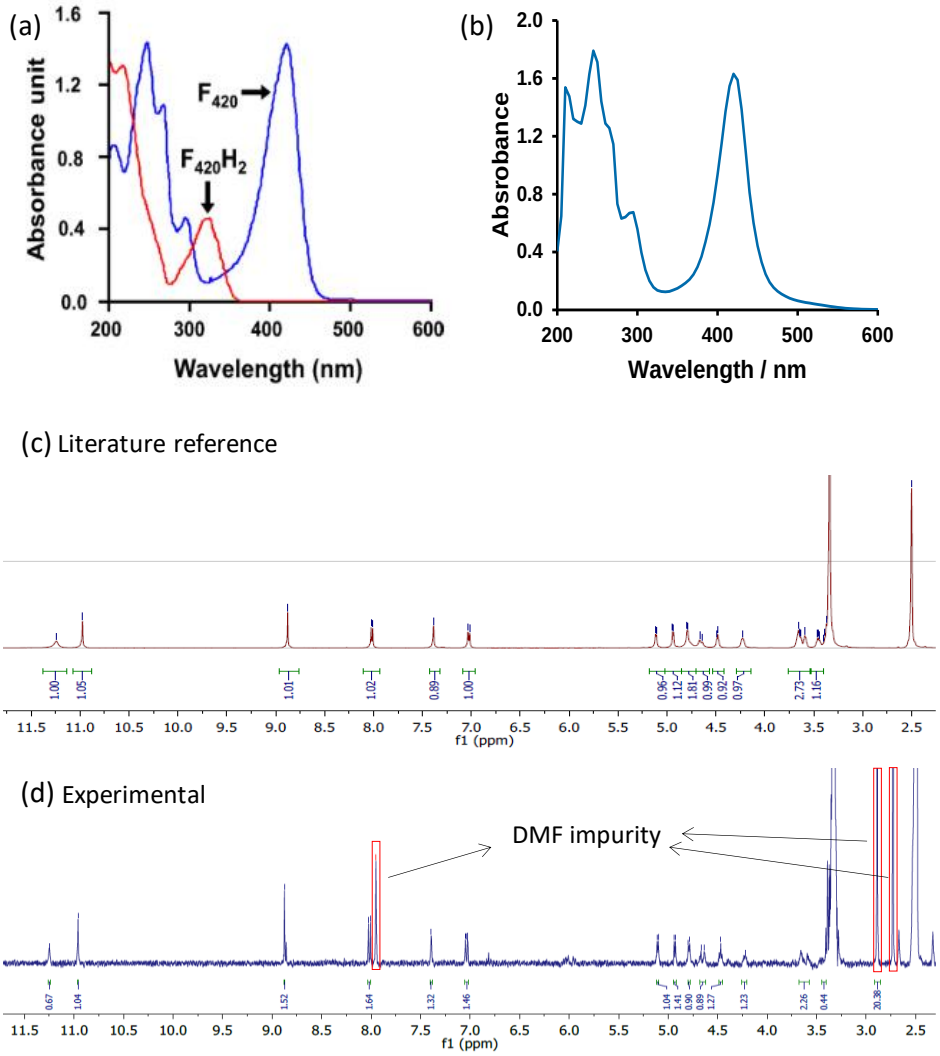


Figure 6. 9. (a) UV-vis absorption spectrum of oxidised and reduced F_{420} reproduced from reference 63. (b) UV-vis spectrum of synthesised F_O in its oxidised state. (c) NMR spectrum of F_O from the literature reproduced from reference 316[316] and (d) synthesised F_O.

6.4.3. Reduction of F_O

The reduction of F_O using Hyd1, Hyd2 and SH was attempted following the procedure outlined in chapter 2, section 2.3.2. A solution of 0.1 mM of the synthesised F_O was prepared in a UV cuvette. Required quantities of Hyd1 or Hyd2 or SH were added to the reaction mixture and spectra obtained during the assay are shown in Figure 6. 10. The absence of any change in the UV-visible activity spectra indicated that no reduction of F_O has taken place with any of the hydrogenases.

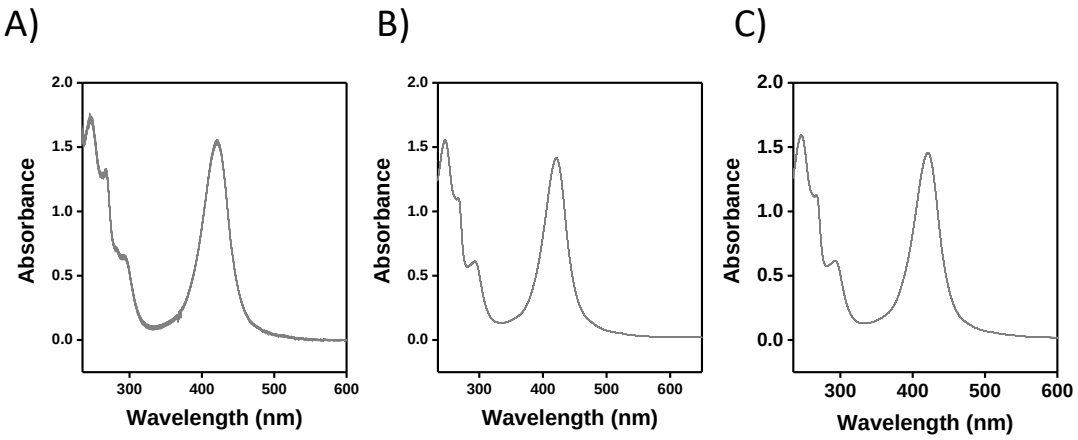


Figure 6. 10. Spectra of the UV-visible activity assay performed for the reduction of F_O using A) Hyd1 and B) Hyd2 and C) SH under H_2 flow present in the cuvette head space.

Reaction conditions: 800 µL scale, 0.1 mM F_O under H_2 flow present in the cuvette headspace in Tris buffer (pH 8, 50 mM) at 25 °C for 30 min.

6.4.4. Reduction of F_{420}

Finally, commercially available F_{420} was purchased from Gecco and its reduction was tested with Hyd1 under H_2. Figure 6. 11. shows the UV-visible spectrum for the activity assay conducted using Hyd1. The absence of any change again indicates that the experiment was unsuccessful. Hyd1 has an over potential of *c.a.* 50-100 mV for H_2 oxidation which also makes this reaction less likely to proceed at a useful rate with this catalyst system.[197]

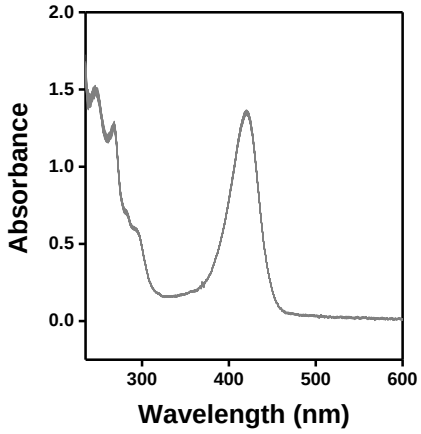


Figure 6. 11. Spectra of the UV-visible activity assay performed for the reduction of F_{420} by Hyd1 under H_2. Reaction conditions: 800 µL scale, 0.2 mM F_{420}, 2.6 mU Hyd1, at 25 °C under H_2 flow in cuvette headspace.

Results obtained for the reduction of F_{420} so far are only from a few preliminary experiments that predominantly comprised UV-visible activity assays, which did not allow the flexibility to study these reactions under different H_2 concentrations. As it is already known that higher H_2 concentrations favour the reduction of F_{420}, it will be interesting to see if the reaction can be drawn at higher H_2 pressures. This can be performed in a pressure vessel. Using an F_{420}-reducing dehydrogenase that natively catalyses this reaction could perhaps offer a more promising solution for F_{420} reduction under H_2. Increasing research on the efficient production of F_{420} reducing enzymes shows more promise to this postulate.[320]

Further, coupling the cofactor regeneration system to an F_{420}-dependent enzyme helps to establish a favourable reaction equilibrium that can drive the reaction forward.

7

Chapter 7 Conclusion and Outlook

This project set out to investigate methods to regenerate cofactors that are less well utilised in industrial biotechnology — flavins and deazaflavins — through H_2-driven biocatalysis. Initial attempts to reduce flavins using the hydrogenase enzyme under H_2 resulted in the unexpected discovery that flavins can be reduced by hydrogenases. This novel reactivity of hydrogenases is the most exciting finding in this thesis which had led to this project taking interesting directions for biocatalytic applications. This new flavin reduction reaction has several benefits when compared to the already existing methods in the literature,[57,344] particularly, the high atom efficiency and the simplicity of the system.[191] Chapter 3 elaborated on the results obtained for the H_2-driven reduction of flavins – FAD and FMN by hydrogenases under a wide range of conditions. The robust nature and exceptional stability of Hyd1 was exploited for flavin reduction over a broad range of temperatures (25 – 70 °C), pH (4-8) and extended reaction time. The use of H_2 means that this system is cleaner and more atom efficient than glucose-driven flavin reduction strategies. These factors demonstrated the potential of this system as an efficient and clean regenerating system for the flavin cofactors.

By combining the Hyd1/flavin system with TsOYE, an OYE ene-reductase, a H_2-driven reduction of ketoisophorone to the selective (*R*)-levodione was accomplished with up to 100 % conversion and up to 99% *ee*. Chapter 4 presented the results from optimising these reactions under various reaction conditions. With *Ts*OYE, The highest Hyd1 TTN of 20,200 and FMN TN of 240 was achieved for a reaction that ran for nearly 134 h. This Hyd1 TTN is in the order of magnitude suitable for use as a catalyst in the pharmaceutical and fine chemical industry.[225] The FMN TN recorded is among the highest values available in the literature. The possibility of using the H_2-driven flavin recycling system for a long reaction time (> 5 days) is an indication of the unusual stability of this system. The longevity of this system, however, could not be properly benchmarked due to the limited data for flavin regeneration techniques available in the literature.

In the second part of chapter 4, several sets of reactions were performed with the Hyd1/ flavin and the GDH/ NADH/ glucose systems as regeneration catalysts using a range of ene-reductases obtained from Johnson Matthey. The aim of this experiment was to study how the Hyd1/ flavin system compares to the conventional GDH/ glucose system. Both the regeneration systems showed moderate to full conversions for various substrate and enzyme combinations. Interestingly, in a few cases, contrasting results were obtained when the same substrate and ene-reductases were operated with the two regeneration systems. For instance, the substrate, 1-acetyl-1-cyclohexene and ene-reductase, ENE-107 showed the best conversion rates when operated with the GDH/ glucose system, however, with the Hyd1/ flavin system, it showed the least conversion. Another major difference between the two regeneration systems was the reaction time. The GDH/ glucose systems showed full conversion of the substrates in just 6 h at 25 °C, however, the same reaction required at least 24 h when it was run with the Hyd1/ flavin system. Nevertheless, it is worth noting that industrial reactions are often performed as an overnight reaction and therefore this longer reaction time may outweigh the other benefits that this system has to offer. The use of glucose as a sacrificial reductant leads to the accumulation of gluconolactone as the end product. This undesired waste makes this process carbon intensive which is not ideal as industries try to accomplish net zero targets. Moreover the cost of supplying purified glucose to run a biocatalysed reaction may not be economic for a large scale reaction. Similarly a direct comparison of the costs of NAD^+ and flavins could not be made, because an accurate industrial price for the flavins could not be accessed. This is probably because flavins are not as commonly employed for industrial biocatalytic processes like that of the nicotinamides. It is likely that flavins may be available at a cheaper rate than nicotinamides. There is also more room to explore how the different grades (purity) of flavin may affect the outcome of a reaction.

Chapter 5 discusses the expansion of this Hyd1/ flavin system to nitroreductases to perform nitro reduction reactions. Employing H_2 as the reductant in place of glucose makes a more substantial difference in these experiments, because for every molecule of nitro compound converted to amine, three equivalents of glucose are consumed, which results in the accumulation of a large amount of waste by-product at the end of the reaction.[36] This experiment was also a demonstration for how reaction protocols for the Hyd1/ flavin system can be translated to different enzymatic systems with ease, making this system attractive for adapting in industry.

Chapter 6 deals with the expansion of this hydrogenase based recycling system to another interesting class of cofactors – the deazaflavins. Deazaflavins remained an under explored class of cofactors in biocatalysis despite their interesting redox properties that allow deazaflavin-dependent enzymes to catalyse transformation of a relatively broader range of substrates.[64] The lack of efficient regeneration systems further impeded their application for useful biocatalytic transformations. In theory, the reduction of F_{420} by H_2 is just feasible thermodynamically, as estimated from the redox potential of the $F_{420}/F_{420}H_2$ and the H^+/H_2 couples (-340 mV and -413 mV respectively at pH 7). Since access to F_{420} and F_O were limited, the initial reactions were performed with 5-deazaflavin, a readily available deazaflavin cofactor. Later F_O was synthesised following a literature procedure and F_{420} was purchased from a commercial source. Several attempts for the reduction of 5-deazariboflavin, F_O and F_{420} by different hydrogenases did not prove fruitful. Hyd1, particularly requires an over potential of 50-100 mV for H_2 oxidation, thus compromising the driving force for H_2-driven F_{420} reduction. Increasing the H_2 pressure would favour H_2-driven F_{420} reduction, so it may be useful to try the reaction under mild H_2 pressures. Using F_{420}-reducing dehydrogenases that natively catalyse this reaction may be helpful. Lastly, coupling this reaction to an F_{420}-dependent enzyme can help to drive the reaction equilibrium forward.

Overall, this thesis has presented a novel and simplified flavin regeneration catalyst involving the hydrogenase enzyme and H_2. Its applicability was successfully demonstrated with a range of ene-reductases and nitroreductases to achieve asymmetric C=C double bond reduction and selective nitro reduction respectively. By circumventing the use of NADH as a cofactor and its corresponding recycling system, which is often the GDH/ glucose system, by-product accumulation at the end of the reaction is prevented. This Hyd1/ flavin recycling has already shown several advantages from a green chemistry perspective.[345,346] To start with, the prevention of unwanted side products already fulfils the first principle. The high atom economy, ambient reaction conditions, use of renewable and environmental friendly materials have made these reactions greener.[345,346] This robust and single enzyme regeneration system holds great promise for cleaner and greener chemical synthesis making it an excellent choice for adoption in industry. The initial experiments with deazaflavin cofactors open up opportunities for new biocatalytic reactions that one can explore in the future.

References

References

1 C. P. S. Badenhorst and U. T. Bornscheuer, *Trends Biochem. Sci.*, 2018, **43**, 180–198.

2 B. A. Sandoval and T. K. Hyster, *Curr. Opin. Chem. Biol.*, 2020, **55**, 45–51.

3 K. Faber, *Biotransformations in Organic Chemistry*, Springer International Publishing, 7th edn., 2011.

4 J. M. Choi, S. S. Han and H. S. Kim, *Biotechnol. Adv.*, 2015, **33**, 1443–54.

5 K. Chen and F. H. Arnold, *Nat. Catal.*, 2020, **3**, 203–213.

6 H. Renata, Z. J. Wang and F. H. Arnold, *Angew. Chem. Int. Ed.*, 2015, **54**, 3351–3367.

7 W. Zhang and F. Hollmann, *Chem. Commun.*, 2018, **54**, 7281–7289.

8 D. Monti, G. Ottolina, G. Carrea and S. Riva, *Chem. Rev.*, 2011, **111**, 4111–4140.

9 J. D. Fischer, G. L. Holliday, S. A. Rahman and J. M. Thornton, *J. Mol. Biol.*, 2010, **403**, 803–824.

10 M. Richter, *Nat. Prod. Rep.*, 2013, **30**, 1324–1345.

11 G. L. Holliday, J. D. Fischer, J. B. O. Mitchell and J. M. Thornton, *FEBS J.*, 2011, **278**, 3835–3845.

12 L. Agledal, M. Niere and M. Ziegler, *Redox Rep.*, 2010, **15**, 2–10.

13 H. O'Neill and J. Woodward, in *Applied Bioctalalysis in Specialty Chemicals and Pharmaceuticals, ACS Symposium Series*, 2001, vol. 776, pp. 103–130.

14 S. Mordhorst and J. N. Andexer, *Nat. Prod. Rep.*, 2020, **37**, 1316–1333.

15 P. W. Bruce Alberts, Alexander Johnson, Julian Lewis, David Morgan, Martin Raff, Keith Roberts, *Molecular Biology of the Cell*, Taylor & Francis, 6th edn., 2014.

16 W. Xiao, R. S. Wang, D. E. Handy and J. Loscalzo, *Antioxidants Redox Signal.*, 2018, **28**, 251–272.

17 R. Miura, *Chem. Rev.*, 2001, **1**, 183–194.

18 B. A. Sandoval, S. I. Kurtoic, M. M. Chung, K. F. Biegasiewicz and T. K. Hyster, *Angew. Chemie - Int. Ed.*, 2019, **58**, 8714–8718.

19 M. S. Jorns, B. Wang and S. P. Jordan, *Biochemistry*, 1987, **26**, 6810–6816.

20 H. I. X. Mager and S. C Tu, *Photochem. Photobiol.*, 1995, **62**, 607–614.

21 S. A. Baker Dockrey and A. R. H. Narayan, *Tetrahedron*, 2019, **75**, 1115–1121.

22 S. Mathew, M. Trajkovic, H. Kumar, Q.-T. Nguyen and M. W. Fraaije, *Chem. Commun.*, 2018, **54**, 11208–11211.

23 C. Greening, T. Jirapanjawat, S. Afroze, B. Ney, C. Scott, G. Pandey, B. M. Lee, R. J. Russell, C. J.

Jackson, J. G. Oakeshott, M. C. Taylor and A. C. Warden, *Front. Microbiol.*, 2017, **8**, 1–10.

24 J. A. Duine and J. A. Jongejan, *Annu. Rev. Biochem.*, 1989, **58**, 403–426.

25 J. A. DUINE, *Eur. J. Biochem.*, 1991, **200**, 271–284.

26 J. P. K. Yao-Qing Shen, Florence Bonnot, Erin M. Imsand, Jordan M. RoseFigura, Kimmen Sjolander, *Biochemistry*, 2013, **51**, 3365–3375.

27 V. L. Davidson, *Compr. Nat. Prod. II Chem. Biol.*, 2010, **7**, 675–710.

28 C. Rodriguez, I. Lavandera and V. Gotor, *Curr. Org. Chem.*, 2012, **16**, 2525–2541.

29 J. Latham, E. Brandenburger, S. A. Shepherd, B. R. K. Menon and J. Micklefield, *Chem. Rev.*, 2018, **118**, 232–269.

30 F. Rudroff, M. D. Mihovilovic, H. Gröger, R. Snajdrova, H. Iding and U. T. Bornscheuer, *Nat. Catal.*, 2018, **1**, 12–22.

31 T. Knaus, C. E. Paul, C. W. Levy, S. De Vries, F. G. Mutti, F. Hollmann and N. S. Scrutton, *J. Am. Chem. Soc.*, 2016, **138**, 1033–1039.

32 X. Wang, T. Saba, H. H. P. Yiu, R. F. Howe, J. A. Anderson and J. Shi, *Chem*, 2017, **2**, 621–654.

33 R. L. Hanson, J. M. Howell, T. L. Laporte, M. J. Donovan, D. L. Cazzulino, V. Zannella, M. A. Montana, V. B. Nanduri, S. R. Schwarz, R. F. Eiring, S. C. Durand, J. M. Wasylyk, W. L. Parker, M. S. Liu, F. J. Okuniewicz, B. C. Chen, J. C. Harris, K. J. Natalie, K. Ramig, S. Swaminathan, V. W. Rosso, S. K. Pack, B. T. Lotz, P. J. Bernot, A. Rusowicz, D. A. Lust, K. S. Tse, J. J. Venit, L. J. Szarka and R. N. Patel, *Enzyme Microb. Technol.*, 2000, **26**, 348–358.

34 A. Weckbecker, H. Gröger and W. Hummel, *Adv. Biochem. Eng. Biotechnol.*, 2010, **120**, 195–242.

35 B. Domínguez, U. Schell, S. Bisagni and T. Kalthoff, *Johnson Matthey Technol. Rev.*, 2016, **60**, 243–249.

36 A. Bornadel, S. Bisagni, A. Pushpanath, I. Slabu, J. LePaih, A. H. Cherney, S. M. Mennen, S. J. Hedley, J. Tedrow and B. Dominguez, *Org. Process Res. Dev.*, 2021, **25**, 648–653.

37 F. Hollmann, I. W. C. E. Arends and K. Buehler, *ChemCatChem*, 2010, **2**, 762–782.

38 V. S. Shende, P. Singh and B. M. Bhanage, *Catal. Sci. Technol.*, 2018, **8**, 955–969.

39 P. G. Bulger, *Industrial Applications of Organocatalysis*, Elsevier Ltd., 2012, vol. 9.

40 T. S. Moody, S. Mix, G. Brown and D. Beecher, *Biocatal. Org. Synth.*, 2015, **2**, 453.

41 F. Hollmann, D. J. Opperman and C. E. Paul, *Angew. Chemie Int. Ed.*, 2021, **60**, 5644–5665.

42 T. Matsuda, R. Yamanaka and K. Nakamura, *Green Biocatal.*, 2016, 307–330.

43 S. E. Milner and A. R. Maguire, *Arkivoc*, 2012, **2012**, 321–382.

44 H. S. Toogood and N. S. Scrutton, *ACS Catal.*, 2018, **8**, 3532–3549.

45 T. Knaus, H. S. Toogood and N. S. Scrutton, in *Green Biocatalysis*, ed. R. N. Patel, Wiley, 1st edn., 2016, pp. 473–488.

46 A. Scholtissek, D. Tischler, A. H. Westphal, W. J. H. van Berkel and C. E. Paul, *Catalysts*, 2017, **7**, 130.

47 M. Hall, C. Stueckler, H. Ehammer, E. Pointner, G. Oberdorfer, K. Gruber, B. Hauer, R. Stuermer, W. Kroutil, P. Macheroux and K. Faber, *Adv. Synth. Catal.*, 2008, **350**, 411–418.

48 N. N. Ulusu, *J. Mol. Evol.*, 2015, **80**, 251–257.

49 J. T. Park, L. M. Gómez Ramos and A. S. Bommarius, *ChemBioChem*, 2015, **16**, 811–818.

50 S. M. A. De Wildeman, T. Sonke, H. E. Schoemaker and O. May, *Acc. Chem. Res.*, 2007, **40**, 1260–1266.

51 H. S. Toogood, J. M. Gardiner and N. S. Scrutton, *ChemCatChem*, 2010, **2**, 892–914.

52 M. M. Grau, J. C. Van Der Toorn, L. G. Otten, P. Macheroux, A. Taglieber, F. E. Zilly, I. W. C. E. Arends and F. Hollmann, *Adv. Synth. Catal.*, 2009, **351**, 3279–3286.

53 C. K. Winkler, D. Clay, M. Entner, M. Plank and K. Faber, *Chem. - A Eur. J.*, 2014, **20**, 1403–1409.

54 C. Stueckler, T. C. Reiter, N. Baudendistel and K. Faber, *Tetrahedron*, 2010, **66**, 663–667.

55 C. E. Paul, S. Gargiulo, D. J. Opperman, I. Lavandera, V. Gotor-Fernández, V. Gotor, A. Taglieber, I. W. C. E. Arends and F. Hollmann, *Org. Lett.*, 2013, **15**, 180–183.

56 F. Hollmann, A. Taglieber, F. Schulz and M. T. Reetz, *Angew. Chemie Int. Ed.*, 2007, **46**, 2903–2906.

57 F. Rudroff, M. D. Mihovilovic, H. Gröger, R. Snajdrova, H. Iding and U. T. Bornscheuer, *Nat. Catal.*, 2018, **1**, 12–22.

58 C. K. Winkler, K. Faber and M. Hall, *Curr. Opin. Chem. Biol.*, 2018, **43**, 97–105.

59 L. Sellés Vidal, C. L. Kelly, P. M. Mordaka and J. T. Heap, *BBA- Proteins Proteomics*, 2018, 1866, 327–347.

60 M. Ismail, L. Schroeder, M. Frese, T. Kottke, F. Hollmann, C. E. Paul and N. Sewald, *ACS Catal.*, 2019, **9**, 1389–1395.

61 D. J. Mansell, H. S. Toogood, J. Waller, J. M. X. Hughes, C. W. Levy, J. M. Gardiner and N. S. Scrutton, *ACS Catal.*, 2013, **3**, 370–379.

62 A. Lygidakis, V. Karuppiah, R. Hoeven, A. Ní Cheallaigh, D. Leys, J. M. Gardiner, H. S. Toogood and N. S. Scrutton, *Angew. Chemie*, 2016, **128**, 9748–9752.

63 C. Greening, F. H. Ahmed, A. E. Mohamed, B. M. Lee, G. Pandey, A. C. Warden, C. Scott, J. G. Oakeshott, M. C. Taylor and C. J. Jackson, *Microbiol. Mol. Biol. Rev.*, 2016, **80**, 451–493.

64 M. Taylor, C. Scott and G. Grogan, *Trends Biotechnol.*, 2013, **31**, 63–64.

65 D. Ghislieri and N. J. Turner, *Top. Catal.*, 2014, **57**, 284–300.

66 G. Grogan and N. J. Turner, *Chem. - A Eur. J.*, 2016, **22**, 1900–1907.

67 J. Mangas-Sanchez, S. P. France, S. L. Montgomery, G. A. Aleku, H. Man, M. Sharma, J. I. Ramsden, G. Grogan and N. J. Turner, *Curr. Opin. Chem. Biol.*, 2017, **37**, 19–25.

68 K. Mitsukura, M. Suzuki, S. Shinoda, T. Kuramoto, T. Yoshida and T. Nagasawa, *Biosci. Biotechnol. Biochem.*, 2011, **75**, 1778–1782.

69 K. Mitsukura, M. Suzuki, K. Tada, T. Yoshida and T. Nagasawa, *Org. Biomol. Chem.*, 2010, **8**, 4533–4535.

70 S. Velikogne, V. Resch, C. Dertnig, J. H. Schrittwieser and W. Kroutil, *ChemCatChem*, 2018, **10**, 3236–3246.

71 J. H. Schrittwieser, S. Velikogne and W. Kroutil, *Adv. Synth. Catal.*, 2015, **357**, 1655–1685.

72 W. Li, A. Khullar, S. Chou, A. Sacramo and B. Gerratana, *Appl. Environ. Microbiol.*, 2009, **75**, 2869–2878.

73 M. Prejanò, X. Sheng and F. Himo, *ChemistryOpen*, , DOI:10.1002/open.202100250.

74 T. Huber, L. Schneider, A. Präg, S. Gerhardt, O. Einsle and M. Müller, *ChemCatChem*, 2014, **6**, 2248–2252.

75 M. Lenz, N. Borlinghaus, L. Weinmann and B. M. Nestl, *World J. Microbiol. Biotechnol.*, 2017, **33**, 1–10.

76 S. C. Cosgrove, A. Brzezniak, S. P. France, J. I. Ramsden, J. Mangas-Sanchez, S. L. Montgomery, R. S. Heath and N. J. Turner, *Imine Reductases, Reductive Aminases, and Amine Oxidases for the Synthesis of Chiral Amines: Discovery, Characterization, and Synthetic Applications*, Elsevier Inc., 1st edn., 2018, vol. 608.

77 M. Schober, C. MacDermaid, A. A. Ollis, S. Chang, D. Khan, J. Hosford, J. Latham, L. A. F. Ihnken, M. J. B. Brown, D. Fuerst, M. J. Sanganee and G. D. Roiban, *Nat. Catal.*, 2019, **2**, 909–915.

78 S. G. Burton and M. Le Roes-Hill, *Multi-Step Enzym. Catal. Biotransformations Chemoenzymatic Synth.*, 2008, 41–60.

79 D. E. Torres Pazmiño, M. Winkler, A. Glieder and M. W. Fraaije, *J. Biotechnol.*, 2010, **146**, 9–24.

80 D. Holtmann and F. Hollmann, *ChemBioChem*, 2016, **17**, 1391–1398.

81 D. Holtmann, M. W. Fraaije, I. W. C. E. Arends, D. J. Opperman and F. Hollmann, *Chem. Commun.*, 2014, **50**, 13180–13200.

82 J. Latham, E. Brandenburger, S. A. Shepherd, B. R. K. Menon and J. Micklefield, *Chem. Rev.*, 2018, **118**, 232–269.

83 N. J. Turner, *7.12 Oxidation: Oxidases*, Elsevier Ltd., 2012, vol. 7.

84 W. P. Dijkman, G. De Gonzalo, A. Mattevi and M. W. Fraaije, *Appl. Microbiol. Biotechnol.*, 2013, **97**, 5177–5188.

85 B. R. K. Menon, D. Richmond and N. Menon, *Catal. Rev. - Sci. Eng.*, 2020, 1–59.

86 H. Ludewig, S. Molyneux, S. Ferrinho, K. Guo, R. Lynch, D. S. Gkotsi and R. J. Goss, *Curr. Opin. Struct. Biol.*, 2020, **65**, 51–60.

87 D. S. Gkotsi, J. Dhaliwal, M. M. McLachlan, K. R. Mulholand and R. J. Goss, *Curr. Opin. Chem. Biol.*, 2018, **43**, 119–126.

88 D. R. M. Smith, S. Grüschow and R. J. M. Goss, *Curr. Opin. Chem. Biol.*, 2013, **17**, 276–283.

89 A. Tressaud, in *Progress in Fuorine Science Series*, Elsevier, 2019, pp. 1–258.

90 D. B. Harper and O. O'Hagan, *Nat. Prod. Rep.*, 1994, **11**, 123–133.

91 S. Dehnen, L. L. Schafer, T. Lectka and A. Togni, *Org. Lett.*, 2021, **23**, 9013–9019.

92 M. F. Carvalho and R. S. Oliveira, *Crit. Rev. Biotechnol.*, 2017, **37**, 880–897.

93 O'Hagan David, Schaffrath Christoph, Cobb Steven L., Hamilton John T. G. and Murphy Carmac D., *Nature*, 2002, **416**, 279–279.

94 L. Wu, F. Maglangit and H. Deng, *Curr. Opin. Chem. Biol.*, 2020, **55**, 119–126.

95 C. H. Wong, L. Daniels, W. H. Orme-Johnson and G. M. Whitesides, *J. Am. Chem. Soc.*, 1981, **103**, 6227–6228.

96 L. Lauterbach, O. Lenz and K. A. Vincent, *FEBS J.*, 2013, **280**, 3058–3068.

97 W. A. Van Der Donk and H. Zhao, *Curr. Opin. Biotechnol.*, 2003, **14**, 421–426.

98 H. Zhao and W. A. Van Der Donk, *Curr. Opin. Biotechnol.*, 2003, **14**, 583–589.

99 O. Lenz, L. Lauterbach and S. Frielingsdorf, *Methods Enzymol.*, 2018, 613, 117–151.

100 J. Ratzka, L. Lauterbach, O. Lenz and M. B. Ansorge-Schumacher, *Biocatal. Biotransformation*, 2011, **29**, 246–252.

101 N. Nakada, I. Okura and F. Hasumi, *J. Mol. Catal.*, 1992, **75**, 23–25.

102 K. Schneider and H. G. Schlegel, *Cell*, 1976, **452**, 66–80.

103 A. Al-Shameri, S. J.-P. Willot, C. E. Paul, F. Hollmann and L. Lauterbach, *Chem. Commun.*, 2020, **56**, 9667–9670.

104 N. Herr, J. Ratzka, L. Lauterbach, O. Lenz and M. B. Ansorge-Schumacher, *J. Mol. Catal. B Enzym.*, 2013, **97**, 169–174.

105 C. H. Wu, P. M. McTernan, M. E. Walter and M. W. W. Adams, *Archaea*, ,

DOI:10.1155/2015/912582.

106 P. Kwan, C. L. McIntosh, D. P. Jennings, R. C. Hopkins, S. K. Chandrayan, C. H. Wu, M. W. W. Adams and A. K. Jones, *J. Am. Chem. Soc.*, 2015, **137**, 13556–13565.

107 J. Preissler, H. A. Reeve, T. Zhu, J. Nicholson, K. Urata, L. Lauterbach, L. L. Wong, K. A. Vincent and O. Lenz, *ChemCatChem*, 2020, **12**, 1–10.

108 M. Horch, L. Lauterbach, O. Lenz, P. Hildebrandt and I. Zebger, *FEBS Lett.*, 2012, **586**, 545–556.

109 T. Burgdorf, E. Van Der Linden, M. Bernhard, Q. Y. Yin, J. W. Back, A. F. Hartog, A. O. Muijsers, C. G. De Koster and S. P. J. Albracht, *J. Bacteriol.*, 2005, **187**, 3122–3132.

110 Y. Shomura, M. Taketa, H. Nakashima, H. Tai, H. Nakagawa, Y. Ikeda, M. Ishii, Y. Igarashi, H. Nishihara, K. S. Yoon, S. Ogo, S. Hirota and Y. Higuchi, *Science*, 2017, **357**, 928–932.

111 L. Lauterbach, Z. Idris, K. A. Vincent and O. Lenz, *PLoS One*, 2011, **6**, e25939.

112 L. Lauterbach, J. Liu, M. Horch, P. Hummel, A. Schwarze, M. Haumann, K. A. Vincent, O. Lenz and I. Zebger, *Eur. J. Inorg. Chem.*, 2011, 1067–1079.

113 T. Burgdorf, O. Lenz, T. Buhrke, E. Van Der Linden, A. K. Jones, S. P. J. Albracht and B. Friedrich, *J. Mol. Microbiol. Biotechnol.*, 2005, **10**, 181–196.

114 J. Preissler, S. Wahlefeld, C. Lorent, C. Teutloff, M. Horch, L. Lauterbach, S. P. Cramer, I. Zebger and O. Lenz, *Biochim. Biophys. Acta - Bioenerg.*, 2018, **1859**, 8–18.

115 L. A. Sazanov and P. Hinchliffe, *Science*, 2006, **311**, 1430–1436.

116 R. Baradaran, J. M. Berrisford, G. S. Minhas and L. A. Sazanov, *Nature*, 2013, **494**, 443–448.

117 H. A. Reeve, L. Lauterbach, P. A. Ash, O. Lenz and K. A. Vincent, *Chem. Commun.*, 2012, **48**, 1589–1591.

118 H. A. Reeve, L. Lauterbach, O. Lenz and K. A. Vincent, *ChemCatChem*, 2015, **7**, 3480–3487.

119 L. Rover, J. C. B. Fernandes, G. D. O. Neto, L. T. Kubota, E. Katekawa and S. H. P. Serrano, *Anal. Biochem.*, 1998, **260**, 50–55.

120 P. M. Vignais and B. Billoud, *Chem. Rev.*, 2007, **107**, 4206–4272.

121 C. Greening, A. Biswas, C. R. Carere, C. J. Jackson, M. C. Taylor, M. B. Stott, G. M. Cook and S. E. Morales, *ISME J.*, 2016, **10**, 761–777.

122 W. Lubitz, H. Ogata, O. Ru and E. Reijerse, *Chem. Rev.*, 2014, **114**, 4081–4148.

123 K. A. Vincent, A. Parkin and F. A. Armstrong, *Chem. Rev.*, 2007, **107**, 4366–4413.

124 T. Hiromoto, K. Ataka, O. Pilak, S. Vogt, M. S. Stagni, W. Meyer-Klaucke, E. Warkentin, R. K. Thauer, S. Shima and U. Ermler, *FEBS Lett.*, 2009, **583**, 585–590.

125 A. R. Finkelmann, H. M. Senn and M. Reiher, *Chem. Sci.*, 2014, **5**, 4474–4482.

126 M. S. Stagni, F. Stellato, M. C. Whaley, S. Vogt, S. Morante, S. Shima, T. B. Rauchfuss and W. Meyer-Klaucke, *Dalt. Trans.*, 2010, **39**, 2972–2983.

127 D. Chen, R. Scopelliti and X. Hu, *Angew. Chemie - Int. Ed.*, 2010, **49**, 7512–7515.

128 P. M. Vignais, B. Billoud and J. Meyer, *FEMS Microbiol. Rev.*, 2001, **25**, 455–501.

129 F. Sargent, *The Model [NiFe]-Hydrogenases of Escherichia coli*, Elsevier Ltd., 1st edn., 2016, vol. 68.

130 M. J. Lukey, M. M. Roessler, A. Parkin, R. M. Evans, R. A. Davies, O. Lenz, B. Friedrich, F. Sargent and F. A. Armstrong, *J. Am. Chem. Soc.*, 2011, **133**, 16881–16892.

131 J. W. Peters, G. J. Schut, E. S. Boyd, D. W. Mulder, E. M. Shepard, J. B. Broderick, P. W. King and M. W. W. Adams, *Biochim. Biophys. Acta - Mol. Cell Res.*, 2015, **1853**, 1350–1369.

132 P. A. Ash, S. Kendall-Price, R. M. Evans, S. B. Carr, A. Brasnett, S. Morra, R. Hidalgo, A. J. Healy, G. Cinque, M. Frogley, F. A. Armstrong and K. A. Vincent, *Chem. Sci.*, 2021, **12**, 12959.

133 R. M. Evans, P. A. Ash, S. E. Beaton, E. J. Brooke, K. A. Vincent, S. B. Carr and F. A. Armstrong, *J. Am. Chem. Soc.*, 2018, **140**, 10208–10220.

134 T. Goris, A. F. Wait, M. Saggu, J. Fritsch, N. Heidary, M. Stein, I. Zebger, F. Lendzian, F. A. Armstrong, B. Friedrich and O. Lenz, *Nat. Chem. Biol.*, 2011, **7**, 310–318.

135 H. Ogata, W. Lubitz and Y. Higuchi, *J. Biochem.*, 2016, **160**, 251–258.

136 G. Sawers, *Antonie Van Leeuwenhoek*, 1994, **66**, 57–88.

137 A. Dubini, R. L. Pye, R. L. Jack, T. Palmer and F. Sargent, *Int. J. Hydrogen Energy*, 2002, **27**, 1413–1420.

138 A. Volbeda, P. Amara, C. Darnault, J.-M. Mouesca, A. Parkin, M. M. Roessler, F. A. Armstrong and J. C. Fontecilla-Camps, *PNAS*, 2012, **109**, 5305–5310.

139 A. Volbeda, C. Darnault, A. Parkin, F. Sargent, F. A. Armstrong and J. C. Fontecilla-Camps, *Structure*, 2013, **21**, 184–190.

140 P. Wulff, C. Thomas, F. Sargent and F. A. Armstrong, *J. Biol. Inorg. Chem.*, 2016, **21**, 121–134.

141 M. J. Lukey, A. Parkin, M. M. Roessler, B. J. Murphy, J. Harmer, T. Palmer, F. Sargent and F. A. Armstrong, *J. Biol. Chem.*, 2010, **285**, 3928–3938.

142 J. Fritsch, P. Scheerer, S. Frielingsdorf, S. Kroschinsky, B. Friedrich, O. Lenz and C. M. T. Spahn, *Nature*, 2011, **479**, 249–253.

143 M. E. Pandelia, W. Nitschke, P. Infossi, M. T. Giudici-Orticoni, E. Bill and W. Lubitz, *Proc. Natl. Acad. Sci. U. S. A.*, 2011, **108**, 6097–6102.

144 R. M. Evans, A. Parkin, M. M. Roessler, B. J. Murphy, H. Adamson, M. J. Lukey, F. Sargent, A. Volbeda, J. C. Fontecilla-camps and F. a Armstrong, *J. Am. Chem. Soc.*, 2013, **135**, 2694–2707.

145 T. Buhrke, O. Lenz, N. Krauss and B. Friedrich, *J. Biol. Chem.*, 2005, **280**, 23791–23796.

146 M. Van Gastel, M. Stein, M. Brecht, O. Schröder, F. Lendzian, R. Bittl, H. Ogata, Y. Higuchi and W. Lubitz, *J. Biol. Inorg. Chem.*, 2006, **11**, 41–51.

147 S. E. Lamle, S. P. J. Albracht and F. A. Armstrong, *J. Am. Chem. Soc.*, 2004, **126**, 14899–14909.

148 P. A. Ash, S. E. T. Kendall-Price, R. M. Evans, S. B. Carr, A. R. Brasnett, S. Morra, J. S. Rowbotham, R. Hidalgo, A. J. Healy, G. Cinque, M. D. Frogley, F. A. Armstrong and K. A. Vincent, *Chem. Sci.*, 2021, **12**, 12959–12970.

149 H. Ogata, T. Krämer, H. Wang, D. Schilter, V. Pelmenschikov, M. Van Gastel, F. Neese, T. B. Rauchfuss, L. B. Gee, A. D. Scott, Y. Yoda, Y. Tanaka, W. Lubitz and S. P. Cramer, *Nat. Commun.*, 2015, **6**, 1–8.

150 H. Ogata, K. Nishikawa and W. Lubitz, *Nature*, 2015, **520**, 571–574.

151 D. Brazzolotto, M. Gennari, N. Queyriaux, T. R. Simmons, J. Pécaut, S. Demeshko, F. Meyer, M. Orio, V. Artero and C. Duboc, *Nat. Chem.*, 2016, **8**, 1054–1060.

152 P. A. Ash, R. Hidalgo and K. A. Vincent, *ACS Catal.*, 2017, **7**, 2471–2485.

153 R. M. Evans, E. J. Brooke, S. A. M. Wehlin, E. Nomerotskaia, F. Sargent, S. B. Carr, S. E. V. Phillips and F. A. Armstrong, *Nat. Chem. Biol.*, 2016, **12**, 46–50.

154 R. Hidalgo, P. A. Ash, A. J. Healy and K. A. Vincent, *Angew. Chemie - Int. Ed.*, 2015, **54**, 7110–7113.

155 S. E. Beaton, R. M. Evans, A. J. Finney, C. M. Lamont, F. A. Armstrong, F. Sargent and S. B. Carr, *Biochem. J.*, 2018, **475**, 1353–1370.

156 M. Senger, K. Laun, B. Soboh and S. T. Stripp, *Catalysts*, 2018, **8**, 530.

157 C. Pinske, M. Jaroschinsky, S. Linek, C. L. Kelly, F. Sargent and R. G. Sawers, *J. Bacteriol.*, 2015, **197**, 296–306.

158 P. A. Ash and K. A. Vincent, 2018, **5**, 590–595.

159 R. G. Sawers and C. Pinske, *NiFe-Hydrogenase Assembly*, John Wiley & Sons, Ltd, 2017.

160 H. Ogata, W. Lubitz and Y. Higuchi, *Dalt. Trans.*, 2009, **9226**, 7577–7587.

161 Y. Higuchi, N. Yasuoka, M. Kakudo, Y. Katsube, T. Yagi and H. Inokuchi, *J. Biol. Chem.*, 1987, **262**, 2823–2825.

162 H. Ogata, S. Hirota, A. Nakahara, H. Komori, N. Shibata, T. Kato, K. Kano and Y. Higuchi, *Structure*, 2005, **13**, 1635–1642.

163 H. Osuka, Y. Shomura, H. Komori, N. Shibata, S. Nagao, Y. Higuchi and S. Hirota, *Biochem. Biophys. Res. Commun.*, 2013, **430**, 284–288.

164 D. Millo, M. E. Pandelia, T. Utesch, N. Wisitruangsakul, M. A. Mroginski, W. Lubitz, P. Hildebrandt and I. Zebger, *J. Phys. Chem. B*, 2009, **113**, 15344–15351.

165 E. E. Ferrandi and D. Monti, *World J. Microbiol. Biotechnol.*, 2018, **34**, 1–10.

166 A. Gomm and E. O'Reilly, *Curr. Opin. Chem. Biol.*, 2018, **43**, 106–112.

167 C. K. Savile, J. M. Janey, E. C. Mundorff, J. C. Moore, S. Tam, W. R. Jarvis, J. C. Colbeck, A. Krebber, F. J. Fleitz, J. Brands, P. N. Devine, G. W. Huisman and G. J. Hughes, *Science*, 2010, **329**, 305–310.

168 A. R. Aguillón, A. S. Miranda, I. I. Junior and R. O. M. A. Souza, *Synth. Approaches to Nonaromatic Nitrogen Heterocycles*, 2020, 667–697.

169 S. A. Kelly, S. Pohle, S. Wharry, S. Mix, C. C. R. Allen, T. S. Moody and B. F. Gilmore, *Chem. Rev.*, 2018, **118**, 349–367.

170 J. R. Cao, F. F. Fan, C. J. Lv, H. P. Wang, Y. Li, S. Hu, W. R. Zhao, H. Bin Chen, J. Huang and L. H. Mei, *Front. Chem.*, 2021, **9**, 1–11.

171 D. Wetzl, M. Gand, A. Ross, H. Müller, P. Matzel, S. P. Hanlon, M. Müller, B. Wirz, M. Höhne and H. Iding, *ChemCatChem*, 2016, **8**, 2023–2026.

172 H. A. Reeve, L. Lauterbach, O. Lenz and K. A. Vincent, *ChemCatChem*, 2015, **7**, 3480–3487.

173 S. B. Carr, R. M. Evans, E. J. Brooke, S. A. M. Wehlin, E. Nomerotskaia, F. Sargent, F. A. Armstrong and S. E. V. Phillips, *Biochem. Soc. Trans.*, 2016, **44**, 863–868.

174 E. J. Brooke, R. M. Evans, S. T. A. Islam, G. M. Roberts, S. A. M. Wehlin, S. B. Carr, S. E. V. Phillips and F. A. Armstrong, *Biochemistry*, 2017, **56**, 132–142.

175 R. M. Evans and S. E. Beaton, *Methods Enzymol.*, 2018, **613**, 91–116.

176 S. E. Beaton, R. M. Evans, A. J. Finney, C. M. Lamont, F. A. Armstrong, F. Sargent and S. B. Carr, *Biochem. J.*, 2018, **475**, 1353–1370.

177 T. Yagi, K. Kimura, H. Daidoji, F. Sakai, S. Tamura and H. Inokuchi, *J. Biochem.*, 1976, **79**, 661–671.

178 D. L. Pavia, G. M. Lampman, G. S. Kriz and J. R. Vyvyan, *Introduction to spectroscopy*, cengage learning, 5th edn., 2004.

179 E. . Morgan, *Vogel's textbook of practical organic chemistry. 5th edn.*, 1989.

180 K. Schwinn, N. Ferré and M. Huix-Rotllant, *Phys. Chem. Chem. Phys.*, 2020, **22**, 12447–12455.

181 P. Mondal, K. Schwinn and M. Huix-Rotllant, *J. Photochem. Photobiol. A Chem.*, 2020, **387**, 112164.

182 P. F. Heelis, *Chem. Soc. Rev.*, 1982, **11**, 15–39.

183 P. Macheroux, in *Methods in Molecular Biology*, eds. S. K. Chapman and G. A. Reid, Humana Press, Totowa, NJ, 1999, pp. 1–247.

184 Y. T. Kao, C. Saxena, T. F. He, L. Guo, L. Wang, A. Sancar and D. Zhong, *J. Am. Chem. Soc.*, 2008, **130**, 13132–13139.

185 I. Ahmad and F. H. M. Vaid, *Flavins: Photochemistry and Photobiology*, 2006.

186 M. W. Fraaije and A. Mattevi, *Trends Biochem. Sci.*, 2000, **25**, 126–132.

187 A. M. Edwards, in *Methods in Molecular Biology*, eds. S. Weber and E. Schleiker, Humana Press, New York, 2014, pp. 3–13.

188 R. K. Kar, A. F. Miller and M. A. Mroginski, *Wiley Interdiscip. Rev. Comput. Mol. Sci.*, 2021, 1–22.

189 V. Massey, *Biochem. Soc. Trans.*, 2000, **28**, 283–296.

190 G. Massey, V.; Palmer, *Biochemistry*, 1966, **5**, 3181.

191 S. Joseph Srinivasan, S. E. Cleary, M. A. Ramirez, H. A. Reeve, C. E. Paul and K. A. Vincent, *Angew. Chemie - Int. Ed.*, 2021, **60**, 13824–13828.

192 C. Walsh, *Acc. Chem. Res.*, 1986, **19**, 216–221.

193 R. S. Wolfe, G. D. Vogels and L. D. Eirich, *Biochemistry*, 1978, **17**, 4583–4593.

194 D. E. Edmondson, B. Barman and G. Toliin, *Biochemistry*, 1972, **11**, 1133–1138.

195 E. Haid, P. Lehmann and J. Ziegenhorn, *Clin. Chem.*, 1975, **21**, 884–887.

196 F. Fruscione, L. Sturla, G. Duncan, J. L. Van Etten, P. Valbuzzi, A. De Flora, E. Di Zanni and M. Tonetti, *J. Biol. Chem.*, 2008, **283**, 184–193.

197 M. J. Lukey, A. Parkin, M. M. Roessler, B. J. Murphy, J. Harmer, T. Palmer, F. Sargent and F. A. Armstrong, *J. Biol. Chem.*, 2010, **285**, 3928–3938.

198 M. M. Bradford, *Anal. Biochem.*, 1976, **72**, 248–254.

199 S. J. Compton and C. G. Jones, *Anal. Biochem.*, 1985, **151**, 369–374.

200 https://www.buchiglas.com/en/products/pressure-reactors-stirred-autoclaves/small pressure-reactors-10-450ml/tinyclave-steel.html, March, 2022.

201 M. C. R. Rauch, M. Pesic, M. M. E. Huijbers, M. Pabst, C. E. Paul, M. Pešić, I. W. C. E. Arends and F. Hollmann, *Biochim. Biophys. Acta - Proteins Proteomics*, 2020, **1868**, 140303.

202 L. A. Moran, R. H. Horton, G. K. Scrimgeour and M. D. Perry, *Principles of Biochemistry*, 2012.

203 A. L. Lehninger, D. L. Nelson and M. M. Cox, *Lehninger Prinicples of Biochemistry*, 2005.

204 S. Vogt, M. Schneider, H. Schä Fer-Eberwein and G. Nö, *Anal. Chem.*, 2014, **86**, 7530–7535.

205 J. C. Fontecilla-camps, A. Volbeda, C. Cavazza and Y. Nicolet, *Chem. Rev.*, 2007, **107**, 4273–4303.

206 S. Dementin, B. Burlat, A. L. De Lacey, A. Pardo, G. Adryanczyk-Perrier, B. Guigliarelli, V. M. Fernandez and M. Rousset, *J. Biol. Chem.*, 2004, **279**, 10508–10513.

207 I. Sumner and G. A. Voth, *J. Phys. Chem. B*, 2012, **116**, 2917–2926.

208 B. J. Murphy, F. Sargent and F. A. Armstrong, *Energy Environ. Sci.*, 2014, **7**, 1426–1433.

209 L. A. Flanagan and A. Parkin, *Biochem. Soc. Trans.*, 2016, **44**, 315–328.

210 C. Pinske, S. Krüger, B. Soboh, C. Ihling, M. Kuhns, M. Braussemann, M. Jaroschinsky, C. Sauer, F. Sargent, A. Sinz and R. G. Sawers, *Arch. Microbiol.*, 2011, **193**, 893–903.

211 G. Brown, T. S. Moody, M. Smyth and S. J. C. Taylor, *RSC Catal. Ser.*, 2018, **2018**-**Janua**, 229–256.

212 H. S. Toogood and N. S. Scrutton, *Curr. Opin. Chem. Biol.*, 2014, **19**, 107–115.

213 T. L. Kieft, J. K. Fredrickson, T. C. Onstott, Y. A. Gorby, H. M. Kostandarithes, T. J. Bailey, D. W. Kennedy, S. W. Li, A. E. Plymale, C. M. Spadoni and M. S. Gray, *Appl. Environ. Microbiol.*, 1999, **65**, 1214–1221.

214 D. J. Opperman and E. Van Heerden, *J. Appl. Microbiol.*, 2007, **103**, 1907–1913.

215 D. Johannes Opperman, L. Ann Piater and E. van Heerden, *J. Bacteriol.*, 2008, **190**, 3076–3082.

216 D. J. Opperman, B. T. Sewell, D. Litthauer, M. N. Isupov, J. A. Littlechild and E. van Heerden, *Biochem. Biophys. Res. Commun.*, 2010, **393**, 426–431.

217 D. Reardon and G. K. Farber, *FASEB J.*, 1995, **9**, 497–503.

218 R. K. Wierenga, *FEBS Lett.*, 2001, **492**, 193–198.

219 K. Kitzing, T. B. Fitzpatrick, C. Wilken, J. Sawa, G. P. Bourenkov, P. Macheroux and T. Clausen, *J. Biol. Chem.*, 2005, **280**, 27904–27913.

220 H. S. Toogood, J. M. Gardiner and N. S. Scrutton, *ChemCatChem*, 2010, **2**, 892–914.

221 B. V. Adalbjörnsson, H. S. Toogood, A. Fryszkowska, C. R. Pudney, T. A. Jowitt, D. Leys and N. S. Scrutton, *ChemBioChem*, 2010, **11**, 197–207.

222 K. M. Fox and P. A. Karplus, *Structure*, 1994, **2**, 1089–1105.

223 A. Fryszkowska, H. Toogood, M. Sakuma, J. M. Gardiner, G. M. Stephens and N. S. Scrutton, *Adv. Synth. Catal.*, 2009, **351**, 2976–2990.

224 J. Bernard, E. van Heerden, I. W. C. E. Arends, D. J. Opperman and F. Hollmann, *ChemCatChem*, 2012, **4**, 196–199.

225 J. J. Dong, E. Fernández-Fueyo, F. Hollmann, C. E. Paul, M. Pesic, S. Schmidt, Y. Wang, S. Younes and W. Zhang, *Angew. Chemie - Int. Ed.*, 2018, **57**, 9238–9261.

226 T. A. Rogers and A. S. Bommarius, *Chem Eng Sci*, 2010, **65**, 2118–2124.

227 M. M. C. H. Van Schie, C. E. Paul, I. W. C. E. Arends and F. Hollmann, *Chem. Commun.*, 2019, **55**, 1790–1792.

228 M. K. Peers, H. S. Toogood, D. J. Heyes, D. Mansell, B. J. Coe and N. S. Scrutton, *Catal. Sci. Technol.*, 2016, **6**, 169–177.

229 C. E. Paul and F. Hollmann, *Appl. Microbiol. Biotechnol.*, 2016, **100**, 4773–4778.

230 C. Kohlmann, W. Märkle and S. Lütz, *J. Mol. Catal. B Enzym.*, 2008, **51**, 57–72.

231 F. Hollmann, K. Hofstetter, T. Habicher, B. Hauer and A. Schmid, *J. Am. Chem. Soc.*, 2005, **127**, 6540–6541.

232 R. Ruinatscha, C. Dusny, K. Buehler and A. Schmid, *Adv. Synth. Catal.*, 2009, **351**, 2505–2515.

233 F. Hollmann, K. Hofstetter and A. Schmid, *Trends Biotechnol.*, 2006, **24**, 163–171.

234 K. Fisher, S. Mohr, D. Mansell, N. J. Goddard, P. R. Fielden and N. S. Scrutton, *Catal. Sci. Technol.*, 2013, **3**, 1505–1511.

235 U. Schwaneberg, D. Appel, J. Schmitt and R. D. Schmid, *J. Biotechnol.*, 2000, **84**, 249–257.

236 F. Hollmann, A. Schmid and E. Steckhan, *Angew. Chemie - Int. Ed.*, 2001, **40**, 169–171.

237 M. Finnegan, E. Linley, S. P. Denyer, G. McDonnell, C. Simons and J. Y. Maillard, *J. Antimicrob. Chemother.*, 2010, **65**, 2108–2115.

238 F. Hollmann and A. Schmid, *Biocatal. Biotransformation*, 2004, **22**, 63–88.

239 A. Tosstorff, C. Kroner, D. J. Opperman, F. Hollmann and D. Holtmann, *Eng. Life Sci.*, 2017, **17**, 71–76.

240 S. Staniland, T. Angelini, A. Pushpanath, A. Bornadel, E. Siirola, S. Bisagni, A. Zanotti-Gerosa and B. Domínguez, *Johnson Matthey Technol. Rev.*, 2020, **64**, 529–536.

241 F. P. Byrne, S. Jin, G. Paggiola, T. H. M. Petchey, J. H. Clark, T. J. Farmer, A. J. Hunt, C. Robert McElroy and J. Sherwood, *Sustain. Chem. Process.*, 2016, **4**, 1–24.

242 D. M. Ruiz and R. E. De Castro, *J. Ind. Microbiol. Biotechnol.*, 2007, **34**, 111–115.

243 G. R. Castro and T. Knubovets, *Crit. Rev. Biotechnol.*, 2003, **23**, 195–231.

244 M. M. C. H. van Schie, J. D. Spöring, M. Bocola, P. Domínguez de María and D. Rother, *Green Chem.*, 2021, **23**, 3191–3206.

245 K. Lalitha, Y. S. Prasad and S. Nagarajan, *State of the art and perspectives of green solvents in biocatalysis*, Elsevier Inc., 2021.

246 K. Stott, K. Saito, D. J. Thiele and V. Massey, *J. Biol. Chem.*, 1993, **268**, 6097–6106.

247 W. B. Black, L. Zhang, W. S. Mak, S. Maxel, Y. Cui, E. King, B. Fong, A. Sanchez Martinez, J. B. Siegel and H. Li, *Nat. Chem. Biol.*, 2020, **16**, 87–94.

248 H. K. Chenault, E. S. Simon and G. M. Whitesides, *Biotechnol. Genet. Eng. Rev.*, 1988, **6**, 221–270.

249 P. L. Graham, *An introduction to medicinal chemistry*, Oxford university Press, Oxford, 1995.

250 S. A. Lawrence, *Amines: Syntheis, Properties and Applications*, Cambridge University Press,

Cambridge, 6th edn., 2004.

251 T. C. Nugent, *Chiral Amine Synthesis Methods, Developments and Applications*, Wiley-VCH.

252 C. C. Marvin, *Synthesis of Amines and Ammonium Salts*, Elsevier Ltd., 2014, vol. 6.

253 M. Breuer, K. Ditrich, T. Habicher, B. Hauer, M. Keßeler, R. Stürmer and T. Zelinski, *Angew. Chemie - Int. Ed.*, 2004, **43**, 788–824.

254 A. S. Travis, *Manufacture and Uses of the Anilines: A Vast Array of Processes and Products*, 2007, vol. 38.

255 R. S. Boddu, O. Perumal and K. Divakar, *Biotechnol. Appl. Biochem.*, 2021, **68**, 1518–1530.

256 J. Song, Z. F. Huang, L. Pan, K. Li, X. Zhang, L. Wang and J. J. Zou, *Appl. Catal. B Environ.*, 2018, **227**, 386–408.

257 D. Formenti, F. Ferretti, F. K. Scharnagl and M. Beller, *Chem. Rev.*, 2019, **119**, 2611–2680.

258 P. Serna and A. Corma, *ACS Catal.*, 2015, **5**, 7114–7121.

259 A. Corma and P. Serna, *Science*, 2006, **313**, 332–335.

260 M. Boronat, P. Concepción, A. Corma, S. González, F. Illas and P. Serna, *J. Am. Chem. Soc.*, 2007, **129**, 16230–16237.

261 M. Orlandi, D. Brenna, R. Harms, S. Jost and M. Benaglia, *Org. Process Res. Dev.*, 2018, **22**, 430–445.

262 J. D. Roberts and M. C. Caserio, *Basic Principles of Organic Chemistry, second edition*, W. A. Benjamin, Inc., California, 2nd edn., 1977.

263 L. R. Sassykova, Y. A. Aubakirov, S. Sendilvelan, Z. K. Tashmukhambetova, N. K. Zhakirova, M. F. Faizullaeva, A. A. Batyrbayeva, R. G. Ryskaliyeva, B. B. Tyussyupova and T. S. Abildin, *Orient. J. Chem.*, 2019, **35**, 22–38.

264 S. D. Roughley and A. M. Jordan, *J. Med. Chem.*, 2011, **54**, 3451–3479.

265 H. R. Dasgupta, S. Mukherjee and P. Ghosh, *Tetrahedron Lett.*, 2019, **60**, 151028.

266 H. U. Blaser, H. Steiner and M. Studer, *ChemCatChem*, 2009, **1**, 210–221.

267 H. Goksu, H. Sert, B. Kilbas and F. Sen, *Curr. Org. Chem.*, 2016, **21**, 794–820.

268 G. Wienhöfer, I. Sorribes, A. Boddien, F. Westerhaus, K. Junge, H. Junge, R. Llusar and M. Beller, *J. Am. Chem. Soc.*, 2011, **133**, 12875–12879.

269 S. Park, I. S. Lee and J. Park, *Org. Biomol. Chem.*, 2013, **11**, 395–399.

270 V. Popat and N. Padhiyar, *Int. J. Chem. Eng. Appl.*, 2013, **4**, 401–405.

271 S. M. Kelly and B. H. Lipshutz, *Org. Lett.*, 2014, **16**, 98–101.

272 W. F. Bruce and L. A. Perez-Medina, *J. Am. Chem. Soc.*, 1970, **69**, 2571.

273 M. Orlandi, F. Tosi, M. Bonsignore and M. Benaglia, *Org. Lett.*, 2015, **17**, 3941–3943.

274 A. W. H. Dawood, R. O. M. A. de Souza and U. T. Bornscheuer, *ChemCatChem*, 2018, **10**, 951–955.

275 M. D. Patil, G. Grogan, A. Bommarius and H. Yun, *Catalysts*, 2018, **8**, 254.

276 C. A. Martinez, R. Kumar, J. Wong and C. C. B. F. Reactions, *Biocatalysis*, John Wiley & Sons, Ltd, 2nd edn., 2020.

277 H. Gröger, *Appl. Microbiol. Biotechnol.*, 2019, **103**, 83–95.

278 T. Knaus, W. Böhmer and F. G. Mutti, *Green Chem.*, 2017, **19**, 453–463.

279 J. Löwe, A. A. Ingram and H. Gröger, *Bioorganic Med. Chem.*, 2018, **26**, 1387–1392.

280 M. Alexeeva, A. Enright, M. J. Dawson, M. Mahmoudian and N. J. Turner, *Angew. Chemie - Int. Ed.*, 2002, **41**, 3177–3180.

281 E. Cigan, B. Eggbauer, J. H. Schrittwieser and W. Kroutil, *RSC Adv.*, 2021, **11**, 28223–28270.

282 D. Ghislieri, A. P. Green, M. Pontini, S. C. Willies, I. Rowles, A. Frank, G. Grogan and N. J. Turner, *J. Am. Chem. Soc.*, 2013, **135**, 10863–10869.

283 J. H. Schrittwieser, B. Groenendaal, S. C. Willies, D. Ghislieri, I. Rowles, V. Resch, J. H. Sattler, E. M. Fischereder, B. Grischek, W. D. Lienhart, N. J. Turner and W. Kroutil, *Catal. Sci. Technol.*, 2014, **4**, 3657–3664.

284 N. J. Turner and M. D. Truppo, *Biocatalytic Routes to Nonracemic Chiral Amines*, 2010.

285 S. C. Cosgrove, J. I. Ramsden, J. Mangas-Sanchez and N. J. Turner, *Methodol. Amin. Synth.*, 2021, 243–283.

286 F. Leipold, S. Hussain, D. Ghislieri and N. J. Turner, *ChemCatChem*, 2013, **5**, 3505–3508.

287 S. Hussain, F. Leipold, H. Man, E. Wells, S. P. France, K. R. Mulholland, G. Grogan and N. J. Turner, *ChemCatChem*, 2015, **7**, 579–583.

288 R. S. Heath, M. Pontini, S. Hussain and N. J. Turner, *ChemCatChem*, 2016, **8**, 117–120.

289 G. A. Aleku, S. P. France, H. Man, J. Mangas-Sanchez, S. L. Montgomery, M. Sharma, F. Leipold, S. Hussain, G. Grogan and N. J. Turner, *Nat. Chem.*, 2017, **9**, 961–969.

290 P. N. Scheller, M. Lenz, S. C. Hammer, B. Hauer and B. M. Nestl, *ChemCatChem*, 2015, **7**, 3239–3242.

291 P. Matzel, M. Gand and M. Höhne, *Green Chem.*, 2017, **19**, 385–389.

292 T. W. Thorpe, S. P. France, S. Hussain, J. R. Marshall, W. Zawodny, J. Mangas-Sanchez, S. L. Montgomery, R. M. Howard, D. S. B. Daniels, R. Kumar, F. Parmeggiani and N. J. Turner, *J. Am. Chem. Soc.*, 2019, **141**, 19208–19213.

293 J. N. Copp, A. M. Mowday, E. M. Williams, C. P. Guise, A. Ashoorzadeh, A. V. Sharrock, J. U. Flanagan, J. B. Smaill, A. V. Patterson and D. F. Ackerley, *Cell Chem. Biol.*, 2017, **24**, 391–403.

294 E. M. Williams, R. F. Little, A. M. Mowday, M. H. Rich, J. V. E. Chan-Hyams, J. N. Copp, J. B. Smaill, A. V. Patterson and D. F. Ackerley, *Biochem. J.*, 2015, **471**, 131–153.

295 M. D. Roldán, E. Pérez-Reinado, F. Castillo and C. Moreno-Vivián, *FEMS Microbiol. Rev.*, 2008, **32**, 474–500.

296 G. N. Parkinson, J. V. Skelly and S. Neidle, *J. Med. Chem.*, 2000, **43**, 3624–3631.

297 A. L. Lovering, E. I. Hyde, P. F. Searle and S. A. White, *J. Mol. Biol.*, 2001, **309**, 203–213.

298 R. E. Williams and N. C. Bruce, *Microbiology*, 2002, **148**, 1607–1614.

299 P. R. Race, A. L. Lovering, R. M. Green, A. Ossor, S. A. White, P. F. Searle, C. J. Wrighton and E. I. Hyde, *J. Biol. Chem.*, 2005, **280**, 13256–13264.

300 C. A. Haynes, R. L. Koder, A. F. Miller and D. W. Rodgers, *J. Biol. Chem.*, 2002, **277**, 11513–11520.

301 W. Pitsawong, J. P. Hoben and A. F. Miller, *J. Biol. Chem.*, 2014, **289**, 15203–15214.

302 H. H. Nguyen-Tran, G. W. Zheng, X. H. Qian and J. H. Xu, *Chem. Commun.*, 2014, **50**, 2861–2864.

303 K. Durchschein, M. Hall and K. Faber, *Green Chem.*, 2013, **15**, 1764–1772.

304 Y. Yanto, M. Hall and A. S. Bommarius, *Org. Biomol. Chem.*, 2010, **8**, 1826–1832.

305 A. F. Miller, J. T. Park, K. L. Ferguson, W. Pitsawong and A. S. Bommarius, *Molecules*, 2018, **23**, 211.

306 F. Li, J. Cui, X. Qian and R. Zhang, *Chem. Commun.*, 2004, 2338–2339.

307 PCT/US20 19/066026, 2020.

308 J. Yves de Saint Laumer, S. Leocata, E. Tissot, L. Barous, D. M. Kampf, P. Merle, A. Boschung, M. Seyfried and A. Chaintreau, *J. Sep. Sci.*, 2015, **38**, 3209–3217.

309 P. Feng, K. N. Lee, J. W. Lee, C. Zhan and M. Y. Ngai, *Chem. Sci.*, 2016, **7**, 424–429.

310 M. V Shah, J. Antoney, S. W. Kang, A. C. Warden, C. J. Hartley, H. Nazem-Bokaee, C. J. Jackson and C. Scott, *Catalysts*, 2019, **9**, 868.

311 P. Cheeseman, A. Toms-Wood and R. S. Wolfe, *J. Bacteriol.*, 1972, **112**, 527–531.

312 B. Ney, F. H. Ahmed, C. R. Carere, A. Biswas, A. C. Warden, S. E. Morales, G. Pandey, S. J. Watt, J. G. Oakeshott, M. C. Taylor, M. B. Stott, C. J. Jackson and C. Greening, *ISME J.*, 2017, **11**, 125–137.

313 M. L. Mascotti, H. Kumar, Q. T. Nguyen, M. J. Ayub and M. W. Fraaije, *Sci. Rep.*, 2018, **8**, 1–10.

314 F. Jacobson and C. Walsh, *Biochemistry*, 1984, **23**, 979–988.

315 L. M. I. de Poorter, W. J. Geerts and J. T. Keltjens, *Microbiology*, 2005, **151**, 1697–1705.

316 K. Tanaka, T. Kimachi, M. Kawase and F. Yoneda, *J. Chem. Soc. Chem. Commun.*, 1988, **2**, 524–526.

317 M. S. Hossain, C. Q. Le, E. Joseph, T. Q. Nguyen, K. Johnson-Winters and F. W. Foss, *Org. Biomol. Chem.*, 2015, **13**, 5082–5085.

318 S. Ebert, P. G. Rieger and H. J. Knackmuss, *J. Bacteriol.*, 1999, **181**, 2669–2674.

319 B. Ney, C. R. Carere, R. Sparling, T. Jirapanjawat, M. B. Stott, C. J. Jackson, J. G. Oakeshott, A. C. Warden and C. Greening, *Front. Microbiol.*, 2017, **8**, 1–11.

320 M. V. Shah, H. Nazem-Bokaee, J. Antoney, S. W. Kang, C. J. Jackson and C. Scott, *Sci. Rep.*, 2021, **11**, 1–16.

321 V. Massey and P. Hemmerich, *J. Biol. Chem.*, 1977, **252**, 5612–5614.

322 E. L. Hendrickson and J. A. Leigh, *J. Bacteriol.*, 2008, **190**, 4818–4821.

323 M. A. Oyugi, G. Bashiri, E. N. Baker and K. Johnson-Winters, *Biochemistry*, 2016, **55**, 5566–5577.

324 E. Purwantini and B. Mukhopadhyay, *Proc. Natl. Acad. Sci.*, 2009, **106**, 6333–6338.

325 M. C. Taylor, C. J. Jackson, D. B. Tattersall, N. French, T. S. Peat, J. Newman, L. J. Briggs, G. V. Lapalikar, P. M. Campbell, C. Scott, R. J. Russell and J. G. Oakeshott, *Mol. Microbiol.*, 2010, **78**, 561–575.

326 F. H. Ahmed, A. E. Mohamed, P. D. Carr, B. M. Lee, K. Condic-Jurkic, M. L. O'Mara and C. J. Jackson, *Protein Sci.*, 2016, **25**, 1692–1709.

327 M. Insińska-Rak, E. Sikorska, J. L. Bourdelande, I. V. Khmelinskii, W. Prukała, K. Dobek, J. Karolczak, I. F. Machado, L. F. V Ferreira, A. Komasa, D. R. Worrall and M. Sikorski, *J. Mol. Struct.*, 2006, **783**, 184–190.

328 R. S. Wolfe, G. D. Vogels and L. D. Eirich, *Biochemistry*, 1978, **17**, 4583–4593.

329 L. A. Davis, M. A. Oyugi, J. Howard, J. Corrales, A. Aziz, C. Mandimutsira, J. Girme, A. Agbonoga, G. Bashiri, E. N. Baker and K. Johnson-Winters, *Inorganica Chim. Acta*, 2021, **524**, 120417.

330 Q. T. Nguyen, G. Trinco, C. Binda, A. Mattevi and M. W. Fraaije, *Appl. Microbiol. Biotechnol.*, 2017, **101**, 2831–2842.

331 K. C. Costa, P. M. Wong, T. Wang, T. J. Lie, J. A. Dodsworth, I. Swanson, J. A. Burn, M. Hackett and J. A. Leigh, *Proc. Natl. Acad. Sci. U. S. A.*, 2010, **107**, 11050–11055.

332 A. P. Shuber, E. C. Orr, M. A. Recny, P. F. Schendel, H. D. May, N. L. Schauer and J. G. Ferry, *J. Biol. Chem.*, 1986, **261**, 12942–12947.

333 S. F. Tzeng, M. P. Bryant and R. S. Wolfe, *J. Bacteriol.*, 1975, **121**, 192–196.

334 J. Kunow, B. Schwörer, K. O. Stetter and R. K. Thauer, *Arch. Microbiol.*, 1993, **160**, 199–205.

335 K. Seelbach, B. Riebel, W. Hummel, M. R. Kula, V. I. Tishkov, A. M. Egorov, C. Wandrey and U. Kragl, *Tetrahedron Lett.*, 1996, **37**, 1377–1380.

336 H. Kumar, Q. T. Nguyen, C. Binda, A. Mattevi and M. W. Fraaije, *J. Biol. Chem.*, 2017, **292**, 10123–10130.

337 S. Vitt, K. Ma, E. Warkentin, J. Moll, A. J. Pierik, S. Shima and U. Ermler, *J. Mol. Biol.*, 2014, **426**, 2813–2826.

338 M. L. Mascotti, M. J. Ayub and M. W. Fraaije, *Proteins*, 2021, **89**, 1497–1507.

339 C. Martin, G. Tjallinks, M. Trajkovic and M. W. Fraaije, *ChemBioChem*, 2020, **22**, 156–159.

340 H. Ichikawa, G. Bashiri and W. L. Kelly, *J. Am. Chem. Soc.*, 2018, **140**, 10749–10756.

341 W. Li, S. Chou, A. Khullar and B. Gerratana, *Appl. Environ. Microbiol.*, 2009, **75**, 2958–2963.

342 G. Heiss, K. W. Hofmann, N. Trachtmann, D. M. Walters, P. Rouvière and H. J. Knackmuss, *Microbiology*, 2002, **148**, 799–806.

343 J. Drenth, M. Trajkovic and M. W. Fraaije, *ACS Catal.*, 2019, **9**, 6435–6443.

344 J. Latham, E. Brandenburger, S. A. Shepherd, B. R. K. Menon and J. Micklefield, *Chem. Rev.*, 2018, **118**, 232–269.

345 H. E.D. M. Saleh and M. Koller, *Green Chemistry*, 2018.

346 A. Ivanković, A. Dronjic, A. Bevanda Martinovic and S. Talic, *Int. J. Sustain. Green Energy*, 2017, **6**, 39–48.

Appendix

A. Procedure for determining the concentrations of Hdyd1

Bradford assays were performed using Bradford Protein Assay Kit from Thermo Scientific and contained BSA ampules (Bovine Serum Albumin) to use as a relative standard. Since Bradford assays yield a non-linear curve with increasing protein concentrations, it is advisable to perform a standard curve alongside the unknown for every assay. Therefore, a series of dilutions of the relative standard, BSA were prepared using the stock BSA with guidelines from the manual which contained the following table:

Table 1. Guideline for preparing serial dilutions of BSA to use as a relative standard and determine enzyme concentrations

Vial	**Volume of diluent µL**	**Volume and source of BSA µL**	**Final BSA concentration µg/ mL**
S1	0	300 µL of stock	2000
S2	125	375 µL of stock	1500
S3	325	325 µL of stock	1000
S4	175	175 of vial B dilution	750
S5	325	325 of vial C dilution	500
S6	325	325 of vial E dilution	250
S7	325	325 of vial F dilution	125
S8	400	100 of vial G dilution	25
S9	400	0	0 = Blank

In total, duplicates of the nine BSA dilutions (10 µL) and 3 Hyd1 dilutions (10 µL) were loaded into the microplate at the indicated positions. Using a multi-channel pipette, 200 µL of the Bradford reagent were mixed with the standard and unknown samples and the mixtures were left to incubate at room

temperature for 5 – 10 minutes. The positions at which all samples and standards were loaded for a typical assay can be seen below

Table 2. A model of 96- well plate showing the contents in each well. The grey area did not have samples

	1	2	3	4	5	6
A	S1	S1	S9	S9	Blank.....	Blank.....
B	S2	S2	Hyd1-220 (1)	Hyd1-220 (1)	Blank.....	Blank.....
C	S3	S3	Hyd1-220 (2)	Hyd1-220 (2)	Blank.....	Blank.....
D	S4	S4	Hyd1-220 (3)	Hyd1-220 (3)	Blank.....	Blank.....
E	S5	S5	Hyd1-223 (1)	Hyd1-223 (1)	Blank.....	Blank.....
F	S6	S6	Hyd1-223 (2)	Hyd1-223 (2)	Blank.....	Blank.....
G	S7	S7	Hyd1-223 (3)	Hyd1-223 (3)	Blank.....	Blank.....
H	S8	S8	Blank	blank	Blank.....	Blank.....

The spectrophotometer was set to 595 nm and the absorbance of samples, standards and blank was measured. A sample data obtained from the plate reader for estimating concentrations of two different batches of Hyd1 can be seen below:

Results from a Bradford assay showing the absorbance measured using a plate reader

Linear regression fit based on Protein 595 in ng/mL (595) Absorbance

	1	2	3	4	5	6	7	8	9	10	11	12
A	511.354	516.575	115.622	115.429	1.423	2.148	3.309	11.48	-0.269	2.293	3.405	3.454
B	463.344	701.073	267.194	255.591	0.214	6.306	4.662	3.841	2.245	2.874	3.695	-1.961
C	420.555	1312.1	224.213	213.479	-0.801	3.309	1.907	8.047	0.118	1.81	0.408	0.504
D	368.678	308.581	180.989	158.894	0.553	4.276	0.118	0.698	5.243	0.94	4.372	1.616
E	313.415	277.686	187.903	178.427	2.583	5.581	7.128	2.148	5.533	4.227	8.434	-2.59
F	225.421	268.838	152.173	131.432	2.68	1.133	1.278	1.423	-0.753	1.52	5.484	2.728
G	157.395	149.127	138.539	147.58	2.874	4.421	0.359	2.922	6.403	2.825	1.326	0.504
H	139.119	124.615	2.197	-0.317	0.698	6.016	5.436	5.533	0.746	-1.236	5.001	7.37

A standard curve (as shown in Figure 1) was plotted using the average absorbance values of standards S1 to S9 (entries in blue). The blank absorbance value was subtracted from the measured values to exclude any unwanted absorptions. Any outliers were omitted, for instance entries 2B and 2C were not

used for calculations in this experiment as the values were unusually high. Hyd1 concentrations (entries in green) were then estimated by substituting their absorbance values for the polynomial equation acquired for the standard curve. Thus, the concentration of Hyd1-220 and Hyd1-223 batches were estimated using the Bradford assay and were measured to be *c.a* 4.5 and 2.5 mg/ mL respectively.

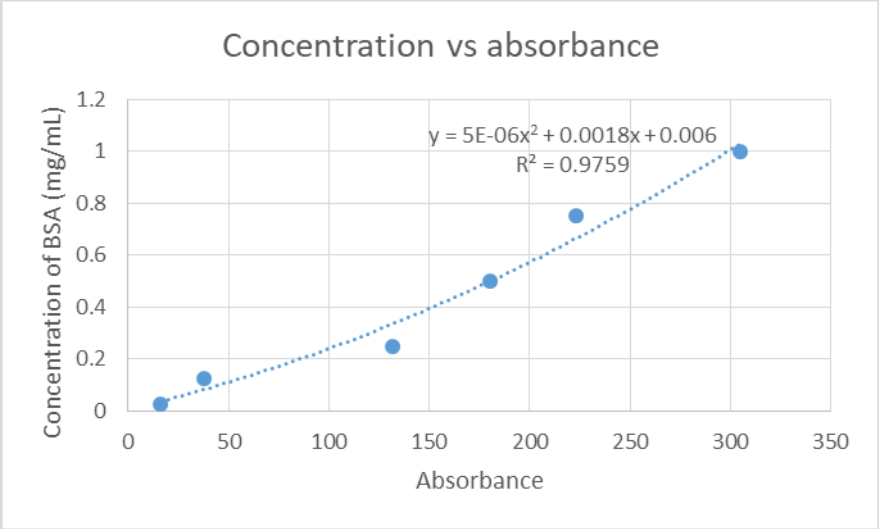
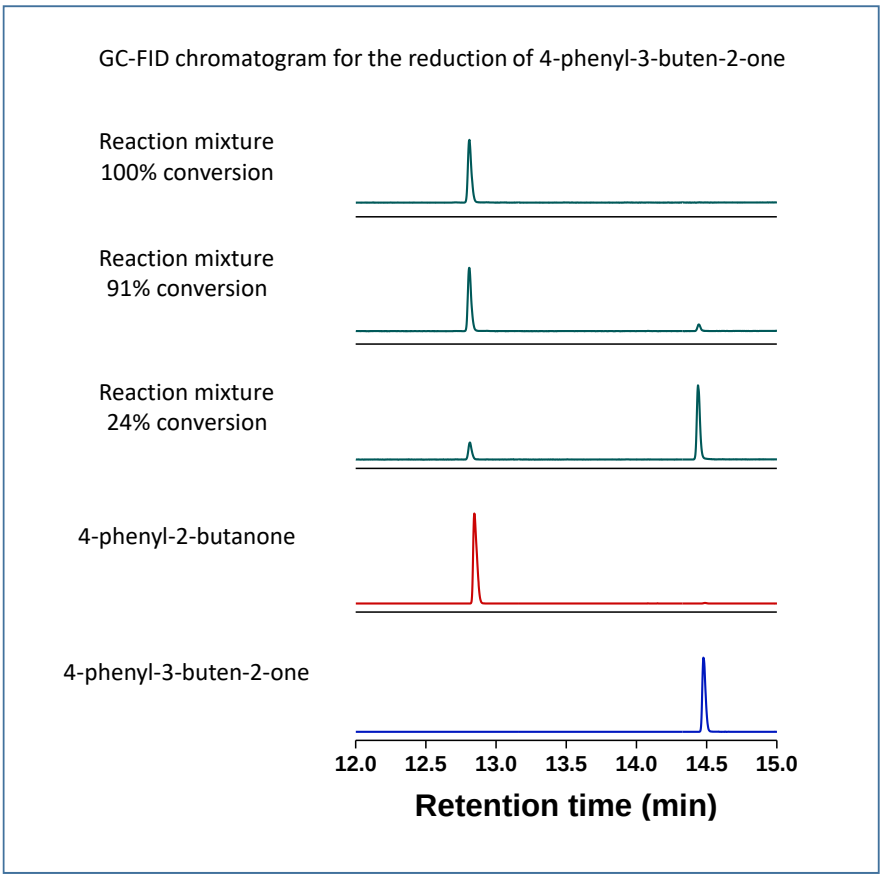


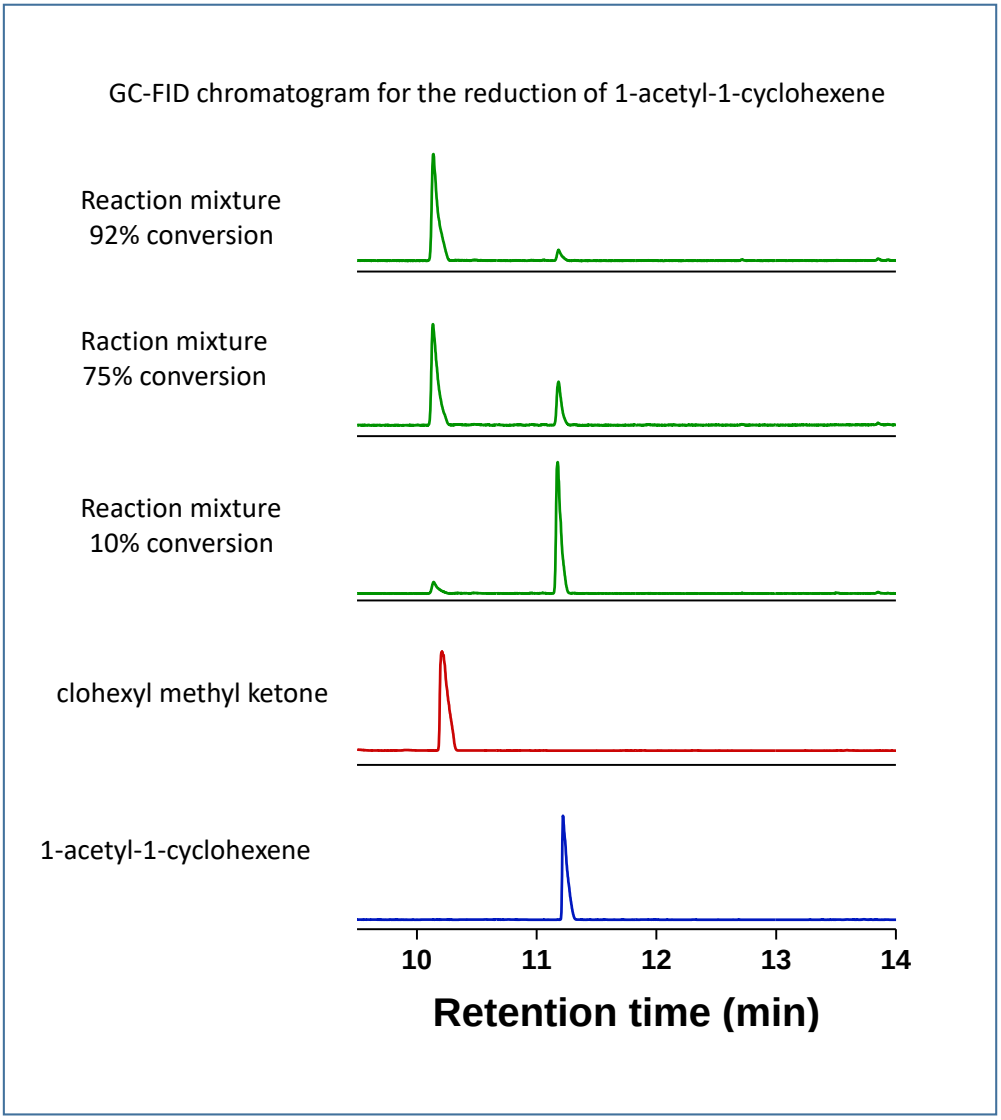
Figure 1. A standard curve and polynomial equation obtained for the absorbance of varying concentrations of BSA at 595 nm

B. GC-FID chromatogram for different reactions

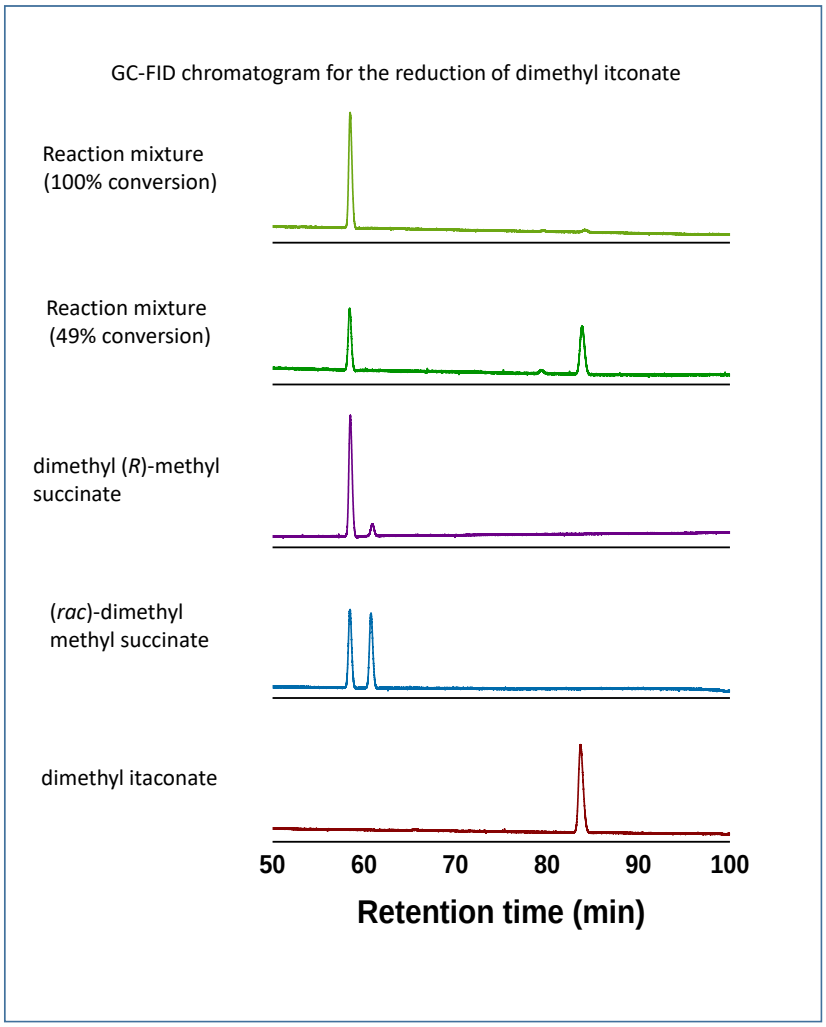
(i) Biocatalytic reduction of 4-phenyl-3-buten-2-one



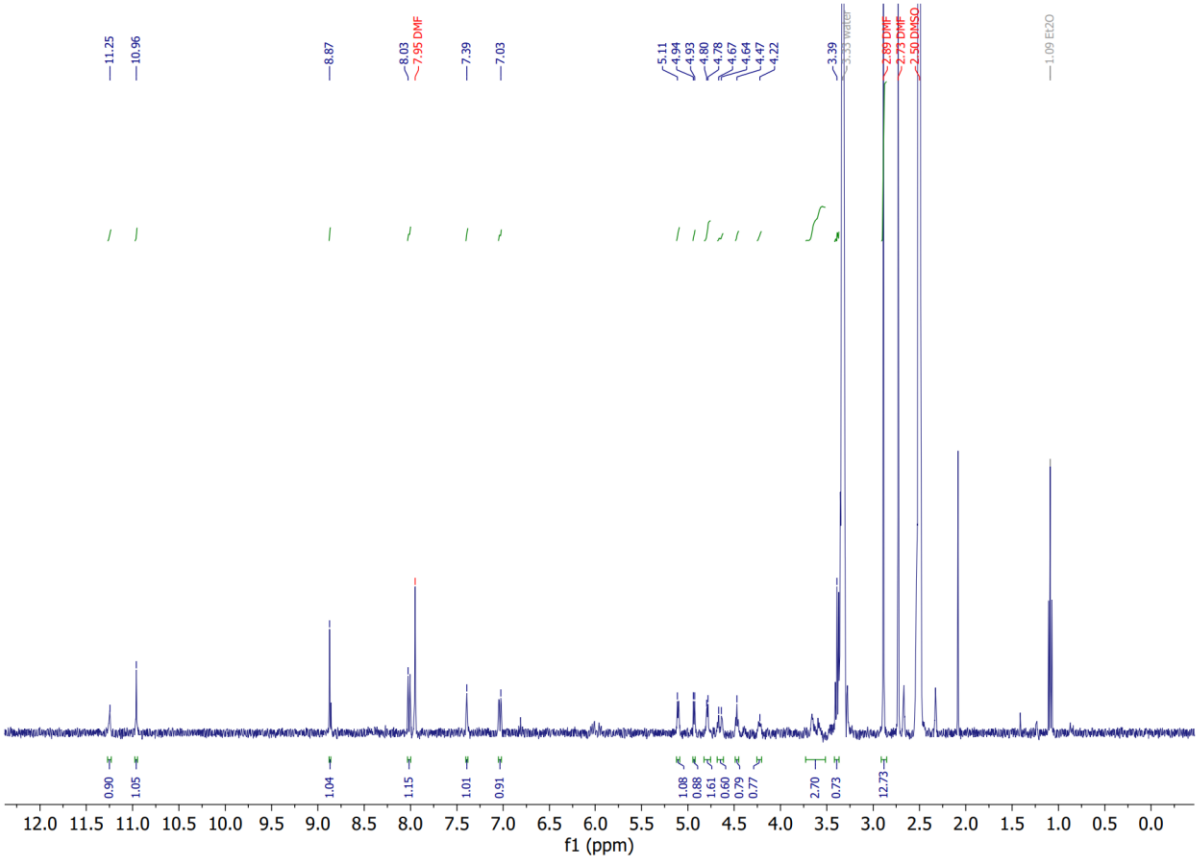
(ii) Biocatalytic reduction of 1-acetyl-1-cyclohexene



(iii) Biocatalytic reduction of Dimethyl itaconate



C. ^{1}H NMR spectrum of laboratory synthesised F_O



^{1}H NMR (400 MHz, DMSO) δ 11.25 (s, 1H), 10.96 (s, 1H), 8.87 (s, 1H), 8.03 (d, J = 8.8 Hz, 1H), 7.39 (s, 1H), 7.05 (d, J = 8.8 Hz, 1H), 5.11 (d, J = 5.5 Hz, 1H), 4.94 (d, J = 5.5 Hz, 1H), 4.78 (d, J = 7.2 Hz , 2H), 4.64 (d, J = 12 Hz, 1H), 4.49 – 4.44 (m, 1H), 4.22 (s, 1H), 3.72-3.51 (m, 3H), 3.41-3.36 (m, 1H).